



**HAL**  
open science

# Hypothalamic control of hippocampal area CA2 activity

Vincent Robert

► **To cite this version:**

Vincent Robert. Hypothalamic control of hippocampal area CA2 activity. *Neurons and Cognition* [q-bio.NC]. Université Sorbonne Paris Cité, 2018. English. NNT : 2018USPCB232 . tel-02984778

**HAL Id: tel-02984778**

**<https://theses.hal.science/tel-02984778>**

Submitted on 1 Nov 2020

**HAL** is a multi-disciplinary open access archive for the deposit and dissemination of scientific research documents, whether they are published or not. The documents may come from teaching and research institutions in France or abroad, or from public or private research centers.

L'archive ouverte pluridisciplinaire **HAL**, est destinée au dépôt et à la diffusion de documents scientifiques de niveau recherche, publiés ou non, émanant des établissements d'enseignement et de recherche français ou étrangers, des laboratoires publics ou privés.



MEMBRE DE  
**U<sup>S</sup>PC**  
Université Sorbonne  
Paris Cité



Université Paris Descartes

**Ecole doctorale 158 : Cerveau, Cognition, Comportement**

*Centre de Psychiatrie et Neurosciences / Equipe Chevalayre - Piskorowski*

# **Hypothalamic control of hippocampal area CA2 activity**

Par Vincent ROBERT

Thèse de doctorat de Neurosciences

Dirigée par Rebecca PISKOROWSKI, PhD & Vivien CHEVALEYRE, PhD

Présentée et soutenue publiquement le 16/05/2018

Devant un jury composé de :

Liset Menendez DE LA PRIDA, PhD (Rapporteur)

Paul SALIN, PhD (Rapporteur)

Claire LEGAY, PhD, PU (Président du jury)

Audrey MERCER, PhD (Examineur)

Philippe ASCHER, PhD, Professeur émérite (Examineur)

Jean-Christophe PONCER, PhD (Examineur invité)

Karim BENCHENANE, PhD (Examineur invité)

# Acknowledgements

It is with sincere enthusiasm that I thank all the persons involved in the completion of this thesis.

I thank Rebecca Piskorowski and Vivien Chevaleyre for taking me on as a PhD student, teaching me many technical and intellectual aspects of research, supervising my work, and guiding me through these years. Thank you for your availability, your encouragements, your insightful advices and for setting such a pleasant atmosphere in the lab. I am proud to have learnt science from you. During these years, I have not only received an invaluable training from you but also found exceptional mentors who never failed to help me move forward through good and hard times with thoughtfulness and friendship. Rebecca, thank you for your patience, your support, your trust, and your enthusiasm in passing on your expertise. I can only hope to become a researcher like you in the future.

I thank the members of my thesis committee, Claire Legay, Liset Menendez de la Prida, Paul Salin, Audrey Mercer, Philippe Ascher, Jean-Christophe Poncer and Karim Benchenane. It is an honor to have you evaluate my work. I thank Manuel Mameli for being part of my progress committee.

I thank all the present and past members of the lab for useful discussions, help with experiments, and all the fun times we had. In particular, I thank Ludivine Therreau and Kaoutsar Nasrallah. Thank you Ludivine for your invaluable help with surgeries, genotyping, and histology. Thank you Kaoutsar for helping me when I started and for your thoughtfulness and positive attitude that never failed to bring serenity in the lab, it was amazing working with you.

I thank the Ecole Normale Supérieure de Cachan, the French Ministère de la Recherche, and the Fondation pour la Recherche Médicale (FDT20170437387) for funding my work.

I thank the members of the McHugh lab for providing the Csf2rb2-Cre mouse line, the AAV.Synapsin.DIO.hM4D(Gi).mCherry virus, and *in vivo* experiments.

I thank Mario Penzo and Bo Li who trained me and became my friends during the year I spent in Cold Spring Harbor labs, showing me that I was capable of doing science which was critical in my decision to go for a PhD.

I thank my family. In particular, I thank my mother for her never-failing support and care, and for her genuine curiosity about my topics of interest. Thank you Julie for your positive attitude. I thank my father for his attention and interest in my work. I thank my grandparents for their encouraging attitude. Thank you Françoise for helping me grow up and sparking my scientific curiosity.

I thank my friends, who were always there for me through good and hard times, having your friendship is truly inspirational. Thank you Clément for the amazing experiences and exchanges we had together, for always pushing me forward and never letting me down. Thank you Poppy for all the happy times and music we shared, for understanding who I am and picking me up every time I fall. Thank you Joss for your unshakable positivity, genuine altruism and for always helping to keep balance in my life be it with laughter or comfort. Thank you Coralie-Anne for all the fun times and fascinating scientific discussions we shared during our thesis years, and for always looking up what is best for me. I thank Mélanie Tobin for the years of our lives that we shared during this thesis. Thank you Benoit, Arnaud, Loulou, Elsa, Lucas, Mathilde, Victor, Charles, Benjamin, Julien, Théo, Anil, Thibault, Antoine, Edith, Agathe, Pierre, Audrey, Cécile, Jean-Marie, Guillaume, Gustavo, Alex, Daphnée.

I thank Mélanie for her kindness, thoughtfulness, tolerance, joyfulness, generosity, and confidence in me, which never fail to bring me happiness and help me overcome difficulties.

*I dedicate this work to my aunt,  
Françoise Mantz*

# Table of contents

<b><u>ACKNOWLEDGEMENTS</u></b> .....	<b>2</b>
<b><u>TABLE OF CONTENTS</u></b> .....	<b>5</b>
<b><u>LIST OF ABBREVIATIONS</u></b> .....	<b>8</b>
<b><u>LIST OF FIGURES AND TABLES</u></b> .....	<b>11</b>
<b><u>I - INTRODUCTION</u></b> .....	<b>13</b>
<u>I.1 - ROLES OF THE HIPPOCAMPUS AND THE HYPOTHALAMUS IN MEMORY</u> .....	13
<u>I.2 - BRAIN CIRCUITS RELEVANT TO EPISODIC MEMORY</u> .....	14
<u>I.2.a - Flow of information in the canonical hippocampal loop</u> .....	15
<u><i>I.2.a.i - Hippocampal anatomy and cellular composition</i></u> .....	15
<u><i>I.2.a.ii - Inter-regional connectivity and information processing</i></u> .....	20
<u>I.2.b - Integration of area CA2 inputs and outputs in the hippocampal circuit</u> .....	23
<u><i>I.2.b.i - Intra-hippocampal connectivity of area CA2</i></u> .....	23
<u><i>I.2.b.ii - Area CA2 long-range afferences and efferences</i></u> .....	26
<u>I.3 - PHYSIOLOGICAL FEATURES OF HIPPOCAMPAL-DEPENDENT MEMORY FORMATION</u> .....	30
<u>I.3.a - Network activity patterns underlying learning and memory</u> .....	30
<u><i>I.3.a.i - Theta and gamma oscillations</i></u> .....	30
<u><i>I.3.a.ii - Sharp wave / ripples</i></u> .....	34
<u>I.3.b - Mnemonic functions of the hippocampus and hypothalamus</u> .....	35
<u><i>I.3.b.i - Spatial coding and memory</i></u> .....	35
<u><i>I.3.b.ii - Emotional, novel and social aspects of memory</i></u> .....	42
<u>I.4 - GOALS OF THE THESIS</u> .....	43
<b><u>II - MATERIAL AND METHODS</u></b> .....	<b>45</b>
<u>II.1 - ANIMALS</u> .....	45
<u>II.2 - STEREOTAXIC VIRAL INJECTIONS</u> .....	46
<u>II.3 - ACUTE HIPPOCAMPAL SLICES PREPARATION</u> .....	47
<u>II.4 - ELECTROPHYSIOLOGICAL RECORDINGS</u> .....	47
<u>II.5 - OPTOGENETIC STIMULATION</u> .....	48
<u>II.6 - IMMUNOCHEMISTRY AND CELL IDENTIFICATION</u> .....	48
<u>II.7 - DATA ANALYSIS AND STATISTICS</u> .....	50
<u>II.8 - EXPERIMENTAL STRATEGY</u> .....	51
<b><u>III - RESULTS</u></b> .....	<b>59</b>

<u>III.1 - SPONTANEOUS NETWORK ACTIVITY OF HIPPOCAMPAL AREA CA2 UNDER CONDITIONS OF ENHANCED CHOLINERGIC TONE</u> .....	59
<u>III.1.a - Introduction</u> .....	59
<u>III.1.b - Results</u> .....	60
<u>III.2 - HYPOTHALAMIC CONTROL OF HIPPOCAMPAL AREA CA2 ACTIVITY BY DIRECT EXCITATION AND FEEDFORWARD INHIBITION</u> .....	81
<u>III.2.a - Introduction</u> .....	81
<u>III.2.b - Results</u> .....	82
<u>III.3 - INFLUENCE OF SuM INPUTS ON HIPPOCAMPAL AREA CA2 DRIVE ONTO CA1</u> .....	115
<u>III.3.a - Introduction</u> .....	115
<u>III.3.b - Results</u> .....	117
<b><u>IV - DISCUSSION AND FUTURE DIRECTIONS</u></b> .....	<b>131</b>
<u>IV.1 - ROLES OF AREA CA2 IN HIPPOCAMPAL NETWORKS AND RHYTHMS</u> .....	131
<u>IV.1.a - Similarities and differences of network activity in area CA2 and CA3</u> .....	132
<u>IV.1.b - Bursts of action potentials in CA2 PNs</u> .....	133
<u>IV.1.c - Integration of area CA2 in theta and gamma hippocampal rhythms</u> .....	134
<u>IV.2 - RELEVANCE OF SuM INPUTS TO HIPPOCAMPAL AREA CA2 PHYSIOLOGY</u> .....	135
<u>IV.2.a - SuM inputs to area CA2 form a microcircuit where PV+ basket cells strongly inhibit deep pyramidal neurons in area CA2 and CA3</u> .....	135
<u>IV.2.b - SuM input and space coding in area CA2</u> .....	136
<u>IV.2.c - SuM input and hippocampal oscillations</u> .....	137
<u>IV.2.d - Gating of area CA2 activity by PV+ INs and significance for pathologies</u> ....	138
<u>IV.2.e - Differential modulation of DG and area CA2 by SuM inputs and consequences on hippocampus-dependent memory formation</u> .....	139
<u>IV.2.f - Relevance of the SuM excitatory drive to CA2 PNs</u> .....	140
<u>IV.3 - CONTROL OF HIPPOCAMPAL ACTIVITY AND OUTPUT BY SuM INPUTS</u> .....	141
<u>IV.3.a - Cholinergic modulation of SuM inputs</u> .....	142
<u>IV.3.b - Synchronization of CA2 activity by SuM inhibitory drive</u> .....	143
<u>IV.3.c - Transient silencing of CA1 activity by the SuM-CA2-CA1 circuit</u> .....	144
<b><u>V - REFERENCES</u></b> .....	<b>149</b>
<b><u>VI - APPENDICES</u></b> .....	<b>176</b>
<u>VI.1 - CHRONIC LOSS OF CA2 TRANSMISSION LEADS TO HIPPOCAMPAL HYPEREXCITABILITY</u>	
176	
<u>VI.1.a - Introduction</u> .....	176

<u>VI.1.b - Paper</u> .....	177
<u>VI.2 - HIPPOCAMPAL AREA CA2 : PROPERTIES AND CONTRIBUTION TO HIPPOCAMPAL</u> <u>FUNCTION</u> .....	178
<u>VI.2.a - Introduction</u> .....	178
<u>VI.2.b - Paper</u> .....	178
<b><u>RÉSUMÉ</u></b> .....	<b>179</b>
<b><u>ABSTRACT</u></b> .....	<b>180</b>

# List of abbreviations

4-AP : 4-aminopyridine  
Ication-Ca<sup>2+</sup> : calcium-dependent non-selective cation current  
AAV : adeno-associated virus  
ACSF : artificial cerebro-spinal fluid  
AHP : after-spike hyperpolarization  
Amp : ampicillin  
AMPA :  $\alpha$ -amino-3-hydroxy-5-methyl-4-isoxazolepropionic acid  
ANOVA : analysis of variance  
AP : action potential  
APV : (2R)-amino-5-phosphonovaleric acid; (2R)-amino-5 phosphonopentanoate  
BAC : bacterial artificial chromosome  
BC : basket cell  
CA : *Cornu Ammonis*  
CACNG5 : calcium voltage-gated channel auxiliary subunit gamma 5  
CAV : canine adenovirus  
CCh : carbachol  
CCK : cholecystokinin  
ChR2 : channelrhodopsin 2  
C<sub>M</sub> : membrane capacitance  
CNO : clozapine N-oxide  
Cre : Cre recombinase  
Csf2rb2 : colony stimulating factor 2 receptor  $\beta$  2  
DAMGO : [D-Ala<sup>2</sup>, N-MePhe<sup>4</sup>, Gly-ol]-enkephalin  
DG : dentate gyrus  
DIO : double inverted open reading frame  
DOR :  $\delta$  opioid receptor  
DPDPE : [D-Pen<sup>2</sup>,D-Pen<sup>5</sup>]enkephalin  
DREADD : designer receptor exclusively activated by designer drug  
DSP : digital signal processor  
EC : entorhinal cortex  
EEG : electroencephalogram  
EF1a : elongation factor 1 alpha  
EGFP : enhanced green fluorescent protein  
EGTA : ethylene glycol-bis( $\beta$ -aminoethyl ether)-N,N,N',N'-tetraacetic acid  
EPSC : excitatory post-synaptic current  
EPSP : excitatory post-synaptic potential  
EYFP : enhanced yellow fluorescent protein  
FLP : flipase  
FRT : flipase recognition target  
GABA :  $\gamma$ -aminobutyric acid

GAD65 : glutamic acid decarboxylase 65kDa  
 GC : granule cell  
 GH : growth hormone  
 HEPES : 4-(2-hydroxyethyl)-1-piperazineethanesulfonic acid  
 hM4D(Gi) : modified human muscarinic receptor 4  
 $I_h$  : hyperpolarization-activated cation current  
 $I_{KsAHP}$  : slow potassium AHP current  
 iLTD : long-term depression of inhibition  
 $I_M$  : M current  
 IN : interneuron  
 $I_{NaP}$  : persistent sodium current  
 IPSC : inhibitory post-synaptic current  
 IPSP : inhibitory post-synaptic potential  
 KO : knock-out  
 LED : light-emitting diode  
 LFP : local field potential  
 LIA : large irregular amplitude  
 mAChR : muscarinic acetylcholine receptor  
 MF : mossy fibers  
 MOR :  $\mu$ -opioid receptor  
 MPA3K15 : Mitogen-Activated Protein Kinase Kinase Kinase 15  
 NBQX : 2,3-dihydroxy-6-nitro-7-sulfamoyl-benzo[f]quinoxaline-2,3-dione  
 NMDA : N-methyl D-aspartate  
 NMDG : N-methyl-D-glucamin  
 NOS : nitric oxide synthase  
 NPY : neuropeptide Y  
 N-unit : SWR non-positively modulated unit  
 N-unit : SWR positively modulated unit  
 PBS : phosphate buffered saline  
 PCP-4 : purkinje cell protein 4  
 PCR : polymerase chain reaction  
 PH : posterior hypothalamus  
 PN : pyramidal neuron  
 PPR : paired-pulse ratio  
 PSP : post-synaptic potential  
 PV : parvalbumin  
 PVN : paraventricular nucleus  
 RGS14 : Regulator of G-protein signaling 14  
 $R_M$  : membrane resistance  
 RPO : reticular nucleus pontis oralis  
 SC : Schaffer collaterals  
 sEPSC : spontaneous excitatory post-synaptic current  
 SIA : small irregular amplitude

sIPSC : spontaneous inhibitory post-synaptic current  
SL : *stratum lucidum*  
SLM : *stratum lacunosum moleculare*  
SM : *stratum moleculare*  
SO : *stratum oriens*  
SP : *stratum pyramidale*  
SR : *stratum radiatum*  
SuM : supramammillary nucleus  
SWR : sharp wave / ripple  
SWS : slow wave sleep  
Syn : synapsin  
TE : thorny excrescence  
TREK : potassium two pore domain channel subfamily K member 2  
TTX : tetrodotoxin  
vg : viral genome  
VGAT : vesicular GABA transporter  
VGluT2 : vesicular glutamate transporter isoform 2  
VIP : vasoactive intestinal peptide  
 $V_M$  : membrane potential  
VTA : ventral tegmental area  
WPRE : woodchuck hepatitis virus post-transcriptional regulatory element

# List of figures and tables

<u>Figure I.2.1. Hippocampal anatomy in a transverse slice.</u> .....	16
<u>Figure I.2.2. Flow of information in the tri-synaptic loop of the hippocampus.</u> .....	22
<u>Figure I.2.3. Integrated view of area CA2 in the intra- and extra-hippocampal circuits.</u> .....	29
<u>Figure I.3.1. Activity of area CA2 from in vivo experiments.</u> .....	41
<u>Figure II.8.1. Experimental workflow of the study on CCh-induced network activity.</u> .....	53
<u>Figure II.8.2. Experimental workflow of the study on SuM input to area CA2.</u> .....	56
<u>Figure II.8.3. Experimental workflow of the study on the consequences of SuM activation on area CA2 and CA1 activity.</u> .....	58
<u>Figure III.1.1. Carbachol induces gamma-like oscillations in hippocampal area CA2 and CA3.</u> .....	61
<u>Figure III.1.2. Temporal relations of CCh-induced oscillations from area CA2 and CA3.</u> .....	63
<u>Figure III.1.3. Effects of chemogenetic silencing of CA2 PNs on CCh-induced oscillations.</u> .....	65
<u>Figure III.1.4. CA2 PNs fire bursts of APs following CCh application.</u> .....	68
<u>Figure III.1.5. Characteristics of charbachol-induced CA2 PN spontaneous activity.</u> .....	71
<u>Figure III.1.6. Effect of CCh on spontaneous excitatory and inhibitory events in CA2 PNs.</u> .....	73
<u>Figure III.1.7. Excitatory and inhibitory transmission shape bursts of action potentials in CA2 pyramidal cells.</u> .....	77
<u>Figure III.1.8. Bursts of action potentials in CA2 pyramidal cells are modulated by the ongoing field oscillation.</u> .....	79
<u>Figure III.2.1. Selective labeling of SuM neurons that project to hippocampal area CA2.</u> .....	85
<u>Figure III.2.2. CA2-projecting SuM neurons express VGluT2.</u> .....	86
<u>Figure III.2.3. SuM input provides excitatory glutamatergic transmission to diverse population of PNs in area CA2.</u> .....	90
<u>Figure III.2.4. Reconstruction of pre-synaptic SuM fibers and post-synaptic PNs in area CA2.</u> .....	91
<u>Figure III.2.5. SuM light-evoked mono-synaptic excitation as well as mono- and di-synaptic inhibition onto DG GCs.</u> .....	95
<u>Figure III.2.6. SuM axon stimulation recruits feedforward inhibition.</u> .....	100
<u>Figure III.2.7. Area CA2 PNs receive a net inhibitory drive from SuM that controls summation and AP firing properties.</u> .....	104

<u>Figure III.2.8. SuM inputs strongly excite basket cell interneurons in area CA2.</u> .....	108
<u>Figure III.2.9. SuM inputs provide excitation to Parvalbumin-expressing BCs.</u> .....	110
<u>Figure III.2.10. Parvalbumin-expressing BCs mediate the feedforward inhibition recruited by photostimulation of SuM fibers.</u> .....	114
<u>Figure III.3.1. Reduction of SuM excitatory and inhibitory transmission by carbachol.</u> .....	119
<u>Figure III.3.2. SuM control of CA2 PN bursting activity.</u> .....	122
<u>Figure III.3.3. Immediate consequences of SuM activation on CA1 activity.</u> .....	125
<u>Figure III.3.4. Delayed consequences of SuM activation on CA1 activity.</u> .....	128
<u>Figure IV.3.1. Integrated view of brain state-dependent SuM and area CA2 activity.</u> .....	147
<u>Table III.1.1. Characteristics of charbachol-induced CA2 PN spontaneous activity.</u> .....	70
<u>Table III.2.1. Electrophysiological properties of pyramidal neurons in SuM innervated area</u> .....	88
<u>Table III.2.2. Properties of deep and superficial pyramidal neurons in areas CA2 and CA3a</u> .....	88
<u>Table III.2.3. Characteristics of SuM light-evoked transmission onto PNs in area CA2.</u> .....	92
<u>Table III.2.4. Characteristics of SuM light-evoked responses in deep and superficial pyramidal neurons in areas CA2 and CA3a.</u> .....	93
<u>Table III.2.5. Electrophysiological properties of interneurons in SuM-innervated area.</u> .....	106
<u>Table III.2.6. Characteristics of SuM light-evoked transmission onto interneurons &amp; pyramidal cells.</u> 106	
<u>Table III.3.1. Consequences of SuM photostimulation over area CA2 on CA1 PNs.</u> .....	130

# **I - Introduction**

## **I.1 - Roles of the hippocampus and the hypothalamus in memory**

To form memories, the brain has the remarkable ability to encode, store and retrieve information. This cognitive function is critical for survival, adaptation to a changing environment, and life in society. Memory is a complex process that encompasses several systems spanning different structures of the central nervous system. This section briefly reviews important features of memory and introduces relevant brain regions, in particular the hippocampus and hypothalamus.

From human studies, much has been learned about how the brain forms memories. Memory is divided into short- and long-term based on the time course of the retained information. These two categories are handled by different parts of the brain, as evidenced by patients with long-term memory loss who can still perform well in a working memory task that requires keeping information available during a short period of time (Baddeley, 2003). Long-term memory is further divided in declarative and non-declarative based on the nature of the information retained. Declarative memory is the process in which items that can be explicitly expressed. Non-declarative memory regroups unconscious forms of memory (Cohen and Squire, 1980; Squire and Zola-Morgan, 1991). Non-declarative memory nevertheless implies learning such that a given input will reliably trigger a corresponding output. Reflex pathways, conditioned associations, priming processes and procedural abilities fall into the non-declarative class of memory (Squire and Zola-Morgan, 1991; Tulving and Schacter, 1990). Declarative memory applies to the process of memory formation and recall of conscious items, either semantic if they are general facts or episodic when they involve personal information. Episodic memory is therefore defined as the memory of events concerning the self that can be explicitly recollected. Strikingly, these different forms of long-term memory rely on specific brain structures that could be discovered in patients with lesions in the corresponding dedicated areas. Indeed, the seminal study of patient H.M. revealed a specific role for the hippocampus and related structures in episodic memory (Squire and Wixted, 2011). Following bi-lateral resection of medial temporal lobes to remove epileptic foci, H.M. developed a full anterograde and partial retrograde amnesia (Scoville and Milner, 1957). Remarkably, procedural and short-term memory were unaffected by H.M.'s lesions, and so was his retrograde long-term memory to the extent remote times before the surgery (Sagar et al., 1985; Squire and Wixted, 2011). Combined

with clinical observations from other amnesic patients and experimental work in monkeys and rodents, these findings firmly establish a selective role for the hippocampus in episodic memory (Mishkin, 1978; Mumby, 2001; Scoville and Milner, 1957; Zola-Morgan et al., 1986; Zola-Morgan et al., 1994). Furthermore, the anterograde nature of H.M.'s amnesia revealed that the hippocampus is necessary for learning and forming new episodic memories.

Although these findings converged on a central role for the hippocampus in episodic memory, it also appeared that the hippocampus was not the sole brain structure responsible for learning and memory. Indeed, the preserved past knowledge of H.M. proved that the hippocampus is not the ultimate storage site for long-term episodic memories. Moreover, H.M.'s lesions were not restricted to the hippocampus and additional work in monkeys and rodents reported that hippocampal lesions alone leave certain aspects of memory unaffected (Mishkin, 1978; Mumby, 2001; Squire and Zola-Morgan, 2001; Zola-Morgan et al., 1994). Perhaps not too surprising given their close relations with the hippocampus, the entorhinal cortex and amygdala are also involved in episodic memory (Mishkin, 1978; Squire and Zola-Morgan, 2001). Another brain structure implicated in memory, notably in humans, is the hypothalamus. This diencephalic area suffers extensive damage in a pathological condition called Korsakoff's syndrome (Mair et al., 1979). Often caused by chronic alcoholism, Korsakoff's syndrome is characterized by damage to the thalamus and the hypothalamic mamillary region, resulting in memory impairments in humans and mice models of the disease (Daniel, 2005; Mair et al., 1979). Interestingly, the hippocampus itself is mostly spared in Korsakoff's syndrome (Daniel, 2005) suggesting that injuries to brain structures connected to the hippocampus can cause similar memory deficits as hippocampal lesions. Indeed, the mamillary region of the hypothalamus is closely associated with the hippocampus as the mamillary bodies receive hippocampal projections and the supramamillary nucleus innervates the hippocampus (Pan and McNaughton, 2004a). However, even with this, there is paucity of physiological investigations of this hypothalamo-hippocampal circuit.

## **I.2 - Brain circuits relevant to episodic memory**

In order to understand how episodic memory can be formed, stored and mobilized in the central nervous system, one needs to examine the brain structures involved, how they are connected and what neurons they host. Therefore, this section describes the anatomy, global and local connectivity, and cellular composition of the hippocampal formation with emphasis on area CA2.

## **I.2.a - Flow of information in the canonical hippocampal loop**

### **I.2.a.i - Hippocampal anatomy and cellular composition**

The hippocampus is a bilateral archicortical structure folded under the cerebral cortex and is widely conserved in numerous species including humans and rodents. In mice, the hippocampus is a prominent structure that occupies a large volume of the brain extending on a rostro-caudal and dorso-ventral axis from a septal pole to a temporal pole in a curved shape. Besides its local circuitry, the hippocampus is connected to several brain structures. The main glutamatergic afference to the hippocampus comes from layers II and III of the entorhinal cortex (EC) (Steward and Scoville, 1976; Witter et al., 1989). Another major glutamatergic input resides in the hippocampus itself, as left and right hippocampi are inter-connected (Blackstad, 1956). GABAergic neurons in the septum project to the hippocampus where they specifically innervate interneurons (Freund and Antal, 1988; Freund and Buzsáki, 1996). The septum also provides cholinergic inputs to the hippocampus (Shute and Lewis, 1963). Other neuromodulatory afferences to the hippocampus include noradrenaline from the locus coeruleus (Swanson and Hartman, 1975), serotonin from the raphe (Freund et al., 1990), dopamine from the ventral tegmental area and substantia nigra (Gasbarri et al., 1994). Additional projections to the hippocampus arise from the amygdala (Kemppainen et al., 2002), thalamus (Witter, 1996), and hypothalamus (Cui et al., 2013; Maglóczy et al., 1994). Efferent projections of the hippocampus are diverse as well. The major hippocampal output is the EC, thus establishing a reciprocal loop with this structure, either directly or via the subiculum (Naber et al., 2001). Reciprocal connections also consist of hippocampal projections to the septum, amygdala, and hypothalamus (Groen and Wyss, 1990; Swanson and Cowan, 1977). In addition, the hippocampus sends outputs to the neocortex olfactory bulb, nucleus accumbens and thalamus (Groen and Wyss, 1990; Gulyás et al., 1998; Jay et al., 1989; Swanson and Cowan, 1977).

Like most regions of the brain, the hippocampus hosts two main kinds of neurons : the majority are principal cells and the minority interneurons (INs). Classically, principal cells are excitatory as they use the neurotransmitter glutamate while interneurons release GABA and are therefore inhibitory (excepted during the development of the central nervous system (Rivera et al., 1999)). Principal cells can drive excitation within and across regions and are therefore considered as the main communication units of the brain. Interneurons are involved in local interactions but also drive inhibition between brain areas through long-range projections (Caputi et al., 2013). In the hippocampal formation, neurons are segregated in different regions

that have anatomical and functional specificities : the dentate gyrus (DG), and *Cornu Ammonii* (CA) areas CA3, CA2 and CA1 (Lorente de No, 1934). These regions are further subdivided in their radial axis corresponding to the different parts of the principal cells parallel dendritic arborization. Indeed, principal cells are organized in a laminar way such that all somas are aligned, thus forming the pyramidal layer (*stratum pyramidale*, SP). The dendrites of these principal cells extend in a preferential direction perpendicular to SP and are therefore aligned parallel to each other on either side of SP. The outer layer formed by basal dendrites of pyramidal neurons (PNs) is called *stratum oriens* (SO), and the apical dendrites fill the inner layers of the hippocampus. The juxta-somatic inner layer in area CA3 is called *stratum lucidum* (SL) and corresponds to axonal tracks of the dentate gyrus granule cells, the mossy fibers (MF). Axons from area CA3 PNs, the Schaffer collaterals, run through the proximal part of the apical dendrites forming a layer called *stratum radiatum* (SR). Finally, the distal part of the apical dendritic arbor is contacted by afferent fibers from the entorhinal cortex (EC) in the *stratum lacunosum moleculare* (SLM).

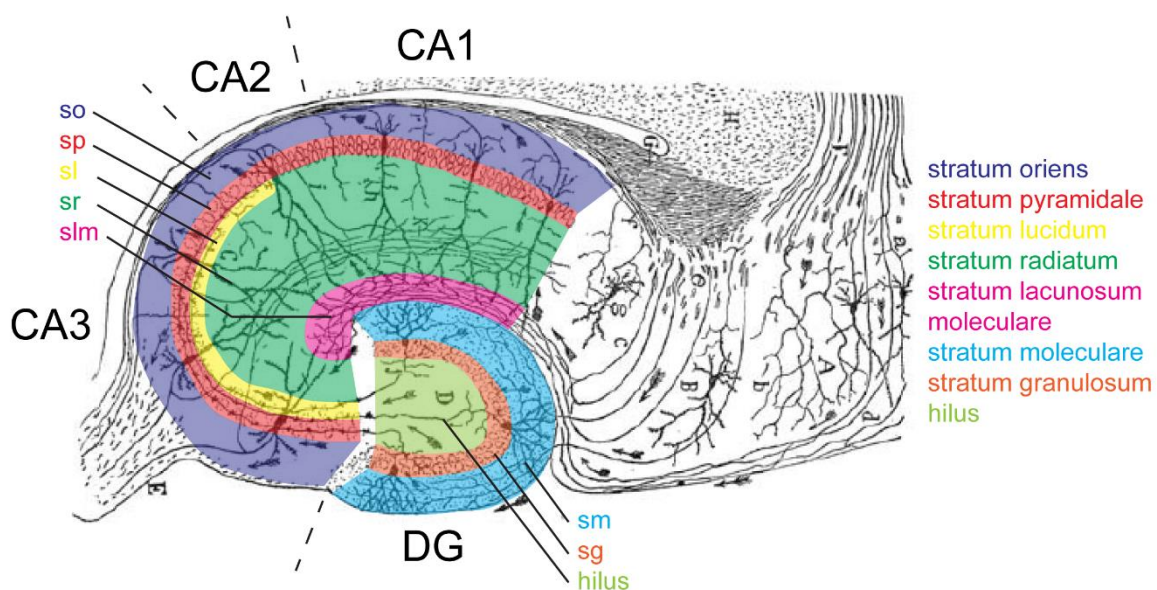


**Figure I.2.1. Hippocampal anatomy in a transverse slice.**

Drawing of Golgi stain illustrating the cytoarchitecture and connections within the different hippocampal subfields with highlighted laminar organization (adapted from Ramon y Cajal, 1911).

Within this common structural organization, principal cells from each region display specific characteristics in terms of morphology, dendritic arborization, electrophysiological properties, connectivity, and gene expression profiles (discussed here and in Section I.2.a.ii). Principal

cells of the DG, the granule cells (GCs), have small ovoid cell bodies and a highly polarized dendritic tree that arborizes only on their basal side in *stratum moleculare* (SM) (Claiborne et al., 1990). Their axons emerge on the apical side in the hilus and extend towards area CA3 in SL. Pyramidal neurons (PNs) of area CA3 are large cells with basal dendrites in SO and bifurcated apical ones in SL, SR and SLM. The dendritic portion in SL displays thorny excrescences (TEs) where MF from the DG make synaptic contact. Preferential axonal projections of CA3 PNs varies according to their location on the CA3a (closer to CA2) – b – c (closer to DG) axis. CA3a PNs give rise to extensive recurrent connections and project to proximal CA1 (closer to CA2). CA3c PNs contribute less to the recurrent system and project more towards distal CA1 (closer to the subiculum) (Ishizuka et al., 1990; Li et al., 1994). CA1 PNs have smaller somas and a different apical dendritic organization than CA3. In contrast to CA3, CA1 PNs apical dendrites do not bifurcate in two apical branches but instead arborize extensively in SR where CA3 afferent axons project, and more modestly in SLM (Bannister and Larkman, 1995). CA2 PNs differ from both CA3 and CA1 in that they have large soma, bifurcated apical dendrites that do not display TEs and arborize very little in SR but dramatically in SLM where inputs from EC form synapses (Chevalyere and Siegelbaum, 2010; Mercer et al., 2007; Piskorowski and Chevalyere, 2012). Electrophysiological properties of CA2 PNs are also unique with respect to CA1 and CA3 PNs. CA2 PNs show a low membrane resistance, hyperpolarized resting membrane potential, low hyperpolarizing sag current, and no after spike hyperpolarization (Chevalyere and Siegelbaum, 2010; Piskorowski et al., 2016; Sun et al., 2017). Besides variations on the proximo-distal axis, PNs vary according to their somatic location on the radial axis of the hippocampus. In area CA1, deep cells closer to SO and superficial cells closer to SR differ in terms of genetic expression, afferent innervation, efferent projections, and physiological functions (Danielson et al., 2016; Lee et al., 2014; Masurkar et al., 2017; Mizuseki et al., 2011; Valero et al., 2015). In particular, CA2 PNs drive stronger excitation on deep compared to superficial CA1 PNs (Kohara et al., 2013; Valero et al., 2015). Interestingly, *in vivo* functional differences between deep and superficial PNs have recently been reported in area CA2 (Oliva et al., 2016a), however the cellular and circuit mechanisms underlying these observations are not yet elucidated.

Besides excitatory pyramidal neurons, the hippocampus contains inhibitory interneurons that gate the inputs and outputs of PNs, shape network oscillations and participate in synaptic plasticity. In contrast with pyramidal neurons that form a relatively homogeneous population, interneurons are extremely diverse in terms of morphology, electrophysiological properties and

expression of genetic markers, reflecting their involvement in various distinct functions (Freund and Buzsáki, 1996; Somogyi and Klausberger, 2005). INs can be classified based on morphological features that allow functional predictions such as the location of their soma, the extension of their dendritic tree, and the targets of their axonal projections. Additional genetic and electrophysiological criteria provide further refinement of often overlapping classifications. A first functional group of INs target the dendrites of PNs and are therefore likely to control their afferent synaptic inputs. O-LM cells have their soma and dendrites located in SO and project their axon all the way to SLM (Maccaferri et al., 2000; McBain et al., 1994), thus potentially controlling EC inputs onto distal PNs or INs dendrites (Somogyi and Klausberger, 2005). O-LM cells express somatostatin (SOM) and fire action potentials quite regularly (Maccaferri et al., 2000). Bi-stratified INs also target PNs and INs dendrites but in SO and SR where they potentially control afferent excitatory inputs from CA3 on proximal dendrites (Buhl et al., 1994; Somogyi and Klausberger, 2005). They have a soma in SP or SO, dendrites extending in SO and SR, express SOM and show little accommodation in their firing pattern (Maccaferri et al., 2000; Pawelzik et al., 1999). SC-associated cells show a similar targeting of their axon to SR but have their soma located in SR, dendrites spanning SLM through SO, express cholecystokinin (CCK) and significantly accommodate their AP firing (Pawelzik et al., 2002; Vida et al., 1998). The other broad class of INs have axons targeting the soma or axon initial segment of PNs and are therefore in position of controlling their output. It is especially the case for axo-axonic cells whose axon targets axon initial segment of PNs and are thus likely to affect action potential generation in these cells (Somogyi and Klausberger, 2005). Axo-axonic cells extend their dendrites from SO through SLM, express parvalbumin (PV), and fire action potentials with either little or marked accommodation (Buhl et al., 1994a; Somogyi and Klausberger, 2005). The major IN type controlling PN output is the basket cell (BC) population, named after the dense peri-somatic net formed by axons from these cells (Buhl et al., 1994a). BCs have their soma in SP or SR, their dendrites spanning all CA *strata*, and express either PV or CCK (Maccaferri et al., 2000; Pawelzik et al., 2002). Remarkably, PV-expressing BCs are mostly fast-spiking whereas CCK-expressing BCs are mostly regular-spiking (Pawelzik et al., 2002).

Regardless of their type, INs can be involved in different type of wiring in hippocampal networks. The source of INs excitation can be local PNs that are subsequently inhibited by the INs : this scenario is called feedback inhibition. Feedback inhibition controls the duration and spread of excitation in PNs and can therefore pace their activity (Bartos et al., 2011).

Alternatively, feedforward inhibition happens when a common excitatory inputs targets both PNs and INs that can inhibit the PNs even before their AP discharge. Feedforward inhibition curtails excitation in post-synaptic PNs thus increasing the temporal precision of their AP firing (Pouille and Scanziani, 2001). In addition, INs can be engaged in mutual inhibition if they target one another, much like recurrent excitation amongst PNs but with opposite effect. Finally, certain populations of INs such as BCs are electrically coupled by gap junctions allowing for the propagation of membrane potential variations amongst these networks of INs.

Like the pyramidal neurons in area CA2, there is mounting evidence that the interneurons in this region have unique properties and potentially play significant roles in memory formation and disease. Studies performing hippocampal-wide comparison of different subclasses of interneurons based on immunological markers have revealed that CA2 comprises a peculiar composition of interneurons as compared to CA1 and CA3 (Botcher et al., 2014). While most immunohistological studies overlook area CA2 when quantifying interneuron density, recent studies have performed detailed quantification of interneuron densities along with concomitant staining of CA2-specific proteins. One very thorough study performed in rat hippocampus examined the density and stratum-localization of interneurons by staining for GAD-67, parvalbumin (PV), CCK, caretinin, calbindin, reelin, somatostatin, NPY and VIP, all with CA2 borders well-defined by either PCP-4 or alpha-actinin 2 staining (Botcher et al., 2014). This study and others found that area CA2 contains the highest density of PV-expressing interneurons (Botcher et al., 2014; Piskorowski and Chevaleyre, 2013). Furthermore, area CA2 contains the highest density of reelin-expressing neurons in the hippocampus (Botcher et al., 2014), which is very interesting given the various signaling roles of reelin in the adult hippocampus (Kupferman et al., 2014).

Using sharp recordings, Mercer et al. performed elegant and detailed analysis of individual CA2 interneurons in hippocampal slices from rats. Their work revealed unexpected morphological and electrophysiological properties of basket cells and bistratified cells in this region (Mercer et al., 2012a; 2012b). Area CA2 hosts two types of PV-expressing (PV+) basket cells: a minority resemble classical CA1 basket cells with narrow dendritic arborization in the septo-temporal axis, no sag potential and non-adapting fast spiking firing pattern, while the majority have a broad dendritic arborization, substantial sag potential and an adapting firing pattern normally encountered in CA1 O-LM interneurons (Mercer et al., 2007). Wide-arbor basket cells further differed by displaying excitatory post-synaptic potentials (EPSPs) elicited by pre-synaptic CA2 pyramidal neuron stimulation that were less depressing and longer in duration

due to a NMDAR component (Mercer et al., 2012a). Strikingly, similar observations were made regarding bistratified cells in area CA2, which consisted of narrow and wide-arbor subpopulations, indicating that the width of dendritic arborization, rather than axonal targeting, could serve as a reliable determinant of electrophysiological properties of interneurons in area CA2 (Mercer et al., 2007; 2012a). Finally, a novel type of interneuron was described in area CA2 with similar electrophysiological properties and morphologies as wide-arbor bistratified cells but with axons restricted to SR (SP–SR interneurons) (Mercer et al., 2012b). How these unusual types of basket cells, bistratified cells and SP–SR interneurons participate in controlling information flow in the hippocampal network remains to be understood.

### **I.2.a.ii - Inter-regional connectivity and information processing**

As described above, the hippocampal formation comprises different regions with specific connectivity allowing for information processing. Inputs from layers II of the medial and lateral entorhinal cortex (EC) transfer information to the DG that then targets area CA3 proximal dendrites through the mossy fibers (MF) in the *stratum lucidum* (SL), CA3 subsequently makes synaptic contact on the proximal dendrites of area CA1 through the Schaffer collaterals in SR and CA1 returns information to the EC, thus forming the tri-synaptic loop (Andersen et al., 1971). Additional routes running through the SLM allow the EC to directly impinge on the distal dendrites of pyramidal neurons in all CA regions (Ruth et al., 1982; 1988; Steward and Scoville, 1976). Much can be learnt about the functions of this tri-synaptic loop by considering the physiology of each region and the computation performed at each step of the circuit.

Afferent information to the hippocampus come from EC inputs that convey multimodal sensory (Canto et al., 2008), metric (Hafting et al., 2005) and directional signals (Taube et al., 1990). Axons from the EC run through the perforant path and make glutamatergic synapses onto the dendrites of granule cells in *stratum moleculare* (SM) (Deller et al., 1996). This information is processed by the dentate gyrus to allow pattern separation, i.e. the discrimination of similar inputs by sending a specific output. Indeed, dentate gyrus lesions impair spatial pattern separation in rats (Gilbert et al., 2001). This remarkable function of the dentate gyrus can be explained by the underlying physiology of its network. Although electrotonically compact, granule cells have a hyperpolarized resting membrane potential (Spruston and Johnston, 1992) making it potentially difficult for EC excitatory inputs to elicit action potential firing in post-synaptic granule cells. In addition, both EC inputs and granule cells excite dentate gyrus interneurons, thus recruiting feedforward and feedback inhibition, respectively (Freund and Buzsáki, 1996; Han et al., 1993; Kneisler and Dingledine, 1995; Sloviter, 1991). Altogether,

these characteristics confer low excitability to dentate gyrus granule cells (Jung and McNaughton, 1993; Penttonen et al., 1997). Therefore, excitatory transmission from EC inputs is likely to result in the activation of only a sparse population of granule cells. This is believed to allow pattern separation in the dentate gyrus as similar EC inputs would result in different granule cells outputs.

Axons from the dentate gyrus granule cells form the mossy fibers (MF) that run through SL towards the very proximal part of CA3 PN. The synapse between mossy fibers and CA3 PN consists of a mossy presynaptic bouton and a large postsynaptic differentiation called thorny excrescence. A single granule cell axon contacts thorny excrescences of a limited number of postsynaptic CA3 PNs (Acsády et al., 1998), thus keeping the pattern separated information orthogonalized. Efficacy of transmission at these synapses can be high and can reliably trigger action potential firing in CA3 PN provided pre-synaptic granule cells fire repeatedly (Henze et al., 2002). In addition, mossy fibers also project onto CA3 interneurons (Acsády et al., 1998) that in turn drive feedforward inhibition onto CA3 PNs. Much like the dentate gyrus, CA3 PNs and INs receive EC inputs in SLM (Kiss et al., 1996; Witter et al., 1989). From the information conveyed by these two upstream inputs, area CA3 performs pattern completion, i.e. builds a coherent output from partial inputs (Rolls, 1996). Pattern completion in area CA3 has been evidenced by the reactivation of CA3 ensembles after exposure to similar contexts (Vazdarjanova and Guzowski, 2004), and by impaired recall in mice lacking NMDARs in CA3 PNs (Nakazawa et al., 2002). A notable feature of the CA3 network that likely underlies pattern completion is the prominent recurrent excitation between CA3 PNs (Miles and Wong, 1986). These recurrent excitatory connections between CA3 PNs, together with sparse but strong input from the dentate gyrus (Geiger and Jonas, 2000; Henze et al., 2002) and the recruitment of interneurons that drive feedback inhibition (Miles, 1990), are thought to allow the reactivation of “meaningful” CA3 PN ensembles from sparse dentate gyrus inputs. It should be noted that pattern completion is highly specific as small changes in context can lead to orthogonalization of spatial representation in area CA3 (Leutgeb et al., 2004).

CA3 PNs in turn project onto CA1 PN proximal dendrites via the Schaffer collaterals in SR. The CA3 – CA1 PN synapses have been shown to bring about modest levels of excitation (Larkman et al., 1991; Sayer et al., 1990). Afferent CA3 axons also recruit feedforward inhibition onto CA1 PNs by exciting local CA1 interneurons (Lacaille, 1991). Entorhinal inputs provide another source of excitation (Yeckel and Berger, 1990) to CA1 PNs and to interneurons that can contribute in feedforward inhibition (Kiss et al., 1996). However, excitatory synapses

formed in SLM by EC axons are inefficient in driving CA1 PN action potential firing because of EPSPs generated in SLM are dampened by filtering on their way from the distal dendrites to the soma (Andreasen and JDC, 1998; Golding et al., 2005; Magee, 1998). Therefore, EC inputs require summation with other sources of excitation to drive activity in postsynaptic CA1 PNs. This puts area CA1 in a good position to act as an integrator of current experience through EC inputs and past experience “kept in memory” relayed by the DG – CA3 – CA1 path. Furthermore, excitatory recurrent connections are rare in area CA1 (Deuchars and Thomson, 1996) while feedback inhibition is prominent (Ali and Thomson, 1998; Ali et al., 1998; Buhl et al., 1994a). Altogether, these properties of the CA1 network are thought to allow weighted representations of past and present experience to be formed and sent to outside of the hippocampus. Efferent projections from CA1 PNs target the entorhinal cortex, directly or via the subiculum, hence closing the loop (Naber et al., 2001).

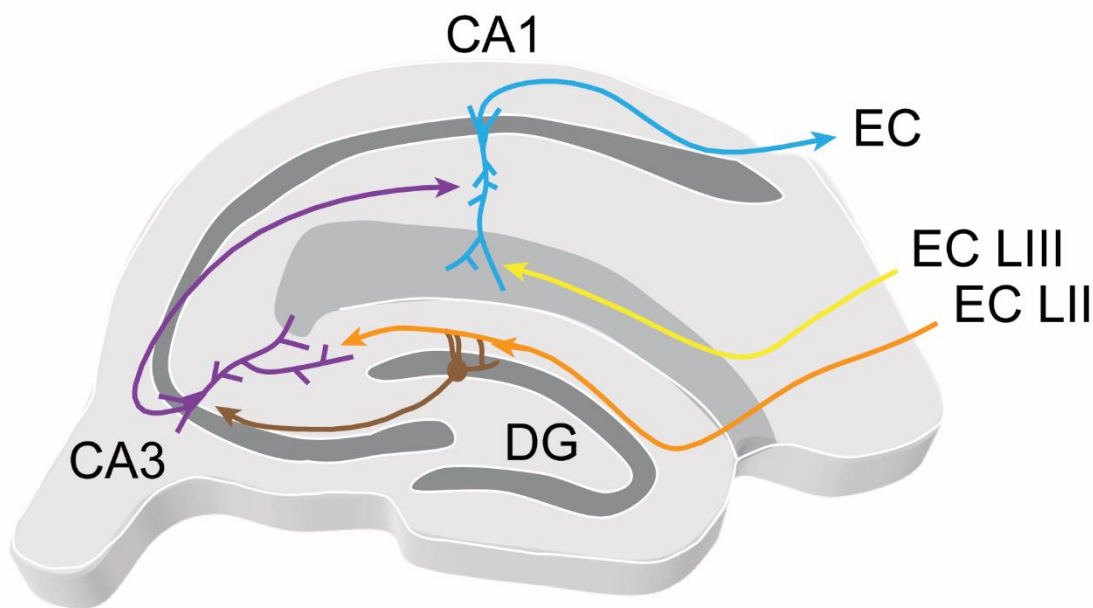


**Figure I.2.2. Flow of information in the tri-synaptic loop of the hippocampus.**

Diagram illustrating the EC – DG – CA3 – CA1 – EC circuit.

The accumulated knowledge of the functions of the tri-synaptic loop led to the idea that it supports memory formation in the hippocampus through pattern separation in the DG, pattern completion in area CA3, and integration in area CA1. However, *in vivo* testing of this view by disruption of the transmission between CA3 and CA1 led to unexpected results. Indeed, major aspects of hippocampal-dependent spatial memory were unaffected by lesions or genetic block

of the CA3 – CA1 transmission (Brun et al., 2002; Nakashiba et al., 2008). The mono-synaptic EC – CA1 loop was proposed to rescue mnemonic functions of the hippocampus in the absence of the tri-synaptic loop. However, this interpretation is in contradiction with the inability of EC inputs to efficiently drive CA1 PNs. Shortly thereafter, the discovery of a di-synaptic loop bypassing the DG and area CA3 but rather involving area CA2 provided an alternative hypothesis for the rescue of hippocampal memory formation in the absence of transmission between CA3 and CA1 (Chevaleyre and Siegelbaum, 2010).

## **I.2.b - Integration of area CA2 inputs and outputs in the hippocampal circuit**

### **I.2.b.i - Intra-hippocampal connectivity of area CA2**

To understand and support the role of area CA2 in information transfer through the hippocampus, one must characterize its connections with other hippocampal areas. The intra-hippocampal inputs to area CA2 have been studied using tracing, optogenetics and electrophysiology *in vivo* and *ex vivo*. Area CA2 receives direct input in SLM from the EC (Bartasaghi and Gessi, 2004; Chevaleyre and Siegelbaum, 2010; Cui et al., 2013; Hitti and Siegelbaum, 2014; Kohara et al., 2013). *In vivo* recordings from anesthetized guinea pigs reported that area CA2 is the first CA region to be active in response to EC input stimulation (Bartasaghi and Gessi, 2004), indicating a strong synaptic connection. This synaptic input was further elucidated with acute mouse brain slice recordings, revealing that mild electrical stimulation of these inputs is sufficient to make CA2 pyramidal neurons fire action potentials (APs) (Chevaleyre and Siegelbaum, 2010). This strong synaptic connection in area CA2 contrasts with distal CA1 cortical inputs, which has both high levels of feedforward inhibition as well as a large  $I_h$  current that prevents strong excitation of CA1 PNs (Chevaleyre and Siegelbaum, 2010; Nolan et al., 2004). Thus, it is possible that cortical inputs directly excite CA2 PNs, which then project to CA1 PNs, forming a di-synaptic hippocampal circuit. The EC – CA2 connection was further examined using conventional retrograde tracing from area CA2 in mice. Cui et al. reported afferent projections from primarily layer II EC cells, with a few layer III cells (Cui et al., 2013). Further, the generation of two different transgenic mouse lines expressing Cre recombinase specifically in CA2 pyramidal neurons allowed Hitti and Siegelbaum with the Amigo2-Cre line and Kohara et al. with the MAP3K15-Cre line to examine this input in a highly controlled manner. Both studies confirmed a strong layer II EC

with sparsely labeled layer III cells following retrograde rabies tracing (Hitti and Siegelbaum, 2014; Kohara et al., 2013).

DG granule cell mossy fibers form functional synapses with CA2 pyramidal neurons, as shown by optogenetic stimulation (Kohara et al., 2013). Mossy fiber inputs onto CA2 PNs have been shown to differ from the well-studied DG – CA3 synapse. As originally observed by Lorenté de No, CA2 pyramidal neurons lack the thorny excrescences that are stereotypical for the mossy fiber – CA3 synapse (No 1934) (Kohara et al., 2013). Furthermore, the DG – CA2 synapse has relatively much lower levels of excitatory transmission as compared to CA3 (Sun et al., 2017). This input is capable of driving feedforward inhibition by recruitment of CA2 interneurons (Kohara et al., 2013). Interestingly, it has been proposed from immunohistological studies that newborn DG granule cells project their axons to area CA2 (Llorens-Martín et al., 2015). This synapse merits further examination, as the DG was unlabeled in retrograde studies performed in the rat (Cui et al., 2013), indicating a potential species-specific difference. Furthermore, in the Amigo2-cre line, this connection was not identified with retrograde tracing (Hitti and Siegelbaum, 2014) but was with experiments performed in the MAP3K15-Cre line (Kohara et al., 2013). These differences may be due to technical differences between vectors and transgenic lines.

Conventional and rabies-based retrograde labeling in mice showed that CA2 pyramidal neurons receive inputs from both CA3 PNs as well as CA2 PNs (Cui et al., 2013; Hitti and Siegelbaum, 2014). Interestingly, stimulation of CA3 Schaffer collaterals in SR on acute slices from mice revealed that this input is dominated by a strong feedforward inhibitory drive in area CA2, unlike in CA1 (Chevalyere and Siegelbaum, 2010). This strong feedforward inhibitory transmission between CA3 and CA2 strongly contrasts with the strong direct excitation and limited feedforward inhibition observed following distal EC input stimulation (Chevalyere and Siegelbaum, 2010). In the context of information transfer, this large feedforward inhibition recruited by area CA3 onto CA2 indicates that area CA2 may not be recruited by CA3 neurons and may be bypassed in the tri-synaptic circuit. This alternative pathway for information flow had been previously proposed based on field recordings and voltage-sensitive dye imaging studies of entire hippocampal slices (Sekino et al., 1997). This study found that, in the majority of instances, no activity was detected in area CA2 following stimulation of the hilus. However, in some instances, a delayed activation of CA2 was detected that led to a larger and delayed signal propagation of area CA1. This early and insightful work may be revealing a potential role of area CA2 in hippocampal network function. Remarkably, the PV+ population of

interneurons is the substrate of a long-term depression of the CA3 to CA2 feedforward inhibition (Piskorowski and Chevaleyre, 2013) that subsequently allows CA2 to be recruited by CA3 inputs (Nasrallah et al., 2015). Hence, the inhibitory gating of area CA2 activity is also unique and shows dysfunctions in schizophrenia due to a loss of PV+ interneurons (Piskorowski et al., 2016).

The intra-hippocampal outputs of area CA2 have been investigated with tracing experiments, *ex vivo* electrophysiology and genetically restricted optogenetics. Interestingly, by selectively infecting EC neurons with rabies viruses in mice and conventional retrograde tracing in both mice and rats, Rowland et al. showed that area CA2 sends a return projection to EC layer II neurons (Rowland et al., 2013). Although this observation stands alone from other studies using either conventional or genetically targeted anterograde viral tracing from area CA2 (Cui et al., 2013; Hitti and Siegelbaum, 2014), the retrograde method used by Rowland et al. is not restricted to a specific pre-synaptic cell type and is potentially more efficient in labeling. This intriguing finding merits replication and further investigation. Using unilateral viral anterograde labeling of CA2 neurons in mice, Cui et al. reported ipsi- and contra-lateral projections to areas CA1, CA2 and CA3 (Cui et al., 2013). Paired recordings from CA2 and CA1 pyramidal neurons on acute hippocampal slices from mice directly proved an excitatory monosynaptic connection from CA2 to CA1 that appeared several-fold stronger than the CA3 to CA1 connection (Chevaleyre and Siegelbaum, 2010). Taking advantage of the Amigo2-Cre transgenic mouse line, Hitti et al. also reported axons of CA2 pyramidal neurons projecting to every CA area (Hitti and Siegelbaum, 2014). The CA2 to CA1 inputs were further examined with optogenetics using the MAP3K15-Cre mouse line, revealing that CA2 PNs have different excitatory drive along the radial CA1 axis, providing a much stronger excitation to deep CA1 pyramidal neurons (Kohara et al., 2013). This is quite interesting, as the deep and superficial CA1 pyramidal neurons project to different cortical and limbic regions (Lee et al., 2014). Using a different CA2-specific mouse Cre line driven by the calcium voltage-gated channel auxiliary subunit gamma 5 (CACNG5) promoter region, Boehringer et al. examined CA2 pyramidal neuron output to areas CA1 and CA3 in acute slices. This study showed that, while area CA2 recruits direct excitation and feedforward inhibition in both areas CA1 and CA3, the inhibitory drive of CA2 predominates in CA3 (Boehringer et al., 2017). In summary, by projecting to every CA subfield, CA2 pyramidal neurons are poised to act on the entire hippocampal network: there is a reciprocal control of E/I balance between areas CA2 and CA3, whereas CA2 acts very

strongly to preferentially excite deep CA1 pyramidal neurons, thereby influencing hippocampal output.

### **I.2.b.ii - Area CA2 long-range afferences and efferences**

In addition to forming the hub of an intrinsic hippocampal network, area CA2 is connected with several extrahippocampal structures. Retrograde tracing from area CA2 and anterograde labeling of vasopressinergic neurons in the paraventricular nucleus of the hypothalamus (PVN) revealed that area CA2 is targeted by inputs containing vasopressin (Cui et al., 2013). The PVN is strongly activated in stressful and social situations and results in the release of oxytocin and vasopressin throughout the brain (reviewed by Iovino et al., 2017), thus area CA2 is likely to be directly modulated during these circumstances. Additional long-range inputs to area CA2 have been described from the medial septum, diagonal band of Broca and median raphe that were labeled after retrograde marker injections in area CA2 of mice (Cui et al., 2013). Projections from these 3 regions were confirmed with rabies-based retrograde tracing from CA2 pyramidal neurons in the Amigo2-Cre and MAP3K15-Cre mouse lines (Hitti and Siegelbaum, 2014; Kohara et al., 2013).

Another hypothalamic projection to area CA2 arises from neurons in the supramammillary nucleus (SuM) (Haglund et al., 1984; Vertes, 1992). Albeit a relatively small area, the SuM has a significant role in the central nervous system through its connections with numerous brain structures. It receives inputs from other hypothalamic nuclei and also from the raphe, the habenula, the central gray, the septum and cortical regions (Pan and McNaughton, 2004). The SuM outputs are diverse as well and include reciprocal connections several hypothalamic areas, the raphe, the central gray, the septum and the cingulate and infralimbic cortex (Pan and McNaughton, 2004; Vertes, 1992). In addition, the SuM sends projections to the locus coeruleus, the thalamus, the amygdala, the EC and the hippocampus (Pan and McNaughton, 2004; Vertes, 1992). Neurons in the SuM are chemically diverse and have been reported to express calretinin, CCK, VGluT2, VGAT, dopamine, VIP, substance P and nitric oxide synthase (NOS) (Pan and McNaughton, 2004). In the hippocampus, afferent axons originate from calretinin-, VGluT2-, VGAT-, NOS-, VIP-, CCK- and substance P-expressing neuronal populations in the SuM (Berger et al., 2001; Borhegyi and Leranth, 1997; Haglund et al., 1984; Kiss et al., 2000; Pedersen et al., 2017). Interestingly, a subpopulation of SuM neurons has been shown to project both to the hippocampus and to the septum (Borhegyi et al., 1997; Vertes and McKenna, 2000). In contrast, inputs to area CA2 and the DG are likely provided by different populations of SuM neurons (Borhegyi and Leranth, 1997; Soussi et al., 2010). Indeed, SuM

afferent axons to the DG co-express glutamatergic (VGluT2) and GABAergic markers (VGAT or GAD65) (Boulland et al., 2009; Soussi et al., 2010). These axons co-release glutamate and GABA onto DG granule cells (Pedersen et al., 2017) and potentially interneurons (Leranth and Nitsch, 1994; Nitsch and Leranth, 1996). Transmission from the SuM to the DG has been shown to facilitate population spikes evoked by performant path stimulation of EC inputs, potentially by increasing activity in granule cells and decreasing it in interneurons (Mizumori et al., 1989). In contrast, area CA2 is targeted by VGluT2-expressing SuM axons only that presumably form synapses exclusively on pyramidal neurons in the rat (Kiss et al., 2000; Maglóczy et al., 1994; Soussi et al., 2010). These CA2-projecting SuM axons also express calretinin and substance P (Berger et al., 2001; Borhegyi and Leranth, 1997; Nitsch and Leranth, 1993). This projection has also been reported in mice (Cui et al., 2013; Hitti and Siegelbaum, 2014; Kohara et al., 2013) and primates (Berger et al., 2001), where it is present in prenatal hippocampus and proposed to play a role in hippocampal rhythms necessary for proper development. Until now, functional investigation of the glutamatergic SuM – CA2 transmission has never been carried out, and neither has the neuromodulation of hippocampal networks by substance P released from SuM.

Neurons in area CA2 also send projections outside the hippocampal circuit to a number of brain regions, sometimes establishing reciprocal connections. Tracing studies in rodents indicate that this is the case for the SuM, the medial septum and the diagonal band of Broca (Cui et al., 2013). The lateral septum has also been reported as a long-range output of area CA2 by anterograde tracings in mice (Cui et al., 2013). These extrahippocampal projections were not observed when using the Amigo2-Cre specific of CA2 pyramidal neurons mouse line (Hitti and Siegelbaum, 2014) and are thus potentially due to a different population of neurons in area CA2, either long-range projecting interneurons or a subpopulation of pyramidal neurons not labeled by this Cre line.

The tendency of long-range reciprocal connections between area CA2 and other cerebral structures raises the possibility of mutual influences between these regions and the hippocampal network via area CA2. However, functional characterizations of these bi-directional connections are still missing and should provide a more comprehensive understanding of the interplay between area CA2 and the rest of the brain.

In summary, the cellular composition, neuronal physiology, intrinsic and extrinsic connectivity patterns of area CA2 make it uniquely positioned in the hippocampal network. A general feature of area CA2 is its low overall excitability conferred by a high density of INs and hyperpolarized

non-resistive PNs. As opposed to CA1, the net input received by CA2 PNs from CA3 is dominated by feedforward inhibition. Interestingly, this CA3 – CA2 feedforward inhibition is highly plastic whereas the CA3 – CA2 excitatory synapse is not. Also contrasting with CA1, distal EC inputs efficiently provide excitation to CA2 PNs thus potentially bypassing the tri-synaptic loop. Area CA2 strongly drives excitation in area CA1 and provides inhibition back to area CA3, thereby possibly isolating the di-synaptic loop from the tri-synaptic one. Interestingly, area CA2 receives and sends long range inputs and outputs that may favor or prevent activity of CA2 PNs thus influencing the rest of the hippocampal network by switching between CA3- and CA2-dominated loops.

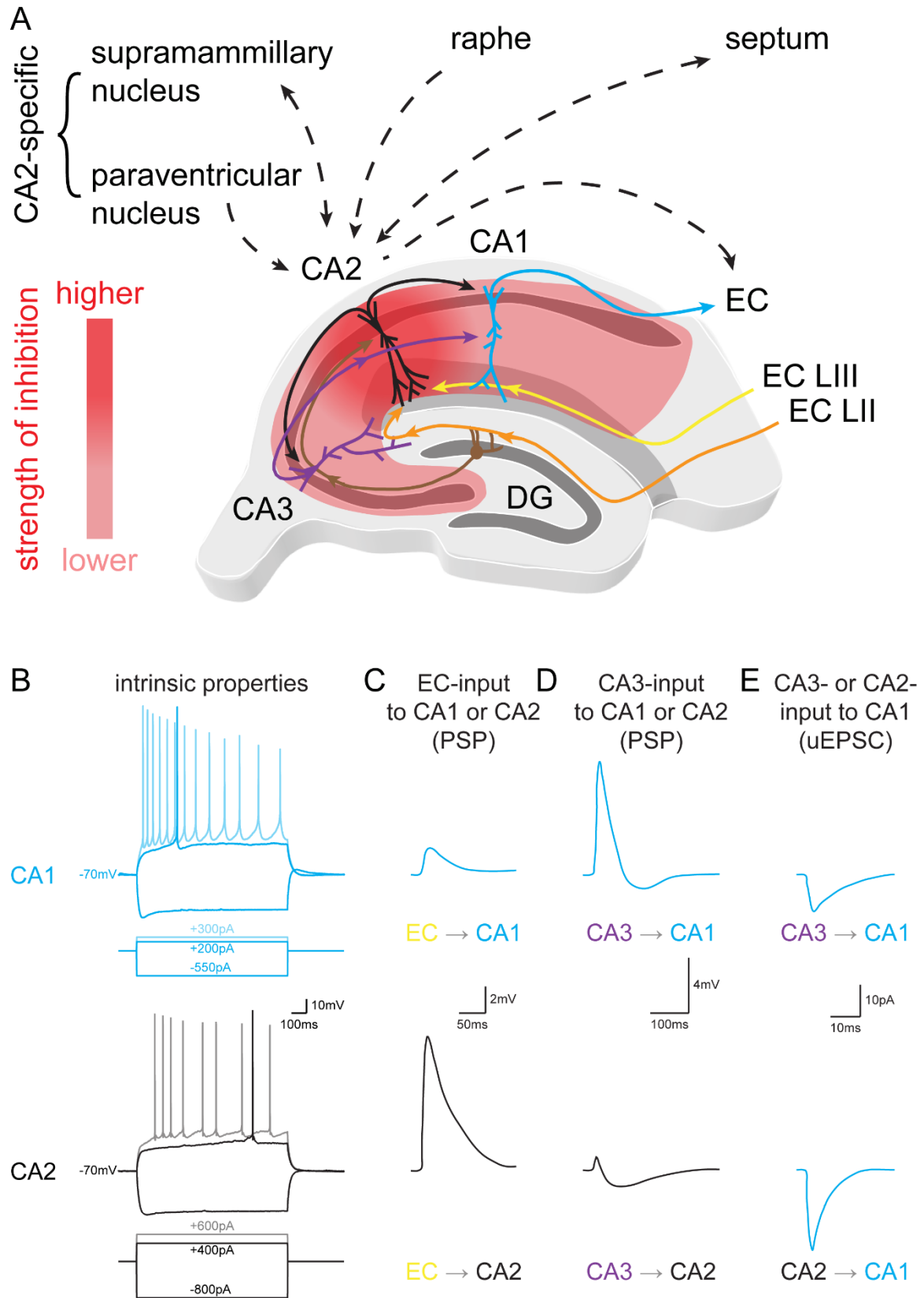


**Figure I.2.3. Integrated view of area CA2 in the intra- and extra-hippocampal circuits.**

**A.** Diagram illustrating the input and output connections of area CA2 and the distribution of interneurons in hippocampal CA areas. **B.** Sample traces illustrating differences between CA1 and CA2 pyramidal

neurons in intrinsic excitability. **C.** Example traces of post-synaptic potentials recorded from CA1 and CA2 pyramidal neurons in response to EC input stimulation. **D.** Examples traces of post-synaptic potentials recorded from CA1 and CA2 pyramidal neurons in response to CA3 input stimulation. **E.** Examples traces of unitary excitatory post-synaptic responses recorded from CA1 pyramidal neurons in response to CA3 or CA2 pre-synaptic cell stimulation.

Illustrations in **C**, **D** and **E** are inspired by (Chevalleyre and Siegelbaum, 2010).

### **I.3 - Physiological features of hippocampal-dependent memory formation**

While being conceptually useful, the information transfer theory derived from neuronal connectivity within hippocampal networks provides only a “static” view of the system that does not reflect its operational states. To alleviate this limitation, this section details physiological activity patterns in the hippocampus and related functions with highlights on the contributions of area CA2.

#### **I.3.a - Network activity patterns underlying learning and memory**

##### **I.3.a.i - Theta and gamma oscillations**

PNs of the hippocampus are organized laminarily with their somas aligned and their dendrites parallel, thus forming electrical dipoles. In such a network, synchronous changes in membrane potential from populations of neurons generate an electrical field potential that can be recorded extra-cellularly either locally (local field potential, LFP) or superficially (electroencephalogram, EEG). This allows the examination of activity in neuronal networks *in vivo* and led to the discovery of several patterns occurring during different brain states : theta, beta, gamma, sharp waves / ripples (SWR), large and small irregular amplitude (LIA and SIA) (Vanderwolf, 1969). Theta and gamma rhythms are present during active wake and REM sleep while SWR occur during quiet wake and slow wave sleep (SWS) when LIA is predominant (Buzsáki, 2015).

Theta waves correspond to rhythmic oscillations ranging from 6 to 12 Hz (in rodents) encountered in the hippocampus and several related brain structures, either as proper field potential oscillations or as rhythmic AP discharges in this frequency band. These include a number cortical areas, the amygdala, septum, hypothalamus, thalamus, VTA and raphe (Buzsáki, 2002; Vertes and Kocsis, 1997). In the hippocampus, theta oscillations are prominent in all layers and subregions although their amplitude is largest in CA1 (Buzsáki, 2002). Of note, hippocampal networks are current generators of theta oscillations but not their sole pacemaker,

as isolation of the hippocampus from the septum abolishes the hippocampal theta (Vertes and Kocsis, 1997). Indeed, rhythmic activity in the theta range exists in brain structures afferent to the hippocampus : namely the septum, EC and SuM (Alonso and García-Austt, 1987a; 1987b; Kocsis and Vertes, 1994; Stewart and Fox, 1990). EC inputs impinging on distal dendrites bring about rhythmic excitation generating current sinks in SLM (Buzsáki, 2002). In addition, the septum is critical for hippocampal theta waves as it provides both permissive cholinergic and pacemaking GABAergic inputs (Buzsáki, 2002; Pan and McNaughton, 2004; Vertes and Kocsis, 1997). Remarkably, hippocampal neurons possess a repertoire of conductances allowing intrinsic resonance in the theta and gamma frequency range (Wang, 2010). Therefore, although septal cholinergic afferents to the hippocampus are diffuse and do not contribute to the post-synaptic potentials underlying theta, acetylcholine released by these fibers causes modifications in these conductances leading to a global depolarization of hippocampal neurons (Madison et al., 1987). This effect of elevated cholinergic tone setting hippocampal networks in a theta prone state led to the definition of an atropine-sensitive theta, named after the cholinergic antagonist atropine that abolishes it as opposed to an atropine-resistant theta (Kramis et al., 1975). Further contribution of the septum to hippocampal theta is brought about by rhythmic inhibition of local INs by hippocampus-projecting GABAergic septal INs (Freund and Antal, 1988; Hangya et al., 2009; Tóth et al., 1997). Peri-somatic targeting hippocampal INs entrained by periodic septal inhibition in turn trigger rhythmic inhibitory post-synaptic potentials in PNs, thus generating a current source in SP (Buzsáki, 2002). Finally, rhythmic activation of the intra-hippocampal CA3 – CA1 SC contribute to another current sink in CA1 SR (Buzsáki, 2002). Altogether, specific sets of conductances and rhythmic excitatory and inhibitory synaptic inputs on different dendritic compartments trigger oscillations of the membrane potential of hippocampal neurons at theta frequencies. This sets windows of excitability that differ depending on the neuronal population, thus leading to action potential firing by PNs and INs at specific preferential phases of the theta cycle (Fox et al., 1986; Klausberger et al., 2003; 2005). Indeed, average firing rates of PNs are highest around the negative peak of the CA1 SP theta and are preceded by INs from the pyramidal layer whose maximal discharges occurs 60° earlier (Csicsvari et al., 1999). It should be noted that these are only indicative values as preferred theta phases vary across cell types and depends on behavior (as discussed later in Section I.3.b.i - ). Still, PNs of areas CA3, CA2 and CA1 of the hippocampus seem to form a relatively homogeneous population with regards to theta oscillations : recent *in vivo* studies that examined PN properties in different CA regions reported either no differences (Kay et al., 2016; Mankin et al., 2015), or slightly stronger theta

modulation and earlier preferred theta phase of CA3 PNs compared to CA2 and CA1 PNs (Oliva et al., 2016a).

Besides the septum and EC, the SuM is of particular interest for the generation and control of theta oscillations in the hippocampus by extra-hippocampal sources. It has been described as the first nucleus where neurons display phasic rather than tonic firing in the so-called “ascending theta synchronizing path” that also comprises the reticular nucleus pontis oralis (RPO), posterior hypothalamus (PH), septum and hippocampus (Kirk, 1998). Indeed, neurons in the SuM fire in bursts at theta frequency coherent with hippocampal theta in anaesthetized rats (Kirk et al., 1996; Kocsis and Vertes, 1994). The SuM is in close relation with both the hippocampus by direct projections and the septum through reciprocal connections (Borhegyi and Freund, 1998; Leranth and Kiss, 1996; Vertes, 1992; Vertes and McKenna, 2000). Of note, theta activity in the SuM is not solely relayed by its interactions with the septum as it remains upon inactivation of the septum (Kirk, 1997; Kirk et al., 1996). Under anesthesia, the SuM influence over hippocampal theta is massive as evidenced by a reduction in frequency and amplitude of theta oscillations in the hippocampus upon disruption of SuM activity by pharmacological agents or lesions (Kirk and McNaughton, 1993; McNaughton et al., 1995; Thinschmidt et al., 1995). Although less pronounced, this effect remains in freely behaving animals (McNaughton et al., 1995; Pan and McNaughton, 1997; 2002). Altogether, these findings point out the SuM as a critical actor in the regulation of hippocampal theta oscillations, either through its direct projections to the hippocampus or via the septum.

Often concurring with theta, gamma waves are higher-frequency oscillations (30-100 Hz) also occurring throughout hippocampal layers and subregions, as well as in other brain areas including the cortex (Buzsáki and Wang, 2012; Colgin, 2016). Detailed analysis of gamma oscillations reveal that they can be subdivided based on their frequency, origin, amplitude-phase coupling relation to theta, and laminar organization (Belluscio et al., 2012; Bragin et al., 1995; Colgin et al., 2009; Schomburg et al., 2014). First, fast-gamma (also referred to as epsilon) spans frequencies from 90 to 150 Hz, is largest at the theta trough, and is confined to CA1 SP (Belluscio et al., 2012). Next, mid-gamma occupies the 50 to 90 Hz band of frequencies, shows maximal amplitude at the peak of theta, and is localized in SLM and DG consistent with its entorhinal origin (Belluscio et al., 2012; Bragin et al., 1995; Chrobak and Buzsáki, 1998; Colgin et al., 2009; Csicsvari et al., 2003; Schomburg et al., 2014). Finally, slow-gamma ranges from 30 to 50 Hz, is highest during the descending phase of theta, originates in area CA3 and therefore predominates in CA1 SR (Belluscio et al., 2012; Bragin et

al., 1995; Chrobak and Buzsáki, 1998; Colgin et al., 2009; Csicsvari et al., 2003; Schomburg et al., 2014).

Much like theta oscillations, cellular and circuit mechanisms underlying gamma oscillations have been examined using various approaches. Modelling studies based on physiological data indicate that gamma oscillations can emerge in neuronal networks consisting either of interneurons only engaged in mutual inhibition and driven by a common excitatory source (I-I or ING model), or of pyramidal cells and interneurons through recurrent excitation and feedback inhibition (E-I or PING model) (Buzsáki and Wang, 2012; Wang, 2010). In support of the latter, *in vivo* examination of action potential firing relative to the gamma cycle revealed that PNs discharge before INs in the recurrent CA3 network, but also drive CA1 INs consistent with feedback and feedforward inhibitory circuits respectively (Csicsvari et al., 2003). Given the intrinsic nature of slow gamma in hippocampal networks, several studies took advantage of the possibility to induce gamma oscillations in acute slices to further elucidate the mechanism involved. Indeed, elevation of the cholinergic tone by bath application of carbachol (CCh) induces gamma oscillations *ex vivo* that resemble the slow-gamma seen *in vivo* (Fisahn et al., 1998; Mann et al., 2005). These approaches notably allowed to validate the central role of fast-spiking PV-expressing basket cells in gamma oscillations, as they generate an active current source in SP through rhythmic perisomatic inhibition (Gulyás et al., 2010; Mann et al., 2005). In addition, they confirmed that intra-hippocampal gamma oscillations build up through recurrent excitation and feedback inhibition in area CA3 and are subsequently transferred to area CA1 by feedforward inhibition (Mann et al., 2005; Oren et al., 2006; Zemankovics et al., 2013).

Area CA2 has yet to be incorporated in this scheme although its intra- and extra-hippocampal connections indicate that it is involved in gamma oscillations. Indeed, area CA2 displays recurrent excitation (Cui et al., 2013; Hitti and Siegelbaum, 2014) and feedback inhibition (Mercer et al., 2012a; 2012b) much like CA3 and is therefore endowed with the necessary features for generating gamma oscillations. Furthermore, its strong excitatory drive from EC (Chevalleyre and Siegelbaum, 2010), reciprocal inhibitory influences with CA3 (Boehringer et al., 2017), and potent excitatory output onto CA1 (Chevalleyre and Siegelbaum, 2010; Kohara et al., 2013), places area CA2 in an ideal position to participate in mid-, slow-, and fast-gamma respectively. In addition, one can predict a role for area CA2 in theta phase coupling of gamma amplitude as it receives theta-locked inputs from the SuM (Kirk et al., 1996; Kocsis and Vertes, 1994). Finally, *in vivo* and *ex vivo* work describe the initiation site of slow-gamma waves in

area CA3a, i.e. in the vicinity of CA2 which may have been overlooked in these studies (Csicsvari et al., 2003; Mann et al., 2005).

### **I.3.a.ii - Sharp wave / ripples**

In contrast with prolonged theta oscillations that dominate the hippocampal EEG during active wake and REM sleep, brief and fast oscillatory events called sharp wave / ripples (SWRs) emerge in states of quiet wakefulness and SWS (Buzsáki, 2015). SWRs consist of a short (~100 ms) dendritic negative deflection of the local field potential (LFP) in CA1 SR (the sharp wave) superimposed with a fast (140–200 Hz) oscillation in the pyramidal layer (the ripple) (Buzsáki, 2015). Contrary to theta and mid-gamma that are brought about in hippocampal networks by extrinsic inputs, SWRs are intrinsically generated as they remain after lesion of afferent structures to the hippocampus (Suzuki and Smith, 1988). Indeed, SWRs originate in areas CA3 and CA2 whose recurrent excitatory connections allow a buildup of excitation culminating in burst firing of PNs (Buzsáki, 1986; Csicsvari et al., 1999b; Mizuseki et al., 2012; Oliva et al., 2016; Schlingloff et al., 2014). Initiation of SWRs might involve a post-inhibitory rebound of PN excitation as a trigger and additional disinhibition by silencing CCK-expressing INs through cannabinoids released by CA3 PNs as they start firing APs (Hájos et al., 2013; Lasztóczy et al., 2011; Papatheodoropoulos, 2010). CA3 PNs then synchronously excite CA1 cells through the SC thus generating a large sink in CA1 SR, the sharp wave (Buzsáki, 1986; Csicsvari et al., 1999b). In response to CA3 strong excitatory inputs, CA1 PNs rhythmically fire APs seen as the repeated negative peaks in CA1 SP signing the ripple (Schlingloff et al., 2014; Schomburg et al., 2012). In addition, phasic excitation from CA3 PNs recruits PV-expressing BCs that in turn provide perisomatic inhibition to CA1 (Csicsvari et al., 1999a; Hájos et al., 2013). Both feedforward from CA3 and feedback inhibition from CA1 produce synchronized IPSPs in CA1 SP that contribute to the upward peaks on the ripple (Csicsvari et al., 1999a; Schomburg et al., 2012). Although triggered by a build-up of excitation in the CA3 recurrent network, SWRs require adequate GABAergic transmission that paces action potential firing during this fast oscillation (Schlingloff et al., 2014; Stark et al., 2014). This phasic inhibition is likely provided by PV-expressing BCs as they fire APs at ripple frequencies phase-locked to the oscillation through mutual inhibition (Csicsvari et al., 1999a; Hájos et al., 2013; Klausberger et al., 2003; Schlingloff et al., 2014; Stark et al., 2014). Finally, SWRs are likely terminated by hyperpolarization of PNs through activation of GABA<sub>B</sub> receptors following high interneuronal activity (English et al., 2014). When considered at the scale of hippocampal circuits, SWRs have been shown to travel from CA3a / CA2 towards CA3c and then reach CA1 where

superficial PNs are more entrained than deep PNs (Csicsvari et al., 2000; Oliva et al., 2016a; Stark et al., 2014; Valero et al., 2015). Discharging CA1 PNs subsequently transfer information outside the hippocampus to cortical areas (Buzsáki, 2015).

While PNs typically increase their action potential firing during SWRs, there are intriguing findings from in vivo studies that describe non-stereotypic firing patterns of CA2 pyramidal neurons during SWRs, indicating that this region is contributing to hippocampal network dynamics in an unusual way. Kay et al. performed in vivo recordings of SWRs and hippocampal unit activity in all CA regions in rats during sleep, rest and while performing a spatial memory task (Kay et al., 2016). They reported two populations of putative pyramidal cells in area CA2 that had opposite modulations of their firing rates during SWRs. CA2 P-units (“positively modulated”) showed increased firing rates during SWRs, much like cells in other hippocampal subfields. Conversely, CA2 N-units (“non-positively modulated”) fired less APs during SWRs. Unlike CA2-P, CA3 and CA1 units that classically showed increased activity during locomotion and SWRs, CA2 N-units displayed increased firing rates during non-SWR immobility (Kay et al., 2016). This unusual firing behavior in area CA2 was supported by experiments using high density silicon probes inserted parallel to the transverse axis of the hippocampus that simultaneously recorded potentials in every layer of each CA region during awake immobility and non-REM sleep (Oliva et al., 2016a). In this study, the authors show that a population of pyramidal neurons in CA2 ramp up their activity prior to SWR initiation after which they become silent, while another population fires more APs during SWRs (Oliva et al., 2016a). Furthermore, Valero et al. used sharp electrodes to record CA2 pyramidal firing in vivo and reported a reduction in firing during SWRs (Valero et al., 2015). Lastly, in vivo whole-cell recordings in area CA2 showed that the membrane potential of PNs undergoes a hyperpolarization during SWR (Matsumoto et al., 2016). Interestingly, pyramidal neurons in area CA2 have also been proposed to participate in the generation of SWR, as deep cells ramp up their activity prior to SWR initiation and superficial cells fire earliest during SWR events compared to CA3 and CA1 (Oliva et al., 2016a). Moreover, SWRs could also be generated in area CA2 and directly transferred to CA1 (Oliva et al., 2016a).

### **I.3.b - Mnemonic functions of the hippocampus and hypothalamus**

#### **I.3.b.i - Spatial coding and memory**

A major aspect of episodic memory supported by the hippocampus is the formation and storage of internal representations of the environment. This spatial coding is achieved by place cells,

i.e. pyramidal neurons that increase their action potential firing when the animal visits a discrete location called place field (Christian and Deadwyler, 1986; O'Keefe, 1976; O'Keefe and Dostrovsky, 1971). Location-specific activity of place cells is likely to be the result of the processing by hippocampal networks of directional, metric and multimodal sensory information provided to the hippocampus by upstream structures. Indeed, EC hosts grid cells that fire action potentials repeatedly at discrete location of an animal's displacement through the environment, thus providing a metric of distance travelled (Hafting et al., 2005). In addition, head direction cells that discharge action potentials preferentially when the animal's head faces certain angles were found in areas related to the hippocampus (Taube et al., 1990). Remarkably, place cells are highly specific of a particular location, such that each place displays usually only one fairly small place field in a given environment (Muller et al., 1987; O'Keefe, 1976). In addition, changing environments causes modifications of place cell features : place fields can change location, disappear or appear from new place cells (Bostock et al., 1991; Muller and Kubie, 1987). Indeed, only a small fraction of hippocampal PNs are actively recruited as place cell in a particular environment (Thompson and Best, 1989). It follows that different combinations of place cells can provide specific internal representations of different environments (Wilson and McNaughton, 1993). This leads to the question of how a particular set of PNs is selected to represent a given environment. Contrary to sensory systems, there is no known topological organization of place cells in the hippocampus, as nearby PNs do not tend to code for locations close in space (Redish et al., 2001). Instead, spatial representations are first learned and then kept in memory : place cells emerge as an animal begins to explore an environment and subsequently form a stable representation of the environment (Frank et al., 2004; Lever et al., 2002; Wilson and McNaughton, 1993). Another mnemonic property of hippocampal spatial coding is evidenced by the remapping of spatial representations upon environmental variations to different degrees (Bostock et al., 1991; Leutgeb et al., 2005; Muller and Kubie, 1987). Interestingly, two types of remapping reminiscent of pattern separation and completion have been described : global remapping in which place fields change locations and rate remapping when place fields remain at their location but the corresponding place cells vary their action potential firing (Leutgeb et al., 2005).

Of note, both theta oscillation and SWR play important roles in spatial coding. As an animal crosses a place field, the action potential firing of the corresponding place cell gradually shifts its preferred theta phase from late to early in the cycle, a phenomenon called phase precession (O'Keefe and Recce, 1993). As place fields are successively visited, the AP discharge of

corresponding place cells is distributed at different phases of theta cycles (Skaggs et al., 1996). Therefore, place cells fire in an organized manner reflecting the animal's path during theta epochs, thus forming theta sequences. Strikingly, sleep enhances the correlation of place cells with nearby place fields (Skaggs and McNaughton, 1996; Wilson and McNaughton, 1994). This observation suggests that a plasticity process occurs during sleep and stabilizes the information encoded in theta sequences during wake. SWRs are an ideal candidate as their disruption during sleep impairs memory consolidation (Girardeau et al., 2009). Furthermore, theta sequences re-emerge during SWRs as compressed replays (Lee and Wilson, 2002). Altogether, these findings critically link theta oscillations and SWR to spatial coding, learning and memory. However, the precise role of the different hippocampal subregions, especially that of area CA2, in these functions is not fully understood.

Place cells have been discovered and extensively studied in areas CA1 and CA3 but only recently characterized in area CA2. Surprisingly, several studies have reported striking differences in spatial coding in area CA2 as compared to CA1 and CA3. Place cells in area CA2 are more abundant, display larger and more numerous place fields per place cell and fire more action potentials on average without increased peak "in-field" firing leading to a lower spatial information content than in area CA1 and CA3, as evidenced by *in vivo* recordings in behaving rats (Alexander et al., 2016; Lee et al., 2015; Lu et al., 2015; Mankin et al., 2015; Oliva et al., 2016b). Other differences include lower theta phase precession (Fernández-Ruiz et al., 2017; Mankin et al., 2015; Oliva et al., 2016b). Together with this low-precision spatial coding, space representation in area CA2 is less specific than in neighboring areas: CA2 place cells fail to remap on changing of enclosure (Lu et al., 2015; Mankin et al., 2015), or on displacement of local or global cues (Lee et al., 2015).

These observations raise the question of what role, if any, area CA2 plays in spatial coding in the hippocampal network. By recording place cell activity in every hippocampal CA subfield as rats successively explored different familiar environments during sessions spanning up to 2 days, Mankin et al. were able to examine CA2 place cell remapping (Mankin et al., 2015). Strikingly, they showed that patterns of activity in area CA2 varied as the same environment was presented repeatedly for several hours. Contextual changes, however, were found to induce little differences in CA2 remapping. Thus, the authors hypothesized that remapping in area CA2 provides an internal representation of elapsed time, due to a combination of rate remapping and place field gain/loss or drift (Mankin et al., 2015). Similar observations were made in different experimental approaches in two studies (Lee et al., 2015; Lu et al., 2015). Using simultaneous

recordings along the CA3 to CA1 axis, Lu et al. compared remapping upon exposure to rooms with different wall colors or to different rooms. They reported lower global and rate remapping induced by context in area CA2 than CA3 and preferential remapping in area CA2 with times increasing from 10 min to up to 31 h (Lu et al., 2015). Lee et al. examined the coherence of place cell activity in CA2 and different CA3 subfields as rats were exposed to an environment where local and global cues were rotated between sessions. This paradigm enabled them to show that place cells in area CA2 were more prone to follow local cues and rotate rather than to remap. Further, they characterized CA2 place cell ensembles as less stable than CA3 in coding the same environment as time passed across 4 days (Lee et al., 2015). In summary, these studies report that area CA2 shows low discrimination between different familiar environments (Mankin et al., 2015), undergoes poor partial and global remapping when challenged with varying environments (Lu et al., 2015) and that area CA2 displays more pattern completion dictated by local cues than remapping (Lee et al., 2015).

Alexander et al. challenged rats with familiar or novel social or object stimulations presented in subsequent sessions of exploration of a familiar arena. Recordings of CA1 and CA2 place cells in this paradigm revealed remapping in area CA2 induced by novel or familiar social exposure and by novel but not familiar object presentation, suggesting that spatial representations in this region can be specific depending on which cues are presented (Alexander et al., 2016).

Interestingly, using immediate–early gene expression to label active cells, Wintzer et al. showed that different cell ensembles are activated in area CA2 upon exposure to a familiar versus novel environment, similar to other CA regions. However, when only small contextual changes were introduced, only area CA2 displayed different active cell ensembles, hence functioning as a conflict detector within tens of minutes of exposure (Wintzer et al., 2014). On a similar time scale, spatial representation of a familiar environment is disrupted in area CA2 by interleaved exposure to a known but different context, although discrimination between contexts is itself low (Mankin et al., 2015).

The apparent discrepancy between both studies can be reconciled, as the introduction of a subtle change to a familiar environment (Wintzer et al., 2014) and exposure to a different but familiar environment (Mankin et al., 2015) are essentially discrete but salient variations of external surroundings conflicting with internal representations detected by area CA2 that then remaps within tens of minutes. Overall, from these experiments, spatial coding in area CA2 seems broad and unspecific, potentially allowing binding of temporal elements with space but can be

sharpened by social, novel or conflicting stimulations. Whether these seemingly unrelated functions are really different aspects of a specific type of episodic memory remains unclear. Given that blocking area CA2 synaptic output only disrupts social memory, future work will clarify the relationship of these spatial functions by encoding social aspects of episodic memory.

All the above experiments examine the role of area CA2 in spatial encoding during the traditional paradigm of place cell activity, that is, when the animal is actively moving through a receptive field. However, when animals are stationary, spatial information is still maintained in the absence of place cell firing. A recent breakthrough concerning the hippocampal mechanisms allowing this spatial encoding during immobility has shown that cells in area CA2 play a central and unexpected role (Kay et al., 2016).

Surprisingly, area CA2 N-units fire more action potentials during non-SWR epochs of immobility and were found to code for spatial location during immobility and sleep (Kay et al., 2016). These cells fired in a very location-specific manner that inversely correlated with locomotion. This was accompanied by a hippocampal-wide pattern of activity distinct from SWR called N-wave (Kay et al., 2016). Thus, area CA2 hosts a peculiar subpopulation of pyramidal neurons that entrain the hippocampal network allowing spatial coding during immobility and sleep, which potentially allows subsets of cells in CA1 to code for nesting position (Jarosiewicz et al., 2002).

Hence, in accordance with its unique and extensive intra- and extra-hippocampal connectivity, area CA2 appears to be critically involved in triggering hippocampal wide patterns of activity relevant for spatial coding during immobility and sleep (N-wave) as well as memory consolidation (SWR). This raises the issue of understanding how a region displaying poor spatial coding during exploration could then orchestrate hippocampal events tied to spatial memory during rest.

Information on this matter has been gained by manipulating area CA2 activity by using tetanus toxin light-chain expression to block CA2 pyramidal neuron output chronically in mice (Boehringer et al. 2017). It was this study that revealed a loss of feedforward inhibition from CA2 to CA3 that leads to hyperexcitability in area CA3 (Boehringer et al., 2017). This transformed normal CA1 and CA3 place field firing into spatially-triggered network hyperexcitability events with increased theta power preceded by a ramping up of CA1 and CA3 pyramidal neuron firing. In addition, in mice with synaptic transmission blocked in CA2 pyramidal neurons, SWRs were partially replaced by epileptiform-like discharges.

Interestingly, these mice showed impairments of contextual habituation. When acutely inhibiting CA2 pyramidal neurons with inhibitory DREADDs, Boehringer et al. observed an abnormal remapping of CA1 and CA3 pyramidal neurons that tended to cluster their firing into hotspots. Altogether, these results indicate a critical role of CA2-mediated inhibition of CA3 that potentially parses hippocampal network excitability and allows for physiological levels of enhanced excitability inside a place field. Hence, although area CA2 is not encoding spatial information during exploration, this region is involved in shaping place field activity in CA1 and CA3.

What makes area CA2 special in regards to spatial coding ? Besides its unique PN properties, interneuronal composition, and relations to other hippocampal subregions, area CA2 is directly influenced by the SuM which is involved in spatial learning and memory. Given the importance of theta oscillations in this process, it is only natural to suggest a mnemonic role for SuM as it controls the hippocampal theta. Indeed, several studies have reported a joint effect on theta and memory after interfering with SuM activity (Pan and McNaughton, 2004). Silencing of SuM with a GABAergic agonist leads to a decreased hippocampal theta together with delayed spatial learning (Pan and McNaughton, 1997). Impairments of spatial memory (Aranda et al., 2008; Shahidi et al., 2004), working memory (Aranda et al., 2006; Shahidi et al., 2004), and contextual fear memory (Pan and McNaughton, 2002) have also been described upon SuM lesion or pharmacological block of action potential firing in SuM neurons. In addition, disruption of serotonergic neuromodulation in SuM causes deficits in spatial learning accompanied by alterations of hippocampal theta (Gutiérrez-Guzmán et al., 2012; Hernández-Pérez et al., 2015). Therefore, regardless of some discrepancies between studies likely due to variable approaches (eg Pan and McNaughton, 1997; vs 2002), the SuM is clearly involved in spatial learning and memory although the underlying mechanisms are yet to be determined.

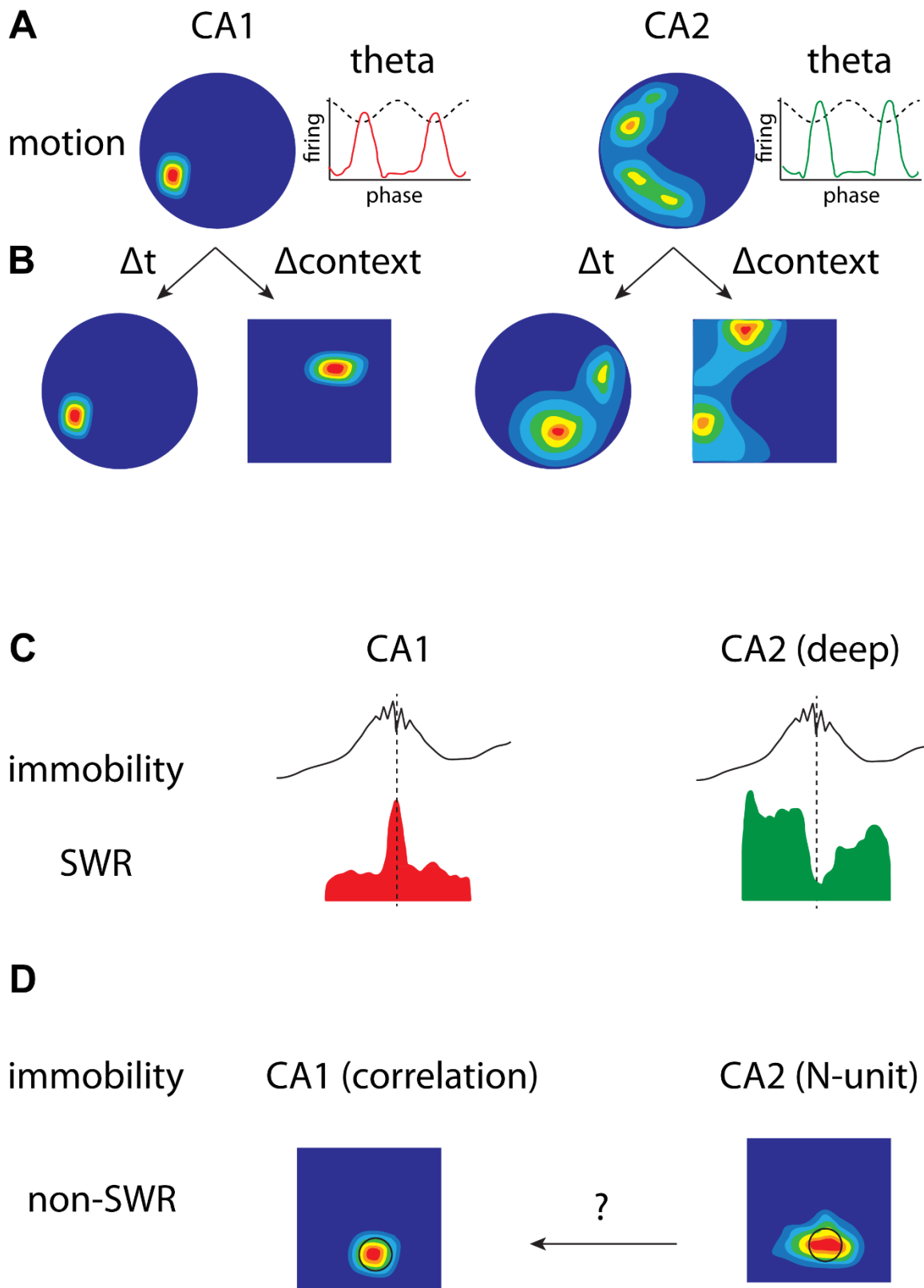


**Figure I.3.1. Activity of area CA2 from in vivo experiments.**

**A**, Place fields and theta phase preference plots of CA1 (left) and CA2 (right) place cells during exploration. Warm colors in heat maps indicate high firing rates. Phase preference plots are relative to theta recorded in CA1 SP. **B**, Place fields showing remapping of place cells with time or context

modification in CA1 (left) and CA2 (right). Warm colors in heat maps indicate high firing rates. **C**, Peri-SWR firing histograms of CA1 (left) and CA2 (right) cells during immobility. Histograms are aligned to the trough of the sharp wave recorded in CA1 indicated by a dashed line. **D**, Population activity correlation map of CA1 place cells between exploration and non-SWR sleep (left) and place field of CA2 place cell during non-SWR sleep (right). Warm colors in heat maps indicate high firing rates. Black circles indicate nesting position.

Illustrations are adapted from: CA1 & CA2 place fields during exploration and remapping with time / context (Mankin et al. 2015); CA1 & CA2 units theta phase preference of firing (Oliva et al. 2016a); CA1 & CA2 units peri-SWR firing histograms (Oliva et al. 2016b); CA2 N-unit place field during non-SWR sleep (SIA) (Kay et al. 2016); CA1 place cells population activity correlation map of exploration vs SIA (Jarosiewicz et al. 2002).

### **I.3.b.ii - Emotional, novel and social aspects of memory**

The hippocampus is well known for its role in the formation of episodic memory, a person's unique memory of specific events that encloses the questions "who?", "what?", "where?" and "when?" (Squire et al., 2007). The spatial aspect of this memory has been well studied, in particular with the discovery of place cells (O'Keefe and Dostrovsky, 1971a). The other aspects of episodic memory have been much less studied.

There is compelling evidence that area CA2 plays a central role in social aspects of memory formation. Wersinger et al. first presented evidence for this role of area CA2 in this form of memory. Using repetitive exposure of a male mouse to a female mouse (10-min exposures every 5 min, repeated ten times), they showed that wild-type males are able to discriminate between novel and familiar stimulus mice more quickly than mice lacking the vasopressin V1b receptor (Wersinger et al., 2002). They also showed using a more challenging paradigm (30-min interval between trials) that V1b receptor KO mice did not appear to have reduced interaction with a familiar female mouse. A few years later, the V1b receptor was shown to be expressed only in discreet regions of the brain, with a very high expression in area CA2 (Young et al., 2006). These data suggest that vasopressin release in area CA2 acting on V1b receptors plays a role in social recognition memory.

The importance of CA2 in social memory was further confirmed by two lesion studies. The first study used transgenic mice (Amigo2-cre) to express the tetanus toxin specifically in CA2 pyramidal neurons in order to prevent transmission between these cells and their targets (Hitti and Siegelbaum, 2014a). The second study performed an excitotoxic lesion of dorsal CA2 by injecting NMDA in area CA2 in rats (Stevenson and Caldwell, 2014). Both studies reported a

strong impairment in social memory formation, gauged by the lack of decrease in interaction time between the experimental subject and a familiar conspecific. Thus, both studies concluded that area CA2 is necessary for the formation of social recognition memory. In agreement with this idea, optogenetic activation of vasopressinergic fibers in area CA2 has been shown to strongly increase the duration of social memory in mice (Smith et al., 2016). Altogether, these data show that area CA2 is necessary for social memory formation and that modulation of activity in CA2 with PVN-mediated vasopressin release results in an increase in social memory duration.

While the PVN vasopressinergic innervation of area CA2 seems critical for its social functions, little is known about the role of the SuM to CA2 connection. However, area CA2 is involved in conflict detection (Wintzer et al., 2014) and the SuM has been shown to be highly activated during novelty (Ito et al., 2009). Therefore, SuM inputs to area CA2 might participate to the detection of salient novel information. In line with this hypothesis, the SuM is involved reward-related tasks (Ikemoto, 2005; Ikemoto et al., 2004), thus potentially conveying emotional signals to area CA2. Although direct evidence is missing, the variations of CA2 activity seen upon exposure to novel objects or animal (Alexander et al., 2016a) might be brought about by the inputs it receives from the SuM.

#### **I.4 - Goals of the thesis**

In this section, we have presented the anatomy, connectivity, physiology and functions of the hippocampus, a cerebral structure critically involved in learning and memory. The description of the specificities of each hippocampal region has highlighted their particular roles in information processing. Even so, this introduction also revealed that several aspects of hippocampal circuitry and physiology are still not well understood. In particular, the contributions of area CA2 to hippocampal network activity remain underexplored. As suggested by its role in social memory, spatial coding and SWR generation, area CA2 is clearly involved in important hippocampal functions. In addition, hippocampal rhythms are influenced by extra-hippocampal inputs amongst which the SuM directly connects area CA2. Therefore, understanding the patterns of activity underlying hippocampal-dependent learning and memory requires area CA2 to be taken into consideration.

Because the SuM participates to the control of hippocampal theta oscillations and projects directly to area CA2, the main goal of this thesis was to characterize the functional aspects of this connection. First, given theta states are associated with oscillatory activity of hippocampal

neurons receiving cholinergic inputs from the septum, we wished to determine the properties of cellular and network activity in area CA2 under conditions of elevated cholinergic tone. This question was addressed in a first study using carbachol application to induce gamma-like oscillations in acute hippocampal slices from mice. Then, we aimed to decipher the local circuit engaged by the long-range SuM input in area CA2 and its influence over CA2 pyramidal neurons activity. We focused on this point in a second study using optogenetics to stimulate SuM afferent fibers to area CA2 and probe the consequences of their activation *ex vivo*. Finally, we asked what consequences SuM inputs had on area CA2 during carbachol-induced network activity and what the resulting output of area CA2 onto area CA1 was. These investigations were carried out in collaboration with *in vivo* approaches from the McHugh laboratory complementing our third study performed with optogenetics on acute hippocampal slices.

## II - Material and methods

### II.1 - Animals

All procedures involving animals were performed in accordance with institutional regulations. Animal sample sizes were estimated using power tests with standard deviations and ANOVA values from pilot experiments. A 15 % failure rate was assumed to account for stereotaxic injection errors and slice preparation complications. No alterations of neurotransmission were observed in the transgenic lines used in this study.

#### Use of the Tg(Slc17ab-icre)10Ki mouse line (VGluT2-Cre)

we used the Tg(Slc17ab-icre)10Ki mouse line that was previously generated (Borgius et al., 2010) to express the Cre recombinase under the control *slc17a6* gene coding for the vesicular glutamate transporter isoform 2 (VGluT2).

#### Use of the Pvalbtm1(cre)Arbr/J mouse line (PV-Cre)

we used the Pvalbtm1(cre)Arbr/J mouse line that was previously generated (Hippenmeyer et al., 2005) to express the Cre recombinase under the control *Pvalbm* gene coding for parvalbumin (PV).

#### Use of the Cacng5-Cre mouse line

we used the Cacng5-Cre mouse line that was previously generated (Boehringer et al., 2017) to express the Cre recombinase under the control *cacng5* gene coding for the voltage-dependent calcium channel gamma subunit 5 specifically expressed in CA2 PNs.

#### Generation of the *csf2rb2-Cre* mouse line by the McHugh laboratory

The bacterial artificial chromosome (BAC) RP23-233L7 (BACPAC Resources Center) containing *Mus musculus* colony stimulating factor 2 receptor, beta 2, low-affinity (granulocyte-macrophage) (*csf2rb2*) was modified using the Quick & Easy BAC Modification Kit (Gene Bridges GmbH) to insert a Cre-FRT-Amp-FRT cassette at the start site of *csf2rb2*

translation. The ampicillin (Amp) marker was deleted utilizing Flp-706 recombination and the Cre-modified BAC's were confirmed by PCR analysis. The confirmed Cre-modified RP23-233L7 BAC was subsequently purified using the QIAGEN Large Construct Kit (QIAGEN). To prepare the modified BAC for microinjection, 50 µg of Cre-modified RP23-233L7 BAC was linearized using AscI (New England Biolabs (NEB)) and then buffer exchanged using the Sepharose CL-4B matrix (Pharmacia/Pfizer) into an injection buffer composed of 10 mM Tris-HCl, pH 7.4, 0.1 mM EDTA, and 100 mM NaCl. The purified BAC was injected into C57BL/6 fertilized pronuclei and fertilized blastocysts were implanted into pseudopregnant females. From the microinjections, three *csf2rb2* B6 founders (lines 252, 267, 271) were generated. The 252 *csf2rb2-Cre* line was determined to express Cre selectively in the supramammillary region using immunohistochemistry with the anti-Cre antibody (AB24607, AbCam). The 252 line was maintained in a pure C57BL/6 background for all the experiments herein described.

## **II.2 - Stereotaxic viral injections**

### Surgical procedure

Animals were anaesthetized with ketamine (100 mg/kg) and xylazine (7 mg/kg). 500 nL of virus was injected into the brain of 4 week-old male wild type C57BL6, Tg(Slc17ab-icre)10Ki (VGluT2-Cre) mice, *csf2rb2-cre*, *Pvalbtm1(cre)Arbr/J* (PV-Cre) or *Cacng5-Cre* mice at 100 nL/min and the injection cannula was left at the injection site for 10 minutes following infusion. SuM was targeted by unilateral midline injections. Bilateral injections were performed in dorsal CA2.

### Viral titers

The adeno-associated viruses AAV9.EF1a.DIO.hChR2(H134R).EYFP and AAV9.hSynapsin.EGFP.WPRE.bGH were used at  $3 \times 10^8$  vg, the AAV.Synapsin.DIO.hM4D(Gi).mCherry was used at  $3.6 \times 10^9$  vg and the AAV2/9.hSyn.hChR2(H134R).EYFP.WPRE.hGH was used at  $3.7 \times 10^{13}$  vg. The retrograde tracer CAV2-cre virus was used at  $2.5 \times 10^{12}$  vg.

### Injections sites coordinates

The loci of the injection sites were as follows: anterior–posterior relative to bregma: -2.8 mm for SuM, -1.6 mm for CA2; medial-lateral relative to midline: 0 mm for SuM, 1.9 mm for CA2; dorsal-ventral relative to surface of the brain: 4.75 mm for SuM, 1.4 mm for CA2.

### **II.3 - Acute hippocampal slices preparation**

Transverse hippocampal slices were prepared at least 3 weeks after viral. In the case of mice injected with AAV.Synapsin.DIO.hM4D(Gi)-mcherry, slices were prepared 6 weeks after viral injection. Animals were deeply anaesthetized with ketamine (100 mg/kg) and xylazine (7 mg/kg), and perfused transcardially with a N-methyl-D-glucamin-based (NMDG) cutting solution containing the following (in mM): NMDG 93, KCl 2.5, NaH<sub>2</sub>PO<sub>4</sub> 1.25, NaHCO<sub>3</sub> 30, HEPES 20, glucose 25, thiourea 2, Na-ascorbate 5, Na-pyruvate 3, CaCl<sub>2</sub> 0.5, MgCl<sub>2</sub> 10. Brains were then rapidly removed, hippocampi were dissected out and placed upright into an agar mold and cut into 400 μm thick transverse slices (Leica VT1200S) in the same cutting solution at 4 °C. Slices were transferred to an immersed-type chamber and maintained in artificial cerebrospinal fluid (ACSF) containing the following (in mM) : NaCl 125, KCl 2.5, NaH<sub>2</sub>PO<sub>4</sub> 1.25, NaHCO<sub>3</sub> 26, glucose 10, Na-pyruvate 2, CaCl<sub>2</sub> 2, MgCl<sub>2</sub> 1. Slices were incubated at 32 °C for approximately 20 minutes then maintained at room temperature for at least 45 minutes prior to transfer to a recording chamber allowing dual perfusion of the slice with ACSF at 5 mL/min at 30 °C.

### **II.4 - Electrophysiological recordings**

Whole-cell or cell-attached patch-clamp of recordings of PNs or INs and local field potential (LFP) recordings were obtained from the CA2, CA1 and CA3 regions. Whole-cell patch-clamp recordings were performed with potassium- or cesium-based intracellular solutions containing the following (in mM): K- or Cs-methyl sulfonate 135, KCl 5, EGTA-KOH 0.1, HEPES 10, NaCl 2, MgATP 5, Na<sub>2</sub>GTP 0.4, Na<sub>2</sub>-phosphocreatine 10 and biocytin (4 mg/mL). Series resistance were < 20 MΩ and were not compensated in voltage-clamp, bridge balance was applied in current-clamp. An experimentally determined liquid junction potential of approximately 2 mV was not corrected for.

Cell-attached recordings were performed using patch pipettes (2-5 MΩ) filled with ACSF for monitoring bursts of APs. Alternatively, regular K<sup>+</sup>- or Cs<sup>+</sup>-based intracellular solution was used for cell-attached recordings when assessing AP firing in response to SuM photostimulation

because these experiments required subsequent whole-cell recordings. LFPs were obtained from area CA2, CA1 and CA3 *strata pyramidale* (SP) using patch pipettes (2-5 M $\Omega$ ) filled with 1 M NaCl.

Data were obtained using a Multiclamp 700B amplifier, sampled at 10 kHz and digitized using a Digidata. The pClamp10 software was used for data acquisition.

Pharmacological agents were added to ACSF at the following concentrations (in  $\mu$ M): 10 CCh to activate cholinergic receptors, 10 NBQX and 50 D-APV to block AMPA and NMDA receptors, 1 SR95531 and 2 CGP55845A to block GABA<sub>A</sub> and GABA<sub>B</sub> receptors, 1 DAMGO to activate  $\mu$ -opioid receptors (MOR), 0.5 DPDPE to activate  $\delta$ -opioid receptors (DOR), 10 clozapine N-oxide (CNO) to activate hM4D(Gi) DREADDs, 100 4-Aminopyridine (4-AP) to block Kv1 potassium channels and 0.2 TTX to prevent sodic action potential (AP) generation.

## **II.5 - Optogenetic stimulation**

ChR2 was excited by 440 nm light delivered by a LED attached to the epifluorescence port of the microscope. Light stimulations trains consisted of 2-10 pulses, 0.5-2 ms long, delivered at 10 Hz, repeated every 10-20 seconds for at least 20 sweeps. Power-response curves of SuM post-synaptic responses in CA2 PNs were carried out with light intensities ranging from 0 to 45 mW/mm<sup>2</sup>. We routinely used a light intensity of 25 mW/mm<sup>2</sup> which was experimentally determined as the lowest irradiance allowing TTX-sensitive maximal responses in all cell types and conditions. Longer trains of 2 minutes at 10 Hz with a light power of 25 mW/mm<sup>2</sup> were used for assessing the effect of SuM inputs on CA2 PN bursting. These trains were triggered manually when the cell had reached a critical pre-burst  $V_M$  inferred from online examination of previous bursts as a point of no return in the depolarization leading to burst discharge. Variability in light onset was minimized and light-on bursts were interleaved with light-off bursts to provide internal control. For the experiments performed in CA1, we used 50 ms long light pulses of 25 mW/mm<sup>2</sup> delivered at 10 Hz for 1 second repeated every 10 seconds.

## **II.6 - Immunocytochemistry and cell identification**

Midbrains containing the injection site were examined post-hoc to ensure that infection was restricted to the SuM.

### Histological procedures

Post-hoc reconstruction of neuronal morphology and SuM axonal projections were performed on slices and midbrain tissue following overnight incubation in 4 % paraformaldehyde in phosphate buffered saline (PBS). Midbrain sections were re-sliced sagittally to 100  $\mu\text{m}$  thick sections. Slices were permeabilized with 0.2 % triton in PBS and blocked overnight with 3 % goat serum in PBS with 0.2 % triton. Primary antibody (life technologies) incubation was carried out in 3 % goat serum in PBS overnight at 4 °C. Channelrhodopsin-2 was detected by chicken primary antibody to GFP (Life technologies) (1:10,000 dilution) and a alexa488-conjugated goat-anti chick secondary. Other primary antibodies used were mouse anti-RGS14 (Neuromab) (1:300 dilution), rabbit anti- PCP4 (Sigma) (1:600 dilution), guinea pig anti-VGluT2 antibody (Milipore) (1:10,000 dilution), rabbit anti-parvalbumin antibody (Swant) (dilution 1:2000). Alexa-546-conjugated streptavidin (life technologies), secondary antibodies and far-red neurotrace (life technologies) incubations were carried out in block solution for 4 hours at room temperature. Images were collected with a Zeiss 710 laser-scanning confocal microscope.

### Classification of neuronal populations

Reconstructed neurons were classified as either PNs or INs based on the extension and localization of their dendrites and axons. CA1, CA2 and CA3 PNs were identified based on their somatic localization, dendritic arborization and presence of thorny excrescences (TE). Among INs with somas located in the pyramidal layer (*stratum pyramidale*, SP), discrimination between BCs and non-BCs was achieved based on the restriction of their axons to SP or not, respectively. When available, firing patterns upon injection of depolarizing current step injection, action potential (AP) half-width, amount of repolarizing sag current upon hyperpolarization from -70 mV to -100 mV by current step injection, membrane resistance ( $R_M$ ) and capacitance ( $C_M$ ) were additionally used for cell identification. CA2 and CA3a PNs displayed similar firing patterns, AP width, sag current,  $R_M$  and  $C_M$ . In contrast, INs had faster firing rates, shorter AP width, higher  $R_M$  and lower  $C_M$  than PNs. BCs further differed from non-BCs by the presence of a larger sag current. All recorded neurons that could not be unequivocally identified as PNs or INs were excluded from analysis.

## II.7 - Data analysis and statistics

Electrophysiological recordings were analyzed using IGORpro (Wavemetrics) and Clampfit (Molecular devices) software.

### Whole-cell recordings

For the clustering of CA2 PN action potentials (APs) in bursts, APs in whole cell recordings were detected automatically by threshold with IGOR TaroTools followed by visual inspection. Kinetics of membrane potential ( $V_M$ ) variations in the vicinity of bursts were measured by linear fits of the  $V_M$  trace as it changed from ACSF- $V_M$  to CCh- $V_M$  or from inter-burst- $V_M$  plus 5 mV to burst- $V_M$  minus 5 mV. AP phases were defined as the phase of the oscillation in area CA2 SP at the time of the AP. Whole-cell recordings during which CA2 PNs did not fire APs or went into depolarization block were excluded from analysis.

For accurate measurements of the kinetics and latencies of SuM light-evoked post-synaptic responses, the following detection process was used. For each cell, average traces were used to create a template waveform that was then fitted to individual traces and measurements were performed on the fitted traces. When only amplitudes of responses were needed, standard average peak detection was used.

When assessing the effect of SuM photostimulation on CA2 PN bursting, comparison of light-on versus light-off bursts in CA2 PNs was performed by aligning all bursts to the pre-burst  $V_M$  defined as the mean  $V_M$  at light onset for each cell.

### LFP recordings

For the analysis of CCh-induced oscillations, LFPs were digitally highpass filtered at 1 Hz and lowpass filtered at 1 kHz *post hoc* using IGOR DSP filters prior to Fourier analysis. Time-frequency analysis was performed on sequential 60 seconds long bins of signal with fast Fourier transform applied to time windows of 1.5 seconds with 50 % overlap multiplied by a Hanning window. Gamma power was defined as the area under the power spectral density between 20 and 40 Hz. LFP recordings that failed to display gamma power above baseline (taken before CCh application) or that were contaminated by noise were excluded from analysis. Wavelet analysis was performed on time windows up to 60 seconds of raw signal decimated to 1 kHz, by computing the complex Morlet wavelet transform of the LFP between 15 and 45 Hz with

Fourier scaling. Phases were extracted from the frequency bearing the maximal magnitude at each time point. Cycles ran from  $-\pi$  to  $\pi$  with a phase of  $-\pi$  defined at the trough of oscillations. Peak-to-peak cycle averages were constructed by averaging raw LFP traces between peaks detected as zero crossings of the derivatives of the corresponding bandpass filtered traces between 20 and 40 Hz with a custom designed digital finite impulse response filter of -60 dB attenuation.

For the detection of extracellular AP firing, LFPs were digitally highpass filtered at 1 kHz *post hoc* to isolate spikes using IGOR DSP filter. APs were then detected automatically by threshold with IGOR TaroTools followed by visual inspection.

### Statistics

Results are reported  $\pm$  SEM. Statistical significance of linear variables was assessed using  $\chi^2$  test, Student's T test, Mann-Whitney U test, Wilcoxon signed-rank test, Kolmogorov-Smirnoff test, Kruskal-Wallis test, one-way or two-way ANOVAs where appropriate.

Circular statistics were used to evaluate the strength of the AP phase-coupling. For each burst of APs, a mean vector ( $r$ ) was constructed by summing unitary vectors ( $R$ ) with angle defined by the phase of each AP in the burst and normalizing to the number of APs ( $n$ ) in the burst:  $|r| = |R|/n$ . This yielded a mean vector ( $r$ ) for each burst with an angle representing the preferred phase of APs in the burst and a radius inversely proportional to the dispersion of individual AP phases around a cycle. Significance of the phase coupling was assessed for each burst by computing the Rayleigh probability of the corresponding mean vector. The circular (SD) was taken as  $SD = \sqrt{-2 \ln |r|}$ .

## **II.8 - Experimental strategy**

### Investigation of single-neuron and LFP activity during carbachol-induced oscillations

In this first set of experiments, transverse acute hippocampal slices were prepared from 6-10 week-old mice. After a baseline recording period of 1-5 minutes, 10  $\mu$ M CCh was continuously applied to these slices while the following experiments were performed. This concentration of CCh was chosen to be consistent with several previous studies working on similar preparations (Fisahn et al., 1998; Gulyás et al., 2010 ; Mann et al., 2005 ; Oren et al., 2006 ; Zemankovics et al., 2013).

LFP recordings were obtained from area CA2 and CA3b SP to evaluate the characteristics of CCh-induced oscillations in both regions and their relation. A subset of these experiments involved bilateral injections of AAVs carrying a Cre-dependent inhibitory DREADD construct targeted in area CA2 of *Cacng5-Cre* mice that express the Cre recombinase specifically in CA2 PNs. These injections were performed on 4 week-old mice, and slices were prepared 6 weeks after that. 10  $\mu$ M CNO was applied 10 minutes after CCh to these slices to selectively silence CA2 PNs expressing the hM4D(Gi)-mcherry receptor and examine the consequences on LFP signals from area CA2 and CA3b.

The pattern of AP firing of CA2 PNs upon CCh application was first assessed by cell-attached recordings from putative CA2 PNs and then by whole-cell patch-clamp recordings of CA2 PNs with *post hoc* confirmation of neuronal identity. When monitoring AP firing induced by CCh in whole-cell configuration, we used current-clamp mode without current injection. In a few instances, transient application of CCh followed by  $V_M$  depolarization through DC current injection after CCh wash-out were used to evaluate the role of CCh in the initial depolarization and subsequent bursts of APs in CA2 PNs. In a subset of experiments, slices were cut with a scalpel blade between area CA2 and CA3a in cutting solution to isolate area CA2 from upstream inputs.

Voltage-clamp recordings of CA2 PNs allowed to quantify the effect of CCh on membrane resistance and on spontaneous excitatory and inhibitory post-synaptic currents.

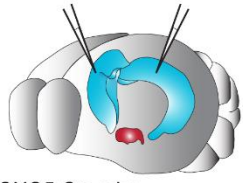
The role of synaptic inputs in shaping bursts of APs in CA2 PNs was assessed by application of 10  $\mu$ M NBQX + 50  $\mu$ M APV and / or 1  $\mu$ M SR95531 + 2  $\mu$ M CGP5584A, 1-2 minutes prior to CCh wash-in.

Simultaneous recordings of LFP in CA2 SP and whole-cell patch-clamp of CA2 PN were performed to probe the temporal relation of CA2 PN AP firing to the field oscillation.

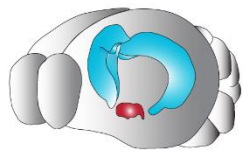
animals & viruses

AAV.Synapsin.DIO.hM4D(Gi).mCherry

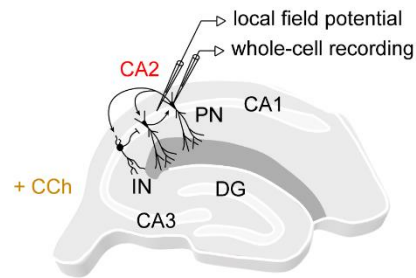
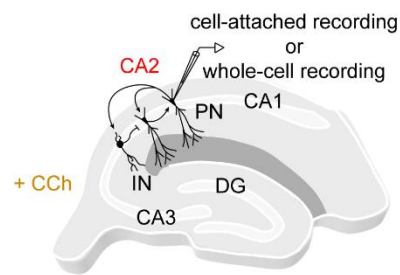
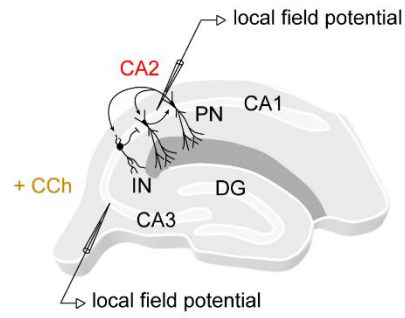
CACNG5-Cre mice



WT mice



recording setup



measurements

time-frequency analysis

pharmacogenetic silencing of CA2 PN

bursts of AP

spontaneous EPSC & IPSC

pharmacology

burst of AP

phase-coupling

pharmacology

**Figure II.8.1. Experimental workflow of the study on CCh-induced network activity.**

Diagrams illustrating the methods used in Section III.1.b

## Examination of the long-range SuM input to area CA2

This second set of experiments involved targeted injections of viral constructs in the brain of genetically engineered mouse lines to map SuM neurons projecting to area CA2 and decipher the neuronal network engaged by these inputs in area CA2.

First, CA2-projecting SuM neurons were identified by injections of retrograde CAV2-Cre in area CA2 and AAV carrying a Cre-dependent EYFP construct in the SuM, followed by immunohistochemical staining of calretinin, VGluT2 and nissl.

Then, Cre-dependent ChR2-EYFP was expressed in SuM neurons by injections of AAVs in the SuM of VGluT2-Cre and Csf2rb2-Cre mice that express the Cre recombinase in SuM neurons. No physiological differences were observed between the two transgenic lines therefore data were pooled. These injections were performed on 4 week-old mice and transverse acute hippocampal slices were prepared at least 4 weeks after that. Cell-attached and whole-cell patch-clamp recordings were obtained from CA2 PNs, CA3 PNs, CA1 PNs, DG GCs, and CA2 INs while SuM afferent axons were photostimulated to determine their post-synaptic targets. *Post hoc* reconstructions of recorded cells allowed their identification and classification. Distinction of CA2 and CA3 PNs in area CA2 was based on the absence or presence of TEs. Classification of deep versus superficial PNs in area CA2 was achieved by measurements of the radial location of their soma relative to the width of the pyramidal layer at the corresponding point of the proximo-distal axis.

Excitatory responses evoked by photostimulation of SuM input were characterized in CA2 and CA3a PNs by voltage- and current-clamp recordings at -70 mV. Application of 10  $\mu$ M NBQX and 50  $\mu$ M APV was used to test the glutamatergic nature of SuM light-evoked EPSCs. 0.2  $\mu$ M TTX was applied to confirm that our photostimulation protocol triggered AP firing in pre-synaptic SuM axons.

Voltage-clamp recordings of DG GCs held at -70 mV and +10 mV were performed to validate the electrophysiological observations made in the newly generated Csf2rb2-Cre line. Sequential application of 10  $\mu$ M NBQX + 50  $\mu$ M APV, and 1  $\mu$ M SR95531 + 2  $\mu$ M CGP5584A was used to assess the co-release of glutamate and GABA described at the SuM to DG GC synapse.

Light-evoked IPSCs upon SuM axons photostimulation were monitored in area CA2 PNs by voltage clamp recordings at +10 mV. The mono-synaptic versus di-synaptic nature of EPSCs versus IPSCs was assessed by application of 10  $\mu$ M NBQX and 50  $\mu$ M APV, or 0.2  $\mu$ M TTX and 100  $\mu$ M 4-AP.

The resulting effect of SuM-driven mono-synaptic excitation and di-synaptic inhibition on PNs in area CA2 was assessed by current-clamp recordings of these cells. The inhibitory control of excitatory responses by feedforward inhibition was probed by blocking inhibitory transmission with 1  $\mu$ M SR95531 and 2  $\mu$ M CGP5584A while monitoring SuM light-evoked EPSPs in CA2 PNs held at -70 mV. To examine the role of the SuM inhibitory drive on CA2 PN activity, current steps were injected to elicit AP firing with or without delivering photostimulation trains at 10 Hz, before and after application of 1  $\mu$ M SR95531 and 2  $\mu$ M CGP5584A.

In order to identify the subtype of IN recruited by the SuM to drive feedforward inhibition of PNs in area CA2, cell-attached and whole-cell patch-clamp recordings were obtained from INs while photostimulating SuM axons. INs were classified *post hoc* based on their somatic location and axonal projections primarily. Intrinsic electrophysiological properties and immunoreactivity for PV were additionally analyzed when available. Voltage- and current-clamp recordings at -70 mV were used to quantify EPSCs and EPSPs evoked by photostimulation of SuM axons in CA2 INs. AP firing in response to SuM input photostimulation was probed in cell-attached configuration before breaking in whole-cell and then in current-clamp mode without current injection (i.e. at resting membrane potential).

To further assess the role of PV-expressing INs in the SuM-driven feedforward inhibition of PNs in area CA2, light-evoked IPSCs were recorded from PNs held at +10 mV in the following experimental conditions. Using VGluT2-Cre and Csf2rb2-Cre mice injected with AAV9.EF1a.DIO.hChR2(H134R).EYFP in the SuM, the  $\mu$ - or  $\delta$ -opioid receptors agonists DAMGO (1  $\mu$ M) or DPDPE (0.5  $\mu$ M) known to depress GABA release from PV-expressing INs were applied. To control for potential effects of 1  $\mu$ M DAMGO or 0.5  $\mu$ M DPDPE on SuM direct excitation, light-evoked EPSCs were recorded at -70 mV in presence of the GABA receptors blockers 1  $\mu$ M SR95531 and 2  $\mu$ M CGP5584A. Alternatively, PV-Cre mice were injected with AAV.Synapsin.DIO.hM4D(Gi).mCherry bilaterally in area CA2 and with AAV2/9.hSyn.hChR2(H134R).EYFP.WPRE.hGH in the SuM, allowing for selective silencing of PV-expressing INs by application of the DREADD agonist CNO (10  $\mu$ M).

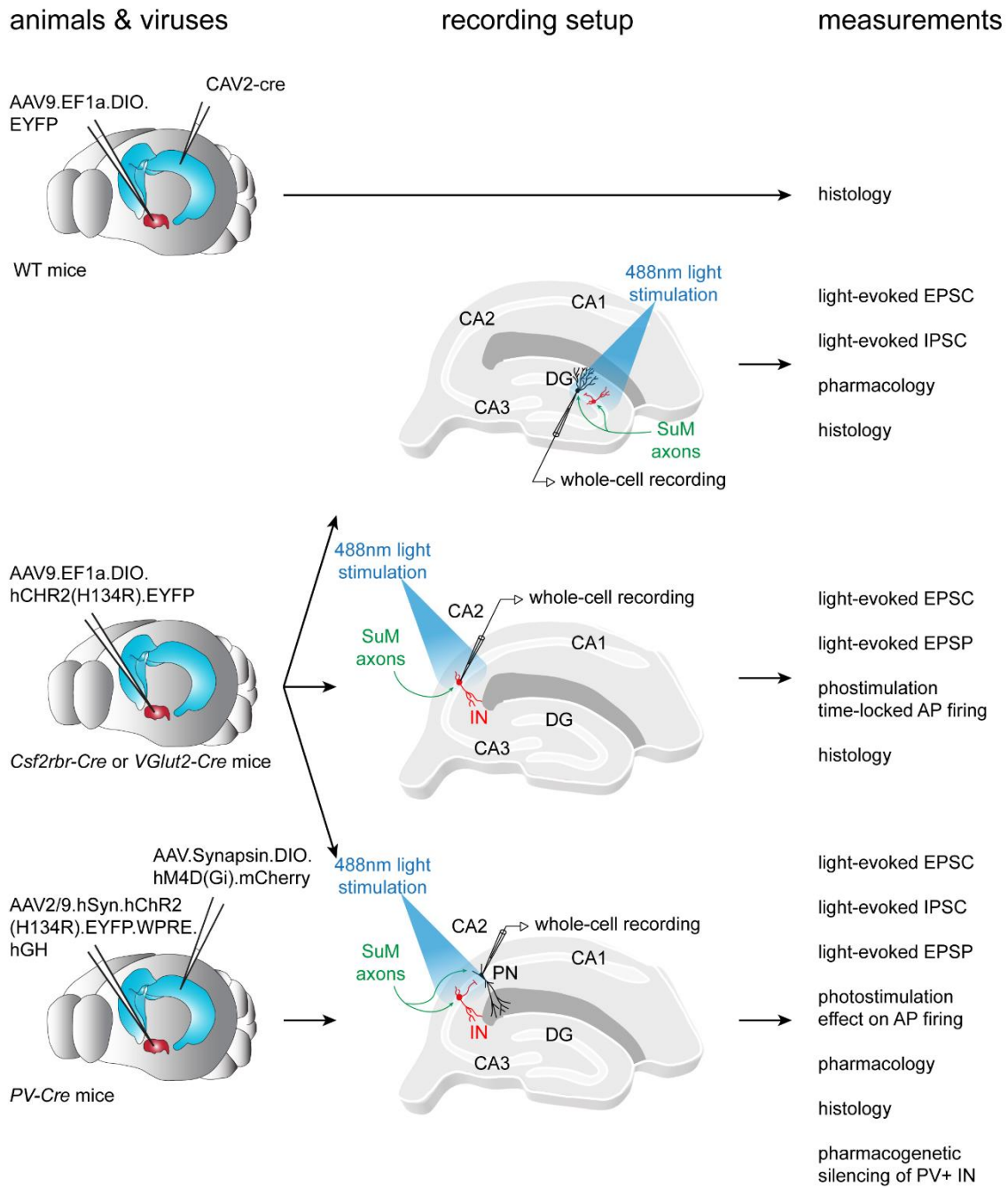


**Figure II.8.2. Experimental workflow of the study on SuM input to area CA2.**

Diagrams illustrating the methods used in Section III.2.b

### Assessment of the consequences of SuM input stimulation on area CA2 and CA1 activity

For this last set of experiments, ChR2-EYFP was expressed in SuM neurons using stereotaxic injections of AAV9.EF1a.DIO.hChR2(H134R).EYFP in VGluT2-Cre and Csf2rb2-Cre mice. Like previously, transverse acute hippocampal slices were prepared at least 4 weeks after surgery, whole-cell patch-clamp and LFP recordings were obtained in area CA2 and CA1 while SuM axons were photostimulated, and 10  $\mu$ M CCh was applied after a baseline period. In parallel, *in vivo* recordings of CA1 single- and multi-unit activity were performed by the McHugh laboratory on Csf2rb2-Cre mice that underwent the same injections and had optic fibers implanted over area CA2.

Voltage-clamp recordings of CA2 PNs held at -70 mV or +10 mV were used to examine the effect of 10  $\mu$ M CCh on SuM excitatory and inhibitory drives. Power response curves of light-evoked EPSCs and IPSCs were obtained by photostimulating SuM axons at increasing light intensities before and after application of 10  $\mu$ M CCh. To isolate the pure excitatory component of SuM synaptic inputs, inhibitory transmission was blocked with 1  $\mu$ M SR95531 and 2  $\mu$ M CGP5584A in some of these experiments.

To investigate the consequence of SuM transmission on CA2 PN burst firing of APs, CA2 PNs were recorded in current-clamp mode without current injection and 10  $\mu$ M CCh was applied. The global firing activity of neurons in area CA2 was simultaneously recorded with a LFP electrode positioned nearby area CA2 SP. Once the CA2 PN recorded in whole-cell configuration starts to fire bursts of APs, its  $V_M$  dynamics were examined online to determine a reliable level of  $V_M$  preceding the bursts without subsequent repolarization (the “pre-burst  $V_M$ ”). Thereafter, 2 minute-long trains of light pulses of 0.5 ms delivered at 10 Hz were used to activate SuM axons when CA2 PNs reached their pre-burst  $V_M$ . These light-on bursts were interleaved with light-off bursts. In a subset of these experiments, 10  $\mu$ M NBQX and 50  $\mu$ M APV were applied to suppress light-evoked synaptic transmission from SuM axons.

*In vivo* recordings of CA1 firing activity were obtained by the McHugh laboratory while photostimulating SuM axons over area CA2 with 50 ms-long light pulses delivered at 10 Hz for one second every 10 seconds on Csf2rb2-Cre mice. The same optogenetic stimulation protocol was used on acute hippocampal slices superfused with 10  $\mu$ M CCh as we performed whole-cell voltage- and current-clamp recordings of CA1 PNs together with LFP recordings of firing activity in area CA1 SP.

animals & viruses

recording setup

measurements

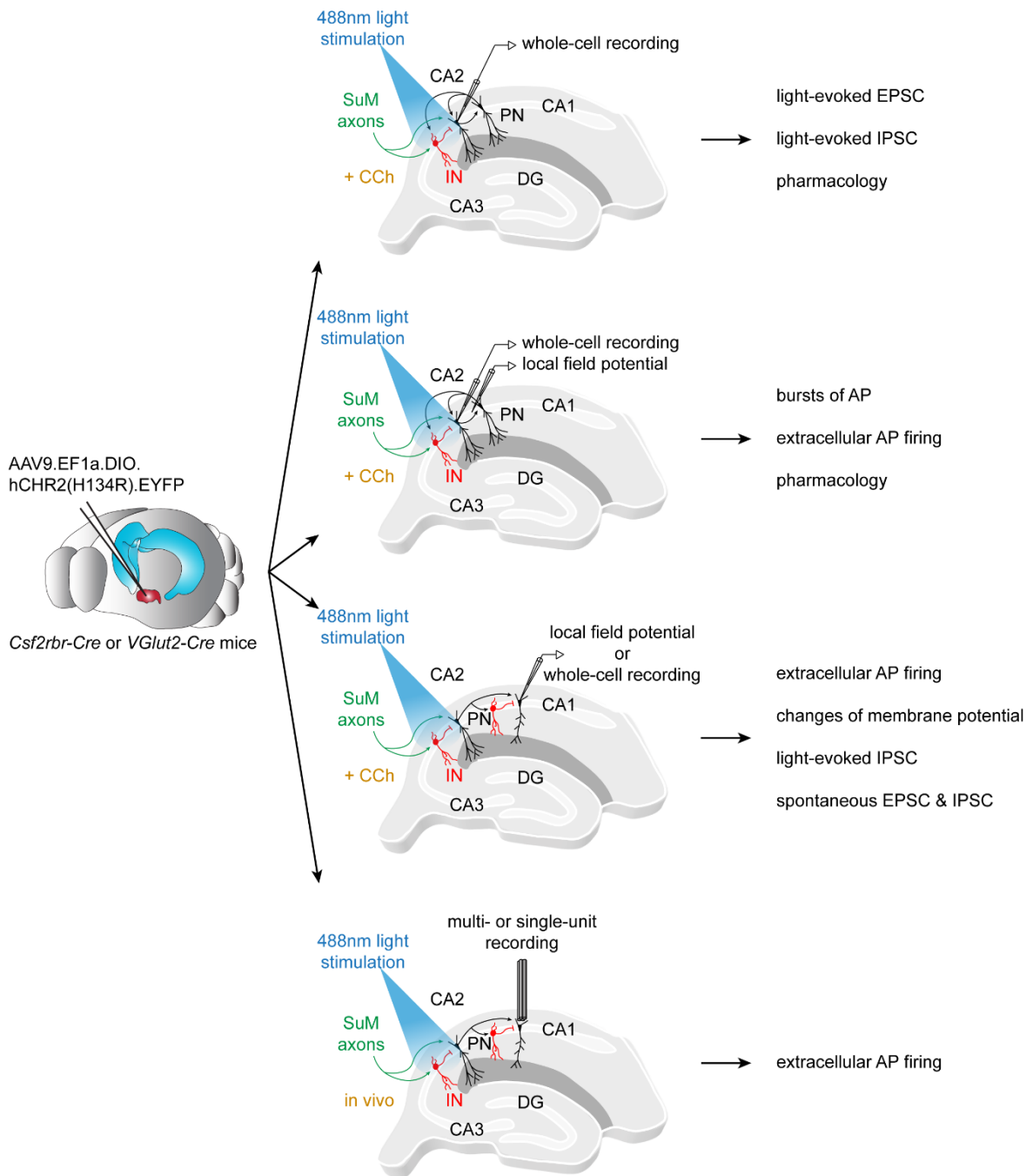


**Figure II.8.3. Experimental workflow of the study on the consequences of SuM activation on area CA2 and CA1 activity.**

Diagrams illustrating the methods used in Section III.3.b

# III - Results

## III.1 - Spontaneous network activity of hippocampal area CA2 under conditions of enhanced cholinergic tone

### III.1.a - Introduction

Theta and gamma rhythms in hippocampal networks are critical for learning and memory (Buzsáki and Moser, 2013; Colgin, 2016). Cellular mechanisms underlying gamma oscillations in area CA3 and CA1 are well documented (Csicsvari et al., 2003; Fisahn et al., 1998; Mann et al., 2005; Oren et al., 2006; Zemankovics et al., 2013), however, as of now, this activity in area CA2 has not been examined. Recent *in vivo* recordings have revealed that neuronal activity in area CA2 is critical for several aspects of hippocampal physiology including initiation of sharp waves / ripples (SWR) (Oliva et al., 2016) and are capable of encoding spatial information during immobility (Kay et al., 2016). These important roles indicate that a better understanding of area CA2 network oscillations is required to better understand hippocampal function.

Thus, we set out to examine the cellular and network mechanisms governing rhythmic activity in area CA2. Area CA3 has been shown to intrinsically generate slow gamma activity in acute slice preparations (Fisahn et al., 1998; Mann et al., 2005; Oren et al., 2006) and shares similarities with area CA2 in terms of network recurrence, inputs and outputs (Boehringer et al., 2017; Chevaleyre and Siegelbaum, 2010; Hitti and Siegelbaum, 2014; Kohara et al., 2013; Sun et al., 2017). We focused our study on pharmacologically-induced *ex vivo* gamma-like activity in area CA2. A wealth of studies focused on CA3 and CA1 have provided evidence that gamma oscillations in the low range, i.e. 30 to 50 Hz, are generated in area CA3 and propagate to area CA1 through feedforward inhibition (Csicsvari et al., 2003; Zemankovics et al., 2013). Both CA2 and CA3 PNs reciprocally recruit strong feed-forward inhibition over one another (Boehringer et al., 2017; Chevaleyre and Siegelbaum, 2010), and CA2 PNs also project onto CA1 PNs (Chevaleyre and Siegelbaum, 2010; Kohara et al., 2013). Therefore, description of cellular and network activity in area CA2 will help the understanding of gamma oscillations by incorporating area CA2 in the hippocampal circuit and taking into account its mutual influences with CA3 and its contribution to driving activity in CA1. To this end, we recorded simultaneous local field potentials (LFPs) from area CA2 and CA3 and obtained whole-cell patch-clamp recordings from CA2 PNs while superfusing acute hippocampal slices with the

cholinergic agonist carbachol (CCh). This approach allowed us to compare network activity in area CA2 and CA3, to explore the activity of CA2 PNs in this condition and relate it to the ongoing oscillation.

We observed that application of the cholinergic agonist carbachol reliably induced gamma-like oscillations in areas CA3 and CA2 as recorded with local field potentials. Comparison of such oscillations between both regions revealed that the power of the signal was lower in area CA2. Patch-clamp recordings of CA2 pyramidal neurons in these conditions revealed their ability to rhythmically fire bursts of action potentials. Excitatory and inhibitory synaptic inputs contributed to the shaping of these action potentials bursts in CA2 PNs. However, synaptic transmission was not necessary as burst firing persisted when blocked. CA2 PN activity was influenced by the network activity as evidenced by phase-coupling of action potential firing to the ongoing field oscillation during bursts. Therefore, our findings reveal the ability of the CA2 neuronal network to undergo gamma-like activity similar to area CA3 and highlight the pattern of action potential firing in CA2 PNs in the presence of increased cholinergic tone.

### **III.1.b - Results**

#### Carbachol induces gamma-like activity in area CA2

Both *in vivo* and *ex vivo* studies have provided evidence that area CA3 can intrinsically generate oscillations in the low gamma range (Csicsvari et al., 2003; Fisahn et al., 1998; Mann et al., 2005; Oren et al., 2006; Zemankovics et al., 2013). Given the newly discovered roles of area CA2 network activity in fundamental aspects of hippocampal physiology such as SWR generation (Oliva et al., 2016) and spatial coding (Kay et al., 2016), and because it shares properties in terms of inputs, outputs and recurrent connections with area CA3 (Chevalyere and Siegelbaum, 2010; Cui et al., 2013; Hitti and Siegelbaum, 2014; Kohara et al., 2013; Sun et al., 2017), we sought to determine how neuronal networks in area CA2 behave when challenged with an increase in cholinergic tone. To this end, we simultaneously recorded local field potentials (LFPs) in area CA2 and CA3 *strata pyramidale* (SP) on acute hippocampal slices and applied the cholinergic agonist carbachol (CCh) (Figure III.1.1A). We assessed the presence and strength of oscillations over time by performing sequential fast Fourier transforms and measuring the average gamma power per minute (defined as the area under the power spectral density curve between 20 and 40 Hz). Upon bath application of 10  $\mu$ M CCh, oscillatory activity could be detected from both CA2 and CA3 SP with peaks of power spectral density in the gamma range (Figure III.1.1B). These oscillations occurred after 1 minute of CCh

application and had a significant gamma power for 15 minutes after CCh application. This time window was used for analysis (Figure III.1.1B;  $n = 34$ ; Kruskal-Wallis test,  $p = 0.007$  for CA2,  $p = 0.003$  for CA3; Wilcoxon signed-rank test between before and after CCh,  $p < 0.001$  for CA2,  $p < 0.001$  for CA3). We observed that network oscillations contained a significantly greater gamma power in area CA3 than CA2 (Figure III.1.1C; gamma powers were  $388 \pm 64.6 \mu\text{V}^2$  in CA2 and  $623 \pm 112 \mu\text{V}^2$  in CA3,  $n = 34$ ; Wilcoxon signed-rank test,  $p = 0.005$ ) with no difference in peak frequencies (Figure III.1.1C; peak frequencies were  $23 \pm 1.0 \text{ Hz}$  in CA2 and  $24 \pm 1.3 \text{ Hz}$  in CA3,  $n = 34$ ; paired Student T test,  $p = 0.53$ ).

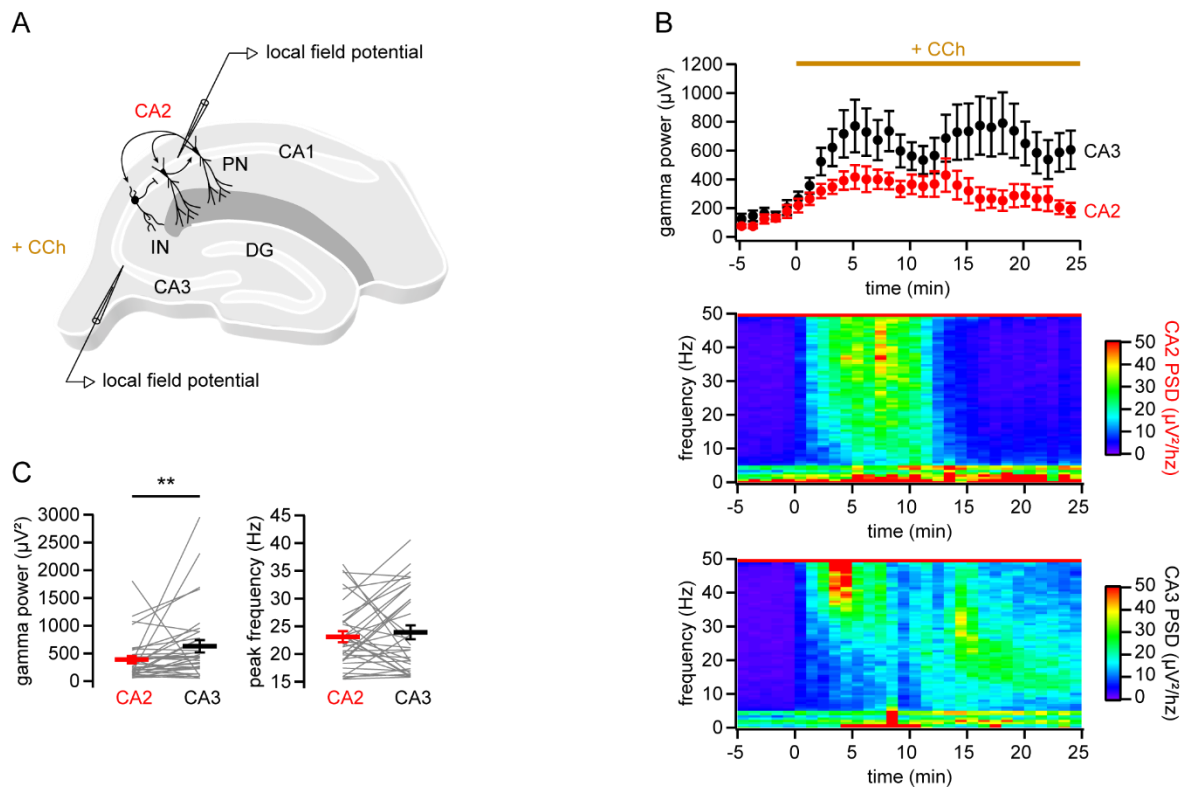


**Figure III.1.1. Carbachol induces gamma-like oscillations in hippocampal area CA2 and CA3.**

**A.** Diagram illustrating the simultaneous LFP recordings from area CA2 and CA3 SP in acute hippocampal slices with application of  $10 \mu\text{M}$  CCh. **B.** Top, time course of the mean gamma power of LFPs recorded in area CA2 (red) and CA3 (black) upon  $10 \mu\text{M}$  CCh application ( $n = 34$ ; error bars represent SEM). Bottom, example spectrograms of signals recorded in area CA2 and CA3 during this time course, warm colors indicate high power. **C.** Comparison of the power (left) and frequency (right) of CCh-induced oscillations recorded from area CA2 and CA3 (individual cells shown as grey lines, population average shown as horizontal line, error bars represent SEM,  $n = 34$ ; Wilcoxon signed-rank test on gamma powers,  $p = 0.005$ ; paired-T test on peak frequencies,  $p = 0.53$ ; error bars represent SEM).

Further analysis was performed using wavelet transforms with Morlet basis on subsets of data spanning 60 seconds during which gamma power was maximal, to extract the magnitude of frequency components in the signal from 15 to 45 Hz (Oren et al., 2006). This method revealed that the magnitude and dominant frequency of oscillations were fluctuating over time in the sub-second range (Figure III.1.2A and Figure III.1.2B). Consequently, the dominant frequencies could differ between CA2 and CA3 during sub-seconds epochs (Figure III.1.2B, Figure III.1.2C) while being similar overall (Figure III.1.1C). Therefore, we extracted phases of oscillations at frequencies bearing the maximal magnitude at each time point (Oren et al., 2006) in CA2 and CA3 to examine the temporal relation between signals from both regions. However, cross-correlation analysis did not reveal a significant lag between field potential oscillations in CA2 and CA3 (CA3 lag versus CA2 =  $0.62 \pm 0.46$  ms,  $n = 34$ ; one-sample T test,  $p = 0.15$ ) nor their respective phases (CA3 lag versus CA2 =  $0.97 \pm 1.23$  ms,  $n = 34$ ; one-sample T test,  $p = 0.44$ ).

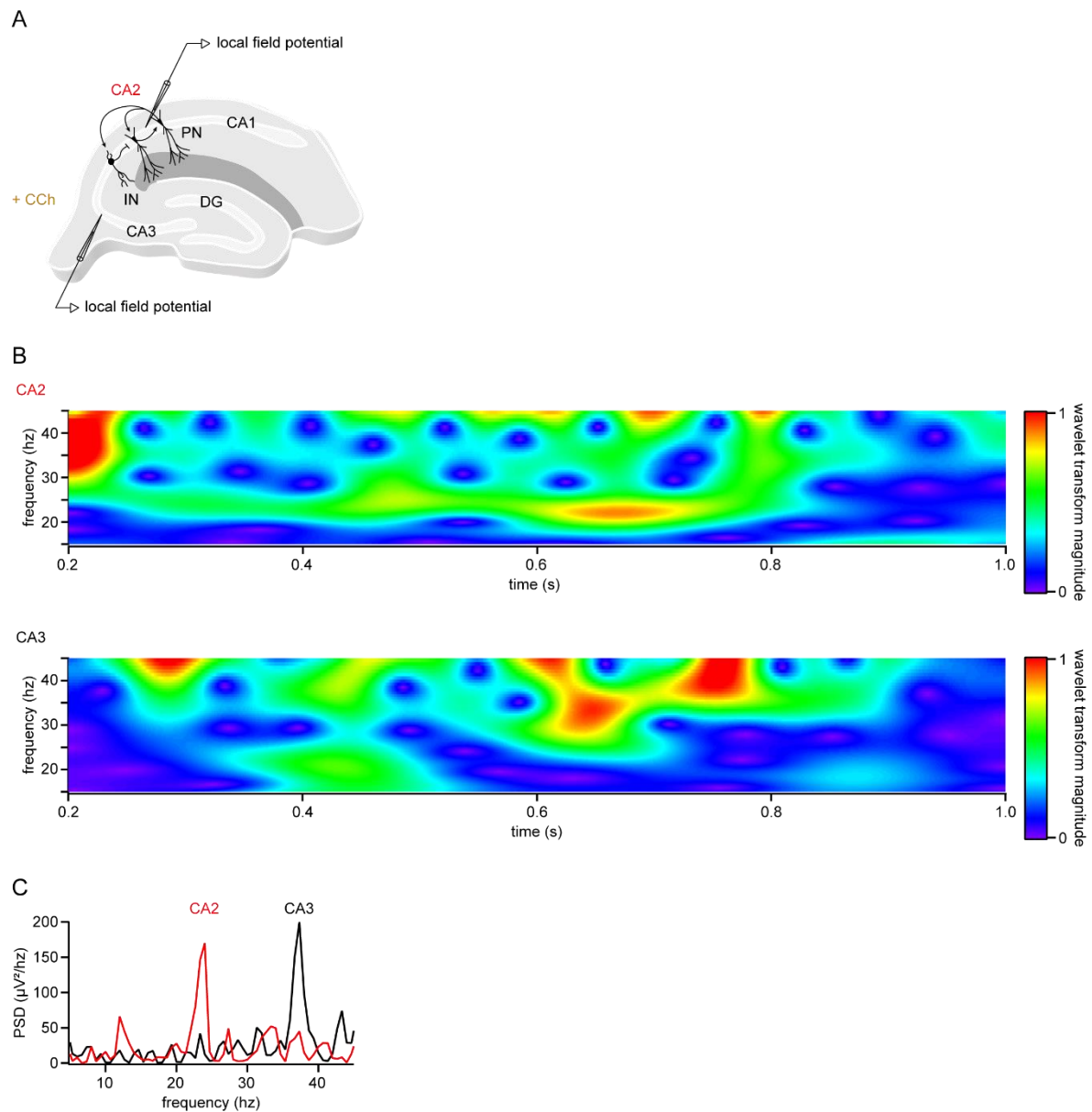


**Figure III.1.2. Temporal relations of CCh-induced oscillations from area CA2 and CA3.**

**A.** Diagram illustrating the simultaneous LFP recordings from area CA2 and CA3 SP in acute hippocampal slices with application of 10  $\mu\text{M}$  CCh. **B.** Normalized magnitude components of the wavelet transforms of raw LFPs recorded in SP from area CA2 (top) and CA3 (bottom), warm colors indicate high magnitude. **C.** Power spectral density functions of LFPs recorded in SP from area CA2 (red line) and CA3 (black line) showing peaks in the gamma range.

These results indicate that CCh-induced oscillations classically described in area CA3 also exist in area CA2. The lack of significant temporal relationship between signals from both regions suggests that oscillations in area CA2 are likely independent from CA3. To further test the interactions of signals from CA2 and CA3, we used chemogenetics to silence CA2 PNs and

examined the consequences on CCh-induced oscillations in both regions. Bilateral injections of AAVs carrying a Cre-dependent construct allowing the expression of the h4MDi inhibitory DREADD were performed in area CA2 of *Cacng5-Cre* mice (Figure III.1.3A). LFP recordings in CA2 and CA3 SP on acute slices from these mice revealed that inhibition of CA2 PNs by application of the DREADD agonist CNO (10  $\mu$ M) significantly reduced CCh-induced oscillations in area CA2 while leaving gamma power unaffected in area CA3 (Figure III.1.3B and Figure III.1.3C; CA2 gamma powers were  $134 \pm 20.9 \mu\text{V}^2$  in control and  $106 \pm 14.2 \mu\text{V}^2$  in CNO hence a  $18 \pm 3.6 \%$  block by CNO,  $n = 16$ ; Wilcoxon signed-rank test,  $p < 0.001$ ; CA3 gamma powers were  $230 \pm 39.0 \mu\text{V}^2$  in control and  $239 \pm 42.7 \mu\text{V}^2$  in CNO,  $n = 16$ ; Wilcoxon signed-rank test,  $p = 0.159$ ). Two conclusions can be drawn from these experiments : first, CA2 PNs are not passively driven by activity from CA3 but instead participate actively in the generation of CCh-induced oscillations in area CA2. Second, signals from area CA3 are not strongly influenced by activity from CA2 in this acute slice model of gamma oscillations.

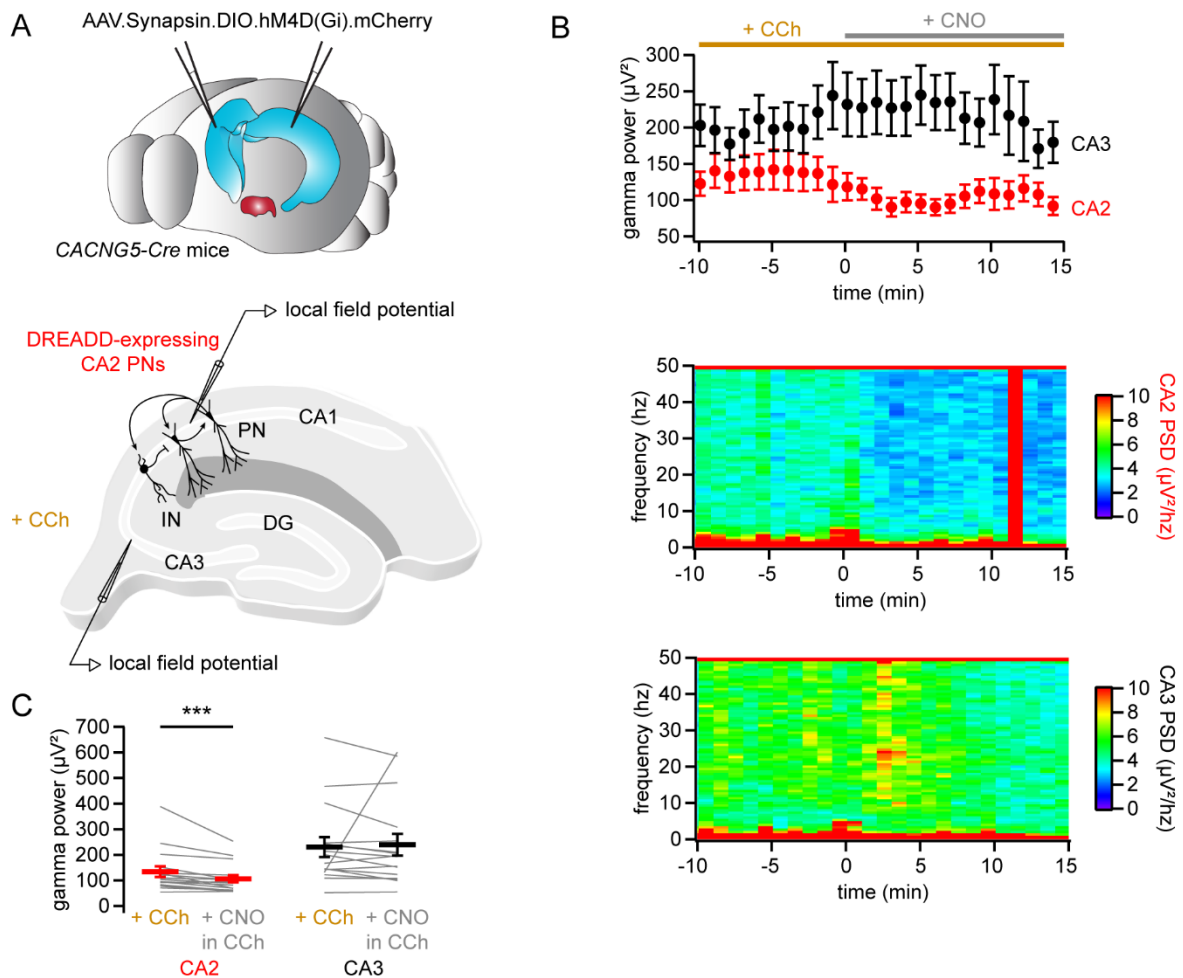


**Figure III.1.3. Effects of chemogenetic silencing of CA2 PN on CCh-induced oscillations.**

**A.** Diagram illustrating the experimental strategy used for chemogenetic silencing of CA2 PNs. **B.** Top, time course of the mean gamma power of LFPs recorded in area CA2 (red) and CA3 (black) in 10  $\mu\text{M}$  CCh upon 10  $\mu\text{M}$  CNO application ( $n = 16$ ; error bars represent SEM). Bottom, example spectrograms of signals recorded in area CA2 and CA3 during this time course, warm colors indicate high power. **C.** Comparison of the power of CCh-induced oscillations recorded from area CA2 (red) and CA3 (black) before and after 10  $\mu\text{M}$  CNO application (individual cells shown as grey lines, population average shown as horizontal line, error bars represent SEM,  $n = 16$ ; Wilcoxon signed-rank test,  $p < 0.001$  for CA2,  $p = 0.159$  for CA3).

### CA2 pyramidal cells undergo slow rhythmic bursting activity during CCh-induced oscillations

Gamma oscillations in area CA3 result from the synchronized activity of pyramidal cells that build up excitation through their excitatory recurrent connections and then recruit feedback inhibition mediated by peri-somatic targeting interneurons which repolarize them, hence completing a cycle (Csicsvari et al., 2003; Fisahn et al., 1998; Mann et al., 2005; Oren et al., 2006; Zemankovics et al., 2013). Given CCh application triggers gamma-like oscillations in

area CA2 that were somewhat different from gamma-like oscillations in CA3, and because CA2 pyramidal neurons display unique properties (Chevalleyre and Siegelbaum, 2010; Srinivas et al., 2017; Pagani et al., 2014; Piskorowski et al., 2016; Sun et al., 2014; Talley et al., 2001), we asked how PNs in area CA2 behave during CCh-induced oscillations (Figure III.1.4A). First, we assessed the firing of action potentials of cells in area CA2 by performing cell-attached recordings with ACSF-filled pipettes to leave the intra-cellular content unperturbed. Prior to CCh application, most cells did not fire action potentials ( $n = 14$  of 15 cells). Although several cells remained silent, the majority showed action potential firing upon CCh wash-in ( $n = 9$  of 15 cells). Interestingly, spiking activity from these cells was often structured in bursts ( $n = 8$  of 9 cells) rather than tonic (Figure III.1.4B). This bursting pattern could either be sustained throughout CCh application ( $n = 5$  cells) or transition to a tonic pattern ( $n = 3$  cells). As burst firing seemed to be the most common type of activity displayed by putative PNs, we wished to confirm the identity of bursting cells and characterize them further. Albeit non-invasive, cell-attached recordings provide limited information on the cell type, electrophysiological properties and synaptic responses of the recorded neuron. Therefore, we turned to whole-cell patch-clamp recordings of CA2 PNs together with LFP recordings from area CA2 SP to access both the supra- and sub-threshold dynamics of CA2 PN  $V_M$  and to relate them to the network activity. Using current-clamp mode without current injection, we could study the evolution of CA2 PNs membrane potential ( $V_M$ ) during the course of CCh application (Table III.1.1, Figure III.1.4C and Figure III.1.5A-L). Upon 10  $\mu$ M CCh wash-in, CA2 PNs increased their membrane potential from resting at  $-75 \pm 1.2$  mV (referred to as ACSF- $V_M$ ) to a depolarized level of  $-64 \pm 1.0$  mV (referred to as CCh- $V_M$ ) (Table III.1.1, Figure III.1.4C and Figure III.1.5C;  $n = 25$ ). This CCh-induced depolarization was slow ( $6.5 \pm 0.8$  mV/min) and variable as CA2 PNs took several minutes ( $6.4 \pm 0.7$  min) to reach the CCh- $V_M$  (Table III.1.1, Figure III.1.4C, Figure III.1.5D and Figure III.1.5E), possibly due to differences in depth of the recording. Voltage-clamp measurements of CA2 PNs membrane properties before and after CCh application revealed that this depolarization was accompanied by a  $56 \pm 6.6$  M $\Omega$  increase in membrane resistance ( $R_M$ ) from  $40 \pm 2.6$  M $\Omega$  to  $95 \pm 7.0$  M $\Omega$  (Table III.1.1, Figure III.1.5B). This indicates that CCh depolarizes CA2 PNs by, at least in part, closing potassium-conducting channels. The initial slow depolarization was followed by regular bursts of action potentials in CA2 PNs that could last throughout CCh application. To maintain consistency with our LFP analysis, we analyzed bursts during the first 15 minutes following CCh wash-in. These bursts occurred at a rather low rate (Table III.1.1, Figure III.1.4C and Figure III.1.5F; inter-burst interval =  $100 \pm 14.7$  s) as CA2 PNs underwent further depolarization of their  $V_M$  during bursts (Table III.1.1,

Figure III.1.4C and Figure III.1.5G; burst- $V_M = -41 \pm 1.0$  mV) interleaved by repolarization in-between bursts to an inter-burst- $V_M$  close to the CCh- $V_M$  (Table III.1.1, Figure III.1.4C and Figure III.1.5H; inter-burst- $V_M = -62 \pm 0.8$  mV). During inter-bursts intervals, CA2 PNs  $V_M$  slowly increased from repolarized levels after a burst to depolarized levels preceding a burst (Figure III.1.4C). However, most of the  $V_M$  variation occurred in the vicinity of bursts with a fast transition from inter-burst- $V_M$  to burst- $V_M$  prior to bursting (Table III.1.1, Figure III.1.4C and Figure III.1.5I; burst rise slope =  $3.5 \pm 0.5$  mV/s) and from burst- $V_M$  to inter-burst- $V_M$  after bursting (Table III.1.1, Figure III.1.4C and Figure III.1.5J; burst decay slope =  $-4.6 \pm 0.8$  mV/s). These transitions demarcated bursts that lasted  $3.8 \pm 0.5$  seconds (Table III.1.1, Figure III.1.4C and Figure III.1.5L) with CA2 PNs firing action potentials at frequencies in the theta range at  $14 \pm 2.6$  Hz (Table III.1.1, Figure III.1.4C and Figure III.1.5K). Thus, CA2 PNs undergo slow rhythmic bursting when challenged with increased cholinergic tone, a behavior previously described in CA3 PNs in similar conditions (Cobb et al., 1999). Importantly, CCh is necessary for CA2 PNs bursting as mimicking the CCh-induced depolarization by injecting current in the absence of CCh led to tonic firing but failed to elicit bursts (Figure III.1.4D). Conversely, CA2 PNs are endowed with a repertoire of conductances sufficient for CCh to induce bursting without the need of synaptic inputs as blocking all synaptic transmission and isolating area CA2 from CA3 by cuts between these regions did not abolish AP bursts in CA2 PNs (Figure III.1.4E).

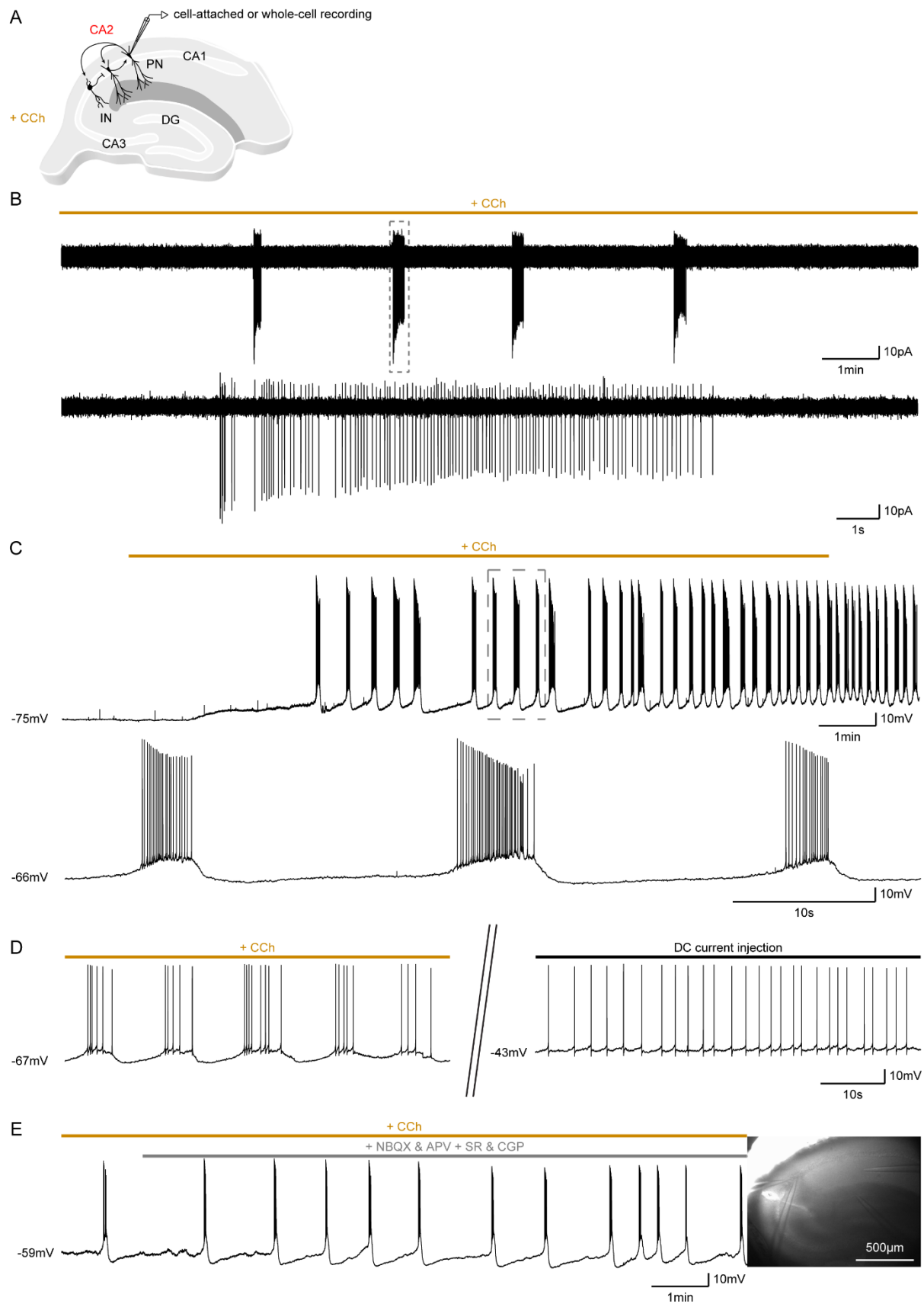


**Figure III.1.4. CA2 PNs fire bursts of APs following CCh application.**

**A.** Diagram illustrating the cell-attached or whole-cell recording configuration of CA2 PN in acute hippocampal slices with application of 10  $\mu$ M CCh. **B.** Sample trace of AP bursts recorded in cell-

attached configuration from a CA2 PN after 10  $\mu$ M CCh application (top) and expanded view of the demarcated window (dashed gray box, bottom). **C.** Sample trace of bursts recorded whole-cell from a CA2 PN after 10  $\mu$ M CCh application (top) and expanded view of the demarcated window (dashed gray box, bottom). **D.** Sample traces recorded whole-cell from the same CA2 PN showing bursts during 10  $\mu$ M CCh application (left) and tonic firing upon DC current injection (right). **E.** Sample trace of bursts recorded whole-cell from a CA2 PN upon 10  $\mu$ M CCh application with excitatory and inhibitory synaptic transmission blocked (10  $\mu$ M NBQX, 50  $\mu$ M APV, 1  $\mu$ M SR95531 & 2  $\mu$ M CGP5584A) in a slice where area CA2 was isolated from CA3 by a cut between regions.

**Table III.1.1. Characteristics of charbachol-induced CA2 PN spontaneous activity.**

	Control	Excitatory and inhibitory transmission blocked  (10 $\mu$ M NBQX, 50 $\mu$ M APV, 1 $\mu$ M SR95531, 2 $\mu$ M CGP5584A)	Excitatory transmission blocked  (10 $\mu$ M NBQX, 50 $\mu$ M APV)	Inhibitory transmission blocked  (1 $\mu$ M SR95531, 2 $\mu$ M CGP5584A)	Statistics
	(n = 25)	(n = 6)	(n = 7)	(n = 6)	
ACSF- $V_M$ (mV)	-75 $\pm$ 1.2	-70 $\pm$ 4.1	-72 $\pm$ 3.1	-80 $\pm$ 1.9	1-way ANOVA test p = 0.054
CCh- $V_M$ (mV)	-64 $\pm$ 1.0	-57 $\pm$ 2.9  p = 0.025 vs CT	-62 $\pm$ 2.1	-64 $\pm$ 1.5	1-way ANOVA test p = 0.036  Tukey <i>post hoc</i>
$\Delta_{ACSF-CCh}$ $V_M$ (mV)	11 $\pm$ 1.0	13 $\pm$ 1.4	9.5 $\pm$ 1.5	16 $\pm$ 1.9	1-way ANOVA test p = 0.065
depolarization slope (mV/min)	6.5 $\pm$ 0.8	8.6 $\pm$ 2.0	9.2 $\pm$ 3.4	9.4 $\pm$ 2.3	Kruskal-Wallis test p = 0.52
burst onset (min)	6.4 $\pm$ 0.7	3.5 $\pm$ 0.6	4.6 $\pm$ 1.8	4.7 $\pm$ 1.2	1-way ANOVA test p = 0.21
inter-burst interval (s)	100 $\pm$ 14.7	36 $\pm$ 5.6  p < 0.05 vs CT	36 $\pm$ 8.3  p < 0.05 vs CT	113 $\pm$ 41.9	Kruskal-Wallis test p = 0.005  Dunn-Holland-Wolfe <i>post hoc</i>
burst- $V_M$ (mV)	-41 $\pm$ 1.0	-42 $\pm$ 2.2	-38 $\pm$ 2.1	-39 $\pm$ 1.9	1-way ANOVA test p = 0.45
inter-burst- $V_M$ (mV)	-62 $\pm$ 0.8	-56 $\pm$ 1.1  p = 0.006 vs CT p = 0.033 vs SR	-56 $\pm$ 1.4  p = 0.001 vs CT p = 0.013 vs SR	-63 $\pm$ 1.9	1-way ANOVA test p < 0.001  Tukey <i>post hoc</i>
$\Delta_{burst-IBI}$ $V_M$ (mV)	22 $\pm$ 1.3	14 $\pm$ 2.2	18 $\pm$ 2.6	24 $\pm$ 2.7	1-way ANOVA test p = 0.047
burst rise slope (mV/s)	3.5 $\pm$ 0.5	3.6 $\pm$ 0.6	5.9 $\pm$ 1.1	59 $\pm$ 26  p < 0.05 vs CT	Kruskal-Wallis test p < 0.001  Dunn-Holland-Wolfe <i>post hoc</i>
burst decay slope (mV/s)	-4.6 $\pm$ 0.8	-4.8 $\pm$ 0.6	-4.3 $\pm$ 0.7	-13.7 $\pm$ 4.0	Kruskal-Wallis test p = 0.087
burst duration (s)	3.8 $\pm$ 0.5	2.4 $\pm$ 0.6	2.6 $\pm$ 0.7	1.1 $\pm$ 0.3  p < 0.05 vs CT	Kruskal-Wallis test p = 0.037  Dunn-Holland-Wolfe <i>post hoc</i>
bursting frequency (Hz)	14 $\pm$ 2.6	6.3 $\pm$ 1.5	9.3 $\pm$ 3.0	23 $\pm$ 5.2  p < 0.05 vs CT	Kruskal-Wallis test p = 0.014  Dunn-Holland-Wolfe <i>post hoc</i>
ACSF- $R_M$ (M $\Omega$ )	40 $\pm$ 2.6				
CCh- $R_M$ (M $\Omega$ )	95 $\pm$ 7.0				
$\Delta_{ACSF-CCh}$ $R_M$ (M $\Omega$ )	56 $\pm$ 6.6				

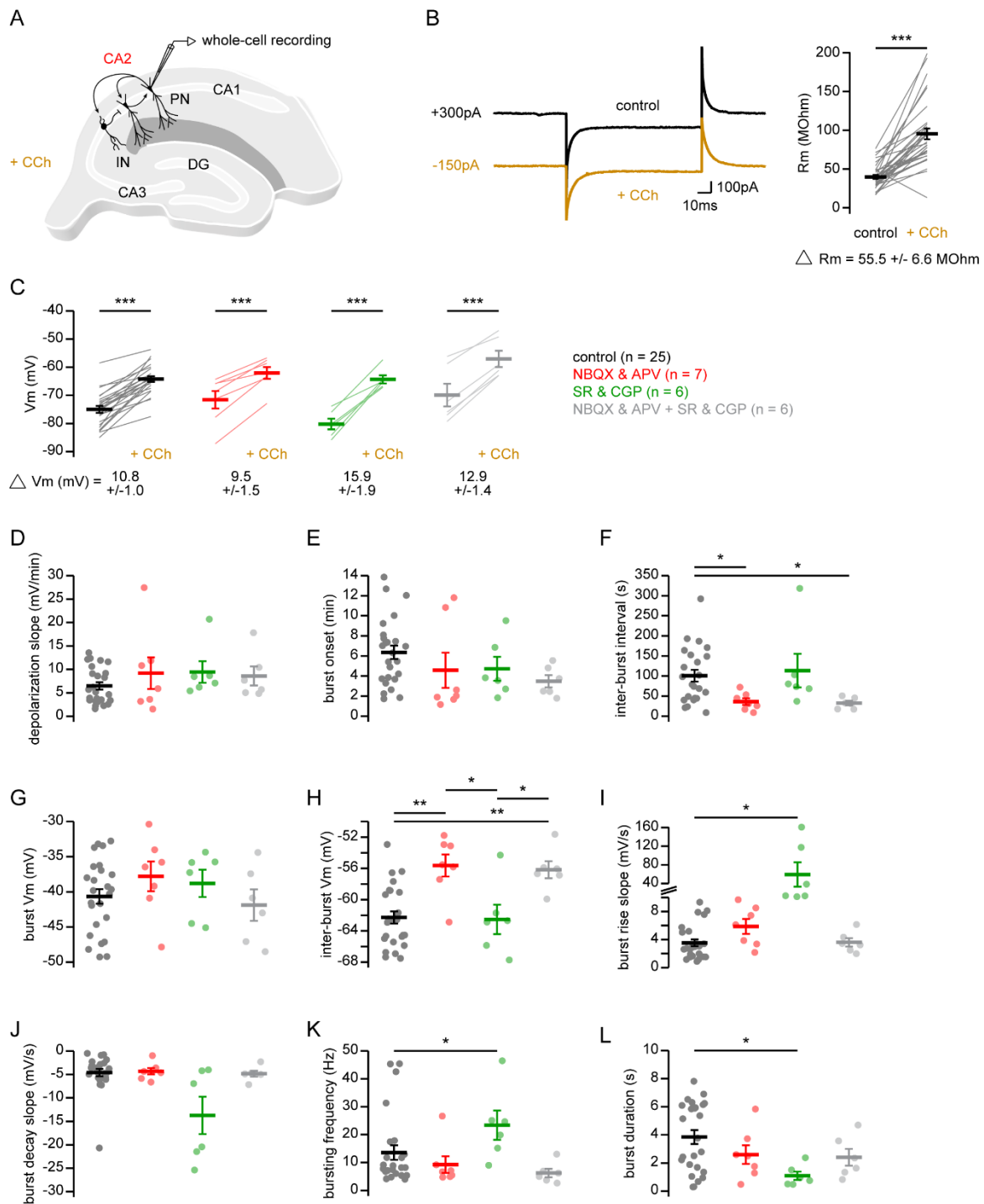


**Figure III.1.5. Characteristics of charbachol-induced CA2 PN spontaneous activity.**

**A.** Diagram illustrating whole-cell recording configuration of CA2 PN in acute hippocampal slices with application of 10  $\mu$ M CCh. **B.** Left, sample traces of the current response of a CA2 PN to a -5 mV hyperpolarizing pulse from -70 mV before and after application of 10  $\mu$ M CCh. Right, comparison of CA2 PNs  $R_m$  before and after application of 10  $\mu$ M CCh (individual cells shown as grey lines, population average shown as horizontal line, error bars represent SEM,  $n = 25$ ; Wilcoxon signed-rank test,  $p < 0.001$ ). **C – L.** Comparisons of CA2 PN  $V_m$  and bursts characteristics with application of 10  $\mu$ M CCh in control (black,  $n = 25$ ), 10  $\mu$ M NBQX & 50  $\mu$ M APV (red,  $n = 7$ ), 1  $\mu$ M SR95531 & 2  $\mu$ M CGP5584A

(green, n = 6) and 10  $\mu$ M NBQX & 50  $\mu$ M APV and 1  $\mu$ M SR95531 & 2  $\mu$ M CGP5584A (grey, n = 6) (individual cells shown as dots, population average shown as horizontal line, error bars represent SEM). **C.**  $V_M$  levels at resting and after the initial depolarization induced by CCh (paired-T tests for ACSF- $V_M$  versus CCh- $V_M$  : control,  $p < 0.001$ ; NBQX & APV,  $p < 0.001$ ; SR95531 & CGP5584A,  $p < 0.001$ ; NBQX & APV and SR95531 & CGP5584A,  $p < 0.001$ ). **D.**  $V_M$  depolarization slope from ACSF- $V_M$  to CCh- $V_M$ . **E.** Burst onset after CCh application. **F.** Inter-burst interval (Kruskal-Wallis test with Dunn-Holland-Wolfe *post hoc* test,  $p = 0.005$ ). **G.** Burst- $V_M$  level. **H.** Inter-burst- $V_M$  levels (1-way ANOVA with Tukey *post hoc* test,  $p < 0.001$ ). **I.** Burst rise slope from inter-burst- $V_M$  to burst- $V_M$  (Kruskal-Wallis test with Dunn-Holland-Wolfe *post hoc* test,  $p < 0.005$ ). **J.** Burst decay slope from burst- $V_M$  to inter-burst- $V_M$ . **K.** AP frequency during bursts (Kruskal-Wallis test with Dunn-Holland-Wolfe *post hoc* test,  $p = 0.014$ ). **L.** Burst duration (Kruskal-Wallis test with Dunn-Holland-Wolfe *post hoc* test,  $p = 0.037$ ).

### Excitatory and inhibitory synaptic transmission contribute to shaping CA2 PN bursting

Given the peculiar bursting behavior observed in CA2 PNs embedded in a network undergoing CCh-induced oscillations, we next examined the contribution of synaptic input to this activity pattern. First, we checked what effect CCh had on excitatory transmission by recording spontaneous excitatory post-synaptic currents (sEPSC) from CA2 PNs (Figure III.1.6A). Voltage-clamp recordings at -70 mV revealed that the sEPSC frequency drastically increased within 5 minutes of CCh application (Figure III.1.6B, Figure III.1.6C and Figure III.1.6D; frequencies were  $1.6 \pm 0.4$  Hz in control and  $7.0 \pm 1.1$  Hz in CCh hence a  $467 \pm 132$  % increase by CCh, n = 8; paired-T test,  $p = 0.002$ ). Interestingly, CCh also affected the frequency distribution of sEPSC which switched from a narrow band of low frequencies to a much broader range of higher frequencies (Figure III.1.6C). Indeed, sEPSC frequencies in CCh extended up to around 15 Hz due to short bouts of excitatory responses reminiscent of the length and firing frequency of CA2 PN bursts (Figure III.1.6B and Figure III.1.6C).

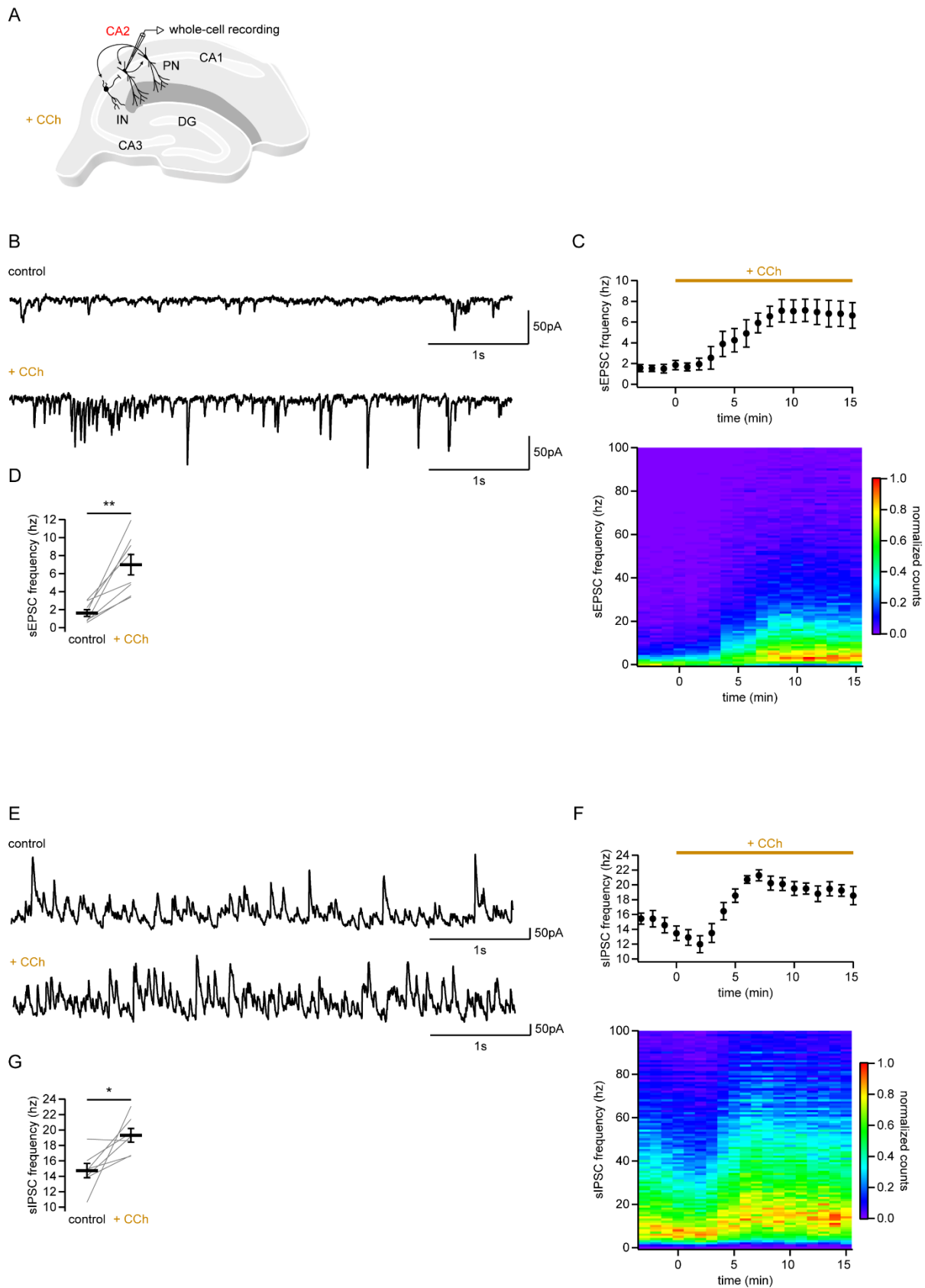


**Figure III.1.6. Effect of CCh on spontaneous excitatory and inhibitory events in CA2 PNs.**

**A.** Diagram illustrating the whole-cell recording configuration of CA2 PN in acute hippocampal slices with application of 10  $\mu$ M CCh. **B.** Sample traces of sEPSCs recorded in a CA2 PN before (top) and

after (bottom) application of 10  $\mu$ M CCh, note high frequency bouts of excitatory events in CCh. **C.** Top, time course of the mean sEPSC frequency recorded in CA2 PNs upon 10  $\mu$ M CCh wash-in (n = 8; error bars represent SEM). Bottom, spectrogram showing the frequency distribution of sEPSCs recorded in CA2 PNs during this time course, warm colors indicate high number of events. **D.** Comparison of sEPSC frequency recorded in CA2 PNs before and after 10  $\mu$ M CCh application (individual cells shown as grey lines, population average shown as horizontal line, error bars represent SEM, n = 8; paired-T test, p = 0.002; error bars represent SEM). **E.** Sample traces of sIPSCs recorded in a CA2 PN before (top) and after (bottom) application of 10  $\mu$ M CCh. **F.** Top, time course of the mean sIPSC frequency recorded in CA2 PNs upon 10  $\mu$ M CCh wash-in (n = 7; error bars represent SEM). Bottom, spectrogram showing the frequency distribution of sIPSCs recorded in CA2 PNs during this time course, warm colors indicate high number of events. **G.** Comparison of sIPSC frequency recorded in CA2 PNs before and after CCh application (individual cells shown as grey lines, population average shown as horizontal line, error bars represent SEM, n = 7; paired-T test, p = 0.026; error bars represent SEM).

Therefore, we assessed the necessity of an intact network for CA2 PNs bursting by blocking all synaptic transmission and isolating area CA2 from CA3 with cuts between both regions in a subset of experiments (Figure III.1.4E). Strikingly, CCh-induced CA2 PNs bursting remained in slices cut between CA2 and CA3 with synaptic transmission blocked (NBQX, APV, SR95531 and CGP55845A) but was somewhat different from control (Figure III.1.4E). We further explored the contributions of synaptic transmission to CA2 PNs bursting on regular slices superfused with NBQX, APV, SR95531 and CGP55845A (Figure III.1.5 and Figure III.1.7A). These experiments confirmed that removing synaptic inputs affected the bursting behavior of CA2 PNs which repolarized less after bursts (Table III.1.1, Figure III.1.5H and Figure III.1.7B; inter-burst- $V_M$  =  $-56 \pm 1.1$  mV in NBQX, APV, SR95531 and CGP55845A, n = 6) leading to an increased bursting rate (Table III.1.1, Figure III.1.5F and Figure III.1.7B; inter-burst intervals =  $36 \pm 5.6$  s in NBQX, APV, SR95531 and CGP55845A, n = 6). Other parameters of CA2 PNs bursting remained unchanged (Table III.1.1, Figure III.1.5 and Figure III.1.7B), indicating that CA2 PNs can intrinsically burst upon CCh application while synaptic inputs contribute to shaping this pattern of activity. As expected, blocking excitatory and inhibitory transmission abolished gamma-like oscillations recorded in the LFP (power in the 20 to 40 Hz band was  $42 \pm 1.8 \mu V^2$  in NBQX, APV, SR95531 and CGP55845A, n = 6; Wilcoxon signed-rank test between before and after CCh, p = 0.22; Mann-Whitney U test versus control, p < 0.001). Consistently, blocking excitatory transmission alone resulted in the same profile of CA2 PNs bursting with only the inter-burst- $V_M$  (Table III.1.1, Figure III.1.5H and Figure III.1.7C; inter-burst- $V_M$  =  $-56 \pm 1.4$  mV in NBQX and APV, n = 7) and inter-burst intervals

(Table III.1.1, Figure III.1.5F and Figure III.1.7C; inter-burst intervals =  $36 \pm 8.3$  s in NBQX and APV,  $n = 7$ ) different from control conditions (Table III.1.1, Figure III.1.5 and Figure III.1.7C). As expected, application of NBQX and APV prevented synchronization of neuronal networks necessary for rhythmogenesis as evidenced by the absence of CCh-induced oscillations in the LFP recording (power in the 20 to 40 Hz band was  $90 \pm 9.5 \mu\text{V}^2$  in NBQX and APV,  $n = 16$ ; Wilcoxon signed-rank test between before and after CCh,  $p = 0.35$ ; Mann-Whitney U test versus control,  $p < 0.001$ ). Hence, although CCh can trigger bursting in CA2 PNs independently of synaptic inputs, excitatory transmission is required for these individual CA2 PN bursts to synchronize and allow network oscillations.

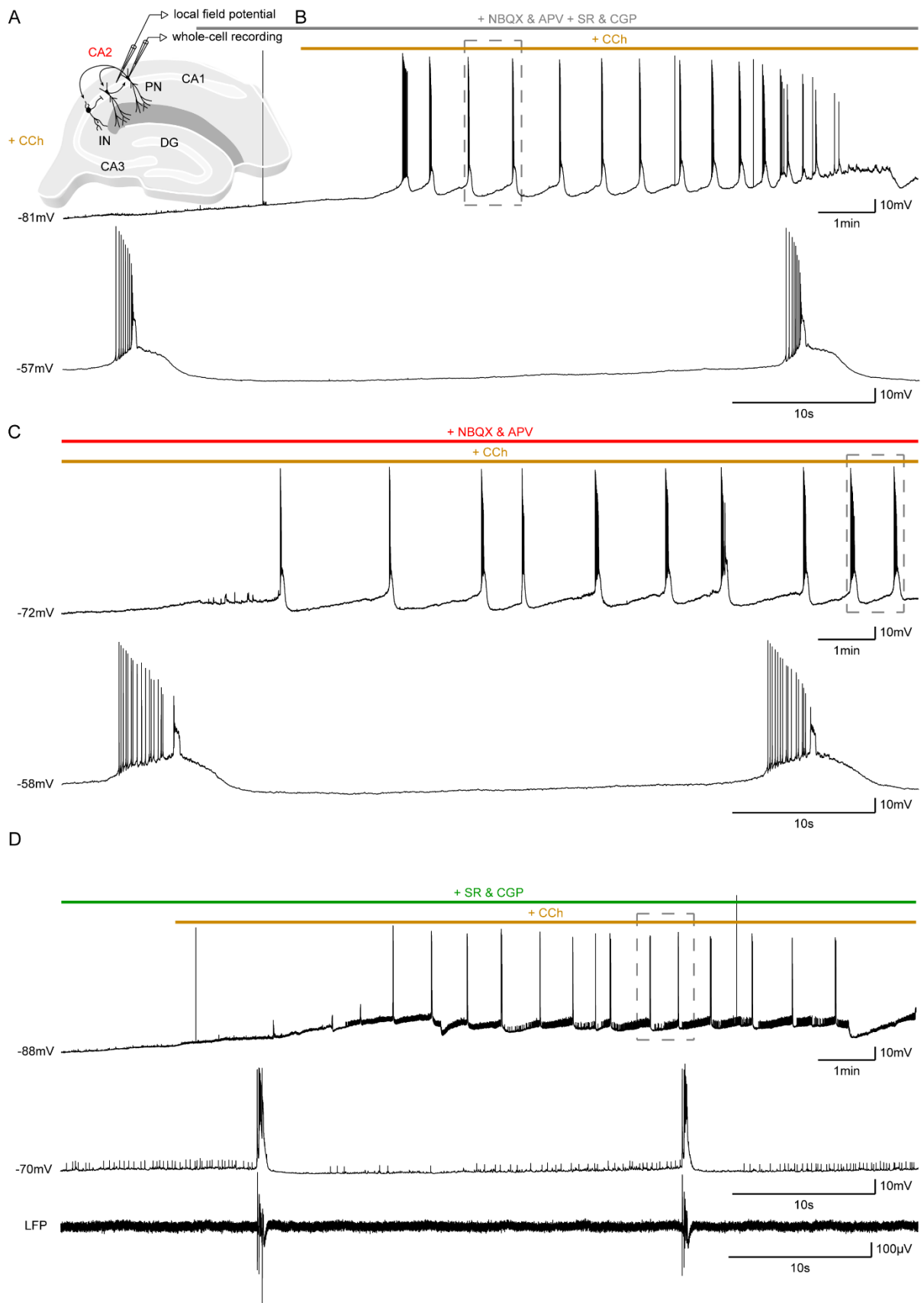


**Figure III.1.7. Excitatory and inhibitory transmission shape bursts of action potentials in CA2 pyramidal cells.**

**A.** Diagram illustrating the simultaneous whole-cell recording configuration of CA2 PNs and LFP recordings from area CA2 SP in acute hippocampal slices with application of 10  $\mu$ M CCh. **B.** Sample trace of AP bursts recorded whole-cell from a CA2 PN following 10  $\mu$ M CCh application with excitatory and inhibitory synaptic transmission blocked by application of 10  $\mu$ M NBQX, 50  $\mu$ M APV, 1  $\mu$ M SR95531 & 2  $\mu$ M CGP5584A (top) and expanded view of the demarcated window (dashed gray box, bottom). **C.** Sample trace of bursts recorded whole-cell from a CA2 PN upon 10  $\mu$ M CCh application with excitatory transmission blocked (top; 10  $\mu$ M NBQX & 50  $\mu$ M APV) and expanded view of the demarcated window (dashed gray box, bottom). **D.** Sample trace of bursts recorded whole-cell from a CA2 PN upon 10  $\mu$ M CCh application with inhibitory synaptic transmission blocked (top; 1  $\mu$ M SR95531 & 2  $\mu$ M CGP5584A) and expanded view of the demarcated window (dashed gray box) with the corresponding LFP recording showing epileptiform-like discharges (bottom).

Another critical component of network oscillations is inhibitory transmission which paces excitation and prevents hyper-synchrony. As previously, we first gauged how inhibitory transmission was affected by CCh by recording spontaneous inhibitory post-synaptic currents (sIPSCs). Monitoring sIPSCs by holding CA2 PNs at a potential of +10 mV showed that CCh application increased the sIPSC frequency within 5 minutes (Figure III.1.6E, Figure III.1.6F and Figure III.1.6G; frequencies were  $15 \pm 0.9$  Hz in control and  $19 \pm 0.9$  Hz in CCh hence a  $36 \pm 15$  % increase by CCh,  $n = 7$ ; paired-T test,  $p = 0.026$ ). In contrast with sEPSC, the distribution of sIPSC across frequency bands did not dramatically change upon application of CCh but rather shifted towards higher frequencies as a whole (Figure III.1.6C and Figure III.1.6F). Hence, we did not observe an obvious link between the sIPSC frequency and the AP bursting of CA2 PNs in CCh. Therefore, we further addressed the role of GABAergic inputs in CCh-induced oscillations in area CA2 by blocking GABA<sub>A</sub> and GABA<sub>B</sub> receptors with SR95531 and CGP55845A. In these conditions, both the LFP and the whole-cell recordings displayed drastic changes which bore signatures of epileptiform events (Figure III.1.7D). Bursts recorded in CA2 PNs became much more sudden and were accompanied by large epileptic waveforms in the LFP which no longer held gamma power (power in the 20 to 40 Hz band was  $61 \pm 11$   $\mu$ V<sup>2</sup> in SR95531 and CGP55845A,  $n = 10$ ; Wilcoxon signed-rank test between before and after CCh,  $p = 0.63$ ; Mann-Whitney U test versus control,  $p < 0.001$ ). More precisely, removal of inhibitory synaptic transmission lead to faster kinetics (Table III.1.1, Figure III.1.5I, Figure III.1.5J and Figure III.1.7D; burst rise slope =  $59 \pm 26$  mV/s in SR95531 and CGP55845A,  $n = 6$ ; burst decay slope =  $-13.7 \pm 4.0$  mV/s in SR and CGP,  $n = 6$ ) and shorter

duration of CA2 PNs bursts (Table III.1.1, Figure III.1.5L and Figure III.1.7D; burst duration =  $1.1 \pm 0.3$  s in SR95531 and CGP55845A,  $n = 6$ ). Furthermore, the bursting frequency was increased in these conditions (Table III.1.1, Figure III.1.5K and Figure III.1.7D; bursting frequency =  $23 \pm 5.2$  Hz in SR95531 and CGP55845A,  $n = 6$ ), thus indicating a role for inhibition in pacing action potential firing during bursts. With inhibition removed, hyper-synchrony emerges in the network leading to very short and sudden bursts of action potentials instead of parsed activity (Figure III.1.7D). Thus, rhythmogenesis in area CA2 relies on a physiological E/I balance brought about by synaptic input that shapes the intrinsic bursting of CA2 PN following CCh application.

#### Action potential firing relation to the field oscillation

Because synaptic transmission is critical for CCh-induced network oscillations and affects CA2 PNs bursting behavior, we further analyzed the relationship between bursts of action potentials in CA2 PNs and the concurrent field oscillation (Figure III.1.8A). First, as ongoing gamma oscillations typically vary their power and peak frequency with time, we investigated whether either parameter differed during CA2 PNs bursts as compared to intervals between bursts. Wavelet analysis of LFP signal relative to CA2 PNs bursting revealed no changes in gamma magnitude or peak frequency related to bursts (wavelet magnitudes were  $0.25 \pm 0.03$  during bursts and  $0.24 \pm 0.3$  between bursts,  $n = 29$ ; Wilcoxon signed-rank test,  $p = 0.29$ ; peak frequencies were  $27 \pm 0.7$  Hz during bursts and  $26 \pm 0.7$  Hz between bursts,  $n = 29$ ; Wilcoxon signed-rank test,  $p = 0.62$ ). This indicates that, although synaptic inputs impact both network oscillations and CA2 PNs bursting, bursts of action potentials in CA2 PNs do not reflect epochs of increased synchronous network activity. However, it is well documented that different neuronal populations preferentially fire action potentials at specific phases of the gamma oscillation (Csicsvari et al., 2003; Mann et al., 2005; Oren et al., 2006; Zemankovics et al., 2013), a phenomenon that relates neuronal activity and synaptic inputs to the activity of the networks they are embedded in. Classically, CA3 PNs fire shortly after the trough of slow gamma oscillations recorded from SP ex vivo (Oren et al., 2006; Zemankovics et al., 2013) while CA3 interneurons prefer later phases (Oren et al., 2006; Zemankovics et al., 2013). In order to check if these relations of phase-coupling firing of neurons with the oscillation were present in CA2 PNs as well, we extracted the timing of action potential firing relative to the CCh-induced oscillation during bursts (Figure III.1.8B). We found that the more than half of CA2 PNs had their firing modulated by the field oscillation during bursts (55.2 %,  $n = 16 / 29$ ).

Examination of individual bursts from each CA2 PN revealed that action potential firing showed significant phase coupling only in a fraction of bursts ( $18.5 \pm 3.4\%$ ,  $n = 16$ ) which was selected for further analysis (Figure III.1.8C). During these bursts, CA2 PNs showed a significant phase preference of  $-2.6 \pm 0.2$  radians ( $n = 16$ ; Rayleigh test,  $p < 0.001$ ) hence near the trough of the gamma-like oscillation which defined  $-\pi/\pi$  phase (Figure III.1.8B and Figure III.1.8D). Thus, this result establishes that the pattern of action potential firing within a burst is dictated by the ongoing network activity.

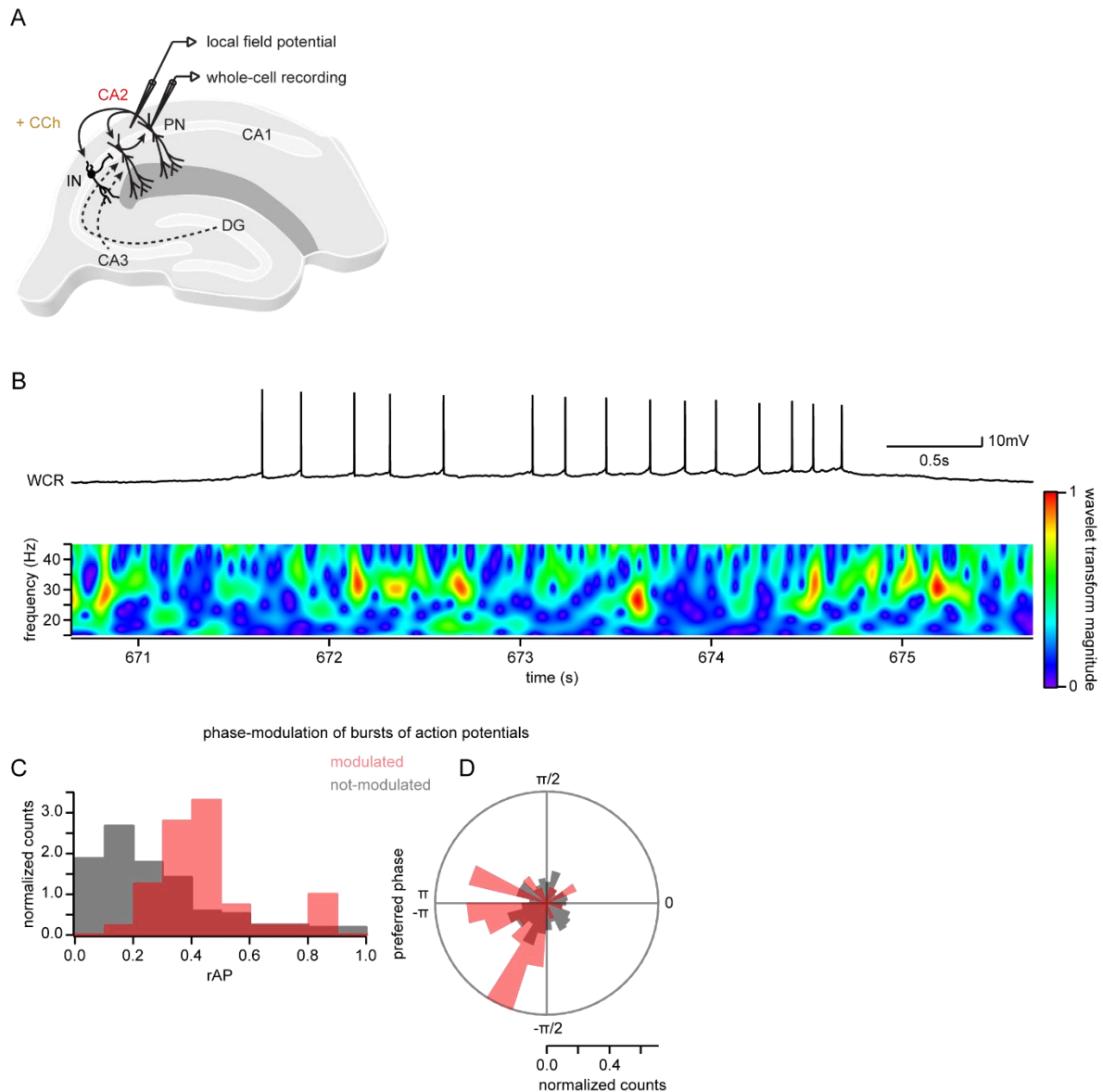


**Figure III.1.8. Bursts of action potentials in CA2 pyramidal cells are modulated by the ongoing field oscillation.**

**A.** Diagram illustrating the simultaneous whole-cell recording configuration of CA2 PNs and LFP recordings from area CA2 SP in acute hippocampal slices with application of 10  $\mu\text{M}$  CCh. **B.** Sample trace of a burst recorded in a CA2 PN (top) and the corresponding normalized magnitude components

of the wavelet transform of the LFP recorded from area CA2 SP (bottom). **C.** Normalized histograms of the modulation strength of action potentials coupling during significantly (red) and non-significantly (black) modulated bursts. **D.** Normalized circular histogram of the preferred phase of action potential firing during significantly (red;  $n = 16$ ; Rayleigh test,  $p < 0.001$ ) and non-significantly (black) modulated bursts.

## **III.2 - Hypothalamic control of hippocampal area CA2 activity by direct excitation and feedforward inhibition**

### **III.2.a - Introduction**

The hippocampus is critical for memory formation and spatial navigation (Buzsáki and Moser, 2013; Eichenbaum and Cohen, 2014), yet basic questions persist regarding the circuitry and cellular components allowing these processes. In particular, it has recently been discovered that area CA2 of the hippocampus forms the basis of a hippocampal-wide network that encodes location during immobility and sleep (Kay et al., 2016). Furthermore, lesions in area CA2 result in reduced social memory (Hitti and Siegelbaum, 2014; Stevenson and Caldwell, 2014). Immediate-early gene expression studies have shown that this area may detect conflict between present and previous experience (Wintzer et al., 2014). In contrast to areas CA1 and CA3, the place cell activity (Alexander et al., 2016; Lee et al., 2015; Lu et al., 2015; Mankin et al., 2015), hippocampal connectivity of area CA2 (Chevaleyre and Siegelbaum, 2010; Kohara et al., 2013) and synaptic plasticity (Piskorowski and Chevaleyre, 2013; Zhao et al., 2007) in this region have only very recently begun being examined *ex vivo* and *in vivo*.

The hypothalamic supramammillary nucleus (SuM) has been shown to project to the dentate gyrus (DG) and hippocampal area CA2 in several species, including rodents and humans (Berger et al., 2001; Haglund et al., 1984; Wyss et al., 1979). There is evidence that the SuM is involved in learning processes, as spatial memory is impaired following silencing of the SuM with pharmacological methods (Aranda et al., 2008; Shahidi et al., 2004) or lesions (Aranda et al., 2006). Furthermore, analysis of cFos expression revealed that this nucleus is highly activated by exposure to a novel environment (Ito et al., 2009). Under urethane anesthesia, SuM neurons fire bursts of action potentials (AP) phase-locked with the hippocampal theta rhythm (Kocsis and Vertes, 1994). The SuM plays a prominent role in the modulation of the hippocampal theta-frequency (Pan and McNaughton, 1997; 2002), possibly by its direct projection to the hippocampus, or by modulation of the medial septum (Borhegyi and Freund, 1998; Vertes, 1992). Serotonin depletion of the SuM leads to deficiencies in spatial learning in the morris water maze, and results in altered hippocampal theta activity (Gutiérrez-Guzmán et al., 2012; Hernández-Pérez et al., 2015).

Even with the anatomical and *in vivo* data, the properties and consequences of SuM activation on area CA2 activity remain unexplored. In this study, we use a combination of histological, *ex*

*in vivo* electrophysiological and optogenetic approaches, to specifically examine the effects of SuM input stimulation on neuronal activity in hippocampal area CA2. We used a viral retrograde approach to identify the SuM cells that project to area CA2 in mice. Then, we used viral injections of Cre-dependent constructs in the SuM of VGlut2-Cre and Csf2rb2-Cre transgenic mice to selectively express channelrhodopsin-2. We performed whole-cell patch-clamp recordings in hippocampal slices from these mice while photostimulating SuM axons to examine their targets and the consequences of their activation in area CA2. We found that SuM axons target both pyramidal neurons (PNs) and interneurons (INs) to which they provide glutamatergic excitation. The SuM excitatory drive was significantly stronger on basket cell-type INs than any other neuronal population. Consequently, we observed substantial feedforward inhibition onto PNs recruited by SuM stimulation. In addition, the excitatory/inhibitory drive from SuM was more inhibitory in deep compared to superficial PN subpopulations, regardless of their CA2 or CA3 morphology. Finally, we found that this inhibition was capable of modulating the action potential jittering of CA2 and CA3a PNs, and thus is likely capable of modulating excitability in this area of the hippocampus.

### **III.2.b - Results**

The supramammillary projection to the hippocampus has been described in retrograde and anterograde studies in the rat, guinea pig and monkey (Borhegyi et al., 1997; Haglund et al., 1984; Kiss et al., 2000; Soussi et al., 2010). In order to determine which cells in the mouse SuM project to hippocampal area CA2, we injected a retrograde canine adenovirus type 2 (CAV-2) into area CA2 of the hippocampus to permit the expression of Cre-recombinase (Cre) in hippocampal-projecting SuM neurons, and an adeno-associated virus (AAV) was injected into the SuM to allow the expression of EGFP under the control of Cre (Figure III.2.1A). In 5 animals the injection of retrograde CAV-2 was sufficiently targeted to area CA2, as indicated by the presence of EGFP-expressing SuM axonal fibers primarily in this hippocampal area (Figure III.2.1B). We stained for calretinin to define the boundaries of the SuM nucleus, and put our mouse anatomical data in context with the anatomical studies from rat (Pan and McNaughton, 2004). Consistent with what has been described, CA2-projecting cells in the SuM are located in the medial regions. These cells were located bilaterally, ventral to the fiber bundles that traverse the SuM (Figure III.2.1C). Furthermore, we found that the majority of these cells were positive for calretinin (Figure III.2.1D).

In order to functionally investigate the SuM projection to area CA2, we used an anterograde strategy in two separate transgenic mouse lines (Figure III.2.1E). It has been shown that the source of vesicular glutamate transporter 2 (VGluT2)-immunopositive boutons in area CA2 originate from the SuM (Halasy et al., 2004), as shown in Figure III.2.2. To further assess where these VGluT2-expressing SuM cells project into the hippocampus, we injected an AAV to express channelrhodopsin(H143R)-YFP (ChR2-EYFP) under the control of Cre recombinase into the SuM of a transgenic mouse line with Cre expression controlled by the VGluT2 promoter, the Tg(Slc17ab-icre)10Ki line (Borgius et al., 2010). In parallel, we used a novel mouse line, the Csf2rb2-Cre line that selectively expresses Cre recombinase in the SuM. We found that with both strategies we could reproducibly restrict expression of ChR2-EYFP in the SuM, and avoid infecting nearby hypothalamic regions that also may project to the hippocampus (Figure III.2.1F). In a subset of experiments involving PV-Cre animals, we used targeted injections of an AAV to express hSyn.hChR2(H134R).EYFP in all SuM neurons regardless of their Cre expression. For all experiments, injection sites were examined *post hoc* to ensure correct targeting of the SuM. With both the VGluT2-Cre and Csf2rb2-Cre lines of transgenic mice, we observed identical patterns of SuM fiber localization in the hippocampus. EYFP-containing SuM axons were found throughout the supragranular layer of the DG and in area CA2 (Figure III.2.1G) where they clustered around the pyramidal layer (stratum pyramidale, SP) and spread in stratum radiatum (SR) consistent with anterograde studies in rats and primates (Berger et al., 2001; Borhegyi and Leranth, 1997b; 1997a; Halasy et al., 2004; Kiss et al., 2000; Soussi et al., 2010). In the CA regions, the SuM fiber projection area was clearly restricted to area CA2, as defined by expression of the CA2-specific markers PCP4 and RGS14, and did not spread to neighboring areas CA3 and CA1 (Figure III.2.1B and Figure III.2.1G). In order to maximize the precision of our experiments, we frequently only achieved partial infection of the SuM nucleus, as indicated by the sparseness of ChR2-EYFP-containing fibers in comparison to the number of VGluT2-stained boutons in this region (Figure III.2.2B and Figure III.2.2C).

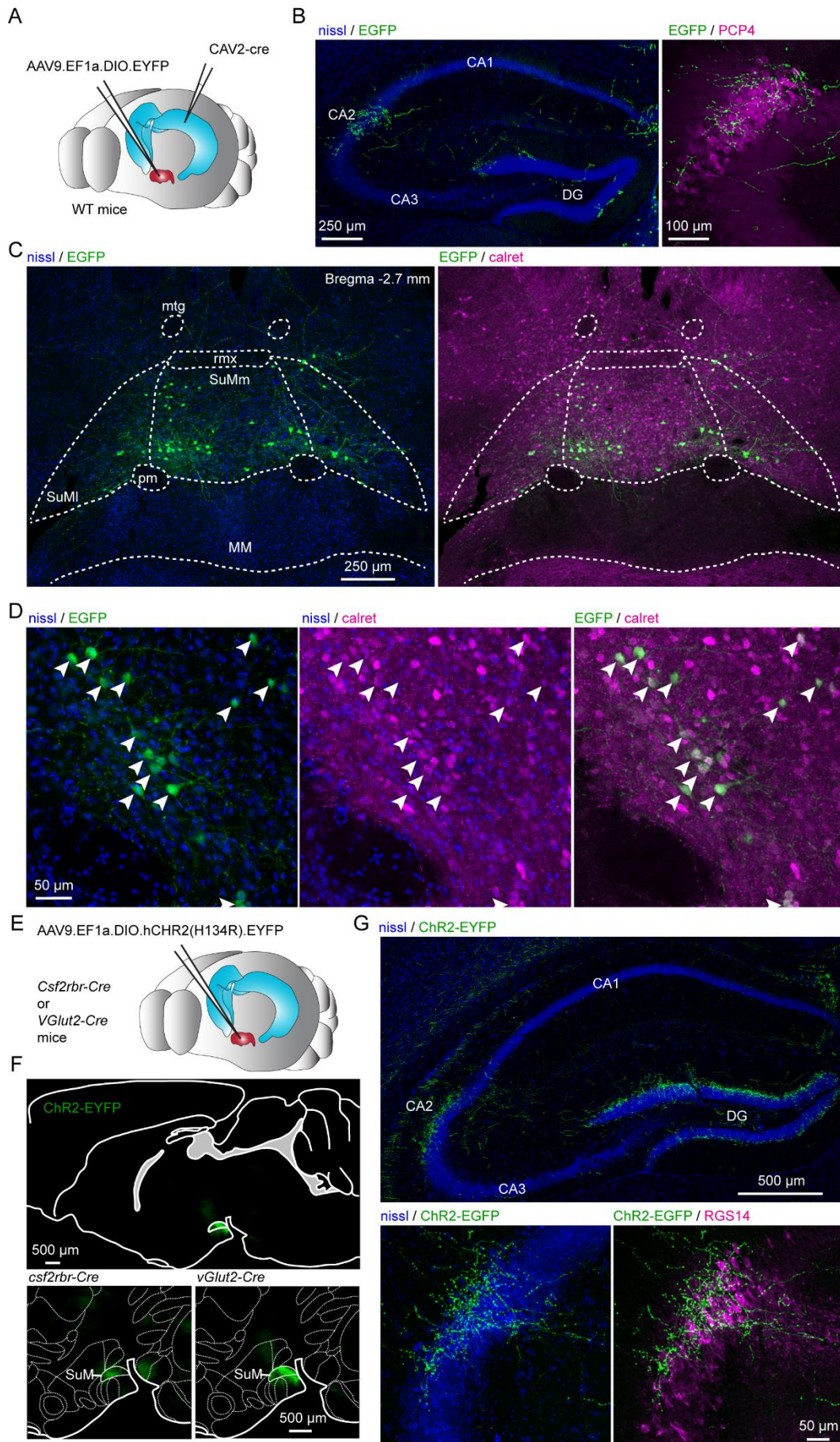


**Figure III.2.1. Selective labeling of SuM neurons that project to hippocampal area CA2.**

**A.** Diagram illustrating the method to selectively label SuM neurons. An AAV allowing the Cre-driven expression of EGFP was injected into the SuM and a retrograde CAV-2 allowing the expression of Cre recombinase was injected into area CA2 of the dorsal hippocampus. **B.** Left, coronal image of hippocampus showing the SuM fibers expressing EGFP (green), and nissl staining (blue). Right, image of area CA2 showing the SuM fibers expressing EGFP (green) and PCP4 staining (magenta) to label area CA2. **C.** Retrograde-labeled SuM neurons that project to hippocampal area CA2. Left, nissl staining (blue) and EGFP expression (green) resulting from dual-infection with the AAV and retrograde CAV-2 Cre-recombinase. Right, calretinin staining (magenta) and EGFP expression (green) in SuM. **D.** Higher magnification image of CA2-projecting neurons in SuM. Left, nissl staining (blue) and EGFP-labeled SuM cells (green). Center, nissl staining (blue) and calretinin labeling (magenta). Right, EGFP-labeled cells (green) and calretinin labelled cells (magenta), arrowheads indicate EGFP-expressing cells. Example results shown, this experiment was repeated with similar results in five mice. **E.** Cartoon illustrating the injection of AAVs into the SuM. **F.** Sagittal image indicating the infected SuM area expressing hCHR2(H134R)-EYFP (green) in VGluT2-Cre (top) and Csf2rbr-Cre (bottom) mouse lines. **G.** Top, hCHR2(H134R)-EYFP -expressing SuM fibers (green) and nissl staining (blue) in the hippocampus. Bottom left, higher magnification image of area CA2 with hCHR2(H134R)-EYFP -expressing SuM fibers (green) and nissl staining (blue); bottom right, hCHR2(H134R)-EYFP -expressing SuM fibers (green) and RGS14 staining (magenta) to label area CA2.

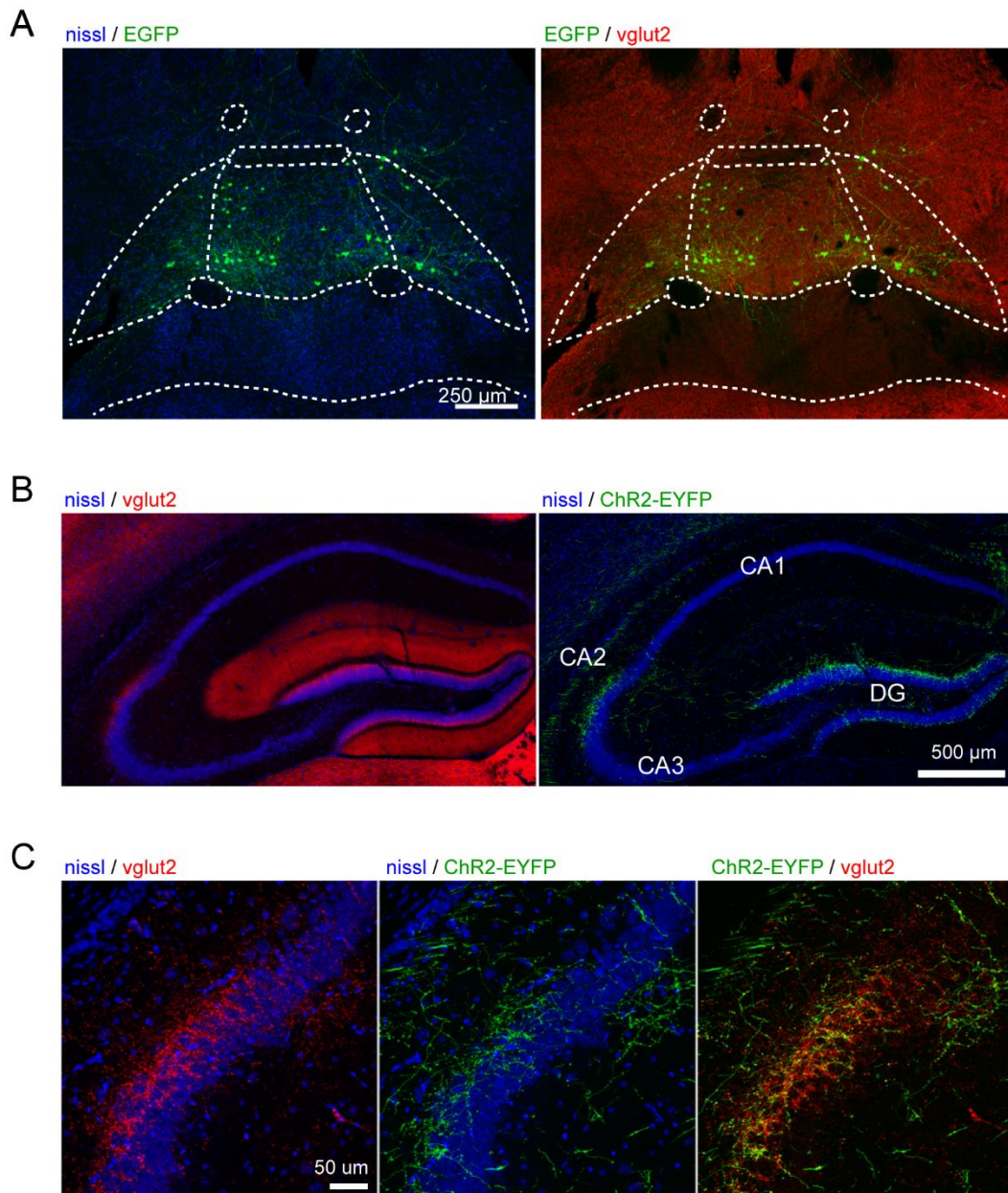


**Figure III.2.2. CA2-projecting SuM neurons express VGLuT2.**

**A.** Retrograde-labelled SuM neurons that project to area CA2. Left, nissl staining (blue) and EGFP expression (green) resulting from dual-infection with the AAV and retrograde CAV-2 Cre-recombinase. Right, VGLuT2 staining (red) and EGFP expression (green) in SuM. **B.** Anterograde-labelled VGLuT2-positive SuM fibers in the hippocampus. Left, VGLuT2 (red) and nissl (blue) staining in the hippocampus. Right, hCHR2(H134R)-EFYP expressing SuM fibers (green) and nissl (blue) staining in the hippocampus. **C.** Higher magnification image of anterograde-labelled VGLuT2-positive SuM fibers in area CA2. Left, VGLuT2 (red) and nissl (blue) staining. Center, hCHR2(H134R)-EFYP expressing SuM fibers (green) and nissl staining (blue). Right, hCHR2(H134R)-EFYP expressing SuM fiber (green) and VGLuT2 staining (red).

### SuM axons provide excitatory glutamatergic input to pyramidal neurons in area CA2

In order to better understand the cellular targets and consequences of SuM input activity in area CA2, we applied the above experimental strategy to express ChR2-EYFP in SuM axonal fibers and activated projecting axons with pulses of 440 nm light in acute hippocampal slices while performing whole-cell patch-clamp recordings of PNs across the hippocampal CA regions (Figure III.2.3A). Following all recordings, we performed post-hoc anatomical reconstructions of recorded cells and axonal fibers (Figure III.2.4), as well as immunohistochemical stainings for CA2-area markers.

We observed that photostimulation of SuM axons elicited excitatory post-synaptic responses in 63 % of PNs ( $n = 166$  of 263 cells) located in area CA2 (Figure III.2.3B). PNs recorded in CA1 (3 %,  $n = 1$  of 36 cells) and CA3b (0 %,  $n = 0$  of 11) further away from the site of SuM fibers innervation showed no excitatory responses, revealing the specificity of SuM inputs to area CA2. PNs in this region shared similar overall dendritic morphologies but differed along two criteria. First, in stratum lucidum some PNs clearly had thorny excrescences (TE) while others had very smooth apical dendrites (Figure III.2.3C and Figure III.2.3D). Based on the presence of TEs, we classified cells as CA2 or CA3 PNs (unequivocal distinction was possible in 148 of 263 cases). Examination of electrophysiological properties of these cells revealed a higher membrane resistance in CA3 PNs than CA2 PNs, but membrane capacitance and resting membrane potential were similar (Table III.2.1, Table III.2.2). Second, the distribution of the locations of PN soma along the radial axis of the hippocampus allowed us to cluster them as deep (closer to stratum oriens, SO) or superficial (closer to stratum radiatum, SR) subpopulations (unequivocal distinction was possible in 157 neurons). Deep and superficial cells showed no differences in electrophysiological properties (Table III.2.1 and Table III.2.2). We found that the connectivity was not different between CA2 and CA3 PNs or between deep and superficial PNs (Table III.2.3 and Table III.2.4). Light-evoked excitatory post-synaptic potentials (EPSPs) and excitatory post-synaptic currents (EPSCs) recorded at -70 mV were of fairly small amplitude (Figure III.2.3C and Figure III.2.3D) that were similar regardless of the PN type or somatic location (Table III.2.3 and Table III.2.4). This small amplitude was not due to under-stimulation of SuM axons as EPSC amplitudes rapidly reached a plateau when increasing light intensity (Figure III.2.3E). We are confident that this transmission is due to action potential-generated vesicle release because all transmission was blocked following application of 0.2  $\mu$ M tetrodotoxin (TTX) (Figure III.2.3E). The pure glutamatergic nature of the SuM input was confirmed by the complete block of light-evoked synaptic transmission

following the application of 10  $\mu\text{M}$  NBQX and 50  $\mu\text{M}$  D-APV (Figure III.2.3F; amplitudes were  $16 \pm 4.8$  pA in control and  $1.8 \pm 0.3$  pA in NBQX & D-APV hence a  $89 \pm 3.5$  % block by NBQX & D-APV,  $n = 6$ ; Wilcoxon signed-rank test,  $p = 0.03$ ). These data confirm that SuM inputs provide long-range glutamatergic excitation to CA2 and CA3 PNs in area CA2.

**Table III.2.1. Electrophysiological properties of pyramidal neurons in SuM innervated area**

	$V_M$ (mV)	$R_M$ (MOhm)	$C_M$ (pF)
CA2 PN ( $n = 81$ )	$-69.8 \pm 0.70$	$59.2 \pm 2.65$	$209 \pm 11.4$
CA3 PN ( $n = 31$ )	$-70.3 \pm 1.06$	$72.4 \pm 4.82$	$211 \pm 15.7$
Statistics	Mann-Whitney U test $p = 0.997$	Student T test $p = 0.020^*$	Mann-Whitney U test $p = 0.625$
PN deep ( $n = 57$ )	$-71.1 \pm 0.76$	$64.0 \pm 3.94$	$200 \pm 12.3$
PN superficial ( $n = 76$ )	$-69.3 \pm 0.67$	$64.9 \pm 3.19$	$196 \pm 11.8$
Statistics	Student T test $p = 0.077$	Mann-Whitney U test $p = 0.777$	Mann-Whitney U test $p = 0.588$

**Table III.2.2. Properties of deep and superficial pyramidal neurons in areas CA2 and CA3a**

	$V_M$ (mV)	$R_M$ (MOhm)	$C_M$ (pF)
CA2 PN deep ( $n = 30$ )	$-71.4 \pm 0.95$	$55.1 \pm 3.88^*$	$223 \pm 18.6$
CA2 PN superficial ( $n = 47$ )	$-68.6 \pm 0.94$	$61.8 \pm 3.65$	$204 \pm 15.6$
CA3 PN deep ( $n = 17$ )	$-71.2 \pm 1.68$	$68.2 \pm 5.47$	$204 \pm 14.7$
CA3 PN superficial ( $n = 14$ )	$-69.2 \pm 1.16$	$77.4 \pm 8.40^*$	$219 \pm 30.4$
Statistics	1-way ANOVA $p = 0.18$	1-way ANOVA $p = 0.037$ Tukey <i>post hoc</i> $p = 0.030^*$	1-way ANOVA $p = 0.85$

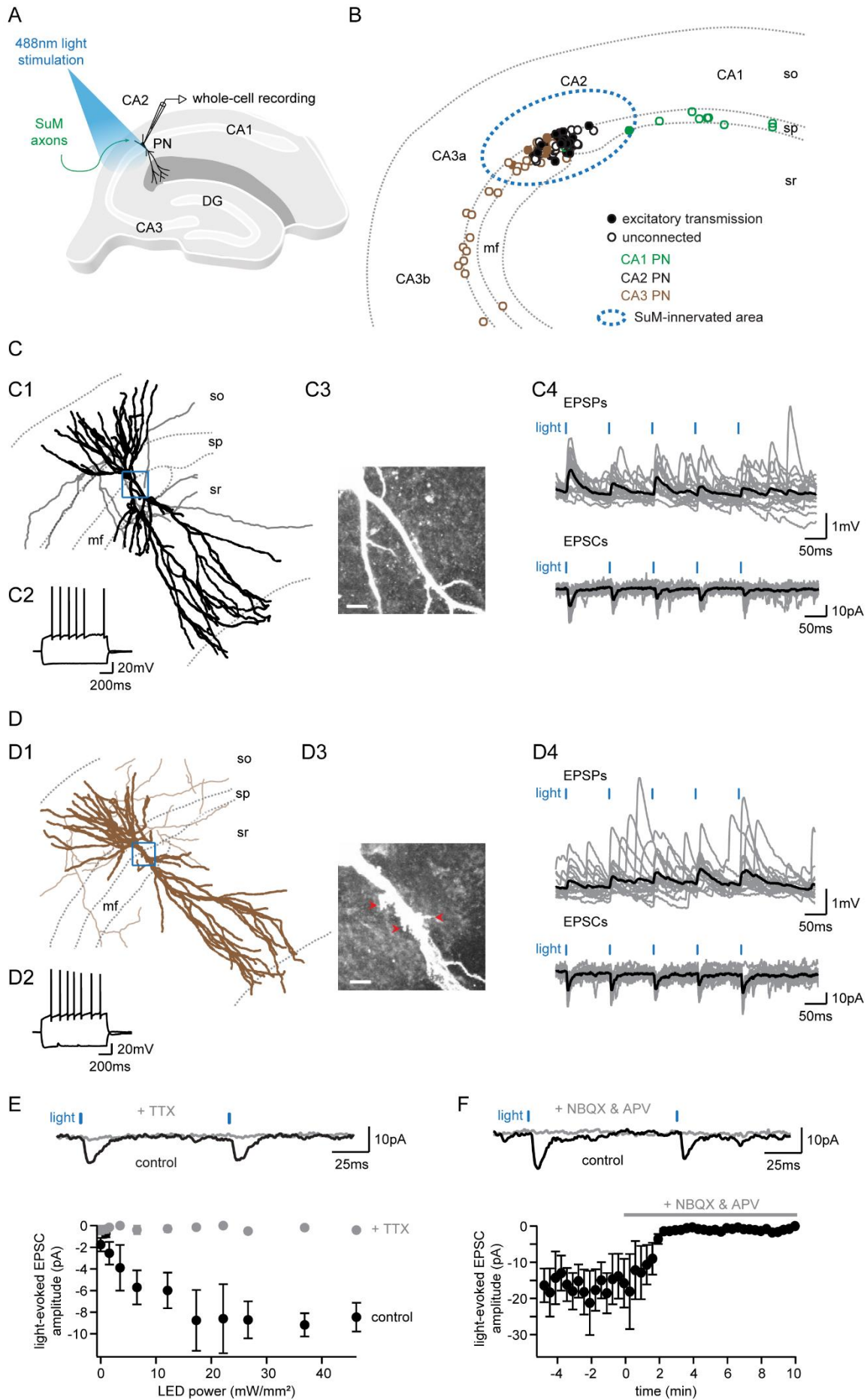
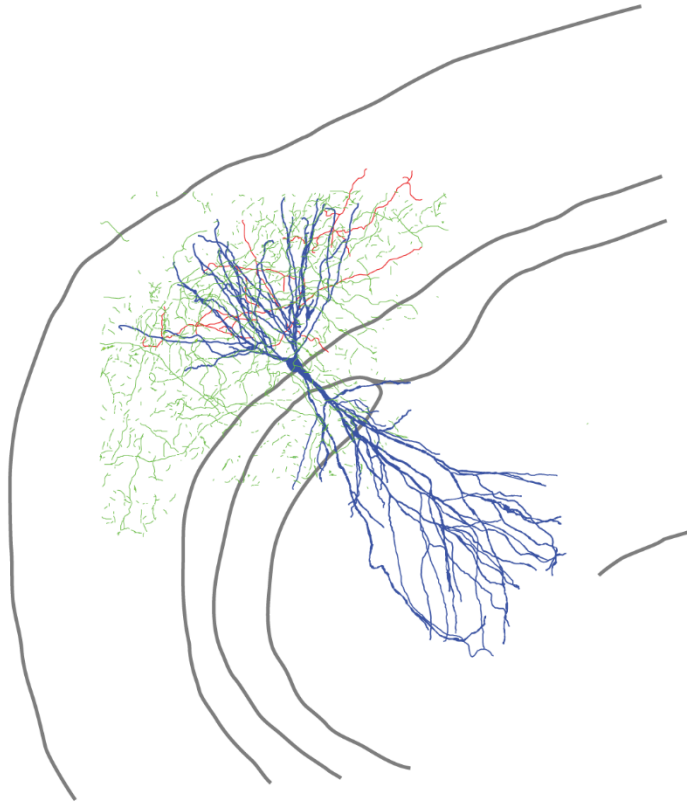


**Figure III.2.3. SuM input provides excitatory glutamatergic transmission to diverse population of PNs in area CA2.**

**A.** Diagram illustrating the whole-cell recording configuration of PNs in area CA2 and SuM fiber stimulation in acute hippocampal slices. **B.** Diagram mapping the location of several PNs recorded in the hippocampus with closed circles indicating connected cells, and open circles indicating no detected transmission. Cells were classified as CA1, CA2 and CA3 based on morphology and location, color indicates cell type, area circled in dotted blue represents region innervated by SuM. **C.** CA2 pyramidal neurons in the SuM-innervated region receive excitatory transmission. **C1.** Example CA2 PN reconstruction (dendrites in black, axons in grey, hippocampal stratum borders shown in dotted line, area demarcated in blue corresponds to the expanded image in **C3**). **C2.** AP firing and repolarizing sag current in response to steps of 800 and -400 pA current injection. **C3.** Biocytin labeling of the recorded cell proximal dendrites, note the absence of TEs, scale bar represents 10  $\mu\text{m}$ . **C4.** Light-evoked EPSPs (top traces, individual traces shown in grey, average trace shown in black) and EPSCs (bottom traces, individual traces shown in grey, average trace shown in black). **D.** CA3 pyramidal neurons in the SuM-innervated region receive excitatory transmission. **D1.** Example CA3 PN reconstruction (dendrites in brown, axons in light brown, hippocampal stratum borders shown in dotted line, area demarcated in blue corresponds to the expanded image in **D3**). **D2.** AP firing and repolarizing sag current in response to steps of 800 and -400 pA current injection. **D3.** Biocytin labeling of the recorded cell proximal dendrites, note the presence of TEs, as indicated by the red arrows; scale bar represents 10  $\mu\text{m}$ . **D4.** Light-evoked EPSPs (top traces, individual traces shown in grey, average trace shown in black) and EPSCs (bottom traces, individual traces shown in grey, average trace shown in black). **E.** Light-evoked EPSCs from SuM inputs are completely blocked following application of tetrodotoxin (TTX). Sample traces (top, control shown in black, +TTX shown in grey) and power-response curves (bottom) of light-evoked EPSC amplitudes recorded in PN before (black) and after application of 0.2  $\mu\text{M}$  TTX (grey) at different light intensities ( $n = 5$ , error bars represent SEM). **F.** Light-evoked EPSCs from SuM inputs are completely blocked following application of NMDA and AMPA receptor blockers (NBQX & APV). Sample traces (top, control shown in black, NBQX & APV shown in grey) and time course (bottom) of light-evoked EPSC amplitudes upon application of 10  $\mu\text{M}$  NBQX & 50  $\mu\text{M}$  APV ( $n = 6$ , error bars represent SEM).

A



B

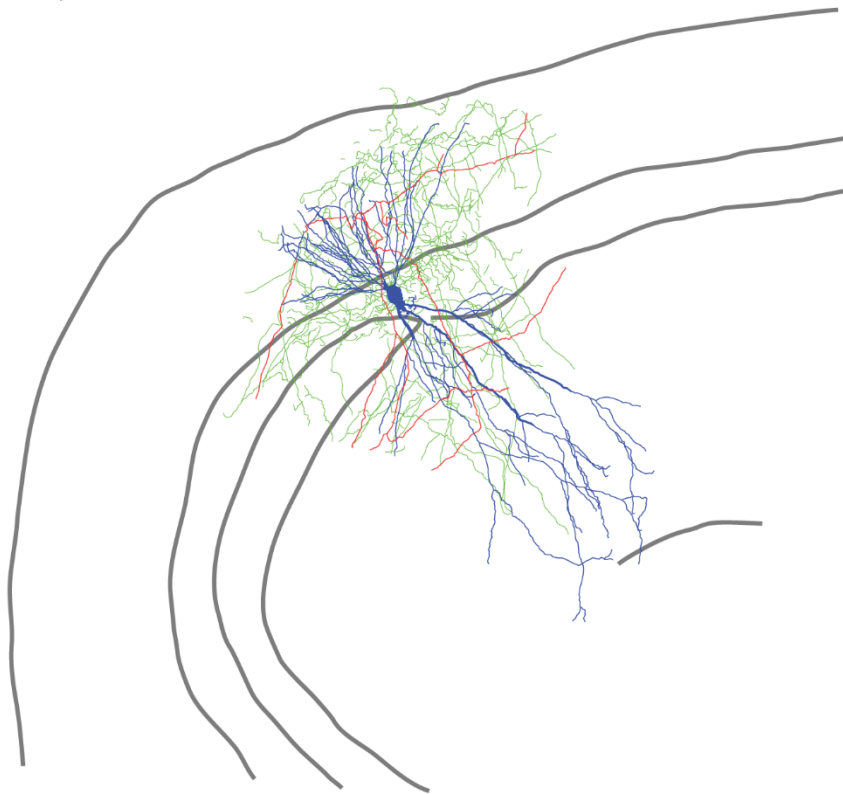


**Figure III.2.4. Reconstruction of pre-synaptic SuM fibers and post-synaptic PNs in area CA2.**

**A, B.** Example reconstructions of PNs and hCHR2(H134R)-EFYP expressing SuM fibers in area CA2 (dendrites shown in blue, axon in red, SuM fibers in green, hippocampal stratum borders in black).

**Table III.2.3. Characteristics of SuM light-evoked transmission onto PNs in area CA2.**

<b>EPSC</b>						
cell type	connectivity (%)	amplitude (pA)	rise time (ms)	decay time (ms)	latency (ms)	success rate
CA2 PN	56 (n = 58 of 103)	16 ± 1.9	2.9 ± 0.1	14 ± 0.8	2.4 ± 0.2	0.44 ± 0.03
CA3 PN	49 (n = 22 of 45)	23 ± 5.9	3.0 ± 0.2	14 ± 0.9	2.7 ± 0.3	0.56 ± 0.06
Statistics	$\chi^2$ test p = 0.572	Mann-Whitney U test p = 0.409	Mann-Whitney U test p = 0.391	Mann-Whitney U test p = 0.797	Mann-Whitney U test p = 0.156	Student T test p = 0.074
PN deep	56 (n = 35 of 63)	15 ± 2.0	3.5 ± 0.2	16 ± 1.0	3.5 ± 0.4	0.39 ± 0.03
PN superficial	56 (n = 53 of 94)	20 ± 3.0	3.1 ± 0.2	15 ± 0.9	2.7 ± 0.3	0.51 ± 0.04
Statistics	$\chi^2$ test p = 0.946	Mann-Whitney U test p = 0.306	Mann-Whitney U test p = 0.051	Mann-Whitney U test p = 0.314	Mann-Whitney U test p = 0.083	Mann-Whitney U test p = 0.072
<b>IPSC</b>						
cell type	connectivity (%)	amplitude (pA)	rise time (ms)	decay time (ms)	latency (ms)	success rate
CA2 PN	35 (n = 19 of 55)	197 ± 41.3	3.8 ± 0.4	25 ± 1.2	6.3 ± 0.7	0.55 ± 0.06
CA3 PN	57 (n = 16 of 28)	145 ± 23.4	4.5 ± 0.4	25 ± 1.2	7.5 ± 0.9	0.54 ± 0.05
Statistics	$\chi^2$ test p = 0.134	Mann-Whitney U test p = 0.870	Student T test p = 0.203	Mann-Whitney U test p = 0.896	Mann-Whitney U test p = 0.303	Student T test p = 0.893
PN deep	47 (n = 16 of 34)	199 ± 40.6	3.8 ± 0.4	25 ± 1.4	7.2 ± 0.8	0.52 ± 0.07
PN superficial	47 (n = 26 of 55)	167 ± 27.5	4.9 ± 0.4	26 ± 1.2	6.8 ± 0.7	0.50 ± 0.05
Statistics	$\chi^2$ test p = 0.987	Mann-Whitney U test p = 0.258	Student T test p = 0.047*	Student T test p = 0.564	Student T test p = 0.706	Student T test p = 0.796

**Table III.2.4. Characteristics of SuM light-evoked responses in deep and superficial pyramidal neurons in areas CA2 and CA3a.**

<b>EPSC</b>						
cell type	connectivity (%)	amplitude (pA)	rise time (ms)	decay time (ms)	latency (ms)	success rate
CA2 PN deep	45 (n = 14 of 31)	19 ± 4.3	3.2 ± 0.3	16 ± 1.8	3.0 ± 0.6	0.42 ± 0.05*
CA2 PN superficial	57 (n = 31 of 54)	17 ± 2.9	2.8 ± 0.2	14 ± 1.0	2.1 ± 0.2	0.48 ± 0.05
CA3 PN deep	55 (n = 11 of 20)	13 ± 1.9	3.1 ± 0.2	13 ± 1.3	2.7 ± 0.5	0.45 ± 0.07#
CA3 PN superficial	44 (n = 10 of 23)	36 ± 12	3.0 ± 0.3	15 ± 1.5	2.4 ± 0.3	0.73 ± 0.07*#
Statistics	$\chi^2$ test $p = 0.815$	Kruskal-Wallis test $p = 0.196$	1-way ANOVA test $p = 0.614$	1-way ANOVA test $p = 0.514$	Kruskal-Wallis test $p = 0.174$	1-way ANOVA test $p = 0.016$ Tukey <i>post hoc</i> $p = 0.016^*$ $p = 0.031\#$
<b>IPSC</b>						
cell type	connectivity (%)	amplitude (pA)	rise time (ms)	decay time (ms)	latency (ms)	success rate
CA2 PN deep	35 (n = 6 of 17)	229 ± 98.1	3.5 ± 0.8	24 ± 1.9	7.3 ± 1.4	0.44 ± 0.12
CA2 PN superficial	32 (n = 11 of 34)	180 ± 50.8	3.9 ± 0.5	25 ± 1.9	5.9 ± 1.0	0.56 ± 0.07
CA3 PN deep	58 (n = 7 of 12)	157 ± 20.9	3.9 ± 0.6	25 ± 2.0	6.6 ± 0.9	0.60 ± 0.08
CA3 PN superficial	60 (n = 9 of 15)	135 ± 39.4	5.1 ± 0.5	24 ± 1.0	8.1 ± 1.3	0.49 ± 0.07
Statistics	$\chi^2$ test $p = 0.418$	Kruskal-Wallis test $p = 0.609$	1-way ANOVA test $p = 0.257$	1-way ANOVA test $p = 0.914$	1-way ANOVA test $p = 0.537$	1-way ANOVA test $p = 0.791$

### Dentate gyrus granule cells receive mono-synaptic glutamatergic as well as mono- and di-synaptic GABAergic inputs from the SuM

Besides the release of glutamate by SuM axons, histological and physiological studies have described co-release of GABA by SuM inputs onto granule cells (GCs) in the dentate gyrus (Pedersen et al., 2017; Soussi et al., 2010). Therefore, we wished to verify that our novel Csf2rb2-Cre line recapitulated the physiological observations made by Pedersen et al. in a VGluT2-Cre line. To this end, we performed voltage-clamp recordings of GCs at -70 mV like previously, and then under conditions optimal for recording inhibitory post-synaptic currents (IPSCs), i.e., with cesium in the pipette solution and the membrane potential clamped at +10 mV (Figure III.2.5A). Photostimulation of SuM axons reliably elicited EPSCs and IPSCs recorded in GCs at -70 mV and +10 mV, respectively (Figure III.2.5B and Figure III.2.5C). Application of NBQX and D-APV abolished EPSCs (Figure III.2.5B and Figure III.2.5D; amplitudes  $13 \pm 3.3$  pA were in control and  $1.2 \pm 0.4$  pA in NBQX & D-APV and SR95531 & CGP55845A hence a  $83 \pm 6.1$  % block by NBQX & D-APV and SR95531 & CGP55845A,  $n = 14$ ; Wilcoxon signed-rank test,  $p < 0.001$ ) and significantly reduced IPSCs amplitude (Figure III.2.5C and Figure III.2.5D; amplitudes were  $74 \pm 24$  pA in control and  $29 \pm 8.6$  pA in NBQX & D-APV hence a  $31 \pm 13$  % block by NBQX & D-APV,  $n = 17$ ; Wilcoxon signed-rank test,  $p = 0.009$ ). Further application of the GABA<sub>A</sub> and GABA<sub>B</sub> receptor antagonists SR95531 (1  $\mu$ M) and CGP55845A (2  $\mu$ M) completely blocked IPSCs (Figure III.2.5C and Figure III.2.5D; amplitudes were  $29 \pm 8.6$  pA in NBQX & D-APV and  $1.3 \pm 0.2$  pA in NBQX & D-APV NBQX & D-APV and SR95531 & CGP55845A hence a  $91 \pm 2.0$  % block by SR95531 & CGP55845A,  $n = 17$ ; Wilcoxon signed-rank test,  $p < 0.001$ ). Altogether, these data replicate the results of Pedersen et al. (Pedersen et al., 2017) showing direct release of both glutamate and GABA at the SuM to GC synapses, thus validating our Csf2rb2-Cre line. Furthermore, the reduction of light-evoked IPSCs upon blockade of excitatory transmission alone demonstrates an additional feedforward inhibitory component of the SuM drive onto GCs in the dentate gyrus.

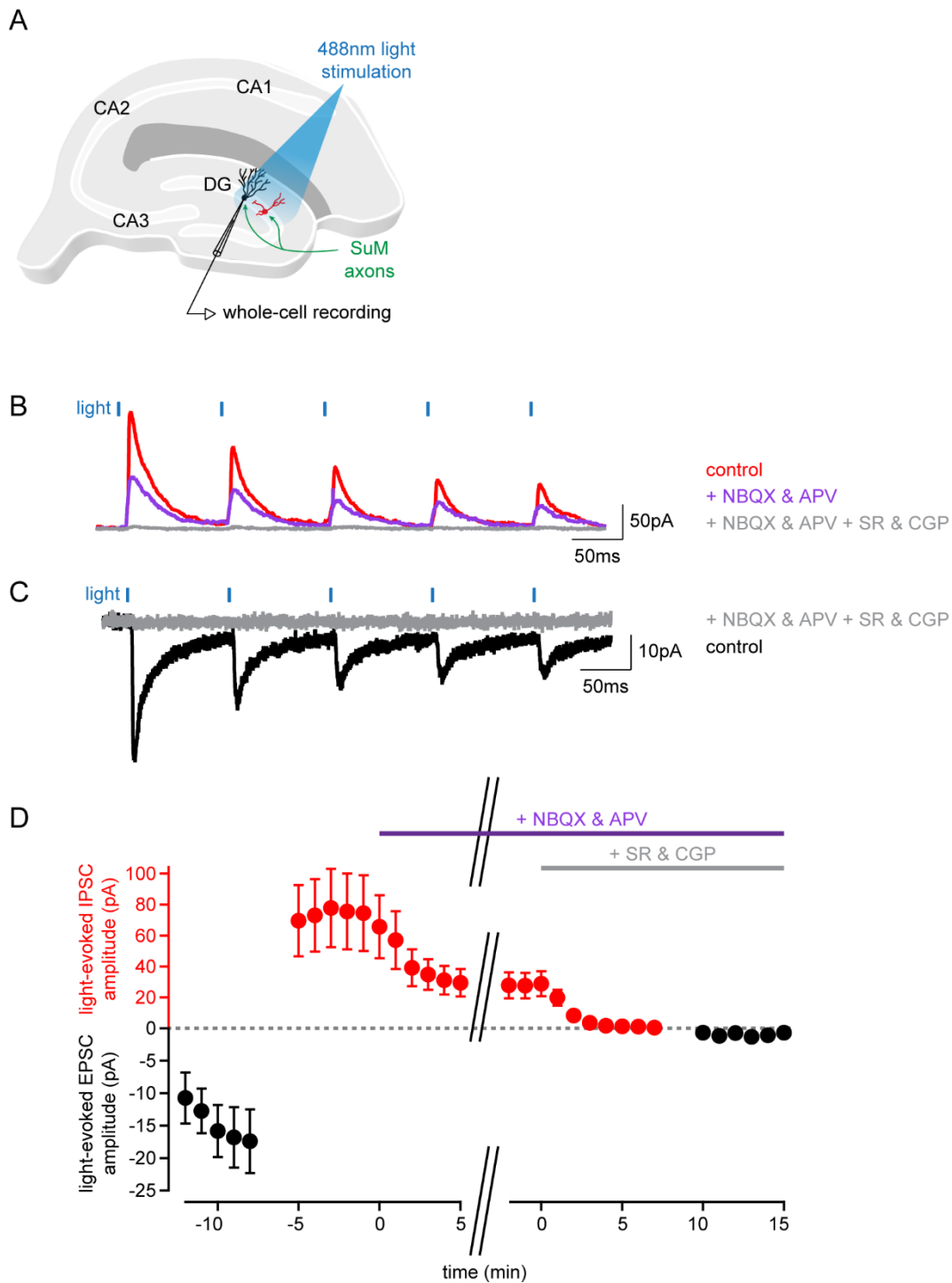


**Figure III.2.5. SuM light-evoked mono-synaptic excitation as well as mono- and di-synaptic inhibition onto DG GCs.**

**A.** Diagram illustrating the whole-cell recording configuration of DG CGs and SuM fibers light stimulation in acute hippocampal slices. **B.** Sample traces of light-evoked IPSCs recorded in GCs before (red) and after (purple) application of 10  $\mu$ M NBQX & 50  $\mu$ M APV, and further application of 1  $\mu$ M SR95531 & 2  $\mu$ M CGP55845A (grey). **C.** Sample traces of light-evoked EPSCs recorded in GCs before (black) and after (grey) application of NBQX, APV, SR95531 & CGP55845A. **D.** Time course of light-evoked EPSC

and IPSC amplitudes upon application of 10  $\mu\text{M}$  NBQX & 50  $\mu\text{M}$  APV, and further application of 1  $\mu\text{M}$  SR95531 & 2  $\mu\text{M}$  CGP55845A (EPSC : n = 14, IPSC : n = 17; error bars represent SEM).

### SuM inputs recruit feedforward inhibition onto CA2 and CA3 pyramidal neurons

With our results from the SuM to GC transmission in mind, we next examined if SuM inputs also target inhibitory neurons and drive feedforward inhibition onto CA2/CA3 PNs, and/or co-release GABA at these synapses (Figure III.2.6A). Using the same strategy as experiments performed in the dentate gyrus, we found that light activation of SuM inputs evoked IPSCs in CA2/CA3 PNs that were consistently much larger in magnitude than the EPSCs observed at -70 mV (Figure III.2.6B). We detected these inhibitory currents in 46 % (n = 69 of 129 cells) of PNs in area CA2 and CA3 (Figure III.2.6C). Inhibitory transmission was never detected in PNs in area CA1 (0 %, n = 0 of 18 cells) and rare but present in CA3b PNs (18 %, n = 2 of 11 cells) (Figure III.2.6C). Connectivity of inhibitory transmission was not different between PNs with or without TEs, nor between superficial and deep PNs (Table III.2.3 and Table III.2.4). IPSC amplitudes were also similar in CA2 and CA3 PNs, as well as in deep and superficial PNs (Table III.2.3 and Table III.2.4).

Interestingly, the light-evoked IPSC latencies were significantly longer with increased jitter as compared to the time course of the light-evoked EPSCs (Figure III.2.6B, Table III.2.3; response latencies were  $2.9 \pm 0.1$  ms for EPSCs, n = 166 PNs;  $6.2 \pm 0.4$  ms for IPSCs, n = 69 PNs; Mann-Whitney U test,  $p < 0.001$ ; Kolmogorov-Smirnoff test,  $p < 0.001$ ). Of note, the IPSC latencies did not differ between cell types or deep and superficial subpopulations (Table III.2.3 and Table III.2.4). Inhibitory responses thus appeared to be di-synaptic, suggesting that SuM axons stimulation recruits feedforward inhibition onto PNs. This was confirmed when blocking excitatory transmission by applying NBQX and D-APV which completely abolished all light-evoked IPSCs (Figure III.2.6D; amplitudes were  $167 \pm 40.3$  pA in control and  $11.6 \pm 2.0$  pA in NBQX & D-APV hence a  $93 \pm 1.9$  % block by NBQX & D-APV, n = 7; paired-T test,  $p = 0.007$ ). We further verified the mono- and di-synaptic natures of EPSCs and IPSCs respectively by applying 0.2  $\mu\text{M}$  TTX and 100  $\mu\text{M}$  4-AP to allow depolarization of pre-synaptic terminals while blocking action-potential driven vesicular release. Under these conditions, EPSCs remained but IPSCs were abolished even with photostimulation increased to 5 ms at 45 mW/mm<sup>2</sup> (Figure III.2.6E; amplitudes were  $20.2 \pm 6.1$  pA for EPSCs and  $110 \pm 50$  pA for IPSCs in control and  $9.3 \pm 7.7$  pA for EPSCs and  $4.8 \pm 0.7$  pA for IPSCs in TTX & 4-AP hence a  $61 \pm 24$  % block of EPSCs and  $88 \pm 4.2$  % block of IPSCs by TTX & 4-AP, n = 7; Wilcoxon

signed-rank test,  $p = 0.22$  for EPSCs and  $p = 0.016$  for IPSCs), consistent with SuM axons providing direct excitation and feed-forward inhibition to area CA2 PNs. These results establish that PNs in this region are di-synaptically inhibited by SuM inputs and rule out any mono-synaptic inhibitory transmission from SuM to area CA2 PNs, in contrast with the dentate gyrus.

### SuM inputs differentially target deep and superficial pyramidal neurons in area CA2

Given the diversity of PNs engaged by SuM inputs in area CA2 and their known different contributions to the hippocampus physiology such as sharp wave ripples (Oliva et al., 2016; Valero et al., 2015), we decided to further examine the net effect of direct excitation and feedforward inhibition in CA2 versus CA3 PNs and deep versus superficial PNs (Figure III.2.6C and Figure III.2.6F). For this purpose, we quantified the connectivities, success rates, amplitudes, potencies (defined as the amplitude multiplied by the success rate), kinetics and latencies of excitatory and inhibitory events in each subtype of PN as well as the E/I ratio where applicable. This analysis revealed no differences in connectivity, success rate, amplitude, potency, rise time, decay time, or latency between CA2 and CA3 PNs for EPSCs or IPSCs (Table III.2.3). Comparison of E/I ratios computed either from pure amplitudes or from combined amplitudes and success rates as potencies did not yield any differences either between CA2 and CA3 PNs (Figure III.2.6G; E/I ratios from amplitudes were  $0.13 \pm 0.03$  for CA2 PNs,  $n = 13$ ;  $0.13 \pm 0.03$  for CA3 PNs,  $n = 7$ ; Mann-Whitney U test,  $p = 0.562$ ; E/I ratios from potencies were  $0.12 \pm 0.03$  for CA2 PNs,  $n = 13$ ;  $0.22 \pm 0.07$  for CA3 PNs,  $n = 7$ ; Mann-Whitney U test,  $p = 0.331$ ). When considering deep and superficial PNs, none of the measurements performed on EPSCs showed any difference, although the rise time of EPSCs appeared slower in deep than in superficial PNs without reaching statistical significance (Table III.2.3). Similarly, most characteristics of IPSCs were similar between deep and superficial PNs, with the exception of the rise time which was faster in deep than in superficial PNs (Table III.2.3). Even so, our analysis unveiled a consistently lower E/I ratio in deep PNs compared to superficial PNs, whether taken from pure amplitudes or potencies (Figure III.2.6G; E/I ratios from amplitudes were  $0.08 \pm 0.01$  for deep PNs,  $n = 15$ ;  $0.19 \pm 0.03$  for superficial PNs,  $n = 26$ ; Mann-Whitney U test,  $p = 0.015$ ; E/I ratios from potencies were  $0.09 \pm 0.03$  for deep PNs,  $n = 15$ ;  $0.22 \pm 0.04$  for superficial PNs,  $n = 26$ ; Mann-Whitney U test,  $p = 0.007$ ). Thus, the deep subpopulation of PNs in area CA2 is likely to be more strongly inhibited by the combination of direct excitatory transmission and feedforward inhibition from the SuM (Figure III.2.6F). Overall, these results support the idea that the microcircuit engaged by SuM inputs

differentially influences PNs according to their radial somatic location rather than their CA2 or CA3 morphology.

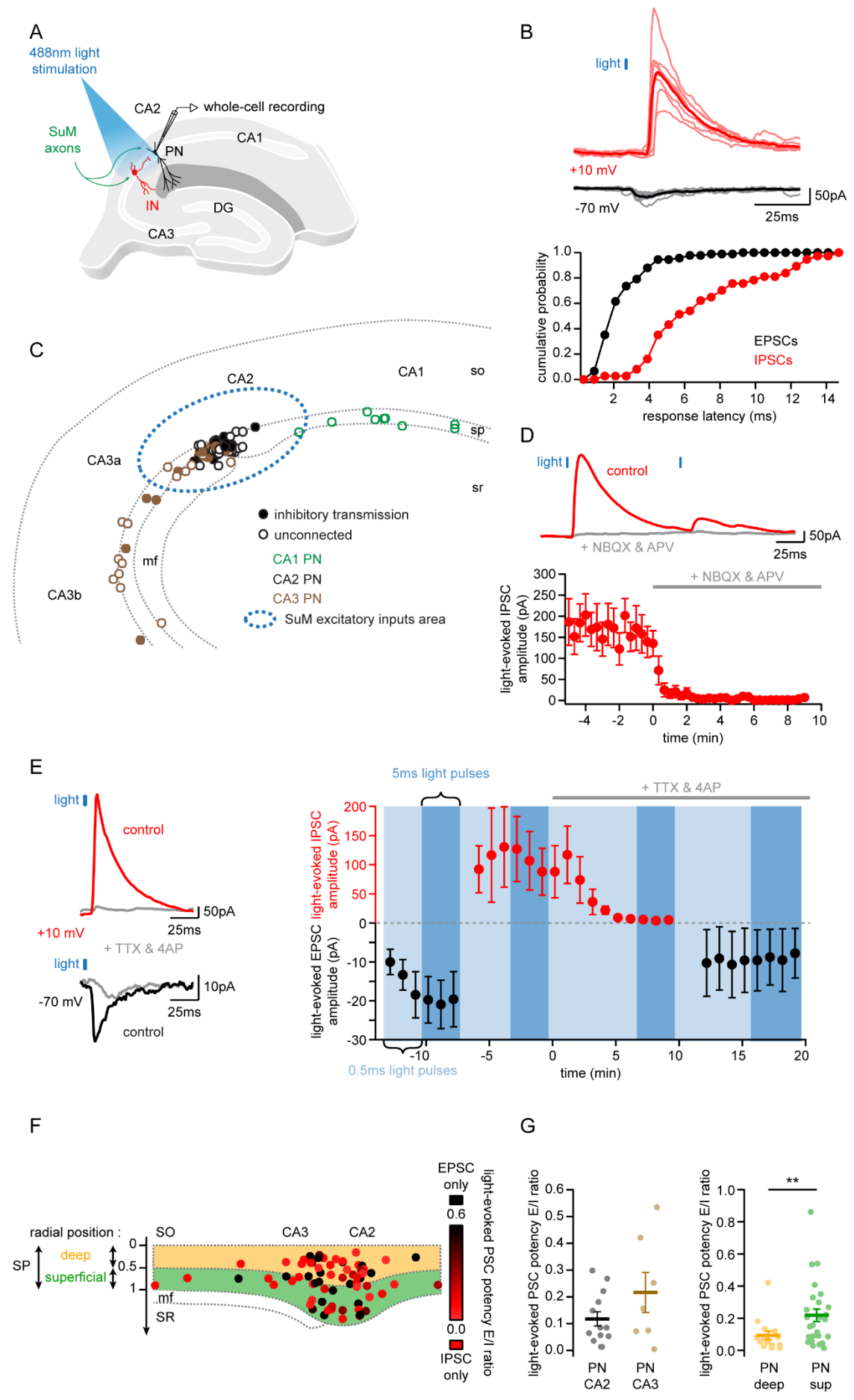


### Figure III.2.6. SuM axon stimulation recruits feedforward inhibition.

**A.** Diagram illustrating the whole-cell recording configuration of PNs in area CA2 and SuM fiber stimulation in acute hippocampal slices. **B.** Using a pipette solution containing Cs<sup>+</sup>, light-evoked currents could be recorded at -70 mV to isolate EPSCs and at +10 mV to isolate IPSCs. Top, sample traces of EPSCs (bottom traces, individual traces shown in grey, average trace shown in black) and IPSCs (top traces, individual traces shown in light red, average trace shown in red) recorded in the same PN, note the increased latency of IPSCs onset compared to EPSCs. Bottom, normalized cumulative distribution of latencies for EPSCs (black, n = 166) and IPSCs (red, n = 69) recorded in PNs. **C.** Diagram mapping the location of several PNs in the hippocampus that receive feedforward transmission from light-evoked SuM inputs with unconnected cells shown as open circles, connected cells as filled circles, color indicates cell type, area circled in dotted blue represents region innervated by SuM. **D.** Inhibitory transmission is completely abolished by the blockade of AMPA and NMDA receptors, consistent with a feedforward mechanism. Sample traces (top, control shown in black, NBQX & APV shown in grey) and time course (bottom) of light-evoked IPSC amplitudes upon application of 10  $\mu$ M NBQX & 50  $\mu$ M APV (n = 7, error bars represent SEM). **E.** Application of TTX & 4-AP abolishes IPSCs and spares EPSCs, consistent with mono-synaptic excitation and di-synaptic inhibition. Left, sample traces shown in black (EPSC) and red (IPSC), following application of TTX & 4-AP shown in grey. Right, time course of light-evoked EPSC and IPSC amplitudes upon application of 0.2  $\mu$ M TTX & 100  $\mu$ M 4-AP (n = 7, error bars represent SEM). **F.** Diagram showing the E/I ratios of EPSCs and IPSCs recorded from PNs in the hippocampus upon light stimulation of SuM inputs. Color scale ranges from red for low to black for high E/I ratios. Radial somatic location normalized to the height of the pyramidal layer ranges from 0 (deep, closest to SO) to 1 (superficial, closest to SR). **G.** SuM inputs bring about differential levels of excitation and inhibition on deep versus superficial PNs. Comparison of E/I ratios for CA2 versus CA3 PNs (left) and deep versus superficial PNs (right) (individual cells shown as dots, population average shown as horizontal line, error bars represent SEM; CA2 PNs : n = 13; CA3 PNs : n = 7; Mann-Whitney U test, p = 0.331; deep PNs : n = 15; superficial PNs : n = 26; Mann-Whitney U test, p = 0.007).

### The feedforward inhibitory drive from SuM controls pyramidal neuron excitability

As SuM provides both direct excitation and feedforward inhibition to area CA2, we examined how light activation of this input could influence several properties of PNs. Using whole-cell recording of pyramidal cells in area CA2 (Figure III.2.7A), we first checked whether feedforward inhibition driven by SuM activation could directly influence the summation of excitatory responses elicited by SuM photostimulation. Blocking inhibitory transmission with the GABA<sub>A</sub> and GABA<sub>B</sub> receptor antagonists SR95531 and CGP55845A led to a significant increase of light-evoked EPSP amplitude recorded in area CA2 PNs (Figure III.2.7B; amplitudes of the first response were  $0.18 \pm 0.05$  mV in control and  $0.24 \pm 0.05$  mV in SR95531 & CGP55845A hence a  $219 \pm 57$  % increase by SR95531 & CGP55845A,  $n = 14$ ; Wilcoxon signed-rank tests,  $p = 0.004$  for the first PSP,  $p = 0.013$  for the second PSP,  $p < 0.001$  for the third PSP), thereby demonstrating a net negative control of SuM-driven excitation by feedforward inhibition. Given SuM axonal stimulation triggers an excitatory-inhibitory sequence in post-synaptic PNs, we asked which effect would prevail on PN excitability. In order to assess that under more physiological conditions, we mimicked an active state in PNs by injecting constant depolarizing current steps sufficient to sustain AP firing during 1second while photostimulating SuM axons at 10 Hz (Figure III.2.7C). We observed that recruitment of SuM inputs significantly delayed the onset of the first AP (Figure III.2.7D; latencies to the first AP were  $221 \pm 19.9$  ms in control and  $233 \pm 19.1$  ms with photostimulation, hence a  $12.1 \pm 4.3$  ms increase upon photostimulation,  $n = 12$ ; paired-T test,  $p = 0.016$ ). In addition, given SuM neurons display theta-locked firing in vivo, we asked if rhythmic inhibition driven by SuM inputs in area CA2 could pace AP firing in PNs by defining windows of excitability. Indeed, photostimulation of SuM axons at 10 Hz led to a significant decrease of variability in the timing of AP firing by PNs (Figure III.2.7E; standard deviations of the first AP timing were  $36.9 \pm 11$  ms in control and  $24.7 \pm 7.4$  ms with photostimulation, hence a  $12.3 \pm 5.3$  ms decrease upon photostimulation,  $n = 12$ ; Wilcoxon signed-rank tests,  $p < 0.001$  for the first AP,  $p = 0.008$  for the second AP,  $p = 0.004$  for the third AP). Both the delay of AP onset and the reduction of AP jitter stemmed from the feedforward inhibition recruited by SuM inputs as application of GABA<sub>A</sub> and GABA<sub>B</sub> receptor antagonists abolished these effects of SuM stimulation (Figure III.2.7C, Figure III.2.7D and Figure III.2.7E; latencies to the first AP were  $232 \pm 19.8$  ms in SR95531 & CGP55845A and  $235 \pm 18.0$  ms with photostimulation,  $n = 6$ ; Wilcoxon signed-rank test,  $p = 0.44$ ; standard deviations of the first AP timing were  $11.9 \pm 2.0$  ms in SR95531 & CGP55845A and  $7.1 \pm 1.5$  ms with photostimulation,  $n = 6$ ; Wilcoxon signed-rank tests,  $p =$

0.22 for the first AP,  $p = 0.16$  for the second AP,  $p = 0.09$  for the third AP). These results reveal that the purely glutamatergic SuM input has an overall inhibitory effect on PN excitability and can influence the timing and jitter of action potential firing.

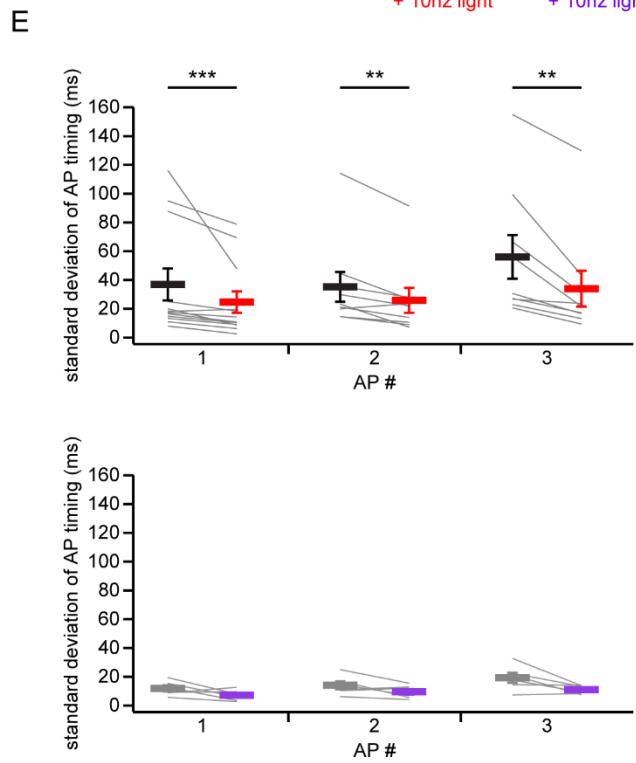
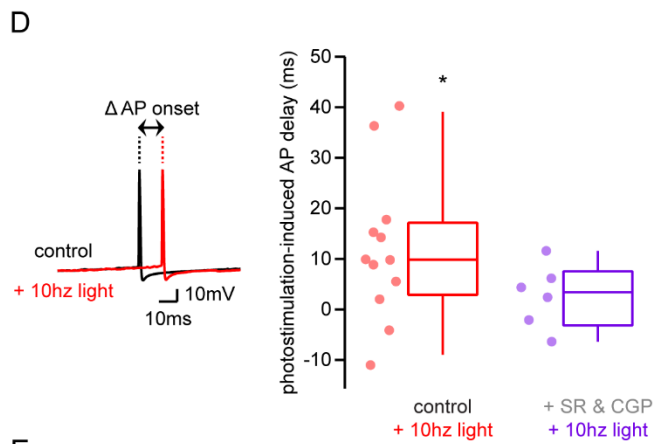
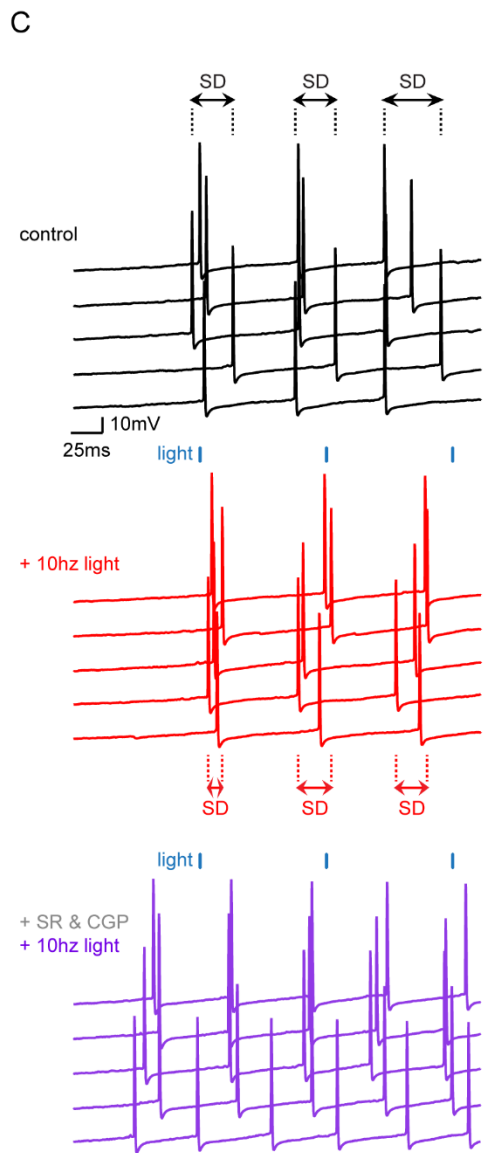
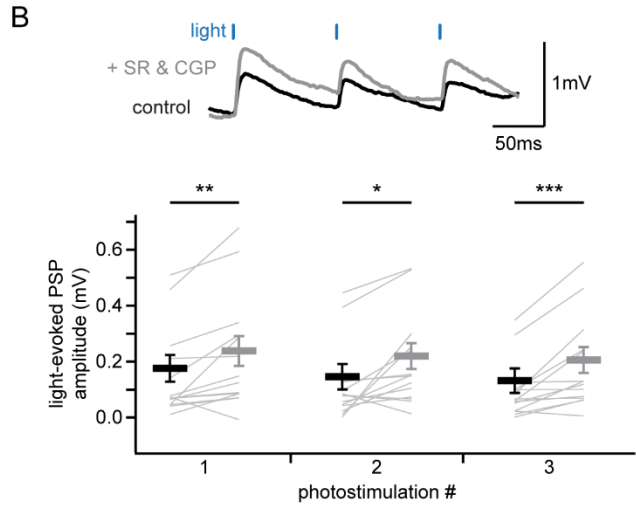
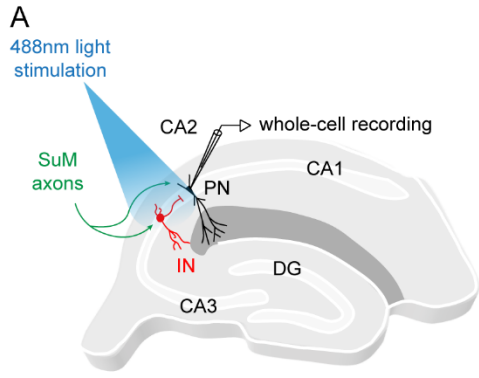


**Figure III.2.7. Area CA2 PNs receive a net inhibitory drive from SuM that controls summation and AP firing properties.**

**A.** Diagram illustrating the whole-cell recording configuration of PNs in area CA2 and SuM fiber stimulation in acute hippocampal slices. **B.** Top, sample traces of three 10 Hz SuM light-evoked PSPs before and after blocking inhibitory transmission (control shown in black, SR95531 & CGP55845A shown in grey). Bottom, comparison of light-evoked PSP amplitudes recorded in PNs before and after application of 1  $\mu$ M SR95531 & 2  $\mu$ M CGP55845A (individual cells shown as grey lines, population average shown as horizontal line, error bars represent SEM,  $n = 14$ ; Wilcoxon signed-rank tests,  $p = 0.004$  for the first PSP,  $p = 0.013$  for the second PSP,  $p < 0.001$  for the third PSP). **C.** Example traces of a CA2 PN action potential firing in response to current injection in the absence (black traces) or presence of 10 Hz photostimulation of SuM inputs (red traces, during the experiment photostimulations were interleaved with controls, but are grouped here for demonstration purposes), and with further application of 1  $\mu$ M SR95531 & 2  $\mu$ M CGP55845A (purple traces). **D.** Action potential onset is increased with 10 Hz SuM input photostimulation. Left, sample traces (control in black, photostimulation in red). Right, comparison of photostimulation-induced delay of AP firing in area CA2 PNs in control and with application of 1  $\mu$ M SR95531 & 2  $\mu$ M CGP55845A in a subset of experiments (control shown in red,  $n = 12$ , paired-T test,  $p = 0.016$ ; 1  $\mu$ M SR95531 & 2  $\mu$ M CGP55845A shown in purple,  $n = 6$ ; Wilcoxon signed-rank test,  $p = 0.44$ ; individual cells shown with dots, averages shown with boxplots). **E.** AP jitter in CA2 PNs is reduced by activation of SuM inputs. Comparison of the standard deviation of AP timing with or without 10 Hz photostimulation in control (top,  $n = 12$ ; Wilcoxon signed-rank test,  $p < 0.001$  for the first AP,  $p = 0.0078$  for the second AP,  $p = 0.0039$  for the third AP; individual cells shown with grey lines, population average shown as horizontal line, error bars represent SEM) and in 1  $\mu$ M SR95531 & 2  $\mu$ M CGP55845A (bottom,  $n = 6$ ; Wilcoxon signed-rank tests,  $p = 0.22$  for the first AP,  $p = 0.16$  for the second AP,  $p = 0.09$  for the third AP).

Basket cells are strongly recruited by SuM inputs

We performed whole-cell recordings from interneurons in area CA2 and CA3a with the goal of determining which class of interneuron mediates the feedforward inhibition recruited by SuM activation (Figure III.2.8A). In contrast with previous reports of an exclusive innervation of PNs by SuM (Maglóczy et al., 1994), we observed robust light-evoked excitatory transmission from SuM axons in 35 out of 62 interneurons (INs) with somas located in SP (Figure III.2.8B, Figure III.2.8C and Figure III.2.8D). Following anatomical biocytin-streptavidin staining and reconstructions of recorded INs (allowing unequivocal identification in 48 of 62 cases), we were able to classify INs based on their physiological properties, somatic location and axonal arborization location. We classified 22 cells as basket cells (BCs) because their axonal arborizations were restricted to SP (Figure III.2.8D). BCs fired APs at high frequency either in bursts or continuously upon depolarizing current injection and showed substantial repolarizing

sag current when hyperpolarized (Table III.2.5). Light-evoked EPSCs and EPSPs were readily observed in the vast majority of BCs (Figure III.2.8B and Figure III.2.8D, Table III.2.6) and reached large amplitudes in some instances. An additional 26 INs with soma in SP classified as non-BCs because their axon did not target SP (Figure III.2.8C). In our recordings, these cells fired in bursts and showed little sag during hyperpolarizing current injection steps (Table III.2.5). We consistently observed no or very minor light-evoked excitatory transmission onto non-BCs (Figure III.2.8C, Table III.2.6). Furthermore, we recorded from 17 INs that had soma in stratum oriens (SO) and 9 in stratum radiatum (SR). Like non-BCs, these INs did not receive strong excitation from SuM fibers (Figure III.2.8B, Table III.2.6). This data is consistent with the conclusion that SuM input preferentially forms excitatory synapses onto basket cells in area CA2 and CA3a.

To fully assess the strength of SuM inputs onto the different cell types, we examined the following parameters for each population: the connectivity, success rate, amplitude, potency, kinetics, and latencies of EPSCs as well as the resulting depolarization of the membrane potential. First, SuM inputs preferentially innervated BCs as evidenced by a higher connectivity of EPSCs in BCs than in PNs or other INs (Table III.2.6). Importantly, excitatory responses had short latencies with limited jitter (Figure III.2.6B, Table III.2.6) indicating that the connection was monosynaptic in all cell types. When voltage-clamping cells at -70 mV, light-evoked EPSCs could be compared between different cell populations. However, not every photostimulation gave rise to an EPSC leading to an average success rate that seemed highest in BCs, although this difference did not reach statistical significance (Table III.2.6). In addition, BCs appeared to receive more excitation from SuM inputs than other cells types, as EPSCs were larger in BCs than in PNs (Table III.2.6). EPSCs recorded in BCs also had faster kinetics than in PNs (Table III.2.6). Interestingly, combining the success rate of EPSCs with their respective amplitudes to compute the potency of the SuM synapses revealed that it was significantly larger in BCs than in PNs and non-BCs (Figure III.2.8E; potencies were  $12 \pm 1.6$  pA for PNs,  $n = 166$ ;  $29 \pm 7.8$  pA for BCs,  $n = 18$ ;  $5.9 \pm 1.5$  pA for non-BCs,  $n = 13$ ; Kruskal-Wallis test with Dunn-Holland-Wolfe *post hoc* test,  $p = 0.022$ ). Consequently, EPSPs recorded at -70 mV were of larger amplitude in BCs than in PNs (Figure III.2.8F; amplitudes were  $0.44 \pm 0.06$  mV for PNs,  $n = 20$ ;  $1.71 \pm 0.57$  mV for BCs,  $n = 10$ ;  $0.53 \pm 0.57$  mV for non-BCs,  $n = 4$ ; Kruskal-Wallis test with Dunn-Holland-Wolfe *post hoc* test,  $p < 0.001$ ). When recording cell-attached or current-clamping BCs at their resting membrane potential ( $V_M$ ), photostimulation of SuM axons was able to evoke AP firing (Figure III.2.8G) in multiple

instances (n = 7 of 13), this was never observed in PNs (n = 0 of 78), non-BCs (n = 0 of 16), SR INs (n = 0 of 9) or SO INs (n = 0 of 8). These results show that SuM projections to area CA2 preferentially provide excitation to BCs that are likely responsible of the feedforward inhibition observed in PNs. This is in accordance with an efficient control of area CA2 PNs excitability by the SuM inhibitory drive as axons from BCs deliver the feedforward inhibition to the peri-somatic region of PNs.

**Table III.2.5. Electrophysiological properties of interneurons in SuM-innervated area.**

	V <sub>M</sub> (mV)	R <sub>M</sub> (MΩ)	C <sub>M</sub> (pF)	firing adaptation index	sag (mV)
Basket cell (n = 16)	-57.3 ± 1.38	144 ± 28.1	64.0 ± 8.70	0.74 ± 0.05	9.4 ± 1.0
non-Basket Cell (n = 12)	-55.6 ± 1.84	224 ± 46.8	52.0 ± 5.90	0.57 ± 0.06	5.9 ± 1.4
interneuron SO (n = 6)	-57.0 ± 3.16	201 ± 21.0	44.7 ± 5.31	0.61 ± 0.11	7.6 ± 1.9
interneuron SR (n = 8)	-60.1 ± 2.89	282 ± 49.8	39.6 ± 3.18	0.65 ± 0.09	8.1 ± 2.1
Statistics	1-way ANOVA test p = 0.527	1-way ANOVA test p = 0.100	Kruskal-Wallis test p = 0.354	1-way ANOVA test p = 0.238	1-way ANOVA test p = 0.292

**Table III.2.6. Characteristics of SuM light-evoked transmission onto interneurons & pyramidal cells.**

cell type	EPSC					
	connectivity (%)	amplitude (pA)	rise time (ms)	decay time (ms)	latency (ms)	success rate
Pyramidal Cell	63 (n = 166 of 263)	19 ± 1.6*	3.4 ± 0.1*	15 ± 0.5*	2.9 ± 0.1	0.46 ± 0.02
Basket Cell	82 (n = 18 of 22)	43 ± 8.7*	1.7 ± 0.3*	8.4 ± 1.3*	3.1 ± 0.4	0.59 ± 0.07
non-Basket Cell	39 (n = 10 of 26)	16 ± 2.8	2.6 ± 0.5	12 ± 1.4	3.4 ± 0.7	0.36 ± 0.06
interneuron SO	12 (n = 2 of 17)					
interneuron SR	11 (n = 1 of 9)					
Statistics	χ <sup>2</sup> test p = 0.006*	Kruskal-Wallis test p = 0.016 Dunn-Holland-Wolfe <i>post hoc</i> p < 0.05*	1-way ANOVA test p < 0.001 Tukey <i>post hoc</i> p < 0.001*	1-way ANOVA test p < 0.001 Tukey <i>post hoc</i> p < 0.001*	1-way ANOVA test p = 0.580	1-way ANOVA test p = 0.066

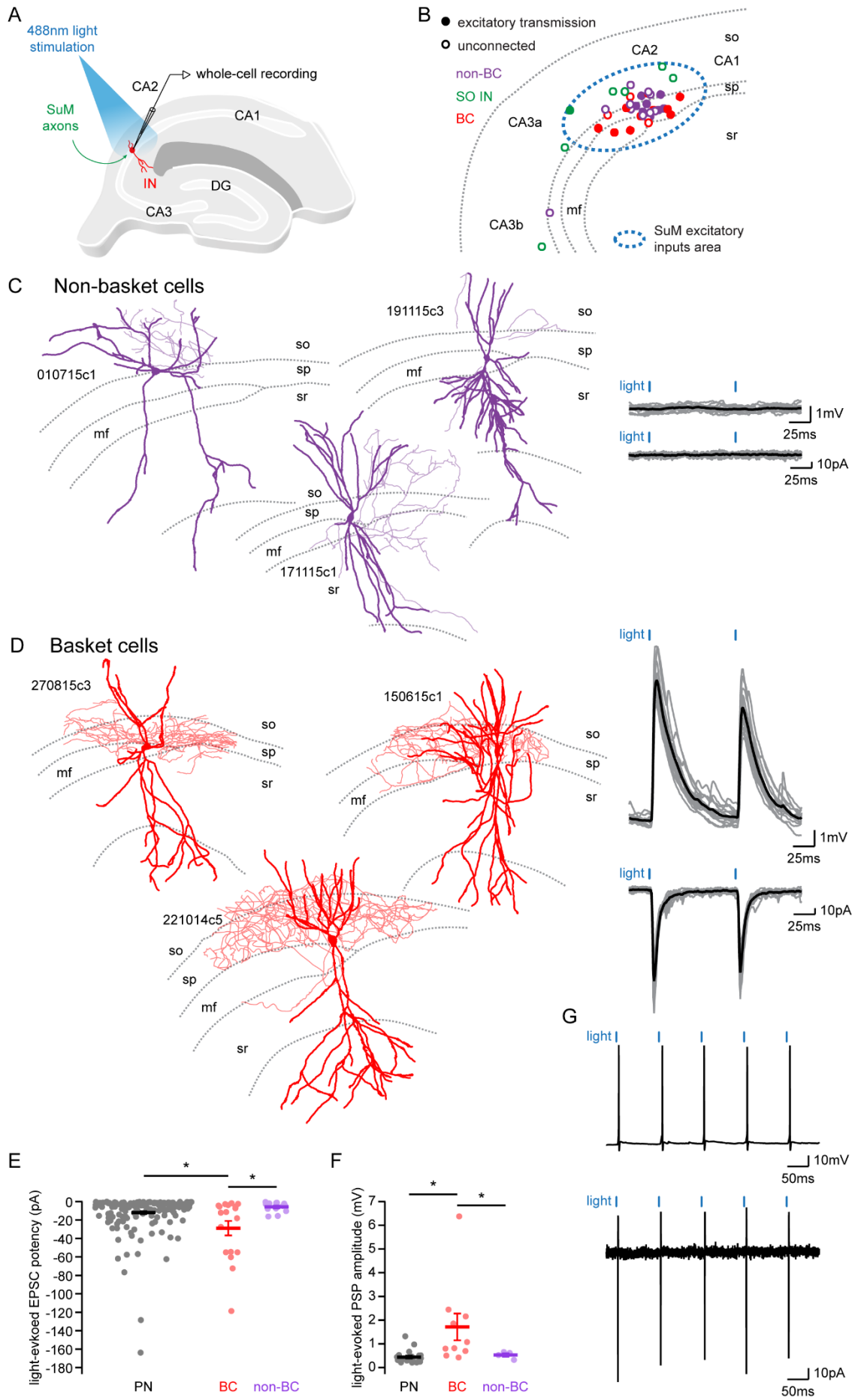


### Figure III.2.8. SuM inputs strongly excite basket cell interneurons in area CA2.

**A.** Diagram illustrating the whole-cell recording configuration of INs in area CA2 and SuM fiber stimulation in acute hippocampal slices. **B.** Diagram mapping several recorded hippocampal INs with open circles indicating connected cells and color indicating IN cell classification, area circled in dotted blue represents region innervated by SuM. **C.** Left, three example non-BC IN reconstructions (dendrites shown in purple, axons shown in light purple, hippocampal borders shown in dotted grey). Right, example of the absence of light-evoked EPSPs and EPSCs from these cells (individual traces in grey, average traces in black) **D.** Left, three examples of BC IN reconstructions (dendrites shown in red, axons shown in light red, hippocampal borders shown in dotted grey). Right, example traces of light-evoked EPSPs and EPSCs (individual traces shown in grey, average trace shown in black). **E.** BCs receive the most potent excitation from SuM. Comparison of light-evoked EPSC potencies recorded from PNs, BCs and non-BCs in area CA2 (individual cells shown as dots, population average shown as horizontal line, error bars represent SEM, PNs : n = 166; BC INs: n = 18; non-BCs: n = 13; Kruskal-Wallis test with Dunn-Holland-Wolfe *post hoc* test, p = 0.022). **F.** SuM input stimulation triggers large EPSPs in BCs. Comparison of light-evoked PSP amplitudes recorded from PNs, BCs and non-BCs in area CA2 (individual cells shown as dots, population average shown as horizontal line, error bars represent SEM, PNs : n = 20; BCs : n = 10; non-BCs : n = 4; Kruskal-Wallis test with Dunn-Holland-Wolfe *post hoc* test, p < 0.001). **G.** BCs fire action potentials time-locked to SuM input stimulation. Example traces of light-evoked action potentials in a BC recorded in current-clamp at resting membrane potential (top) and in cell-attached (bottom) configurations.

### Parvalbumin-expressing basket cells mediate the feedforward inhibition recruited by SuM

In the hippocampus, BCs express either cholecystokinin (CCK) or parvalbumin (PV) (Klausberger and Somogyi, 2008). We found that in response to a 1 second depolarizing pulse, most BCs that received strong SuM excitatory input displayed very fast AP firing with little accommodation in the AP firing frequency (Table III.2.5, Figure III.2.9A, Figure III.2.9B and Figure III.2.9C). This firing behavior is similar to what has been reported for fast spiking PV-expressing BCs in CA1 (Pawelzik et al., 2002). In contrast, CCK-expressing BCs show a lower firing frequency and more accommodation during the train (Pawelzik et al., 2002). This result suggests that BCs connected by the SuM may be expressing PV. To directly confirm this hypothesis, we performed post-hoc immunostaining of recorded interneurons that received strong excitation from SuM input. Because of the dialysis inherent to the whole-cell recording conditions, we encountered staining difficulties for multiple cells. However, PV-immunoreactivity could unequivocally be detected in either the soma or dendrites of 7 connected BCs (Figure III.2.9D). Therefore, this data demonstrates that at least a fraction of the recorded BCs connected by the SuM are expressing PV.

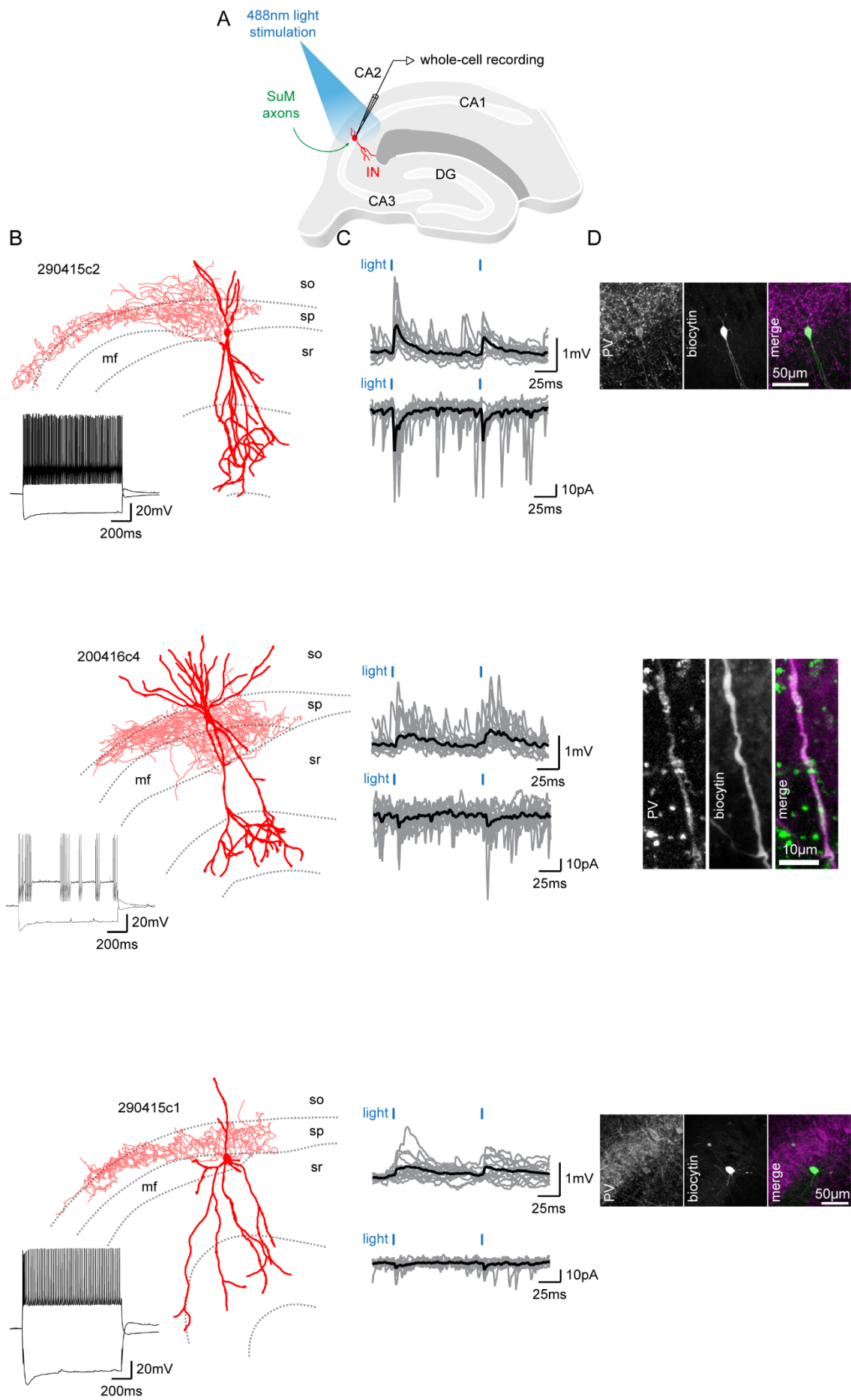


### Figure III.2.9. SuM inputs provide excitation to Parvalbumin-expressing BCs.

**A.** Diagram illustrating the whole-cell recording configuration of INs in area CA2 and SuM fiber stimulation in acute hippocampal slices. **B.** Three biocytin reconstructions of BC INs with dendrites in red and axons in light red. Inset, current clamp steps to -400 pA and +400 pA display high-frequency AP firing and repolarizing sag current. **C.** Corresponding light-evoked EPSCs and EPSPs for three reconstructed neurons (individual traces shown in grey, average trace shown in black). **D.** Corresponding PV immunostaining of three interneurons. Parvalbumin staining, left panel and magenta (right panel); biocytin labeling of the recorded cell, center panel and green (right panel).

Hence, to address whether the lack of PV staining in some cells was a consequence of dialysis or resulted from the fact that non-PV BC are also connected, we made use of a different strategy to differentiate PV and CCK INs. It has previously been demonstrated that PV+ BC transmission can be strongly attenuated by mu opioid receptor activation (MOR) while CCK+ BC transmission is insensitive to MOR activation (Glickfeld et al., 2008). Thus, in order to determine if SuM inputs preferentially target one subpopulation of BC, we recorded from PNs in area CA2 and examined the sensitivity of light-evoked IPSCs to the application of the MOR agonist DAMGO (Figure III.2.10A). We found that there was a complete block of the light-evoked IPSC amplitude following 1  $\mu$ M DAMGO application (Figure III.2.10B; IPSC amplitudes were  $343 \pm 123$  pA in control and  $31 \pm 12.4$  pA in DAMGO hence a  $88 \pm 5.0$  % block by DAMGO,  $n = 6$  PNs; Wilcoxon signed-rank test,  $p = 0.031$ ), while direct excitatory transmission remained unaffected (Figure III.2.10B; EPSC amplitudes were  $7.6 \pm 0.9$  pA in SR95531 & CGP55845A and  $8.7 \pm 3.9$  pA after DAMGO,  $n = 6$  PNs; Wilcoxon signed-rank test,  $p = 0.44$ ).

Because PV+ INs in area CA2 which mediate the SuM feed-forward inhibition are also the substrate of an iLTD of feed-forward inhibition from CA3 mediated by delta opioid receptor (DOR) activation (Piskorowski and Chevaleyre, 2013), we sought to further refine our characterization of the SuM feedforward inhibition by assessing its sensitivity to DOR activation. Application of 0.5  $\mu$ M of the DOR agonist DPDPE led to a long-term reduction of light-evoked IPSCs recorded in CA2 PNs, similar to the iLTD seen at CA3 inputs (Figure III.2.10C; amplitudes were  $168 \pm 28$  pA in control and  $64 \pm 22$  pA in DPDPE hence a  $61 \pm 14$  % block by DPDPE,  $n = 7$ ; paired-T test,  $p = 0.015$ ), while leaving direct EPSCs unaffected (Figure III.2.10C; amplitudes were  $4.0 \pm 1.6$  pA in SR95531 & CGP55845A and  $3.1 \pm 1.1$  pA after DPDPE,  $n = 7$ ; Wilcoxon signed-rank test,  $p = 0.22$ ). Further confirming the PV+ nature of INs responsible for the SuM feedforward inhibition, this result strikingly reveals that both

the local CA3 and long-range SuM inputs converge onto the same population of INs to inhibit area CA2 PNs, thus enabling cross-talk between these routes through synaptic plasticity of PV+ INs.

Following up on this observation, we wished to genetically confirm that PV+ INs are responsible for the SuM feedforward inhibition over area CA2 PNs. As the dichotomy between PV+ versus CCK+ INs sensitivity to opioids has not been directly verified in area CA2, we used inhibitory DREADD to selectively inhibit PV+ INs in area CA2 while monitoring feedforward IPSCs from area CA2 PNs in response to SuM stimulation. To achieve that, we injected AAVs expressing a Cre-dependent h4MDi inhibitory DREADD in area CA2 of PV-Cre mice together with AAVs expressing ChR2 with the pan-neuronal promoter hSynapsin in the SuM (Figure III.2.10D). In 13 instances, this strategy was successful and we observed a substantial reduction of SuM-evoked IPSC amplitude recorded in area CA2 PNs upon application of 10  $\mu$ M of the DREADD ligand CNO (Figure III.2.10E; amplitudes were  $847 \pm 122$  pA in control and  $498 \pm 87$  pA in CNO hence a  $42 \pm 6.0$  % block by CNO,  $n = 13$ ; paired-T test,  $p < 0.001$ ). Although we never observed a complete block of inhibitory responses, this result unequivocally places PV+ INs as mediators of the SuM feed-forward inhibition of area CA2 PNs. The incomplete block of IPSCs in these experiments could be due to several factors. First, quantification of cells co-expressing DREADDs and PV over the total number of PV+ INs in the infected area of the hippocampal slices recorded here revealed a partial infection of PV+ INs by AAVs carrying DREADDs (infection rate =  $75 \pm 3.5$  %,  $n = 13$ ). Second, it is possible that CNO application did not completely silence DREADD-expressing PV+ INs. Third, photostimulation of SuM axons expressing high levels of non-Cre dependent ChR2 might have recruited additional non-PV INs.

Taking advantage of the mCherry tag of the DREADD construct labeling PV+ INs in these animals, we recorded an additional 12 PV+ INs. SuM inputs stimulation lead to AP firing in 6 instances from these cells, 4 of which were revealed to be BCs by *post hoc* reconstruction and confirmed to express PV.

Altogether, these combined results strongly indicate that SuM axons are efficiently and selectively exciting PV+ BCs in area CA2, thus driving a feedforward inhibition onto neighboring PNs. Importantly, while PNs that received excitatory input from SuM were located only in area CA2, some cells that received inhibitory inputs were located in CA3b, far away from the direct reach of SuM axons (Figure III.2.6C). This is in agreement with the fact that axonal projections from connected BCs can extend toward CA3 several hundreds of

micrometers away from the somas of the BCs (Figure III.2.8D, Figure III.2.9B). In contrast, the axons of the connected BCs rarely extend toward CA1 and CA1 PNs recorded in these experiments were never subjected to inhibition recruited by the SuM.

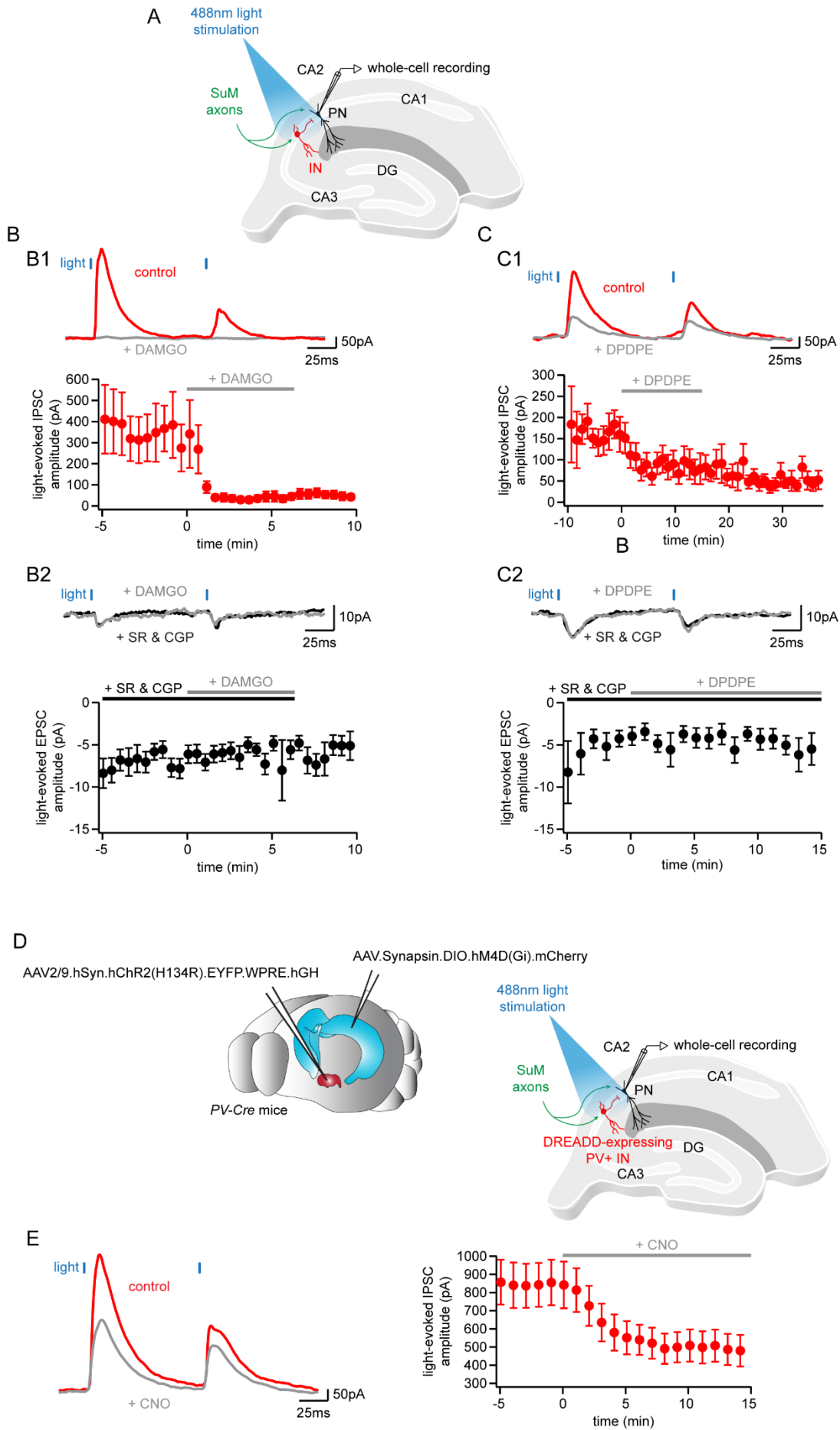


**Figure III.2.10. Parvalbumin-expressing BCs mediate the feedforward inhibition recruited by photostimulation of SuM fibers.**

**A.** Diagram illustrating the whole-cell recording configuration of PNs in area CA2 and SuM fiber stimulation in acute hippocampal slices. **B.** Application of the mu-opioid receptor agonist, DAMGO, results in the complete abolition of light-evoked SuM inhibitory transmission. **B1.** Sample traces (top, control in red, DAMGO in grey) and time course of light-evoked IPSC amplitudes upon application of 1  $\mu$ M DAMGO (bottom,  $n = 6$ , error bars represent SEM). **B2.** Sample traces (top, SR95531 & CGP55845A in black, DAMGO in grey) and time course of light-evoked EPSC amplitudes upon application of 1  $\mu$ M DAMGO in 1  $\mu$ M SR95531 & 2  $\mu$ M CGP55845A (bottom,  $n = 6$ , error bars represent SEM). **C.** Application of the delta-opioid receptor agonist, DPDPE, results in the long-term depression of light-evoked SuM inhibitory transmission. **C1.** Sample traces (top, control in red, DPDPE in grey) and time course of light-evoked IPSC amplitudes upon application of 0.5  $\mu$ M DPDPE (bottom,  $n = 7$ , error bars represent SEM). **D2.** Sample traces (SR95531 & CGP55845A in black, DPDPE in grey) and time course of light-evoked EPSC amplitudes upon application of 0.5  $\mu$ M DPDPE in 1  $\mu$ M SR95531 & 2  $\mu$ M CGP55845A (bottom,  $n = 6$ , error bars represent SEM). **D.** Diagrams illustrating the method to infect SuM neurons and selectively inhibit PV+ INs in area CA2. An AAV allowing the Cre-driven expression of inhibitory DREADD was injected bilaterally into area CA2 of the dorsal hippocampus and another AAV allowing the expression of ChR2 was injected into the SuM of PV-Cre mice. This allowed optogenetic stimulation of SuM inputs and chemogenetic inhibition of PV+ INs by application of the DREADD agonist CNO. **E.** Silencing of PV+ INs by inhibitory DREADDs reduces SuM feed-forward inhibition onto area CA2 PNs. Sample traces (left, control in red, CNO in grey) and time course of light-evoked IPSC amplitudes upon application of 10  $\mu$ M CNO (right,  $n = 13$ , error bars represent SEM).

### **III.3 - Influence of SuM inputs on hippocampal area CA2 drive onto CA1**

#### **III.3.a - Introduction**

Crucial aspects of episodic learning and memory are supported by the hippocampus. Afferent information from the entorhinal cortex (EC) is thought to be sequentially processed by hippocampal circuits in the classical tri-synaptic loop enabling memory formation. In this view, the dentate gyrus (DG) receives EC inputs and projects to area CA3, CA3 pyramidal neurons (PNs) then send outputs to area CA1 that in turn returns information to the EC. Surprisingly, interrupting this loop by blocking the CA3 to CA1 connection does not result in a dramatic compromise of hippocampal-dependent learning and memory (Brun et al., 2002; Nakashiba et al., 2008). This observation argues for another route of information in the hippocampus that could rescue its functions in the absence of transmission from area CA3 to CA1. A good candidate for this role is the long-overlooked area CA2 as it receives strong input from the EC and potently drives area CA1, thus potentially bypassing CA3 (Chevalleyre and Siegelbaum, 2010; Kohara et al., 2013). However, little is known about how area CA2 influences CA1 and what the resulting hippocampal output is. Therefore, physiological investigations of the consequences of area CA2 neuronal activity on CA1 are required to better understand information flow in hippocampal circuits.

Of note, specific patterns of activity are present in hippocampal networks during the encoding, consolidation and retrieval of spatial information. Theta and gamma oscillations as well as sharp wave ripples (SWR) are critically involved in these mnemonic processes (Fuchs et al., 2007; Girardeau et al., 2009; Korotkova et al., 2010). Although the roles of area CA3 and CA1 in rhythmic activity of hippocampal networks have been extensively studied, the contributions of area CA2 have rarely been addressed until lately. Remarkably, recent studies have unveiled a critical role of area CA2 in the generation of SWR and in spatial coding (Boehringer et al., 2017; Kay et al., 2016; Oliva et al., 2016). On the other hand, the functions of area CA2 during brain states of theta and gamma oscillations are still unclear. Strikingly, area CA2 receives direct input from the hypothalamic supramammillary nucleus (SuM) (Haglund et al., 1984; Kiss et al., 2000; Maglóczky et al., 1994; Soussi et al., 2010; Vertes, 1992) that shows theta-locked activity (Kirk et al., 1996; Kocsis and Vertes, 1994) and is involved in the control of hippocampal theta oscillations (Kirk and McNaughton, 1993; McNaughton et al., 1995; Thinschmidt et al., 1995). Hence, area CA2 neuronal activity is likely to be modulated by SuM input during theta states and subsequently affect the output of the hippocampus via CA1.

We have previously shown that the SuM controls the timing of CA2 PN action potential firing by recruiting feedforward inhibition mediated by PV-expressing (PV+) basket cells (BCs). This population of interneurons (INs) is critically involved in virtually all hippocampal rhythms including theta, gamma, and SWR (Fuchs et al., 2007; Gulyás et al., 2010; Hájos et al., 2013; Klausberger et al., 2005; Korotkova et al., 2010; Royer et al., 2012). This prompted us to examine the effect of SuM stimulation on area CA2 activity and the consequences on CA1 PN firing in a physiologically active hippocampal network. Slow gamma oscillations are generated intrinsically in the hippocampus, and this oscillation can be induced in acute hippocampal slices by elevating the cholinergic tone (Fisahn et al., 1998; Mann et al., 2005; Oren et al., 2006; Zemankovics et al., 2013). We have previously observed that application of the cholinergic agonist carbachol (CCh) induces gamma-like oscillations in area CA2 and triggers burst firing of action potentials in CA2 PNs. These bursts of action potentials in CA2 PNs are likely to have a dramatic effect on area CA1 and the resulting hippocampal output. Therefore, we asked how neuronal activity in area CA2 is modulated by the SuM during CCh-induced oscillations and what the resulting consequences are on area CA1 PN activity.

To address this, we used optogenetics to photostimulate SuM projections to area CA2 and performed whole-cell patch-clamp recordings of CA2 and CA1 PNs in acute hippocampal slices following application of 10  $\mu$ M CCh. Cre-dependent channelrhodopsin-2 (ChR2) was specifically expressed in SuM neurons by injection of adeno-associated viruses (AAV) in VGluT2 and Csf2rb2-Cre mouse lines. This allowed us to quantify the strength of excitatory and inhibitory drives of SuM inputs onto CA2 PNs and their effect on burst firing in CCh. We observed a reduction of SuM light-evoked excitatory (EPSC) and inhibitory post-synaptic currents (IPSC) amplitudes and paired-pulse depression in CA2 PNs upon CCh application. The net effect of SuM transmission over CA2 PNs remained inhibitory in CCh and resulted in delayed burst firing from these cells. When examining the consequences of SuM activity on CA2 output transmission in area CA1 during CCh-induced network activity, we observed a drastic reduction of action potential firing in CA1 *stratum pyramidale* (SP) that lasted several seconds following light-stimulation of SuM inputs. Whole-cell recordings of CA1 PNs revealed that this reduction of field activity was paralleled by a hyperpolarization of CA1 PN membrane potential ( $V_M$ ) that prevented action potential firing in a seconds-long time window after SuM axon photostimulation. The time course of spontaneous EPSC and IPSC frequencies in CA1 PNs during this time window showed a transient increase during the light-on period followed by a lasting decrease upon termination of SuM input stimulation. Altogether, our data

demonstrate that the SuM inhibitory drive received by CA2 PNs controls the timing of their burst firing of action potentials that results in a massive and lasting silencing of CA1 PNs during CCh-induced network activity. These results indicate that the hippocampal output from area CA1 is controlled by SuM input through the modulation of area CA2 activity.

### **III.3.b - Results**

#### Carbachol influences the strength and dynamics of SuM transmission onto area CA2

We have previously shown that SuM inputs provide direct excitation and feedforward inhibition to area CA2 PNs resulting in an overall inhibitory drive. This feedforward inhibition is mediated by PV+ BCs that fire action potentials in response to SuM axon photostimulation. In order to study the functional consequences of activating SuM inputs to area CA2 under conditions in which neurons are active, we applied CCh to induce network activity in acute hippocampal slices from injected VGluT2-Cre and Csf2rb2-Cre animals expressing ChR2 in SuM axons. Activation of cholinergic receptors has profound and diverse effects on several hippocampal targets including the depolarization of PNs and the majority of INs, as well as the modulation of glutamate and GABA release (Alger et al., 2014; Cobb and Davies, 2005; Hasselmo, 2006). Because of this, we first assessed whether mono-synaptic excitation and di-synaptic inhibition from SuM inputs onto CA2 PNs was affected by CCh. Whole-cell patch-clamp recordings with Cs<sup>+</sup>-based internal solution were obtained from CA2 PNs and light-evoked excitatory or inhibitory post-synaptic currents from SuM inputs were monitored before and after application of CCh (Figure III.3.1A). Given both resting membrane potential and neurotransmitter release of hippocampal neurons involved in the microcircuit engaged by SuM in area CA2 were affected by CCh, we measured how the amplitudes of EPSCs and IPSCs changed with increasing light intensity. Strikingly, application of 10  $\mu$ M CCh reduced the amplitude of light-evoked EPSCs throughout the power-response curve (Figure III.3.1B; n = 14; two-way ANOVA with repeated measures, p < 0.001). This effect was solely due to changes in excitatory transmission from SuM as it persisted in experiments performed with GABA<sub>A</sub> and GABA<sub>B</sub> receptors blocked by 1  $\mu$ M SR95531 and 2  $\mu$ M CGP55845A (Figure III.3.1C; n = 7; two-way ANOVA with repeated measures, p < 0.001). Examination of the short-term synaptic depression of light-evoked EPSCs before and after CCh wash-in revealed an increase of the paired-pulse ratio (PPR) indicating that CCh decreases the release of glutamate by pre-synaptic SuM axons (Figure III.3.1B and Figure III.3.1C; PPRs were  $0.65 \pm 0.06$  in control and  $1.07 \pm 0.06$  in CCh hence a  $84 \pm 19$  % increase by CCh, n = 14; paired-T test, p < 0.001; PPRs were

0.59 ± 0.06 in SR95531 & CGP55845A and 0.87 ± 0.05 in SR95531 & CGP55845A and CCh hence a 51 ± 11 % increase by CCh, n = 7; paired-T test, p < 0.001). Consistent with this, amplitudes of light-evoked IPSCs recorded in CA2 PNs were also reduced by CCh at all light intensities (Figure III.3.1D; n = 17; two-way ANOVA with repeated measures, p < 0.001). Similarly, inhibitory responses to SuM photostimulation showed less short-term depression after CCh application as evidenced by an increased PPR of IPSC (Figure III.3.1D; PPRs were 0.73 ± 0.07 in control and 1.05 ± 0.05 in CCh hence a 67 ± 18 % increase by CCh, n = 17; paired-T test, p = 0.001). Altogether, these results show that activation of cholinergic receptors in acute hippocampal slices decreases glutamate release from SuM inputs. This was directly demonstrated at the excitatory SuM-CA2 PN synapse and can be inferred to apply to excitation of INs by SuM as well. Consequently, CCh application reduces SuM-driven feedforward inhibition of CA2 PNs by reducing the recruitment of INs or decreasing GABA release from these INs, or both. Therefore, because short-term depression of EPSCs and IPSCs is decreased by CCh, SuM-driven excitation and inhibition in area CA2 is likely to develop more gradually over time during a train in conditions of elevated cholinergic tone.

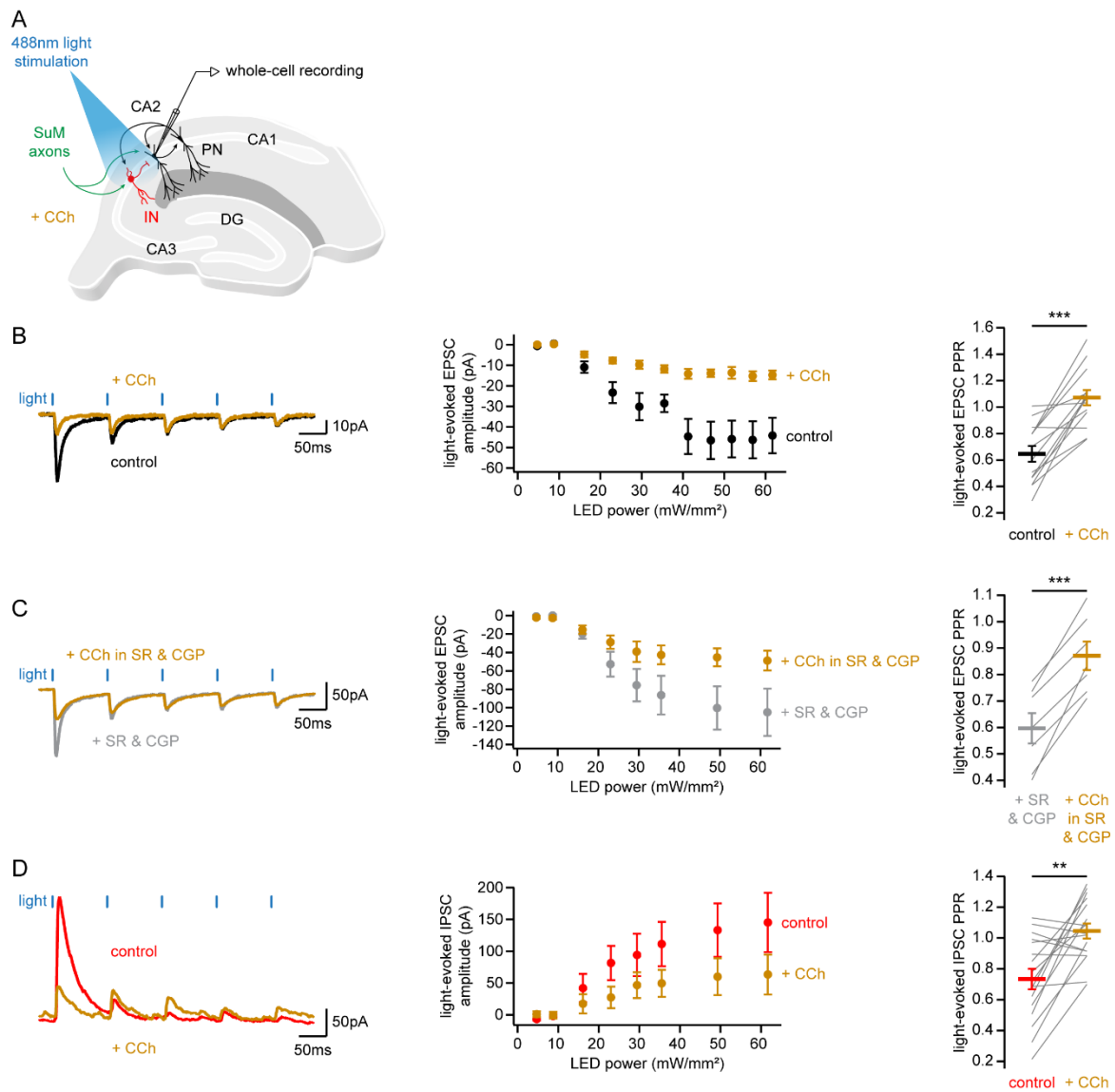


**Figure III.3.1. Reduction of SuM excitatory and inhibitory transmission by carbachol.**

**A.** Diagram illustrating the whole-cell recording configuration of PNs in area CA2 and SuM fiber stimulation in acute hippocampal slices. **B, C, D.** Effect of 10  $\mu$ M CCh on SuM light-evoked PSCs recorded in CA2 PNs under different conditions : voltage clamp at -70mV in control (**B**, control shown in black, CCh shown in orange), voltage clamp at -70mV with inhibitory transmission blocked (**C**, SR95531 & CGP55845A shown in grey, SR95531 & CGP55845A + CCh shown in orange), and voltage clamp at +10mV (**D**, control shown in red, CCh shown in orange). Left, sample traces. Middle, power-response curves (**B**,  $n = 14$ ; two-way ANOVA with repeated measures,  $p < 0.001$ ; **C**,  $n = 7$ ; two-way ANOVA with repeated measures,  $p < 0.001$ ; **D**,  $n = 17$ ; two-way ANOVA with repeated measures,  $p < 0.001$ ; error bars represent SEM). Right, comparison of PPRs (**B**,  $n = 14$ ; paired-T test,  $p < 0.001$ ; **C**,  $n = 7$ ; paired-T test,  $p < 0.001$ ; **D**,  $n = 17$ ; paired-T test,  $p = 0.001$ ; individual cells shown as grey lines, population average shown as horizontal line, error bars represent SEM).

### CA2 pyramidal neuron burst firing of action potentials is controlled by the SuM inhibitory drive

We previously documented a peculiar pattern of burst firing of action potentials from CA2 PNs in the presence of CCh. Because this likely approximates the physiological activity of CA2 PNs during theta and gamma oscillations in the hippocampus in vivo, and because SuM neurons discharge action potentials time-locked to the hippocampal theta, we asked how SuM activity would influence burst firing in CA2 PNs. Using the same strategy as above, we performed whole-cell patch-clamp recordings of CA2 PNs with K<sup>+</sup>-based intracellular solution and monitored their V<sub>M</sub> without current injection (Figure III.3.2A). As previously described, application of 10 μM CCh caused CA2 PNs to depolarize and subsequently fire bursts of action potentials (Figure III.3.2B). Under these conditions, CA2 PN V<sub>M</sub> slowly increases from after-burst hyperpolarization but then rapidly rises when reaching depolarized levels that lead to the next burst. Given these bursts occur at a rather low frequency and most of the V<sub>M</sub> changes happen close to the onset of bursts, we decided to use long trains of light pulses at 10 Hz to stimulate SuM inputs starting shortly before bursts and lasting for 2 minutes (Figure III.3.2B). To achieve this, the dynamics of V<sub>M</sub> depolarization were monitored for several bursts to determine a “pre-burst” V<sub>M</sub> level that reliably preceded burst firing (Figure III.3.2B and Figure III.3.2C). This threshold was adjusted depending on the dynamics of V<sub>M</sub> changes in individual experiments and V<sub>M</sub> values at light onset measured *post hoc* gave an average pre-burst V<sub>M</sub> of  $-53.7 \pm 0.7$  mV (n = 8), ranging from -55.0 mV to -49.3 mV in individual cells. Subsequently, photostimulation trains were initiated when the pre-burst V<sub>M</sub> was reached (Figure III.3.2B). Subsequent “light-on” bursts were interleaved with “light-off” ones serving as internal controls. Both light-on and light-off bursts were analyzed by aligning to the mean pre-burst V<sub>M</sub> corresponding to the onset of the SuM photostimulation for each cell (Figure III.3.2C). This approach revealed that light-on bursts were significantly delayed with regards to the pre-burst V<sub>M</sub> compared to light-off bursts (Figure III.3.2C; burst latencies from pre-burst V<sub>M</sub> were  $11.8 \pm 2.7$  s during light-off epochs and  $29.3 \pm 5.3$  s during light-on epochs hence a  $17.5 \pm 4.3$  s delay induced by photostimulation, n = 8; paired-T test, p = 0.004). This was likely due to the feedforward inhibition recruited by SuM inputs as CA2 PNs transiently repolarized upon photostimulation onset (Figure III.3.2B and Figure III.3.2C). Unfortunately, the role of inhibition recruited by SuM input in delaying bursts could not be directly tested as blocking inhibitory transmission during CCh application transforms bursts into epileptiform-like events (see Figure III.1.7D). Even so, fast synaptic transmission from SuM axons likely accounts for the burst delay as the effect of SuM activation was abolished by blocking excitatory

transmission with 10  $\mu$ M NBQX & 50  $\mu$ M APV in a preliminary subset of experiments (Figure III.3.2C). The delay in burst firing after SuM photostimulation observed from individual CA2 PNs was accompanied by a transient reduction of spiking activity recorded extracellularly in nearby CA2 SP during light-on epochs (Figure III.3.2D; firing rates were  $2.0 \pm 0.2$  Hz during the 2 seconds preceding light onset and  $1.4 \pm 0.1$  Hz during the 2 seconds following light onset hence a  $31 \pm 4.4$  % decrease by photostimulation,  $n = 8$ ; paired-T test,  $p = 0.002$ ). No change of firing rate was observed at these time points during interleaved light-off epochs (Figure III.3.2D; firing rates were  $1.9 \pm 0.2$  Hz during the 2 seconds before reaching pre-burst  $V_M$  and  $2.2 \pm 0.3$  Hz during the 2 seconds after pre-burst reached,  $n = 8$ ; paired-T test,  $p = 0.26$ ). Comparison of field spiking activity between light-off and light-on epochs confirmed a decrease in firing rate following light onset (Figure III.3.2D; firing rates during the 2 seconds following light onset were  $29 \pm 8.2$  % lower than the corresponding time window in light-off epochs,  $n = 8$ ; paired-T test,  $p = 0.018$ ). Therefore, activation of SuM inputs can control the discharges of bursts by CA2 PNs in CCh and potentially pace bursting from several CA2 PNs by enforcing an inhibitory time window. Of note, the reduction in short-term synaptic depression of SuM transmission by CCh seems well suited to accommodate the slow dynamics of the bursting pattern displayed by CA2 PNs.

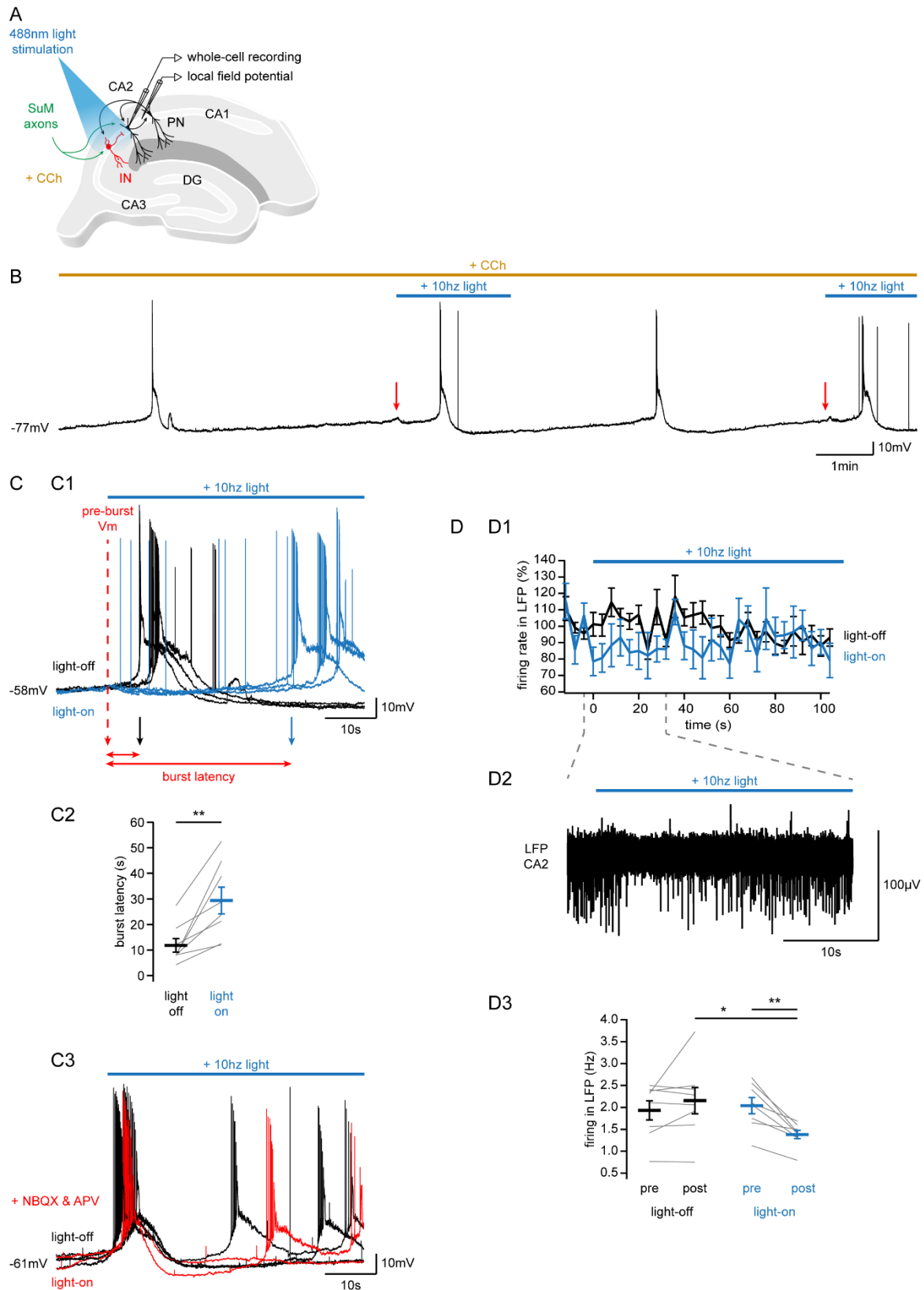


**Figure III.3.2. SuM control of CA2 PN bursting activity.**

**A.** Diagram illustrating the simultaneous whole-cell recording configuration of CA2 PNs and LFP recordings from area CA2 SP and SuM fiber stimulation in acute hippocampal slices with application of 10  $\mu$ M CCh. **B.** Sample trace of bursts recorded whole-cell from a CA2 PN during CCh application with

and without photostimulation of SuM inputs at 10 Hz for 2 minutes, note the repolarization of  $V_M$  upon light onset (red arrows). **C.** SuM fiber photostimulation delays AP bursting of CA2 PNs. **C1.** Sample traces of light-on (blue) and light-off (black) bursts aligned to the pre-burst  $V_M$  for measurements of latencies. **C2.** Comparison of burst latencies relative to pre-burst  $V_M$  in light-off and light-off conditions (individual cells shown as grey lines, population average shown as horizontal line, error bars represent SEM,  $n = 8$ ; paired-T test,  $p = 0.004$ ). **C3.** Example traces of pre-burst  $V_M$ -aligned light-on (red) and light-off (black) bursts recorded in the presence of 10  $\mu\text{M}$  NBQX & 50  $\mu\text{M}$  APV, note the absence of delay upon SuM inputs photostimulation. **D.** Reduced AP firing in area CA2 during photostimulation of SuM inputs. **D1.** Time course of firing rates recorded with extracellularly in CA2 SP during light-on (blue) and light-off (black) bursts, note the transient decrease of firing rate at the population level upon photostimulation of SuM inputs (error bars represent SEM,  $n = 8$ ). **D2.** Sample trace of extracellularly recorded APs from CA2 SP before and during photostimulation of SuM inputs (the trace shown corresponds to the time window demarcated by gray dashed lines), note the strong reduction of AP firing following light onset. **D3.** Comparison of firing rates the LFP recorded from CA2 SP in light-off and light-on bursts before (pre) and during (post) photostimulation of SuM inputs (individual cells shown as grey lines, population average shown as horizontal line, error bars represent SEM,  $n = 8$ ; paired-T test between pre- and post-light-on,  $p = 0.002$ ; paired-T test between post-light-off and post-light-on,  $p = 0.018$ ).

### SuM inputs onto area CA2 produces a silencing output over CA1 activity

As SuM inputs control burst firing of action potentials and likely pace activity in area CA2, we wondered how the subsequent output of CA2 PNs would affect their post-synaptic targets. Because CA2 PNs strongly project to CA1 PNs, this activity is likely to influence CA1 encoding and hippocampal output. We focused our investigation on area CA1 and examined the consequences of CCh-induced CA2 activity shaped by SuM input in that region (Figure III.3.3 and Figure 3A). In collaboration with our study, *in vivo* experiments from the McHugh laboratory using the *Csf2rb2-Cre* line have shown that optogenetic stimulation of SuM inputs in area CA2 strongly affects social recognition memory. In detail, they observed that mice display enhanced exploration of a familiar animal when SuM fibers are photostimulated in area CA2. In addition, using *in vivo* recordings of multi- and single-units in area CA1 from these mice, they have shown a decrease in firing rate in CA1 following light-stimulation of SuM axons over CA2 (Figure III.3.3A and Figure III.3.3B). Therefore, we set out to decipher the SuM – CA2 – CA1 circuit in our *ex vivo* preparation. To this end, we applied their photostimulation protocol that consisted of light stimulation trains of 50 ms-long pulses delivered at 10 Hz for 1 second, repeated every 10 seconds for 2 minutes and interleaved with light-off sweeps of the same duration, with the microscope objective centered on area CA2 (Figure III.3.3 and Figure 3B). Extracellular field recordings in CA1 SP and whole-cell patch-clamp recordings of CA1 PNs were obtained in acute hippocampal slices superfused with CCh and subjected to this light stimulation protocol (Figure III.3.3, Figure 3A and 3B). First, we asked what synaptic events may be responsible for the decreased firing of CA1 units observed 10 – 20 ms after light onset *in vivo* (Figure III.3.3A and Figure III.3.3B). Whole-cell recordings of CA1 PNs showed an absence of EPSCs time-locked to the photostimulation (Figure III.3.3C) in all but one case ( $n = 11/12$ ). In contrast, we often ( $n = 7/12$ ) observed light-evoked IPSCs occurring 10 – 20 ms after light onset in CA1 PNs (Figure III.3.3D). Therefore, the reduction in firing of CA1 units *in vivo* is likely caused by increased inhibitory inputs onto CA1 PNs within 10 – 20 ms of SuM fiber stimulation over area CA2 (Figure III.3.3D).

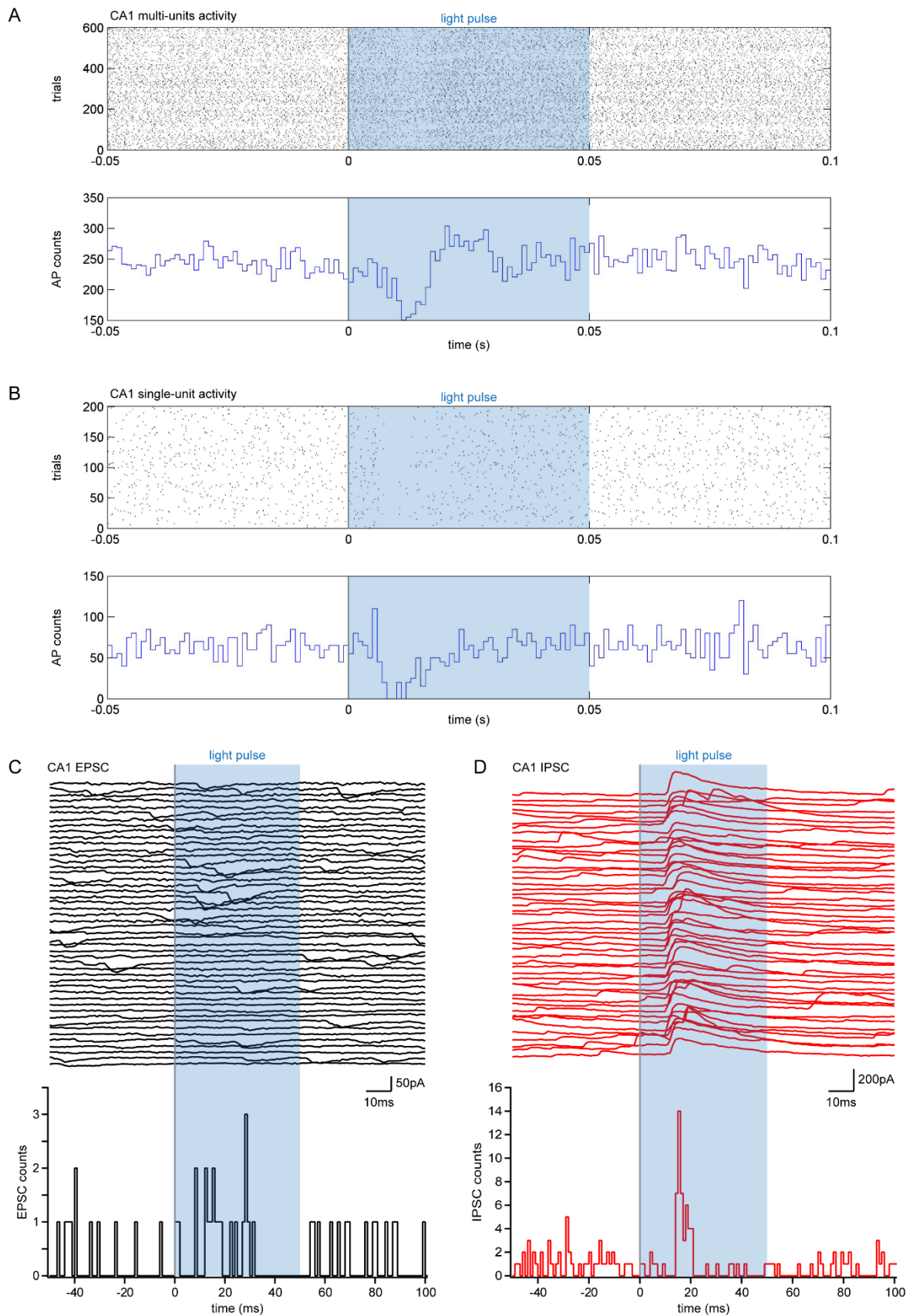


**Figure III.3.3. Immediate consequences of SuM activation on CA1 activity.**

**A.** Example raster plot (top) and corresponding peri-stimulus time histogram (bottom) of CA1 multi-unit activity recorded *in vivo* during photostimulation of SuM input over area CA2. **B.** Example raster plot

(top) and corresponding peri-stimulus time histogram (bottom) of CA1 single-unit activity recorded *in vivo* during photostimulation of SuM input over area CA2. **C.** Example waterfall plot (top) and corresponding peri-stimulus time histogram (bottom) of EPSCs recorded from a CA1 PN *ex vivo* during photostimulation of SuM input over area CA2. **D.** Example waterfall plot (top) and corresponding peri-stimulus time histogram (bottom) of IPSCs recorded from a CA1 PN *ex vivo* during photostimulation of SuM input over area CA2.

In addition to providing mechanistic insight into the cause of CA1 inhibition of AP firing shortly after light onset, these experiments revealed a striking effect of SuM activation on CA1 PN activity at longer time scale. Remarkably, we observed a reduction of spiking activity from CA1 SP that started at the onset of the SuM axons photostimulation and lasted for several seconds (Table III.3.1, Figure III.3.4C; firing rates after photostimulation were  $24.6 \pm 3.2$  % lower than before photostimulation and  $14.5 \pm 3.4$  % lower than during interleaved light-off epochs,  $n = 13$ ; paired-T tests,  $p < 0.001$  and  $p < 0.001$ ). Intracellular recordings of CA1 PNs held close to AP threshold ( $\sim -50$  mV) revealed a hyperpolarization of their  $V_M$  that prevented AP discharge upon SuM input activation and displayed the same time course as the decrease of AP firing observed in the CA1 SP field recording (Table III.3.1, Figure III.3.4D;  $V_M$  after photostimulation hyperpolarized by  $0.51 \pm 0.12$  mV compared to before photostimulation and by  $0.53 \pm 0.12$  mV compared to interleaved light-off epochs,  $n = 15$ ; paired-T tests,  $p < 0.001$  and  $p < 0.001$ ). Of note, although CA1 PNs did not readily depolarize after CCh application in our experiments, the hyperpolarizing effect of SuM photostimulation was still observed in CA1 PNs left at their resting  $V_M$  ( $\sim -70$  mV) without current injection, albeit more modest than the one obtained at  $-50$  mV (Table III.3.1, Figure III.3.4D;  $V_M$  after photostimulation hyperpolarized by  $0.13 \pm 0.06$  mV compared to before photostimulation and by  $0.12 \pm 0.05$  mV compared to interleaved light-off epochs,  $n = 13$ ; paired-T tests,  $p = 0.048$  and  $p = 0.044$ ). We then probed the synaptic events underlying this hyperpolarization by recording spontaneous EPSCs and IPSCs in CA1 PNs under the same conditions and protocol. Surprisingly, we reliably observed a transient increase of spontaneous EPSC frequency in CA1 PNs during the light-stimulation of SuM fibers, followed by a prolonged drop of the frequency of spontaneous events that followed the same time course as the hyperpolarization and reduction in AP firing (Table III.3.1, Figure III.3.4E; sEPSC frequency was increased by  $26.5 \pm 7.9$  % during and decreased by  $24.4 \pm 2.7$  % after compared to before photostimulation,  $n = 12$ ; paired-T tests,  $p = 0.013$  and  $p < 0.001$ ; sEPSC frequency was increased by  $36.6 \pm 14.2$  % during and decreased by  $22.2 \pm 8.3$  % after photostimulation compared to interleaved light-off epochs,  $n = 12$ ; paired-

T tests,  $p = 0.024$  and  $p = 0.010$ ). The frequency of spontaneous IPSCs underwent the same variations as that of sEPSCs, and the transient increase in sIPSC frequency was statistically significant when compared to interleaved light-off epochs (Table III.3.1, Figure III.3.4F; sIPSC frequency was increased by  $7.6 \pm 3.7\%$  during and decreased by  $20.5 \pm 4.3\%$  after compared to before photostimulation,  $n = 12$ ; paired-T tests,  $p = 0.093$  and  $p = 0.001$ ; sIPSC frequency was increased by  $11.1 \pm 5.5\%$  during and decreased by  $17.6 \pm 6.0\%$  after photostimulation compared to interleaved light-off epochs,  $n = 12$ ; paired-T tests,  $p = 0.032$  and  $p = 0.008$ ). No significant change in sEPSC or sIPSC amplitudes were detected (Table III.3.1). This result demonstrates a seconds-long global silencing of excitatory and inhibitory neurons afferent to CA1 PNs caused by activation of SuM inputs to area CA2. Importantly, all parameters measured here were stable in the light-off interleaved epochs (Table III.3.1, Figure III.3.4C-F). Interestingly, preliminary experiments performed with GABA<sub>A</sub> and GABA<sub>B</sub> receptors blocked indicate that the hyperpolarization of CA1 PNs after SuM activation remains in the absence of inhibitory transmission (Figure III.3.4D). This observation, if confirmed, argues for a neuromodulatory mechanism underlying CA1 PN hyperpolarization and reduced activity with SuM stimulation. In support of this hypothesis, voltage-clamp recordings of CA1 PNs at  $-70$  mV show a hyperpolarizing current upon SuM fiber activation that parallels the time course of hyperpolarization, reduced field activity, and decreased frequency of spontaneous events (Figure III.3.4E). Therefore, our data reveal that area CA1 is subjected to a drastic, prolonged and global silencing that results from modifications of area CA2 output by SuM activity. We postulate that the underlying mechanism of this silencing is likely to involve a change in conductances brought about by a yet to be identified.

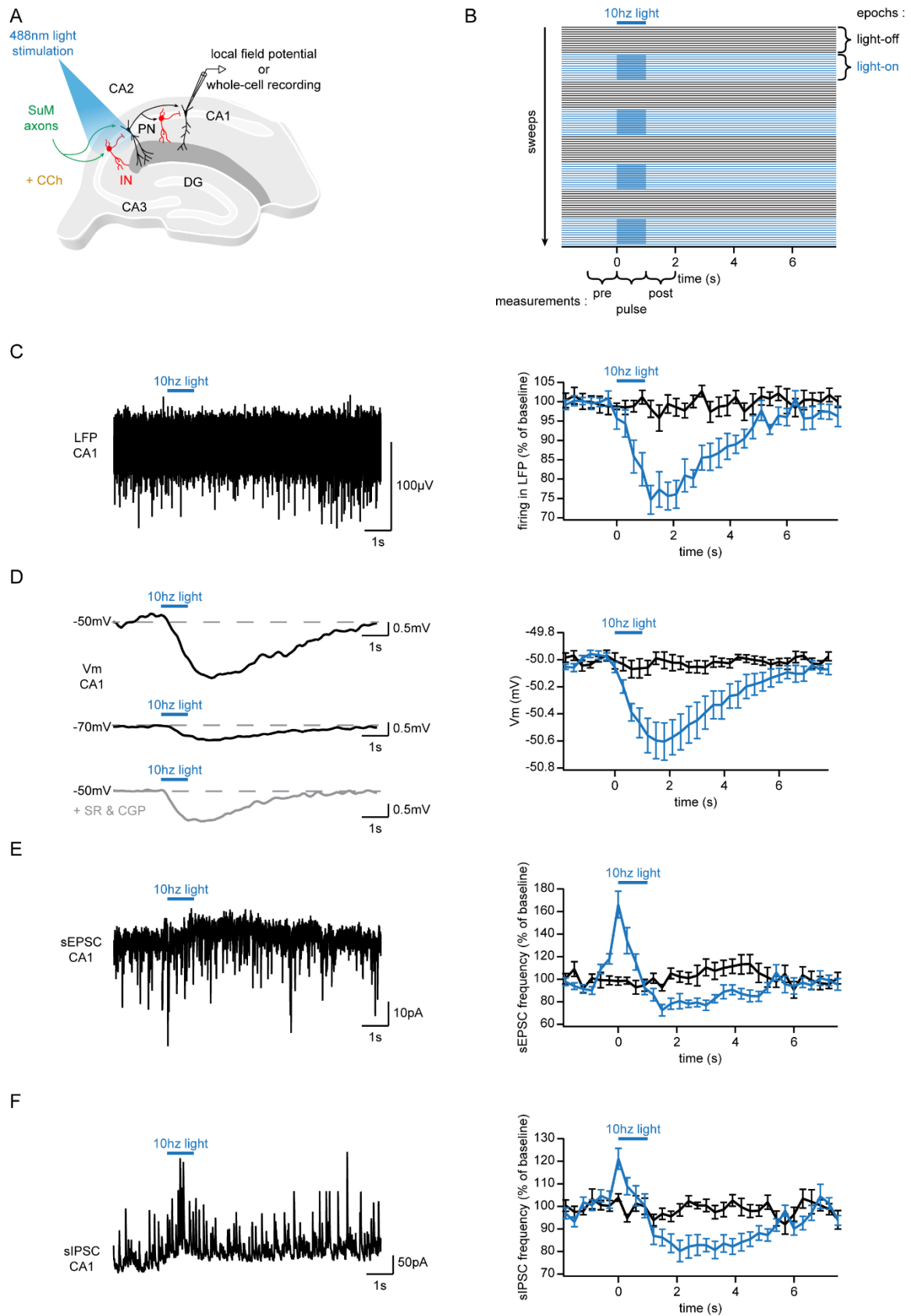


**Figure III.3.4. Delayed consequences of SuM activation on CA1 activity.**

**A.** Diagram illustrating the LFP and whole-cell recording configuration of PNs in area CA1 and SuM fiber stimulation in acute hippocampal slices with application of 10 μM CCh. **B.** Schematic illustration of the

protocol used in this series of experiments. **C.** Top, time course of firing rate in LFP from CA1 SP during light-off (black) and light-on (blue) epochs upon photostimulation of SuM inputs (error bars represent SEM,  $n = 13$ ; paired-T test between pre and post light-on,  $p < 0.001$ , paired-T test between post light-off and post light-on,  $p < 0.001$ ). Bottom, sample trace of extracellularly recorded APs from CA1 SP during a light-on epoch. **D.** Top, time course of CA1 PN  $V_M$  during light-off (black) and light-on (blue) epochs upon photostimulation of SuM inputs (error bars represent SEM,  $n = 15$ , paired-T test between pre and post light-on,  $p < 0.001$ , paired-T test between post light-off and post light-on,  $p < 0.001$ ). Bottom, sample traces of CA1 PN  $V_M$  held at -50 mV (upper black trace), -70 mV (lower black trace), and -50 mV with inhibitory transmission blocked (grey trace) during light-on epochs, note the hyperpolarization of  $V_M$  at both holding potentials and persisting in 1  $\mu\text{M}$  SR95531 and 2  $\mu\text{M}$  CGP55845A. **E.** Top, time course of sEPSC frequency in CA1 PNs during light-off (black) and light-on (blue) epochs upon photostimulation of SuM inputs (error bars represent SEM,  $n = 12$ , paired-T test between pre and pulse light-on,  $p = 0.013$ , paired-T test between pulse light-off and pulse light-on,  $p = 0.024$ , paired-T test between pre and post light-on,  $p < 0.001$ , paired-T test between post light-off and post light-on,  $p = 0.010$ ). Bottom, sample trace of sEPSCs recorded in a CA1 PN during a light-on epoch, note the activation of a hyperpolarizing current after photostimulation of SuM inputs. **F.** Top, time course of sIPSC frequency in CA1 PNs during light-off (black) and light-on (blue) epochs upon photostimulation of SuM inputs (error bars represent SEM,  $n = 12$ , paired-T test between pre and pulse light-on,  $p = 0.093$ , paired-T test between pulse light-off and pulse light-on,  $p = 0.032$ , paired-T test between pre and post light-on,  $p = 0.001$ , paired-T test between post light-off and post light-on,  $p = 0.008$ ). Bottom, sample trace of sIPSCs recorded in a CA1 PN during a light-on epoch.

**Table III.3.1. Consequences of SuM photostimulation over area CA2 on CA1 PNs.**

	Firing rate in LFP (Hz)	$\Delta V_m$ @ $\sim -50mV$ (mV)	$\Delta V_m$ @ $\sim -70mV$ (mV)	sEPSC frequency (Hz)	sEPSC amplitude (pA)	sIPSC frequency (Hz)	sIPSC amplitude (pA)
pre-light-off	10.5 $\pm$ 1.4	N/A	N/A	3.9 $\pm$ 0.5	14.3 $\pm$ 0.6	12.1 $\pm$ 1.0	27.5 $\pm$ 2.5
pulse-light-off	10.5 $\pm$ 1.3	-0.01 $\pm$ 0.05	-0.02 $\pm$ 0.05	3.8 $\pm$ 0.4	14.2 $\pm$ 0.7	12.0 $\pm$ 1.1	27.2 $\pm$ 2.6
post-light-off	10.5 $\pm$ 1.4	0.01 $\pm$ 0.04	-0.01 $\pm$ 0.05	4.1 $\pm$ 0.4	14.1 $\pm$ 0.5	12.0 $\pm$ 1.1	28.2 $\pm$ 2.9
pre-light-on	11.8 $\pm$ 1.6	N/A	N/A	3.9 $\pm$ 0.3	13.9 $\pm$ 0.7	12.6 $\pm$ 1.2	27.6 $\pm$ 2.3
pulse-light-on	10.6 $\pm$ 1.4	-0.20 $\pm$ 0.05	-0.07 $\pm$ 0.05	5.0 $\pm$ 0.6	14.0 $\pm$ 0.6	13.5 $\pm$ 1.4	32.0 $\pm$ 5.1
post-light-on	8.8 $\pm$ 1.2	-0.51 $\pm$ 0.12	-0.13 $\pm$ 0.06	2.9 $\pm$ 0.2	13.7 $\pm$ 0.7	10.1 $\pm$ 1.1	27.7 $\pm$ 2.9
Statistics							
pre-light-on VS pulse-light-on	p = 0.003	p < 0.001	p = 0.080	p = 0.013	p = 0.96	p = 0.093	p = 0.79
pre-light-on VS post-light-on	p < 0.001	p < 0.001	p = 0.048	p < 0.001	p = 0.38	p = 0.001	p = 0.97
pulse-light-on VS post-light-on	p < 0.001	p < 0.001	p = 0.45	p = 0.001	p = 0.33	p = 0.002	p = 0.27
pulse-light-off VS pulse-light-on	p = 0.61	p = 0.008	p = 0.24	p = 0.024	p = 0.70	p = 0.032	p = 0.27
post-light-off VS post-light-on	p < 0.001	p < 0.001	p = 0.044	p = 0.010	p = 0.48	p = 0.008	p = 0.57

## **IV - Discussion and future directions**

The work performed during the course of this thesis explored several aspects of area CA2 physiology and connections with intra- and extra-hippocampal structures in order to better understand the role of area CA2 in hippocampal circuits and its implications in learning and memory. Because area CA2 only recently began to be investigated by *in vivo* experiments and had never been studied in the context of ongoing network activity *ex vivo*, our first goal was to examine the characteristics of CCh-induced gamma-like oscillations in area CA2. Next, as tracing studies reported the innervation of area CA2 by SuM inputs relevant to theta oscillations, our project was to decipher the micro-circuit engaged by the long-range connection from SuM to area CA2. Finally, given CA2 PNs strongly project to area CA1 that constitutes the main hippocampal output, we probed the control of area CA2 activity by SuM inputs and the consequences on activity downstream in area CA1. In this section, we discuss our main experimental findings, place them in the larger context of hippocampal physiology, and propose future directions to complement these studies.

### **IV.1 - Roles of area CA2 in hippocampal networks and rhythms**

In this first series of experiments, we describe the cellular and circuit events underlying network oscillations in area CA2 and provide evidence of how they are related, in comparison with area CA3. Using a pharmacological model of gamma oscillations in acute hippocampal slices, we were able to compare network activity in area CA2 and CA3, as well as elucidate the corresponding dynamics of neuronal activity. We found that the CA2 neuronal network undergoes oscillatory activity in the gamma range in the presence of the cholinergic agonist CCh, similar to what has been reported in area CA3. In these conditions, we observed a peculiar pattern of activity in individual CA2 PNs consisting of bursts of action potentials. Blocking synaptic inputs revealed that CA2 PNs are intrinsically prone to bursting. However, the properties of these bursts were influenced by the activity of the surrounding network as AP timing is likely modulated by the ongoing oscillation. Altogether, these observations highlight important specific characteristics of area CA2 neuronal circuits to bear in mind when considering global hippocampal rhythms.

#### **IV.1.a - Similarities and differences of network activity in area CA2 and CA3**

Like CA3, area CA2 possess fundamental features required for rhythmogenesis in a neuronal network : recurrent excitation (Cui et al., 2013; Hitti and Siegelbaum, 2014) and feedback inhibition (Mercer et al., 2012a; 2012b). The dynamics of cellular activity in relation to the network oscillations have been clarified in area CA3 by a wealth of studies demonstrating that different neuronal populations fire action potentials in an organized manner during the gamma cycle (Csicsvari et al., 2003; Mann et al., 2005; Oren et al., 2006; Zemankovics et al., 2013), linking synaptic currents generating the oscillation with spiking output of neurons in the network. While the basic mechanisms are likely the same in area CA2, a number of peculiarities in this region suggest that it may behave differently than CA3. First, area CA2 hosts the highest density of interneurons, PV+ in particular, in the hippocampus (Botcher et al., 2014; Piskorowski and Chevaleyre, 2013). It is well established that PV+ interneurons are central to gamma oscillations (Fuchs et al., 2007; Gulyás et al., 2010; Korotkova et al., 2010). Thus, the level of inhibition brought about by these interneurons might be higher in CA2 than CA3 PNs. Second, CA2 PNs have a particularly low membrane resistance (Chevaleyre and Siegelbaum, 2010; Piskorowski et al., 2016; Sun et al., 2017), causing synaptic inputs received by a CA2 PN to have a lower impact on  $V_M$  than in a CA3 or CA1 PN. Third, CA2 PNs fire action potentials at lower frequencies and with higher rhythmicity than CA3 and CA1 PNs (Chevaleyre and Siegelbaum, 2010; Sun et al., 2017). Altogether, these observations predict that CA2 PNs will be harder to bring to firing threshold than CA3 PNs but would stay active longer once they start to spike. The sparsity of long bursts of action potentials reported here matches these predictions.

When considering rhythms in the whole hippocampal network, a striking feature is that the same oscillation is present in different subregions in which signals lead or lag relative to one another (Csicsvari et al., 2003; Patel et al., 2012). Obviously, the type of wiring that connects each subregion will determine how the oscillatory wave will travel. Studying the sequential activation of neurons and the relative timing of the oscillation in different subregions allows to identify where the signal originates and how it propagates through the hippocampus. Importantly, slow gamma oscillations have been described to be generated in area CA3 and propagate to CA1 through feedforward inhibition (Csicsvari et al., 2003; Zemankovics et al., 2013). This raises the question of the place of area CA2 in this circuit, as area CA2 and CA3 mainly inhibit each other through feedforward inhibition while CA2 PNs strongly excite CA1

PNs. Our data did not reveal a consistent lead or lag between oscillations from area CA2 and CA3. Whether this reflects that oscillators in area CA2 and CA3 are independent is unclear as we cannot exclude the possibility that axonal projections between regions were severed in our preparation. Future work with simultaneous recordings of gamma oscillations in area CA2 and CA3 *in vivo* is needed to resolve this issue.

#### **IV.1.b - Bursts of action potentials in CA2 PNs**

A major aspect of the dynamics of action potential firing in CA2 PNs unveiled by our study is that they come in bursts when CCh is present, similar to CA3 PNs (Cobb et al., 1999). Furthermore, these bursts occur repeatedly with synaptic transmission blocked. This demonstrates that CA2 PNs possess a combination of conductances allowing intrinsic bursting when challenged with CCh. Although we did not try to identify these conductances, predictions can be made from previous studies in other CA areas and prior information regarding CA2 PNs. Intuitively, the observation that CA2 PNs bursting occurs during membrane potential depolarization and an increase in membrane resistance suggests that CCh induces closure of potassium leak channels in these cells. Indeed, signaling through muscarinic cholinergic receptors (mAChR) decreases potassium conductances  $I_M$ ,  $I_{K_{SAHP}}$ , and leak in cortical principal cells (Alger et al., 2014; Cobb and Davies, 2005). In addition,  $I_h$ ,  $I_{NaP}$  and  $I_{cation-Ca^{2+}}$  are increased by mAChR activation (Alger et al., 2014; Cobb and Davies, 2005; Fisahn et al., 2002; Yamada-Hanff and Bean, 2013). Whether these observations hold for CA2 PNs remains to be determined. Interestingly, CA2 PNs have been described to express high mRNA levels of the potassium leak TREK channel whose increased conductance accounts for excitability defects of CA2 PNs in the  $Df16^{+/-}$  mouse model of schizophrenia (Piskorowski et al., 2016). It is possible that in this mouse model, the hyperpolarized  $V_M$  disrupts CA2 PN bursting, contributing to the deficits in social memory (Piskorowski et al., 2016) and cortico-hippocampal synchrony (Sigurdsson et al., 2010) observed in these mice.

While bursts of action potentials in CA2 PNs in the presence of CCh occurred with excitatory and inhibitory transmission blocked, the properties of these intrinsic bursts were different from those seen in an intact network. The observation that bursts occur more frequently in the absence of synaptic input suggests that excitation and inhibition normally structure the network excitability and paces bursts in individual CA2 PNs. This raises the issue of the potential synchrony of bursts amongst PNs in area CA2. Examination of the LFP signal during bursts did not reveal an increased gamma power during these epochs, thus arguing that bursts do not

represent hyper-synchronous events. On the contrary, blocking inhibitory transmission alone resulted in large epileptiform discharges recorded in the LFP which were never observed in control conditions. Hence, the pattern of activity that we describe in CA2 PNs does not originate from bouts of hyper-excitability but rather reflects physiological dynamics of CA2 PNs action potential firing that is shaped by synaptic inputs.

Finally, an interesting question is the consequence that bursts of action potentials in CA2 PNs will have on their post-synaptic targets in area CA3 and CA1. CA2 PNs strongly excite CA1 PNs (Chevalleyre and Siegelbaum, 2010; Kohara et al., 2013) and drive both excitation and feedforward inhibition onto CA3 PNs (Boehringer et al., 2017). Therefore, bursts of action potentials in CA2 PNs will elicit trains of EPSPs and IPSPs around theta frequency for several seconds in CA1 and CA3 PNs, the consequences of which merit further investigation.

#### **IV.1.c - Integration of area CA2 in theta and gamma hippocampal rhythms**

Although we describe several aspects of area CA2 activity in gamma oscillations, our study could not fully examine the role of area CA2 in oscillations that are absent in acute hippocampal slices. However, predictions can be made based on the connectivity patterns of area CA2 with brain structures involved in theta and gamma oscillations, and from evidence provided by *in vivo* experiments. Indeed, area CA2 is connected by the septum, the EC, area CA3, the DG, and the hypothalamus (Cui et al., 2013; Hitti and Siegelbaum, 2014; Kohara et al., 2013; Pan and McNaughton, 2004). Much like other hippocampal subregions, area CA2 likely receives theta-locked inhibition from the septum and excitatory inputs at theta and gamma frequencies from the EC. In contrast with other CA areas, CA2 is contacted by the SuM, providing an additional rhythmic input during theta oscillations. Area CA2 further differs from CA1 by receiving strong excitatory distal inputs from EC and a potent inhibitory drive from CA3. Somewhat surprisingly still, *in vivo* studies do not report major differences of theta modulation or preferred phase of PNs from CA2 and other CA regions (Kay et al., 2016; Mankin et al., 2015; Oliva et al., 2016). Conversely, CA2 PNs show lower amounts of theta phase precession than CA1 PNs, arguably because of different relative timing of EC and CA3 inputs between those regions (Fernández-Ruiz et al., 2017). Therefore, the uniquely strong excitatory drive from EC and the additional theta-locked input from SuM likely dynamically influence the behavior of CA2 PNs during theta and gamma oscillations. Further, the importance of area CA2 in hippocampal rhythms has been directly tested by blocking synaptic transmission from CA2 PNs (Boehringer et al., 2017). This manipulation leads to hippocampal hyperexcitability, a global increase in theta and gamma

power, and a shift in CA3 PNs preferred theta phase (Boehringer et al., 2017), thus revealing a clear contribution of area CA2 to hippocampal rhythms.

## **IV.2 - Relevance of SuM inputs to hippocampal area CA2 physiology**

In the second study, we provide direct evidence for a functional connection between the hypothalamus and the hippocampus. Using stereotaxic injection of viral vectors in combination with transgenic mouse lines to express channelrhodopsin in a projection-specific manner, we have been able to selectively stimulate SuM axons in area CA2 of the hippocampus, allowing for the direct examination of synaptic transmission. This approach yielded novel functional physiological information about the SuM post-synaptic targets and overall consequences of activation. We found that, consistent with previous anatomical studies, SuM inputs into area CA2 are entirely glutamatergic. However, in contrast to previous reports, we found that SuM inputs form synapses onto both PNs and INs in area CA2. This excitation of INs was sufficient to reliably drive feedforward inhibition onto PNs, and was capable of influencing the jitter and timing of PN action potential firing. At the population level, deep PNs received a stronger inhibitory influence from SuM inputs than superficial PNs. The excitatory drive evoked by light-stimulation of SuM inputs was significantly larger for BC INs, which we demonstrate are predominantly PV+ BCs. Indeed, chemogenetic silencing of these cells as well as reduction of their GABA release by activation of mu or delta opioids receptors decrease SuM-driven feedforward inhibition of CA2 PNs.

### **IV.2.a - SuM inputs to area CA2 form a microcircuit where PV+ basket cells strongly inhibit deep pyramidal neurons in area CA2 and CA3**

Glutamatergic innervation of area CA2 by the SuM has been previously described by tracing studies in rats (Kiss et al., 2000; Soussi et al., 2010) and reported to form synapses exclusively onto PNs (Maglóczy et al., 1994). Our experimental strategy allowed for the direct examination of the post-synaptic targets of SuM glutamatergic axons. Our results confirm that PNs in area CA2 indeed receive excitatory synapses from SuM axons. However, in contrast to what had been proposed in previous studies, we observed that SuM inputs target not only PNs but also INs in area CA2. Importantly, we identified a specific subpopulation of INs as PV+ BCs which were the cell type most potently excited by SuM. These BCs fired action potentials upon SuM input photostimulation, leading to a substantial feedforward inhibition of neighboring PNs. Consistent with the perisomatic targeting of BCs axons, recruitment of BCs

by SuM resulted in the control of PNs excitability. This finding demonstrates that SuM activity can pace action potential firing in PNs through recruitment of PV+ BCs. Furthermore, while excitatory transmission from SuM was restricted to neurons in area CA2, the feedforward inhibition extended in CA3b several hundreds of micrometers away from the termination zone of the SuM fibers. This is in accordance with the pattern of projection of BCs axons that extended toward CA3b. Thus, the SuM inhibitory control of PNs excitability appears more global over both area CA2 and CA3. Of note, SuM direct excitation and feedforward inhibition were equally distributed between CA2 and CA3 PNs.

Aside from regional distinctions such as CA2 versus CA3, hippocampal PNs have been described to differ according to the location of their soma along the radial axis of the pyramidal layer. Numerous physiological differences between deep and superficial PNs have been described in area CA1 (Danielson et al., 2016; Mizuseki et al., 2011), and a recent *in vivo* study revealed that area CA2 also hosts deep and superficial PNs with functional differences (Oliva et al., 2016a). More precisely, Oliva et al. describe a ramping up of deep CA2 PNs activity followed by a suppression of firing prior to sharp wave ripples (SWR) onset, and a peak of superficial CA2 PNs firing preceding the SWR recorded in CA1. When clustering PNs according to their deep or superficial somatic location and quantifying the relative strength of excitation and inhibition in these cells, we observed that SuM inputs exert a stronger overall inhibitory effect on deep PNs than on superficial PNs. Thus, the SuM can differentially influence these two subpopulations of CA2 PNs, which are functionally different. Namely, the preferential inhibitory over excitatory drive of the SuM on deep PNs could participate in promoting superficial PNs activity over deep PNs.

#### **IV.2.b - SuM input and space coding in area CA2**

Unlike in areas CA3 and CA1, place cells in area CA2 have been shown to be less precise and unstable (Kay et al., 2016; Mankin et al., 2015a; Oliva et al., 2016a). However, a recent study by Kay et al. revealed that area CA2 forms the basis of a hippocampal network that encodes location during immobility and sleep (Kay et al., 2016). More precisely, the activity of certain CA2 PNs (N units) was found to negatively correlate with sharp wave ripples (SWR). Consistently, CA2 PNs firing has been shown to decrease during SWR (Valero et al., 2015), and the deep subpopulation of CA2 PNs ramp up their activity before suppression of firing upon SWR occurrence (Oliva et al., 2016b). Furthermore, the activity of N units negatively correlated with locomotive speed, and hippocampal theta power. The firing of these cells was found to

encode location during immobility and in the absence of theta oscillation. We propose that our results provide crucial mechanistic insight about CA2 N units activity. It has been shown that neuronal activity in the SuM is locked to hippocampal theta oscillations (Kirk and McNaughton, 1991) which is prominent during locomotion (Buzsáki, 2002). We demonstrate that long-range SuM axons, which selectively innervate this area, provide a feedforward inhibition via PV+ basket cells in area CA2. Thus, by exciting BCs, the SuM can rhythmically inhibit CA2 and CA3a PNs during theta states associated with locomotion. Conversely, decreased SuM activity during immobility would allow CA2 and CA3a PNs to fire action potentials by relieving them from inhibition. Therefore, SuM activity likely allows for a state-dependent modulation of deep versus superficial CA2 PNs.

#### **IV.2.c - SuM input and hippocampal oscillations**

Oscillatory activity of hippocampal networks in the theta and gamma range support key functions of the hippocampus and are critical for learning and memory (Alexander et al., 2016; Vertes and Kocsis, 1997). Although numerous studies have yielded valuable insights into the generation, mechanisms and functions of these oscillations, the contribution of extra-hippocampal structures and the consequences of their activity on the hippocampus are still not entirely understood. Indeed, the SuM has been established as a key nucleus involved in setting the frequency of the hippocampal theta rhythm (Cui et al., 2013; Hitti and Siegelbaum, 2014; Kohara et al., 2013; Pan and McNaughton, 2004a) but how this control is achieved remains unclear. Activity in SuM is theta-locked and has been shown to strongly influence hippocampal theta frequency in anaesthetized rodents (Ariffin et al., 2010; Jiang and Khanna, 2006; Kirk and McNaughton, 1993) and partially in awake animals (Pan and McNaughton, 1997; 2002; Ruan et al., 2011; Shahidi et al., 2004; Woodnorth et al., 2003). In addition, hippocampal theta activity during spatial learning in a Morris water maze is altered upon serotonin depletion in SuM (Gutiérrez-Guzmán et al., 2012; Hernández-Pérez et al., 2015). SuM influence over hippocampal theta rhythm could be achieved indirectly by SuM outputs to the septum (Jiang and Khanna, 2006; Vertes and Kocsis, 1997), but also through its direct outputs to the DG and hippocampal area CA2 (Vertes, 1992).

The micro circuitry we reveal in this work provides insight into how the SuM activity can affect hippocampal oscillatory activity. The population of INs potently excited by SuM transmission have many features that allow us to classify them as PV+ BCs. They have soma located in the somatic layer with densely packed perisomatic-targeted axons. These cells are fast spiking,

show PV immuno-reactivity, are sensitive to MOR and DOR activation, and their selective silencing reduces SuM driven feed-forward inhibition of area CA2 PNs. BCs are central actors of hippocampal theta and gamma oscillations (Csicsvari et al., 2003a; Mann et al., 2005a; Oren et al., 2006a; Zemankovics et al., 2013). Specifically, PV+ fast-spiking INs participate to both theta and gamma oscillations, and are involved in hippocampal learning (Fuchs et al., 2007a; Gulyás et al., 2010a; Korotkova et al., 2010a). It is believed that during oscillatory activity in the hippocampus, specific interneuron subtypes act to control timing windows to synchronize pyramidal cell discharge. We found that SuM stimulation delays action potential firing and strongly reduces action potential jitter. Thus, the inhibitory post-synaptic targets of SuM axons combine all the characteristics for efficiently affecting hippocampal oscillations.

In addition to its role in theta oscillations, the SuM has been implicated in the regulation of brain states by controlling arousal versus sleep (Pedersen et al., 2017). Indeed, DG-projecting SuM neurons are labelled by c-fos after REM sleep (Billwiller et al., 2017; Renouard et al., 2015). Chemogenetic activation or inhibition of VGluT2+ SuM neurons respectively increases and decreases wake as well as EEG power in the theta and gamma bands (Pedersen et al., 2017). However, the experimental strategy employed in this study does not allow for discrimination between the relative contributions of SuM inputs to CA2 and to DG in driving arousal.

#### **IV.2.d - Gating of area CA2 activity by PV+ INs and significance for pathologies**

The density of PV+ INs in area CA2 is strikingly higher than in neighboring areas CA3 and CA1 (Botcher et al., 2014a; Piskorowski and Chevaleyre, 2013a). This population of INs has been shown to play a powerful role in controlling the activation of CA2 PNs by CA3 inputs (Nasrallah et al., 2015; Piskorowski and Chevaleyre, 2013b). We show in this study that long-range inputs from the SuM can strongly recruit PV+ BCs, which in turn inhibit PNs in this area. Hence, both intra-hippocampal inputs from CA3 and long-range inputs from the SuM converge onto PV+ INs to control CA2 PN excitability and output.

Postmortem studies have reported losses of PV+ INs in area CA2 in several pathological contexts including bipolar disorder (Benes et al., 1998), Alzheimer's disease (Brady and Mufson, 1997), and schizophrenia (Benes et al., 1998; et al., 2004) (for a review see Chevaleyre and Piskorowski, 2016). Consistent with these reports, in a mouse model of the 22q11.2 deletion syndrome, we found a loss of PV staining and deficit of inhibitory transmission in area CA2 that were accompanied by impairments in social memory (Piskorowski et al., 2016). We

postulate that the PV+ INs altered during pathological conditions may be the same population of PV+ BCs recruited by long-range SuM inputs. Thus, the loss of function of PV+ INs in area CA2 could disrupt proper long-range connection between the hippocampus as the hypothalamus and possibly contribute to some of the cognitive impairments observed in schizophrenia animal models. Further, pharmacological mouse models of schizophrenia have reported increased c-fos immunoreactivity in the SuM as well as memory impairments (Castañé et al., 2015). Although several alterations in these models of schizophrenia could lead to deficits of hippocampal-dependent behavior, abnormalities of the SuM projection onto area CA2 appear as a potential mechanism that warrants further investigation.

#### **IV.2.e - Differential modulation of DG and area CA2 by SuM inputs and consequences on hippocampus-dependent memory formation**

Area CA2 is not the sole hippocampal target of SuM inputs as the DG also receives innervation from the SuM (Haglund et al., 1984; Vertes, 1992). Interestingly, afferents to area CA2 and the DG likely originate from distinct neurons in the SuM and might therefore serve different functions (Kiss et al., 2000; Soussi et al., 2010a). While previous studies and our own work have established that VGluT2-expressing SuM inputs target area CA2 where they control CA2 PN excitability through feedforward inhibition, the physiology of SuM transmission to the DG is most likely different. Indeed, SuM axons have been shown to co-release glutamate and GABA on DG granule cells (Boulland et al., 2009; Pedersen et al., 2017; Soussi et al., 2010b; and our own observations). In addition, we demonstrated that SuM inputs also recruit feedforward inhibition onto DG granule cells. These observations raise the question of the net effect of SuM driven excitation and inhibition have on GCs. Although the combination of direct and feedforward inhibition tends to suggest an overall inhibitory effect of SuM transmission onto GCs, *in vivo* results describing an excitatory effect of SuM stimulation argue for a predominance of SuM-driven excitation in DG GCs (Mizumori et al., 1989). In contrast with CA2 PNs, DG GCs are highly resistive and will therefore respond readily to synaptic inputs (Spruston and Johnston, 1992). In addition, overall effects of SuM transmission on DG GCs will depend on the distribution of direct excitatory and inhibitory synapses on the dendritic tree of GCs as well as the location targeted by INs mediating the feedforward inhibition. Hence, the influence of SuM inputs onto DG GC activity is difficult to predict and might vary during different brain states. Current-clamp recordings of DG GCs coupled with SuM stimulation are required to resolve this issue.

Because the SuM, area CA2 and the DG have separately been described to participate in specific hippocampal memory functions, a particularly interesting challenge is to determine how these regions interact or act independently on each function. For instance, SuM activity is involved in working, spatial and contextual fear memory as well as novelty- and reward-laden behaviors (Aranda et al., 2006; Gutiérrez-Guzmán et al., 2012; Hernández-Pérez et al., 2015; Ikemoto, 2005; Ikemoto et al., 2004; Ito et al., 2009; Pan and McNaughton, 1997; 2002; 2004b; Shahidi et al., 2004a; 2004b). Therefore, one may ask which aspects of hippocampal functions carried out by CA2 such as social memory and novelty detection (Hitti and Siegelbaum, 2014b; Wintzer et al., 2014) are due to SuM modulation of CA2 output. Or when considering the DG, how does SuM participate in pattern separation and working memory (Gilbert et al., 2001; Xavier et al., 1999).

In collaboration with our investigation of hippocampal circuits engaged by SuM inputs, the McHugh laboratory has been examining the behavioral effects of activating or silencing SuM projections to either area CA2 or the DG in a spatially-restricted way. Using retrograde virus injections in SuM-Cre animals to selectively express excitatory or inhibitory DREADDs or opsins in either CA2-projecting or DG-projection SuM neurons, they were able to manipulate these inputs during awake behavior. Strikingly, activation or inhibition of SuM inputs to area CA2 during a social task bi-directionally affected social memory. Activation of SuM inputs increased exploration of a familiar mouse whereas silencing these inputs prevented the enhanced exploration of a novel animal. This indicates that SuM inputs play a role in social novelty detection or proper encoding of social information. On the other hand, silencing DG-projecting neurons in a delayed alternation task impaired working memory and object recognition. Therefore, in agreement with distinct physiological features of the SuM to CA2 versus DG projections, these two circuits are specifically involved in different behaviors and hippocampal-dependent learning processes.

#### **IV.2.f - Relevance of the SuM excitatory drive to CA2 PNs**

Our findings clearly prove an overall inhibitory drive of SuM inputs on area CA2 PNs. This point leads to the question of the relevance of the SuM excitatory transmission received by the majority of CA2 and CA3a PNs. Several observations can help in understanding the role of SuM-driven excitation of CA2 PNs. First, CA2 PNs are strongly excited by distal EC inputs that can elicit to action potential firing (Chevaleyre and Siegelbaum, 2010b; Sun et al., 2014). During theta oscillations, both SuM and EC neurons rhythmically fire at theta frequency

(Buzsáki, 2002; Kirk et al., 1996; Kocsis and Vertes, 1994). Therefore, depending on their phase relation relative to the theta cycle, these excitatory inputs could summate in CA2 PNs and influence the timing of their action potential discharge. Second, SuM-driven excitation of area CA2 PNs likely prevails in conditions of decreased activity from PV+ BCs. As discussed above, it might be the case in pathologies such as schizophrenia (Piskorowski et al., 2016b). Besides pathological conditions, PV+ INs in area CA2 can be depressed by a delta opioid receptor-dependent long-term depression of inhibition (iTLD) that can be induced by 10 Hz stimulation of CA3 inputs (Nasrallah et al., 2015; Piskorowski and Chevaleyre, 2013b). Interestingly, preliminary results from our laboratory indicate this iTLD naturally occurs in mice exposed to an enriched environment. In these conditions, the SuM-driven feedforward inhibition mediated by PV+ INs would be reduced, thus allowing a stronger impact of excitatory transmission from SuM inputs onto CA2 PNs. How this modification of E/I drive from SuM affects CA2 PNs remains to be determined. Of note, environmental enrichment has been described to increase theta-nested gamma oscillations in the hippocampus (Shinohara et al., 2013). Given its rhythmic activity with theta, the SuM might contribute to this effect through modified influence over area CA2.

### **IV.3 - Control of hippocampal activity and output by SuM inputs**

In the third study, we report the physiological impact of SuM inputs to area CA2 and the consequences on downstream CA1 in conditions of high cholinergic tone. Using genetically-restricted optogenetics to selectively stimulate SuM axons on acute hippocampal slices superfused with the cholinergic agonist CCh, we investigated the responses of CA2 and CA1 PNs to the activation of SuM inputs during ongoing network activity. This strategy enabled us to decipher the SuM-CA2-CA1 circuit and to quantify the events occurring at each step. First, we demonstrated that SuM direct excitatory and feedforward inhibitory drives are dampened in amplitude but prolonged in time by CCh. Next, we showed that recruitment of inhibition by SuM inputs exerts a temporal control on the bursting of action potentials by CA2 PNs. Finally, we found that the CA2 output shaped by SuM inputs triggers a strong and prolonged reduction of CA1 activity. Therefore, our data provide novel functional information regarding the physiology of hippocampal circuits and highlight a powerful control of hippocampal output by long-range SuM inputs.

### **IV.3.a - Cholinergic modulation of SuM inputs**

Quantification of the SuM light-evoked EPSC and IPSC amplitudes and PPRs in CA2 PNs revealed that CCh decreases glutamate release from SuM axons. While this explanation is straight forward for mono-synaptic excitation, additional factors need to be accounted for when considering the feedforward inhibition recruited by SuM input. First, the dynamics of the excitatory synapses formed by SuM axons onto PNs and INs might differ, although no evidence suggests that it is the case. Second, CCh causes a mixed effect on inhibitory transmission as it depolarizes most interneurons but decreases GABA release ((Alger et al., 2014; Cobb and Davies, 2005). Therefore, one can predict that weaker excitation from SuM would be necessary to bring INs to threshold but that subsequent inhibition of CA2 PNs would be less pronounced in CCh. In addition, the depolarization of INs brought about by CCh might cause INs other than PV+ BCs to be recruited by SuM input and thus participate in the feedforward inhibition of CA2 PNs. Although we did not fully address this point, we occasionally observed an incomplete block of IPSCs by further application of DAMGO after CCh indicating that other INs beside PV+ BCs might be recruited by SuM inputs in these conditions. Patch-clamp recordings of identified IN subtypes and chemogenetic silencing of specific populations of INs are necessary to make firmer conclusions on this matter.

Concerning the pre-synaptic inhibition of SuM axons by CCh, the possibility of pre-synaptic expression of cholinergic receptors by SuM fibers afferent to the hippocampus cannot be ruled out, although tracing studies never reported this. Indeed, cholinergic pre-synaptic inhibition of excitatory transmission has been described in other hippocampal circuits (Hasselmo, 2006). Alternatively, depression of glutamate release from SuM axons could be due to other neuromodulators released by hippocampal neurons when challenged with CCh. In any case, the reduction of SuM light-evoked EPSC and IPSC amplitudes in CCh comes with a decreased short-term depression of these inputs. This is particularly interesting in the context of rhythmic activity of SuM neurons during theta oscillations when the cholinergic tone is high. Under these conditions, the reduced depression of excitatory and inhibitory transmission from SuM would allow its influence over hippocampal post-synaptic targets to be sustained in time. Albeit initially less powerful, the SuM drive would have a stronger impact over time when acetylcholine concentration is high. This likely allows SuM inputs to reliably recruit feedforward inhibition over time, causing significant delays of CA2 PN bursting (Figure 2). At a more global scale, low short-term depression of SuM transmission probably participates in synchronizing

theta oscillations through reciprocal connections with other structures displaying rhythmic activity, such as the septum (Pan and McNaughton, 2004a).

#### **IV.3.b - Synchronization of CA2 activity by SuM inhibitory drive**

In an effort to assess the consequences of SuM inputs onto area CA2 activity in a physiological way, we report that the timing of bursts of action potential discharged by CA2 PNs can be controlled by the SuM inhibitory drive. However, the experimental strategy employed here comes with a number of caveats. First, the onset of SuM inputs photostimulation is clearly biased towards times preceding bursts in the recorded CA2 PN. This choice was made for the following reasons : light-stimulation of SuM axons recruits feedforward inhibition, therefore its impact would have been limited if triggered earlier in the inter-burst interval when CA2 PNs are hyperpolarized. On the contrary, the amount of feedforward inhibition might not have been sufficient to terminate an ongoing burst if light-stimulation had been delivered later, especially because CA2 PNs can intrinsically burst in the absence of synaptic inputs. In addition, PV+ BCs mediating the SuM-driven feedforward inhibition are likely recruited in feedback loops when CA2 PNs fire action potentials during bursts. Although the interaction of the SuM and CA2 excitatory drives onto PV+ BCs would have been extremely interesting to study notably in terms of AP phase coupling to the oscillation, the low number of bursts and their limited duration would have made these measurements noisy. Therefore, triggering SuM activity during the rising phase of bursts seemed the best option as it also yields information about the generation of bursts through recurrent excitatory connections of CA2 PNs captured by the field spiking activity. Indeed, in parallel with the delay of CA2 PN bursting, we observed a reduction in action potential firing recorded extracellularly in CA2 SP. Because they represent the majority of neurons in the pyramidal layer, CA2 PNs are likely to be the source of action potentials recorded with a field electrode in CA2 SP. Therefore, the inhibitory effect of SuM stimulation applies to the population of CA2 PNs as a whole. Although we did not see an increased field spiking activity prior to bursts recorded whole-cell in the light-off condition, the reduction of firing rate in CA2 SP might contribute to the delay of burst firing in the light-on condition by dampening recurrent excitation between CA2 PNs. Surprisingly, we did not observe an increased firing in CA2 SP after the light-induced delay of bursts from CA2 PNs recorded whole cell. This argues for a gradual relief of SuM-driven inhibition allowing CA2 PNs to fire bursts of APs rather than a post-inhibitory rebound of excitation that would cause synchronous burst discharge of CA2 PNs. In agreement with this, CA2 PNs normally fire sparse

bursts of action potentials and do not discharge together, as opposed to hyper-synchrony observed with inhibitory transmission blocked (see Figure III.1.7D). Therefore, it is likely that the prolonged trains of SuM photostimulation suppress firing in area CA2 by differentially delaying CA2 PNs activity depending on their level of depolarization at the onset of the light. As inhibition wanes off later during light trains, CA2 PNs gradually return to burst firing. Hence, SuM activity can efficiently control area CA2 output by pacing burst firing of CA2 PNs through feedforward inhibition.

#### **IV.3.c - Transient silencing of CA1 activity by the SuM-CA2-CA1 circuit**

A major finding of our study is the silencing of CA1 activity resulting from photostimulation of SuM inputs onto area CA2. Indeed, activation of SuM inputs over area CA2 caused a marked and long-lasting reduction of field spiking activity, hyperpolarization, and transient increase followed by lasting decrease of spontaneous EPSCs and IPSC frequencies in area CA1. While revealing a potentially crucial role of SuM in controlling the output of the hippocampus with surprising implications for hippocampal network activity, this result proves difficult to explain given the current information available on the SuM-CA2-CA1 circuit. Solid evidences describe an inhibitory drive of SuM to area CA2 and an excitatory output of CA2 PNs onto CA1. In addition, SuM and CA2 driven feedforward inhibition onto CA1 PNs need to be considered as plausible. Finally, neuromodulatory effects of long-range SuM fibers and local hippocampal neurons engaged in this circuit may be at play. First, it appears clearly that the overall effect of SuM inputs stimulation is inhibitory in area CA1. When considering fast synaptic transmission, this might be explained by decreased excitatory drive from CA2 PNs inhibited by SuM inputs, propagation to area CA1 of the feedforward inhibition recruited by SuM inputs in area CA2, and additional feedforward inhibition from area CA2 to CA1 once CA2 PNs recover from SuM-driven inhibition. The slow aspect of CA1 silencing following SuM activation suggests that it might be mediated by a GABA<sub>B</sub>-mediated effect. However, preliminary experiments with inhibitory transmission blocked revealed that the hyperpolarization of CA1 PNs remained in these conditions. Therefore, although fast synaptic transmission among the circuit described above likely plays a part, it cannot fully explain the silencing of CA1 activity caused by SuM input activation. The slow time course of this effect and its global spread to spontaneous EPSCs and IPSCs argues for a neuromodulatory mechanism. Of note, SuM fibers afferent to the hippocampus contain substance P that could well be released during strong photostimulation of SuM inputs. In area CA1, bath application of substance P excites INs leading to increased

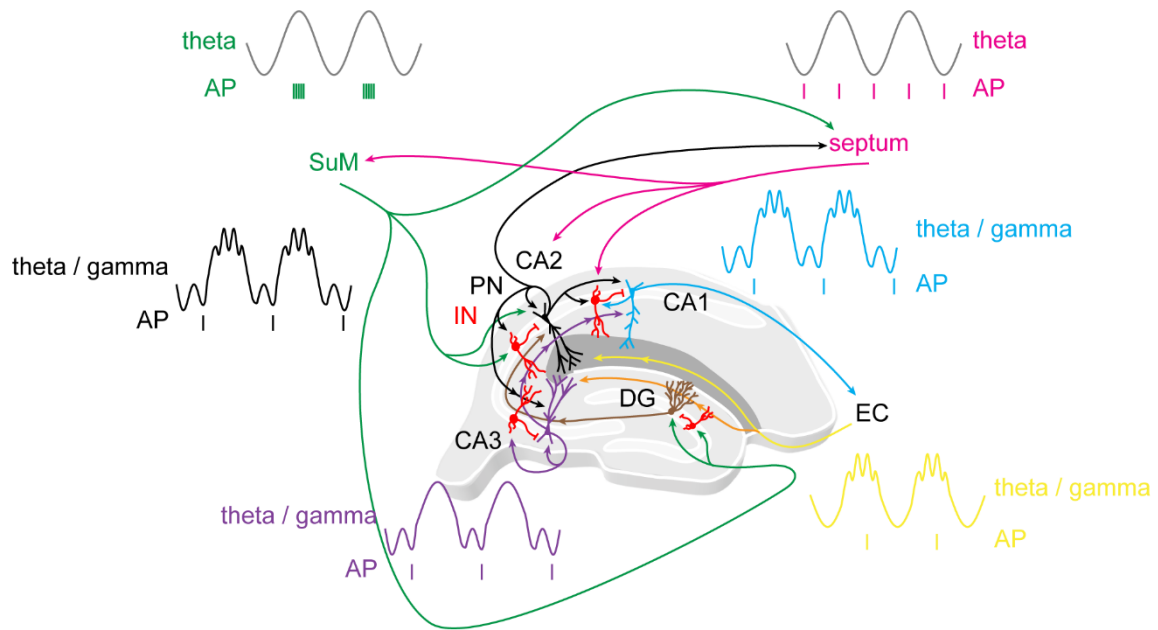
spontaneous inhibition of both PNs and other INs (Ogier and Raggenbass, 2003; Ogier et al., 2008). The CA3 to CA1 excitatory drive is reduced by substance P, potentially because of increased recruitment of inhibition (Kouznetsova and Nistri, 1998). Interestingly, substance P causes a hyperpolarization of CA1 PNs but potentializes the depolarizing effect of subsequent application of CCh (Kouznetsova and Nistri, 2000). Although it is difficult to directly relate this study to our own, the hyperpolarization of CA1 PNs seen upon bath application of substance P make it a likely candidate neuropeptide to explain our results. Indeed, preliminary experiments performed in area CA2 indicate that sustained photostimulation of SuM fibers can trigger release of substance P. Using 2 minutes-long trains of light pulses to stimulate SuM inputs, we observed a decreased amplitude of the CA3 to CA2 feedforward inhibition and obtained a similar effect by bath application of substance P. Therefore, these preliminary experiments give precedent to further investigate the role of substance P in the SuM-driven silencing of CA1 activity. Future experiments will be performed with the same stimulation protocol of SuM inputs while blocking the neurokinin 1 receptor of substance P.

Alternatively, potent and repeated excitation of CA2 and CA1 INs, either directly by SuM or by CA2 PNs through post-inhibitory rebound of excitation, might release a variety of neuromodulators intrinsic to the hippocampus that could cause the suppression of CA1 activity. Neuromodulatory signaling such as CCK, VIP, endocannabinoids, mGluRs, could be implicated in the SuM effect on area CA1, and all of which potentially interfere with cholinergic pathways. Replication of our protocol in the presence of pharmacological blockers will help identify the signaling molecules responsible. In addition, chemogenetic inhibition of specific populations of INs, or of CA2 PNs, will allow to decipher their respective contributions in this phenomenon. Finally, characterizing the INs responsible for the CA2 to CA1 feedforward inhibition will help to understand the influence of SuM on CA1 through CA2 PNs.

Regardless of its origin and mechanism, the silencing of CA1 by SuM activity has important functional potential implications. During hippocampal theta oscillations, CA1 is influenced by CA3, entorhinal and septal inputs that all fire rhythmically (Buzsáki, 2002a). At the same time, SuM neurons fire bursts of action potentials at theta frequency (Buzsáki, 2002a; Kirk et al., 1996a; Kocsis and Vertes, 1994a). Therefore, through its influence over area CA2, the SuM likely participates in the generation of theta oscillations in area CA1 by phasically hyperpolarizing CA1 PNs. In addition, CA2-projecting SuM neurons send collaterals to the septum (Borhegyi et al., 1997; Vertes and McKenna, 2000; our own observations), and area CA2 sends outputs to the septum as well (Cui et al., 2013). Furthermore, the septum targets both area CA2 and the SuM (Cui et al., 2013; Hitti and Siegelbaum, 2014a; Kohara et al., 2013;

Pan and McNaughton, 2004a), thus potentially establishing bi-directional connections. Therefore, the SuM, the septum and area CA2 might form a long-distance loop that could be critical for the synchronization of theta oscillations. These perspectives provide exciting hypothesis to be tested in the future, notably by examining the reciprocal connection between area CA2 and the septum.

## active wake & REM sleep



## quiet wake & slow wave sleep

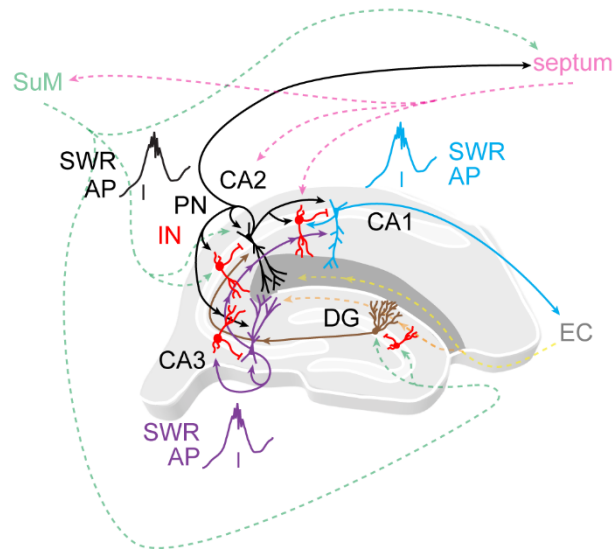
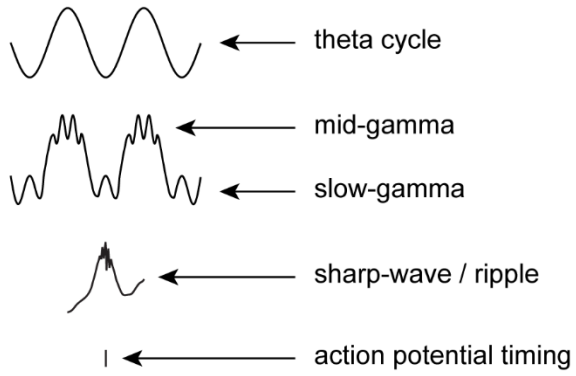


**Figure IV.3.1. Integrated view of brain state-dependent SuM and area CA2 activity.**

Diagrams illustrating the intrinsic and extrinsic connections of the different hippocampal areas and their relative field and firing activity during theta / gamma- and SWRs-dominated brain states.

## legend



## V - References

Acsády, Kamondi, Sík, Freund, and Buzsáki (1998). GABAergic cells are the major postsynaptic targets of mossy fibers in the rat hippocampus. *The Journal of Neuroscience : The Official Journal of the Society for Neuroscience* 18, 3386–403.

Alexander, Farris, Pirone, Zheng, Colgin, and Dudek (2016a). Social and novel contexts modify hippocampal CA2 representations of space. *Nature Communications* 7, ncomms10300.

Alexander, Farris, Pirone, Zheng, Colgin, and Dudek (2016b). Social and novel contexts modify hippocampal CA2 representations of space. *Nature Communications* 7, ncomms10300.

Alger, Nagode, and Tang (2014). Muscarinic cholinergic receptors modulate inhibitory synaptic rhythms in hippocampus and neocortex. *Frontiers in Synaptic Neuroscience* 6, 18.

Ali, and Thomson (1998). Facilitating pyramid to horizontal oriens-alveus interneurone inputs: dual intracellular recordings in slices of rat hippocampus. *The Journal of Physiology* 507, 185–199.

Ali, Deuchars, Pawelzik, and Thomson (1998). CA1 pyramidal to basket and bistratified cell EPSPs: dual intracellular recordings in rat hippocampal slices. *The Journal of Physiology* 507, 201–217.

Alonso, and García-Austt (1987a). Neuronal sources of theta rhythm in the entorhinal cortex of the rat. *Experimental Brain Research* 67, 502–509.

Alonso, and García-Austt (1987b). Neuronal sources of theta rhythm in the entorhinal cortex of the rat. *Experimental Brain Research* 67, 493–501.

Andersen, Bliss, and Skrede (1971). Lamellar organization of hippocampal excitatory

pathways. *Experimental Brain Research* 13.

Andreasen, and JDC, L. (1998). Factors determining the efficacy of distal excitatory synapses in rat hippocampal CA1 pyramidal neurones. *The Journal of Physiology* 507, 441–462.

Aranda, Santín, Begega, Aguirre, and Arias (2006). Supramammillary and adjacent nuclei lesions impair spatial working memory and induce anxiolytic-like behavior. *Behavioural Brain Research* 167, 156–164.

Aranda, Begega, Sánchez-López, Aguirre, Arias, and Santín (2008). Temporary inactivation of the supramammillary area impairs spatial working memory and spatial reference memory retrieval. *Physiology & Behavior* 94, 322–330.

Ariffin, Jiang, Low, and Khanna (2010). Nicotinic receptor mechanism in supramammillary nucleus mediates physiological regulation of neural activity in dorsal hippocampal field CA1 of anaesthetized rat. *Hippocampus* 20, 852–865.

Baddeley (2003). Working memory: looking back and looking forward. *Nature Reviews Neuroscience* 4, nrn1201.

Bannister, and Larkman (1995). Dendritic morphology of CA1 pyramidal neurones from the rat hippocampus: I. Branching patterns. *Journal of Comparative Neurology* 360, 150–160.

Bartasaghi, and Gessi (2004). Parallel activation of field CA2 and dentate gyrus by synaptically elicited perforant path volleys. *Hippocampus* 14, 948–963.

Bartos, Alle, and Vida (2011). Role of microcircuit structure and input integration in hippocampal interneuron recruitment and plasticity. *Neuropharmacology* 60, 730–739.

Belluscio, Mizuseki, Schmidt, Kempter, and Buzsáki (2012). Cross-Frequency Phase–Phase Coupling between Theta and Gamma Oscillations in the Hippocampus. *The Journal of Neuroscience* 32, 423–435.

Benes, Kwok, Vincent, and Todtenkopf (1998). A reduction of nonpyramidal cells in sector CA2 of schizophrenics and manic depressives. *Biological Psychiatry* 44, 88–97.

Berger, Esclapez, Alvarez, Meyer, and Catala (2001). Human and monkey fetal brain development of the supramammillary-hippocampal projections: A system involved in the regulation of theta activity. *Journal of Comparative Neurology* 429, 515–529.

Billwiller, Renouard, Clement, Fort, and Luppi (2017). Differential origin of the activation of dorsal and ventral dentate gyrus granule cells during paradoxical (REM) sleep in the rat. *Brain Structure and Function* 222, 1495–1507.

Blackstad (1956). Commissural connections of the hippocampal region in the rat, with special reference to their mode of termination. *Journal of Comparative Neurology* 105, 417–537.

Boehringer, Polygalov, Huang, Middleton, Robert, Wintzer, Piskorowski, Chevaleyre, and McHugh (2017). Chronic Loss of CA2 Transmission Leads to Hippocampal Hyperexcitability. *Neuron* 94, 642–655.e9.

Borgius, Restrepo, Leao, Saleh, and Kiehn (2010). A transgenic mouse line for molecular genetic analysis of excitatory glutamatergic neurons. *Molecular and Cellular Neuroscience* 45, 245–257.

Borhegyi, and Freund (1998). Dual projection from the medial septum to the supramammillary nucleus in the rat. *Brain Research Bulletin* 46, 453–459.

Borhegyi, and Leranth (1997b). Distinct substance P- and calretinin-containing projections from the supramammillary area to the hippocampus in rats; a species difference between rats and monkeys. *Experimental Brain Research* 115, 369–374.

Borhegyi, and Leranth (1997a). Substance P innervation of the rat hippocampal formation. *Journal of Comparative Neurology* 384, 41–58.

Borhegyi, Maglóczy, Acsády, and Freund (1997). The supramammillary nucleus innervates cholinergic and GABAergic neurons in the medial septum-diagonal band of Broca complex.

Neuroscience 82, 1053–1065.

Bostock, Muller, and Kubie (1991). Experience-dependent modifications of hippocampal place cell firing. *Hippocampus* 1, 193–205.

Botcher, Falck, Thomson, and Mercer (2014). Distribution of interneurons in the CA2 region of the rat hippocampus. *Frontiers in Neuroanatomy* 8, 104.

Boulland, Jenstad, Boekel, Wouterlood, Edwards, Storm-Mathisen, and Chaudhry (2009). Vesicular Glutamate and GABA Transporters Sort to Distinct Sets of Vesicles in a Population of Presynaptic Terminals. *Cerebral Cortex* 19, 241–248.

Brady, and Mufson (1997). Parvalbumin-immunoreactive neurons in the hippocampal formation of Alzheimer's diseased brain. *Neuroscience* 80, 1113–1125.

Bragin, Jandó, Nádasdy, Hetke, Wise, and Buzsáki (1995). Gamma (40-100 Hz) oscillation in the hippocampus of the behaving rat. *The Journal of Neuroscience : The Official Journal of the Society for Neuroscience* 15, 47–60.

Brun, Otnæss, Molden, Steffenach, Witter, Moser, and Moser (2002). Place Cells and Place Recognition Maintained by Direct Entorhinal-Hippocampal Circuitry. *Science* 296, 2243–2246.

Buhl, Halasy, and Somogyi (1994a). Diverse sources of hippocampal unitary inhibitory postsynaptic potentials and the number of synaptic release sites. *Nature* 368, 368823a0.

Buhl, Han, Lorinczi, Stezhka, Karnup, and Somogyi (1994b). Physiological properties of anatomically identified axo-axonic cells in the rat hippocampus. *Journal of Neurophysiology* 71, 1289–1307.

Buzsáki (1986). Hippocampal sharp waves: Their origin and significance. *Brain Research* 398, 242–252.

Buzsáki (2002). Theta Oscillations in the Hippocampus. *Neuron* 33.

Buzsáki, and Moser (2013). Memory, navigation and theta rhythm in the hippocampal-entorhinal system. *Nature Neuroscience* 16, 130–138.

Buzsáki (2015). Hippocampal sharp wave-ripple: A cognitive biomarker for episodic memory and planning. *Hippocampus* 25, 1073–1188.

Buzsáki, and Wang (2012). Mechanisms of Gamma Oscillations. *Annual Review of Neuroscience* 35, 203–225.

Caputi, Melzer, Michael, and Monyer (2013). The long and short of GABAergic neurons. *Current Opinion in Neurobiology* 23, 179–186.

Canto, Wouterlood, and Witter (2008). What Does the Anatomical Organization of the Entorhinal Cortex Tell Us? *Neural Plasticity* 2008, 381243.

Castañé, Santana, and Artigas (2015). PCP-based mice models of schizophrenia: differential behavioral, neurochemical and cellular effects of acute and subchronic treatments. *Psychopharmacology* 232, 4085–4097.

Shute and Lewis (1963). Cholinesterase-Containing Systems of the Brain of the Rat. *Nature* 199, 1160.

Chevaleyre, and Siegelbaum (2010). Strong CA2 Pyramidal Neuron Synapses Define a Powerful Disynaptic Cortico-Hippocampal Loop. *Neuron* 66, 560–572.

Chevaleyre and Piskorowski (2016). Hippocampal area CA2: An overlooked but promising therapeutic target. *Trends in Molecular Medicine* 8, 645-655.

Christian, and Deadwyler (1986). Behavioral functions and hippocampal cell types: evidence for two nonoverlapping populations in the rat. *Journal of Neurophysiology* 55, 331–348.

Chrobak, and Buzsáki (1998). Gamma oscillations in the entorhinal cortex of the freely behaving rat. *The Journal of Neuroscience : The Official Journal of the Society for*

Neuroscience 18, 388–98.

Claiborne, Amaral, and Cowan (1990). Quantitative, three-dimensional analysis of granule cell dendrites in the rat dentate gyrus. *Journal of Comparative Neurology* 302, 206–219.

Cobb, and Davies (2005). Cholinergic modulation of hippocampal cells and circuits. *The Journal of Physiology* 562, 81–88.

Cobb, Bulters, Suchak, Riedel, RGM, M., and Davies (1999). Activation of nicotinic acetylcholine receptors patterns network activity in the rodent hippocampus. *The Journal of Physiology* 518, 131–140.

Cohen, and Squire (1980). Preserved learning and retention of pattern-analyzing skill in amnesia: dissociation of knowing how and knowing that. *Science* 210, 207–210.

Colgin (2016). Rhythms of the hippocampal network. *Nature Reviews Neuroscience* 17, 239–249.

Colgin, Denninger, Fyhn, Hafting, Bonnevie, Jensen, Moser, and Moser (2009). Frequency of gamma oscillations routes flow of information in the hippocampus. *Nature* 462, nature08573.

Csicsvari, Hirase, Czurkó, Mamiya, and Buzsáki (1999a). Oscillatory coupling of hippocampal pyramidal cells and interneurons in the behaving Rat. *The Journal of Neuroscience : The Official Journal of the Society for Neuroscience* 19, 274–87.

Csicsvari, Hirase, Czurkó, Mamiya, and Buzsáki (1999b). Fast network oscillations in the hippocampal CA1 region of the behaving rat. *The Journal of Neuroscience : The Official Journal of the Society for Neuroscience* 19, RC20.

Csicsvari, Hirase, Mamiya, and Buzsáki (2000). Ensemble Patterns of Hippocampal CA3-CA1 Neurons during Sharp Wave–Associated Population Events. *Neuron* 28, 585–594.

Csicsvari, Jamieson, Wise, and Buzsáki (2003). Mechanisms of Gamma Oscillations in the Hippocampus of the Behaving Rat. *Neuron* 37, 311–322.

Cui, Gerfen, and Young (2013). Hypothalamic and other connections with dorsal CA2 area of the mouse hippocampus. *Journal of Comparative Neurology* 521, 1844–1866.

Danielson, Zaremba, Kaifosh, Bowler, Ladow, and Losonczy (2016). Sublayer-Specific Coding Dynamics during Spatial Navigation and Learning in Hippocampal Area CA1. *Neuron* 91, 652–665.

Deller, Martinez, Nitsch, and Frotscher (1996). A novel entorhinal projection to the rat dentate gyrus: direct innervation of proximal dendrites and cell bodies of granule cells and GABAergic neurons. *The Journal of Neuroscience : The Official Journal of the Society for Neuroscience* 16, 3322–33.

Deuchars, and Thomson (1996). CA1 pyramid-pyramid connections in rat hippocampus in vitro: Dual intracellular recordings with biocytin filling. *Neuroscience* 74, 1009–1018.

Eichenbaum, and Cohen (2014). Can We Reconcile the Declarative Memory and Spatial Navigation Views on Hippocampal Function? *Neuron* 83, 764–770.

Fernández-Ruiz, Oliva, Nagy, Maurer, Berényi, and Buzsáki (2017). Entorhinal-CA3 Dual-Input Control of Spike Timing in the Hippocampus by Theta-Gamma Coupling. *Neuron* 93, 1213–1226.e5.

Fisahn, Pike, Buhl, and Paulsen (1998). Cholinergic induction of network oscillations at 40 Hz in the hippocampus in vitro. *Nature* 394, 28179.

Fisahn, Yamada, Duttaroy, Gan, Deng, McBain, and Wess (2002). Muscarinic Induction of Hippocampal Gamma Oscillations Requires Coupling of the M1 Receptor to Two Mixed Cation Currents. *Neuron* 33, 615–624.

Fox, Wolfson, and Ranck (1986). Hippocampal theta rhythm and the firing of neurons in walking and urethane anesthetized rats. *Experimental Brain Research* 62.

Frank, Stanley, and Brown (2004). Hippocampal Plasticity across Multiple Days of Exposure

to Novel Environments. *The Journal of Neuroscience* 24, 7681–7689.

Freund, and Antal (1988). GABA-containing neurons in the septum control inhibitory interneurons in the hippocampus. *Nature* 336, 336170a0.

Freund, and Buzsáki (1996). Interneurons of the hippocampus. *Hippocampus* 6, 347–470.

Freund, Gulyás, Acsády, Görcs, and Tóth (1990). Serotonergic control of the hippocampus via local inhibitory interneurons. *Proceedings of the National Academy of Sciences* 87, 8501–8505.

Fuchs, Zivkovic, Cunningham, Middleton, LeBeau, Bannerman, Rozov, Whittington, Traub, JNP, R., et al. (2007). Recruitment of Parvalbumin-Positive Interneurons Determines Hippocampal Function and Associated Behavior. *Neuron* 53, 591–604.

Gasbarri, Verney, Innocenzi, Campana, and Pacitti (1994). Mesolimbic dopaminergic neurons innervating the hippocampal formation in the rat: a combined retrograde tracing and immunohistochemical study. *Brain Research* 668, 71–79.

Geiger, and Jonas (2000). Dynamic Control of Presynaptic Ca<sup>2+</sup> Inflow by Fast-Inactivating K<sup>+</sup> Channels in Hippocampal Mossy Fiber Boutons. *Neuron* 28, 927–939.

Gilbert, Kesner, and Lee (2001). Dissociating hippocampal subregions: A double dissociation between dentate gyrus and CA1. *Hippocampus* 11, 626–636.

Girardeau, Benchenane, Wiener, Buzsáki, and Zugaro (2009). Selective suppression of hippocampal ripples impairs spatial memory. *Nature Neuroscience* 12, 1222–1223.

Golding, Mickus, Katz, Kath, and Spruston (2005). Factors mediating powerful voltage attenuation along CA1 pyramidal neuron dendrites. *The Journal of Physiology* 568, 69–82.

Groen, and Wyss (1990). Extrinsic projections from area CA1 of the rat hippocampus: Olfactory, cortical, subcortical, and bilateral hippocampal formation projections. *Journal of Comparative Neurology* 302, 515–528.

Gulyás, Tóth, McBain, and Freund (1998). Stratum radiatum giant cells: a type of principal cell in the rat hippocampus. *European Journal of Neuroscience* 10, 3813–3822.

Gulyás, Szabó, Ulbert, Holderith, Monyer, Erdélyi, Szabó, Freund, and Hájos (2010). Parvalbumin-Containing Fast-Spiking Basket Cells Generate the Field Potential Oscillations Induced by Cholinergic Receptor Activation in the Hippocampus. *The Journal of Neuroscience* 30, 15134–15145.

Gutiérrez-Guzmán, Hernández-Pérez, M<sup>Á</sup>, L.-V., Fregozo, M<sup>Á</sup>, G., and Olvera-Cortés (2012). Serotonin depletion of supramammillary/posterior hypothalamus nuclei produces place learning deficiencies and alters the concomitant hippocampal theta activity in rats. *European Journal of Pharmacology* 682, 99–109.

Hafting, Fyhn, Molden, Moser, and Moser (2005). Microstructure of a spatial map in the entorhinal cortex. *Nature* 436, nature03721.

Haglund, Swanson, and Köhler (1984). The projection of the supramammillary nucleus to the hippocampal formation: An immunohistochemical and anterograde transport study with the lectin PHA-L in the rat. *Journal of Comparative Neurology* 229, 171–185.

Hájos, Karlócai, Németh, Ulbert, Monyer, Szabó, Erdélyi, Freund, and Gulyás (2013). Input-Output Features of Anatomically Identified CA3 Neurons during Hippocampal Sharp Wave/Ripple Oscillation In Vitro. *The Journal of Neuroscience* 33, 11677–11691.

Halasy, Hajszan, ÉG, K., Lam, and Leranthy (2004). Distribution and origin of vesicular glutamate transporter 2-immunoreactive fibers in the rat hippocampus. *Hippocampus* 14, 908–918.

Han, Buhl, Lörinczi, and Somogyi (1993). A High Degree of Spatial Selectivity in the Axonal and Dendritic Domains of Physiologically Identified Local-circuit Neurons in the Dentate Gyms of the Rat Hippocampus. *European Journal of Neuroscience* 5, 395–410.

Hangya, Borhegyi, Szilágyi, Freund, and Varga (2009). GABAergic Neurons of the Medial

Septum Lead the Hippocampal Network during Theta Activity. *The Journal of Neuroscience* 29, 8094–8102.

Hasselmo (2006). The role of acetylcholine in learning and memory. *Current Opinion in Neurobiology* 16, 710–715.

Henze, Wittner, and Buzsáki (2002). Single granule cells reliably discharge targets in the hippocampal CA3 network in vivo. *Nature Neuroscience* 5, nn887.

Hernández-Pérez, Gutiérrez-Guzmán, MÁ, L.-V., and Olvera-Cortés (2015). Supramammillary serotonin reduction alters place learning and concomitant hippocampal, septal, and supramammillary theta activity in a Morris water maze. *Frontiers in Pharmacology* 6, 250.

Hippenmeyer, Vrieseling, Sigrist, Portmann, Laengle, Ladle and Arber (2005). A developmental switch in the response of DRG neurons to ETS transcription factor signaling. *PLoS Biol* 3, e159.

Hitti, and Siegelbaum (2014). The hippocampal CA2 region is essential for social memory. *Nature* 508, 88–92.

Ikemoto (2005). The Supramammillary Nucleus Mediates Primary Reinforcement via GABAA Receptors. *Neuropsychopharmacology* 30, 1300660.

Ikemoto, Witkin, Zangen, and Wise (2004). Rewarding Effects of AMPA Administration into the Supramammillary or Posterior Hypothalamic Nuclei But Not the Ventral Tegmental Area. *The Journal of Neuroscience* 24, 5758–5765.

Iovino, Giagulli, Licchelli, Iovino, Guastamacchia, Triggiani (2017). Synaptic inputs of neural afferent pathways to vasopressin- and Oxytocin-secreting neurons of Supraoptic and Paraventricular hypothalamic nuclei. *EMDDT* 16: 276–287.

Ishizuka, Weber, and Amaral (1990). Organization of intrahippocampal projections

originating from CA3 pyramidal cells in the rat. *Journal of Comparative Neurology* 295, 580–623.

Ito, Shirao, Doya, and Sekino (2009). Three-dimensional distribution of Fos-positive neurons in the supramammillary nucleus of the rat exposed to novel environment. *Neuroscience Research* 64, 397–402.

Jay, Glowinski, and Thierry (1989). Selectivity of the hippocampal projection to the prelimbic area of the prefrontal cortex in the rat. *Brain Research* 505, 337–340.

Jiang, and Khanna (2006). Microinjection of carbachol in the supramammillary region suppresses CA1 pyramidal cell synaptic excitability. *Hippocampus* 16, 891–905.

Jung, and McNaughton (1993). Spatial selectivity of unit activity in the hippocampal granular layer. *Hippocampus* 3, 165–182.

Katsumaru, Kosaka, Heizmann, and Hama (1988). Immunocytochemical study of GABAergic neurons containing the calcium-binding protein parvalbumin in the rat hippocampus. *Experimental Brain Research* 72.

Kay, Sosa, Chung, Karlsson, Larkin, and Frank (2016). A hippocampal network for spatial coding during immobility and sleep. *Nature* 531, 185–190.

Kemppainen, Jolkkonen, and Pitkänen (2002). Projections from the posterior cortical nucleus of the amygdala to the hippocampal formation and parahippocampal region in rat. *Hippocampus* 12, 735–755.

Kirk (1997). Supramammillary Neural Discharge Patterns and Hippocampal EEG. *Brain Research Bulletin* 42, 23–26.

Kirk (1998). Frequency Modulation of Hippocampal Theta by the Supramammillary Nucleus, and Other Hypothalamo–Hippocampal Interactions: Mechanisms and Functional Implications. *Neuroscience & Biobehavioral Reviews* 22, 291–302.

Kirk, and McNaughton (1993). Mapping the differential effects of procaine on frequency and amplitude of reticularly elicited hippocampal rhythmical slow activity. *Hippocampus* 3, 517–525.

Kirk, and McNaughton (1991). Supramammillary cell firing and hippocampal rhythmical slow activity. *Neuroreport* 11, 723-725.

Kirk, Oddie, Konopacki, and Bland (1996). Evidence for differential control of posterior hypothalamic, supramammillary, and medial mammillary theta-related cellular discharge by ascending and descending pathways. *The Journal of Neuroscience : The Official Journal of the Society for Neuroscience* 16, 5547–54.

Kiss, Buzsáki, Morrow, Glantz, and Leranth (1996). Entorhinal cortical innervation of parvalbumin-containing neurons (basket and chandelier cells) in the rat ammon's horn. *Hippocampus* 6, 239–246.

Kiss, Á, C., Bokor, Shanabrough, and Leranth (2000). The supramammillo-hippocampal and supramammillo-septal glutamatergic/aspartatergic projections in the rat: a combined [<sup>3</sup>H]d-aspartate autoradiographic and immunohistochemical study. *Neuroscience* 97, 657–669.

Klausberger, and Somogyi (2008). Neuronal Diversity and Temporal Dynamics: The Unity of Hippocampal Circuit Operations. *Science* 321, 53–57.

Klausberger, Magill, Márton, JDB, R., Cobden, Buzsáki, and Somogyi (2003). Brain-state- and cell-type-specific firing of hippocampal interneurons in vivo. *Nature* 421, nature01374.

Klausberger, Marton, O'Neill, JHJ, H., Dalezios, Fuentealba, Suen, Papp, Kaneko, Watanabe, et al. (2005). Complementary Roles of Cholecystokinin- and Parvalbumin-Expressing GABAergic Neurons in Hippocampal Network Oscillations. *The Journal of Neuroscience* 25, 9782–9793.

Knable, Barci, Webster, Meador-Woodruff, and Torrey (2004). Molecular abnormalities of the hippocampus in severe psychiatric illness: postmortem findings from the Stanley Neuropathology Consortium. *Molecular Psychiatry* 9, 609.

Kneisler, and Dingledine (1995). Spontaneous and synaptic input from granule cells and the perforant path to dentate basket cells in the rat hippocampus. *Hippocampus* 5, 151–164.

Kocsis, and Vertes (1994). Characterization of neurons of the supramammillary nucleus and mammillary body that discharge rhythmically with the hippocampal theta rhythm in the rat. *The Journal of Neuroscience : The Official Journal of the Society for Neuroscience* 14, 7040–52.

Kohara, Pignatelli, Rivest, Jung, Kitamura, Suh, Frank, Kajikawa, Mise, Obata, et al. (2013). Cell type-specific genetic and optogenetic tools reveal hippocampal CA2 circuits. *Nature Neuroscience* 17, nn.3614.

Korotkova, Fuchs, Ponomarenko, Engelhardt, and Monyer (2010). NMDA Receptor Ablation on Parvalbumin-Positive Interneurons Impairs Hippocampal Synchrony, Spatial Representations, and Working Memory. *Neuron* 68, 557–569.

Kouznetsova, and Nistri (1998). Modulation by substance P of synaptic transmission in the mouse hippocampal slice. *European Journal of Neuroscience* 10, 3076–3084.

Kouznetsova, and Nistri (2000). Facilitation of cholinergic transmission by substance P methyl ester in the mouse hippocampal slice preparation. *European Journal of Neuroscience* 12, 585–594.

Kramis, Vanderwolf, and Bland (1975). Two types of hippocampal rhythmical slow activity in both the rabbit and the rat: Relations to behavior and effects of atropine, diethyl ether, urethane, and pentobarbital. *Experimental Neurology* 49, 58–85.

Kupferman, Basu, Russo, Guevarra, Cheung, and Siegelbaum (2014). Reelin Signaling Specifies the Molecular Identity of the Pyramidal Neuron Distal Dendritic Compartment. *Cell* 158, 1335–1347.

Lacaille (1991). Postsynaptic potentials mediated by excitatory and inhibitory amino acids in interneurons of stratum pyramidale of the CA1 region of rat hippocampal slices in vitro.

Journal of Neurophysiology 66, 1441–1454.

Larkman, Stratford, and Jack (1991). Quantal analysis of excitatory synaptic action and depression in hippocampal slices. *Nature* 350, 350344a0.

Lasztóczy, Tukker, Somogyi, and Klausberger (2011). Terminal Field and Firing Selectivity of Cholecystokinin-Expressing Interneurons in the Hippocampal CA3 Area. *The Journal of Neuroscience* 31, 18073–18093.

Lee, and Wilson (2002). Memory of Sequential Experience in the Hippocampus during Slow Wave Sleep. *Neuron* 36, 1183–1194.

Lee, Marchionni, Bezaire, Varga, Danielson, Lovett-Barron, Losonczy, and Soltesz (2014). Parvalbumin-Positive Basket Cells Differentiate among Hippocampal Pyramidal Cells. *Neuron* 82, 1129–1144.

Lee, Wang, Deshmukh, and Knierim (2015). Neural Population Evidence of Functional Heterogeneity along the CA3 Transverse Axis: Pattern Completion versus Pattern Separation. *Neuron* 87, 1093–1105.

Leranth, and Kiss (1996). A population of supramammillary area calretinin neurons terminating on medial septal area cholinergic and lateral septal area calbindin-containing cells are aspartate/glutamatergic. *The Journal of Neuroscience : The Official Journal of the Society for Neuroscience* 16, 7699–7710.

Leranth, and Nitsch (1994). Morphological evidence that hypothalamic substance P-containing afferents are capable of filtering the signal flow in the monkey hippocampal formation. *The Journal of Neuroscience : The Official Journal of the Society for Neuroscience* 14, 4079–94.

Leutgeb, Leutgeb, Treves, Moser, and Moser (2004). Distinct Ensemble Codes in Hippocampal Areas CA3 and CA1. *Science* 305, 1295–1298.

Leutgeb, Leutgeb, Barnes, Moser, McNaughton, and Moser (2005). Independent Codes for

Spatial and Episodic Memory in Hippocampal Neuronal Ensembles. *Science* 309, 619–623.

Lever, Wills, Cacucci, Burgess, and O'Keefe (2002). Long-term plasticity in hippocampal place-cell representation of environmental geometry. *Nature* 416, 416090a.

Li, Somogyi, Ylinen, and Buzsáki (1994). The hippocampal CA3 network: An in vivo intracellular labeling study. *Journal of Comparative Neurology* 339, 181–208.

Llorens-Martín, Jurado-Arjona, Avila, and Hernández (2015). Novel connection between newborn granule neurons and the hippocampal CA2 field. *Experimental Neurology* 263, 285–292.

Lorente de No (1934). Studies on the structure of the cerebral cortex. II. *J Psychol Neurol* 113-117

Lu, Igarashi, Witter, Moser, and Moser (2015). Topography of Place Maps along the CA3-to-CA2 Axis of the Hippocampus. *Neuron* 87, 1078–1092.

Maccaferri, David, Roberts, Szucs, Cottingham, and Somogyi (2000). Cell surface domain specific postsynaptic currents evoked by identified GABAergic neurones in rat hippocampus in vitro. *The Journal of Physiology* 524, 91–116.

Madison, Lancaster, and Nicoll (1987). Voltage clamp analysis of cholinergic action in the hippocampus. *The Journal of Neuroscience : The Official Journal of the Society for Neuroscience* 7, 733–41.

Magee (1998). Dendritic hyperpolarization-activated currents modify the integrative properties of hippocampal CA1 pyramidal neurons. *The Journal of Neuroscience : The Official Journal of the Society for Neuroscience* 18, 7613–24.

Maglóczky, Acsády, and Freund (1994). Principal cells are the postsynaptic targets of supramammillary afferents in the hippocampus of the rat. *Hippocampus* 4, 322–334.

Mair, Warrington, and Weiskrantz (1979). Memory disorder in Korsakoff's psychosis: a neuropathological and neuropsychological investigation of two cases. *Brain* 102, 749–783.

Mankin, Diehl, Sparks, Leutgeb, and Leutgeb (2015). Hippocampal CA2 Activity Patterns Change over Time to a Larger Extent than between Spatial Contexts. *Neuron* 85, 190–201.

Mann, Suckling, Hajos, Greenfield, and Paulsen (2005). Perisomatic Feedback Inhibition Underlies Cholinergically Induced Fast Network Oscillations in the Rat Hippocampus *In Vitro*. *Neuron* 45, 105–117.

Masurkar, Srinivas, Brann, Warren, Lowes, and Siegelbaum (2017). Medial and Lateral Entorhinal Cortex Differentially Excite Deep versus Superficial CA1 Pyramidal Neurons. *Cell Reports* 18, 148–160.

Matsumoto, Okamoto, Takagi, Ikegaya (2016). 3-Hz subthreshold oscillations of CA2 neurons *in vivo*. *Hippocampus* 26, 1570–1578.

McBain, DiChiara, and Kauer (1994). Activation of metabotropic glutamate receptors differentially affects two classes of hippocampal interneurons and potentiates excitatory synaptic transmission. *The Journal of Neuroscience : The Official Journal of the Society for Neuroscience* 14, 4433–45.

McNaughton, Logan, Panickar, Kirk, Pan, Brown, and Heenan (1995). Contribution of synapses in the medial supramammillary nucleus to the frequency of hippocampal theta rhythm in freely moving rats. *Hippocampus* 5, 534–545.

Mercer, Trigg, and Thomson (2007). Characterization of Neurons in the CA2 Subfield of the Adult Rat Hippocampus. *The Journal of Neuroscience* 27, 7329–7338.

Mercer, Eastlake, Trigg, and Thomson (2012a). Local circuitry involving parvalbumin-positive basket cells in the CA2 region of the hippocampus. *Hippocampus* 22, 43–56.

Mercer, Botcher, Eastlake, and Thomson (2012b). SP–SR interneurons: A novel class of neurons of the CA2 region of the hippocampus. *Hippocampus* 22, 1758–1769.

Miles (1990). Synaptic excitation of inhibitory cells by single CA3 hippocampal pyramidal cells of the guinea-pig in vitro. *The Journal of Physiology* 428, 61–77.

Miles, and Wong (1986). Excitatory synaptic interactions between CA3 neurones in the guinea-pig hippocampus. *The Journal of Physiology* 373, 397–418.

Mizumori, McNaughton, and Barnes (1989). A comparison of supramammillary and medial septal influences on hippocampal field potentials and single-unit activity. *Journal of Neurophysiology* 61, 15–31.

Mizuseki, Diba, Pastalkova, and Buzsáki (2011). Hippocampal CA1 pyramidal cells form functionally distinct sublayers. *Nature Neuroscience* 14, nn.2894.

Mizuseki, Royer, Diba, and Buzsáki (2012). Activity dynamics and behavioral correlates of CA3 and CA1 hippocampal pyramidal neurons. *Hippocampus* 22, 1659–1680.

Muller, and Kubie (1987). The effects of changes in the environment on the spatial firing of hippocampal complex-spike cells. *The Journal of Neuroscience : The Official Journal of the Society for Neuroscience* 7, 1951–68.

Muller, Kubie, and Ranck (1987). Spatial firing patterns of hippocampal complex-spike cells in a fixed environment. *The Journal of Neuroscience : The Official Journal of the Society for Neuroscience* 7, 1935–50.

Naber, FHL, S., and Witter (2001). Reciprocal connections between the entorhinal cortex and hippocampal fields CA1 and the subiculum are in register with the projections from CA1 to the subiculum. *Hippocampus* 11, 99–104.

Nakashiba, Young, McHugh, Buhl, and Tonegawa (2008). Transgenic Inhibition of Synaptic Transmission Reveals Role of CA3 Output in Hippocampal Learning. *Science* 319, 1260–1264.

Nakazawa, Quirk, Chitwood, Watanabe, Yeckel, Sun, Kato, Carr, Johnston, Wilson, et al.

(2002). Requirement for Hippocampal CA3 NMDA Receptors in Associative Memory Recall. *Science* 297, 211–218.

Nasrallah, Piskorowski, and Chevaleyre (2015). Inhibitory Plasticity Permits the Recruitment of CA2 Pyramidal Neurons by CA3. *Eneuro* 2, ENEURO.0049-15.2015.

Nitsch, and Leranth (1993). Calretinin immunoreactivity in the monkey hippocampal formation—II. Intrinsic gabaergic and hypothalamic non-gabaergic systems: An experimental tracing and co-existence study. *Neuroscience* 55, 797–812.

Nitsch, and Leranth (1996). GABAergic neurons in the rat dentate gyrus are innervated by subcortical calretinin-containing afferents. *Journal of Comparative Neurology* 364, 425–438.

Nolan, Malleret, Dudman, Buhl, Santoro, Gibbs, Vronskaya, Buzsáki, Siegelbaum, Kandel, et al. (2004). A Behavioral Role for Dendritic Integration HCN1 Channels Constrain Spatial Memory and Plasticity at Inputs to Distal Dendrites of CA1 Pyramidal Neurons. *Cell* 119, 719–732.

O'Keefe (1976). Place units in the hippocampus of the freely moving rat. *Experimental Neurology* 51, 78–109.

O'Keefe, and Dostrovsky (1971). The hippocampus as a spatial map. Preliminary evidence from unit activity in the freely-moving rat. *Brain Research* 34, 171–175.

O'Keefe, and Recce (1993). Phase relationship between hippocampal place units and the EEG theta rhythm. *Hippocampus* 3, 317–330.

Ogier, and Raggenbass (2003). Action of tachykinins in the rat hippocampus: modulation of inhibitory synaptic transmission. *European Journal of Neuroscience* 17, 2639–2647.

Ogier, Wrobel, and Raggenbass (2008). Action of tachykinins in the hippocampus: Facilitation of inhibitory drive to GABAergic interneurons. *Neuroscience* 156, 527–536.

Oliva, Fernández-Ruiz, Buzsáki, and Berényi (2016a). Role of Hippocampal CA2 Region in

Triggering Sharp-Wave Ripples. *Neuron* 91, 1342–1355.

Oliva, Fernández-Ruiz, Buzsáki, and Berényi (2016b). Spatial coding and physiological properties of hippocampal neurons in the Cornu Ammonis subregions. *Hippocampus* 26, 1593–1607.

Oren, Mann, Paulsen, and Hájos (2006). Synaptic Currents in Anatomically Identified CA3 Neurons during Hippocampal Gamma Oscillations In Vitro. *The Journal of Neuroscience* 26, 9923–9934.

Pagani, Zhao, Cui, SKW, A., Caruana, Dudek, and Young (2014). Role of the vasopressin 1b receptor in rodent aggressive behavior and synaptic plasticity in hippocampal area CA2. *Molecular Psychiatry* 20, 490–499.

Pan, and McNaughton (1997). The medial supramammillary nucleus, spatial learning and the frequency of hippocampal theta activity. *Brain Research* 764, 101–108.

Pan, and McNaughton (2002). The role of the medial supramammillary nucleus in the control of hippocampal theta activity and behaviour in rats. *European Journal of Neuroscience* 16, 1797–1809.

Pan, and McNaughton (2004). The supramammillary area: its organization, functions and relationship to the hippocampus. *Progress in Neurobiology* 74, 127–166.

Papathodoropoulos (2010). Patterned activation of hippocampal network (~10 Hz) during in vitro sharp wave-ripples. *Neuroscience* 168, 429–442.

Patel, Fujisawa, Berényi, Royer, and Buzsáki (2012). Traveling Theta Waves along the Entire Septotemporal Axis of the Hippocampus. *Neuron* 75, 410–417.

Pawelzik, Bannister, Deuchars, Ilia, and Thomson (1999). Modulation of bistratified cell IPSPs and basket cell IPSPs by pentobarbitone sodium, diazepam and Zn<sup>2+</sup>: dual recordings in slices of adult rat hippocampus. *European Journal of Neuroscience* 11, 3552–3564.

Pawelzik, Hughes, and Thomson (2002). Physiological and morphological diversity of immunocytochemically defined parvalbumin- and cholecystokinin-positive interneurons in CA1 of the adult rat hippocampus. *Journal of Comparative Neurology* 443, 346–367.

Pedersen, Ferrari, Venner, Wang, SBG, A., Vujovic, Arrigoni, Saper, and Fuller (2017). Supramammillary glutamate neurons are a key node of the arousal system. *Nature Communications* 8, 1405.

Penttonen, Kamondi, Sik, Acsády, and Buzsáki (1997). Feed-forward and feed-back activation of the dentate gyrus in vivo during dentate spikes and sharp wave bursts. *Hippocampus* 7, 437–450.

Piskorowski, and Chevaleyre (2012). Synaptic integration by different dendritic compartments of hippocampal CA1 and CA2 pyramidal neurons. *Cellular and Molecular Life Sciences* 69, 75–88.

Piskorowski, and Chevaleyre (2013). Delta-Opioid Receptors Mediate Unique Plasticity onto Parvalbumin-Expressing Interneurons in Area CA2 of the Hippocampus. *The Journal of Neuroscience* 33, 14567–14578.

Piskorowski, Nasrallah, Diamantopoulou, Mukai, Hassan, Siegelbaum, Gogos, and Chevaleyre (2016). Age-Dependent Specific Changes in Area CA2 of the Hippocampus and Social Memory Deficit in a Mouse Model of the 22q11.2 Deletion Syndrome. *Neuron* 89, 163–176.

Pouille, and Scanziani (2001). Enforcement of Temporal Fidelity in Pyramidal Cells by Somatic Feed-Forward Inhibition. *Science* 293, 1159–1163.

Ramon y Cajal (1911). *Histologie du Système Nerveux de l'Homme et des Vertébrés*.

Redish, Battaglia, Chawla, Ekstrom, Gerrard, Lipa, Rosenzweig, Worley, Guzowski, McNaughton, et al. (2001). Independence of firing correlates of anatomically proximate hippocampal pyramidal cells. *The Journal of Neuroscience : The Official Journal of the Society for Neuroscience* 21, RC134.

Renouard, Billwiller, Ogawa, Clément, Camargo, Abdelkarim, Gay, Scoté-Blachon, Touré, Libourel, et al. (2015). The supramammillary nucleus and the claustrum activate the cortex during REM sleep. *Science Advances* 1, e1400177.

Rivera, Voipio, Payne, Ruusuvuori, Lahtinen, Lamsa, Pirvola, Saarma, and Kaila (1999). The K<sup>+</sup>/Cl<sup>-</sup> co-transporter KCC2 renders GABA hyperpolarizing during neuronal maturation. *Nature* 397, 16697.

Rolls (1996). A theory of hippocampal function in memory. *Hippocampus* 6, 601–620.

Rowland, Weible, Wickersham, Wu, Mayford, Witter, and Kentros (2013). Transgenically Targeted Rabies Virus Demonstrates a Major Monosynaptic Projection from Hippocampal Area CA2 to Medial Entorhinal Layer II Neurons. *The Journal of Neuroscience* 33, 14889–14898.

Royer, Zemelman, Losonczy, Kim, Chance, Magee, and Buzsáki (2012). Control of timing, rate and bursts of hippocampal place cells by dendritic and somatic inhibition. *Nature Neuroscience* 15, 769–775.

Ruan, Young, and McNaughton (2011). Minimal driving of hippocampal theta by the supramammillary nucleus during water maze learning. *Hippocampus* 21, 1074–1081.

Ruth, Collier, and Routtenberg (1982). Topography between the entorhinal cortex and the dentate septotemporal axis in rats: I. Medial and intermediate entorhinal projecting cells. *Journal of Comparative Neurology* 209, 69–78.

Ruth, Collier, and Routtenberg (1988). Topographical relationship between the entorhinal cortex and the septotemporal axis of the dentate gyrus in rats: II. Cells projecting from lateral entorhinal subdivision. *Journal of Comparative Neurology* 270, 506–516.

Sagar, Cohen, Corkin, and Growdon (1985). Dissociations Among Processes in Remote Memory. *Annals of the New York Academy of Sciences* 444, 533–535.

Sayer, Friedlander, and Redman (1990). The time course and amplitude of EPSPs evoked at synapses between pairs of CA3/CA1 neurons in the hippocampal slice. *The Journal of Neuroscience : The Official Journal of the Society for Neuroscience* 10, 826–36.

Schlingloff, Káli, Freund, Hájos, and Gulyás (2014). Mechanisms of Sharp Wave Initiation and Ripple Generation. *The Journal of Neuroscience* 34, 11385–11398.

Schomburg, Anastassiou, Buzsáki, and Koch (2012). The Spiking Component of Oscillatory Extracellular Potentials in the Rat Hippocampus. *The Journal of Neuroscience* 32, 11798–11811.

Schomburg, Fernández-Ruiz, Mizuseki, Berényi, Anastassiou, Koch, and Buzsáki (2014). Theta Phase Segregation of Input-Specific Gamma Patterns in Entorhinal-Hippocampal Networks. *Neuron* 84, 470–485.

Sekino, Obata, Tanifuji, Mizuno, and Murayama (1997). Delayed Signal Propagation via CA2 in Rat Hippocampal Slices Revealed by Optical Recording. *Journal of Neurophysiology* 78, 1662–1668.

Shahidi, Motamedi, and Naghdi (2004). Effect of reversible inactivation of the supramammillary nucleus on spatial learning and memory in rats. *Brain Research* 1026, 267–274.

Shinohara, Hosoya, and Hirase (2013). Experience enhances gamma oscillations and interhemispheric asymmetry in the hippocampus. *Nature Communications* 4, ncomms2658.

Sigurdsson, Stark, Karayiorgou, Gogos, and Gordon (2010). Impaired hippocampal–prefrontal synchrony in a genetic mouse model of schizophrenia. *Nature* 464, 763–767.

Skaggs, and McNaughton (1996). Replay of Neuronal Firing Sequences in Rat Hippocampus During Sleep Following Spatial Experience. *Science* 271, 1870–1873.

Skaggs, McNaughton, Wilson, and Barnes (1996). Theta phase precession in hippocampal neuronal populations and the compression of temporal sequences. *Hippocampus* 6, 149–172.

Sloviter (1991). Feedforward and feedback inhibition of hippocampal principal cell activity evoked by perforant path stimulation: GABA-mediated mechanisms that regulate excitability In Vivo. *Hippocampus* 1, 31–40.

Smith, SKW, A., Cymerblit-Sabba, Song, and Young (2016). Targeted activation of the hippocampal CA2 area strongly enhances social memory. *Molecular Psychiatry* 21, 1137.

Somogyi, and Klausberger (2005). Defined types of cortical interneurone structure space and spike timing in the hippocampus. *The Journal of Physiology* 562, 9–26.

Soussi, Zhang, Tahtakran, Houser, and Esclapez (2010). Heterogeneity of the supramammillary–hippocampal pathways: evidence for a unique GABAergic neurotransmitter phenotype and regional differences. *European Journal of Neuroscience* 32, 771–785.

Spruston, and Johnston (1992). Perforated patch-clamp analysis of the passive membrane properties of three classes of hippocampal neurons. *Journal of Neurophysiology* 67, 508–529.

Squire, and Zola-Morgan (1991). The medial temporal lobe memory system. *Science* 253, 1380–1386.

Squire, and Zola-Morgan (1991). The medial temporal lobe memory system. *Science* 253, 1380–1386.

Srinivas, Buss, Sun, Santoro, Takahashi, Nicholson, and Siegelbaum (2017). The Dendrites of CA2 and CA1 Pyramidal Neurons Differentially Regulate Information Flow in the Cortico-Hippocampal Circuit. *Journal of Neuroscience* 37, 3276–3293.

Stark, Roux, Eichler, Senzai, Royer, and Buzsáki (2014). Pyramidal Cell-Interneuron Interactions Underlie Hippocampal Ripple Oscillations. *Neuron* 83, 467–480.

Stevenson, and Caldwell (2014). Lesions to the CA2 region of the hippocampus impair social memory in mice. *European Journal of Neuroscience* 40, 3294–3301.

Steward, and Scoville (1976). Cells of origin of entorhinal cortical afferents to the hippocampus and fascia dentata of the rat. *Journal of Comparative Neurology* 169, 347–370.

Stewart, and Fox (1990). Firing relations of lateral septal neurons to the hippocampal theta rhythm in urethane anesthetized rats. *Experimental Brain Research* 79, 92–6.

Sun, Srinivas, Sotayo, and Siegelbaum (2014). Dendritic Na<sup>+</sup> spikes enable cortical input to drive action potential output from hippocampal CA2 pyramidal neurons. *ELife* 3, e04551.

Sun, Sotayo, Cazzulino, Snyder, Denny, and Siegelbaum (2017). Proximodistal Heterogeneity of Hippocampal CA3 Pyramidal Neuron Intrinsic Properties, Connectivity, and Reactivation during Memory Recall. *Neuron* 95, 656–672.e3.

Swanson, and Cowan (1977). An autoradiographic study of the organization of the efferent connections of the hippocampal formation in the rat. *Journal of Comparative Neurology* 172, 49–84.

Swanson, and Hartman (1975). The central adrenergic system. An immunofluorescence study of the location of cell bodies and their efferent connections in the rat utilizing dopamine-B-hydroxylase as a marker. *Journal of Comparative Neurology* 163, 467–505.

Talley, Solorzano, Lei, Kim, and Bayliss (2001). Cns distribution of members of the two-pore-domain (KCNK) potassium channel family. *The Journal of Neuroscience : The Official Journal of the Society for Neuroscience* 21, 7491–505.

Taube, Muller, and Ranck (1990). Head-direction cells recorded from the postsubiculum in freely moving rats. I. Description and quantitative analysis. *The Journal of Neuroscience : The Official Journal of the Society for Neuroscience* 10, 420–35.

Thinschmidt, Kinney, and Kocsis (1995). The supramammillary nucleus: Is it necessary for the mediation of hippocampal theta rhythm? *Neuroscience* 67, 301–312.

Thompson, and Best (1989). Place cells and silent cells in the hippocampus of freely-

- behaving rats. *The Journal of Neuroscience : The Official Journal of the Society for Neuroscience* 9, 2382–90.
- Tóth, Freund, and Miles (1997). Disinhibition of rat hippocampal pyramidal cells by GABAergic afferents from the septum. *The Journal of Physiology* 500, 463–474.
- Tulving, and Schacter (1990). Priming and human memory systems. *Science* 247, 301–306.
- Valero, Cid, Averkin, Aguilar, Sanchez-Aguilera, Viney, Gomez-Dominguez, Bellistri, and Prida (2015). Determinants of different deep and superficial CA1 pyramidal cell dynamics during sharp-wave ripples. *Nature Neuroscience* 18, 1281–1290.
- Vanderwolf (1969). Hippocampal electrical activity and voluntary movement in the rat. *Electroencephalography and Clinical Neurophysiology* 26, 407–418.
- Vazdarjanova, and Guzowski (2004). Differences in Hippocampal Neuronal Population Responses to Modifications of an Environmental Context: Evidence for Distinct, Yet Complementary, Functions of CA3 and CA1 Ensembles. *The Journal of Neuroscience* 24, 6489–6496.
- Vertes (1992). PHA-L analysis of projections from the supramammillary nucleus in the rat. *Journal of Comparative Neurology* 326, 595–622.
- Vertes, and Kocsis (1997). Brainstem-diencephalo-septohippocampal systems controlling the theta rhythm of the hippocampus. *Neuroscience* 81, 893–926.
- Vertes, and McKenna (2000). Collateral projections from the supramammillary nucleus to the medial septum and hippocampus. *Synapse* 38, 281–293.
- Vida, Halasy, Szinyei, Somogyi, and Buhl (1998). Unitary IPSPs evoked by interneurons at the stratum radiatum-stratum lacunosum-moleculare border in the CA1 area of the rat hippocampus in vitro. *The Journal of Physiology* 506, 755–773.

Wang (2010). Neurophysiological and Computational Principles of Cortical Rhythms in Cognition. *Physiological Reviews* 90, 1195–1268.

Weel, and Witter (1996). Projections from the nucleus reuniens thalami to the entorhinal cortex, hippocampal field CA1, and the subiculum in the rat arise from different populations of neurons. *Journal of Comparative Neurology* 364, 637–650.

Wilson, and McNaughton (1993). Dynamics of the hippocampal ensemble code for space. *Science* 261, 1055–1058.

Wilson, and McNaughton (1994). Reactivation of hippocampal ensemble memories during sleep. *Science* 265, 676–679.

Wintzer, Boehringer, Polygalov, and McHugh (2014). The Hippocampal CA2 Ensemble Is Sensitive to Contextual Change. *The Journal of Neuroscience* 34, 3056–3066.

Witter, Groenewegen, FLD, S., and Lohman (1989). Functional organization of the extrinsic and intrinsic circuitry of the parahippocampal region. *Progress in Neurobiology* 33, 161–253.

Woodnorth, Kyd, Logan, Long, and McNaughton (2003). Multiple hypothalamic sites control the frequency of hippocampal theta rhythm. *Hippocampus* 13, 361–374.

Wyss, Swanson, and Cowan (1979). Evidence for an input to the molecular layer and the stratum granulosum of the dentate gyrus from the supramammillary region of the hypothalamus. *Anatomy and Embryology* 156, 165–176.

Yamada-Hanff, and Bean (2013). Persistent Sodium Current Drives Conditional Pacemaking in CA1 Pyramidal Neurons under Muscarinic Stimulation. *The Journal of Neuroscience* 33, 15011–15021.

Yeckel, and Berger (1990). Feedforward excitation of the hippocampus by afferents from the entorhinal cortex: redefinition of the role of the trisynaptic pathway. *Proceedings of the National Academy of Sciences* 87, 5832–5836.

Xavier, Oliveira-Filho, and Santos (1999). Dentate gyrus-selective colchicine lesion and disruption of performance in spatial tasks: difficulties in “place strategy” because of a lack of flexibility in the use of environmental cues? *Hippocampus* 6, 668-681.

Zemankovics, Veres, Oren, and Hájos (2013). Feedforward Inhibition Underlies the Propagation of Cholinergically Induced Gamma Oscillations from Hippocampal CA3 to CA1. *The Journal of Neuroscience* 33, 12337–12351.

Zhao, Choi, Obrietan, and Dudek (2007). Synaptic Plasticity (and the Lack Thereof) in Hippocampal CA2 Neurons. *The Journal of Neuroscience* 27, 12025–12032.

# VI - Appendices

## VI.1 - Chronic loss of CA2 transmission leads to hippocampal hyperexcitability

### VI.1.a - Introduction

This research article investigates the contributions of area CA2 activity to hippocampal function by using genetics to prevent output synaptic transmission from CA2 PN. First, the excitatory and inhibitory drives from area CA2 onto area CA3 and CA1 are assessed using optogenetics in acute slices, showing that area CA2 recruits a substantial feedforward inhibition in area CA3 that can limit its responsiveness to DG input. Then, the contributions of area CA2 to controlling hippocampal excitability are probed in acute slices by preventing the output synaptic transmission with TeTX in CA2 PNs, revealing increased excitability in the CA3 recurrent network. Next, the consequences of silencing area CA2 output are investigated *in vivo* during exploration with the same strategy, showing that place fields in area CA1 are replaced by spatially-triggered hyperexcitability events and that the CA3 spike-timing preference to theta is shifted in the chronic absence of CA2 PN transmission. Consistently, a clustering of place fields is observed when using chemogenetics to acutely silence CA2 PNs *in vivo* during exploration. Then, analysis of rest epochs *in vivo* in mice expressing TeTX in CA2 PNs reveals a lower occurrence of SWR that are replaced by epileptiform discharges in the chronic absence of synaptic transmission from CA2 PNs. Finally, behavioral tests show that the chronic loss of CA2 transmission in CA2-TeTX mice impairs contextual learning and increases seizure probability.

This research article was published as a collaborative effort from the McHugh laboratory and the Piskorowski / Chevalleyre laboratory in which I worked during my thesis. Specifically, I contributed to performing the following experiments : power-response of light-evoked synaptic transmission from CA2 to CA1 in current clamp before and after blocking inhibitory transmission (Figure 1. CA2 output recruits inhibition in CA3 and filters network excitability) and power-response of the fEPSP amplitude evoked by electrical stimulation of CA3 inputs in CA1 and CA3 in acute slices from animals with TeTX- and mCherry-expressing CA2 PNs (Figure 2. CA2-PC-specific expression of TeTX silences synaptic transmission and increases CA2 recurrent activity).

## **VI.1.b - Paper**

## **VI.2 - Hippocampal area CA2 : properties and contribution to hippocampal function**

### **VI.2.a - Introduction**

This review article focuses on hippocampal area CA2, summarizing the current knowledge on this region and highlighting recent findings. First, the unique connectivity of area CA2 with intra- and extra-hippocampal structures is detailed. Then, we highlight the roles of area CA2 in behavior and hippocampal-dependent memory formation, as well as the contribution of area CA2 to the underlying network activity. Next, the peculiar cellular composition and properties of area CA2 are reviewed. Finally, the specific types of synaptic plasticity occurring in area CA2 are summarized.

This review article was published by the Piskorowski / Chevaleyre laboratory where I worked during my thesis and I contributed to the writing of the following sections : Introduction, CA2 inputs and outputs (Intra-hippocampal connectivity, Long-range input and output), CA2's roles in behavior and hippocampal-dependent memory formation (Place cell activity and potential roles in spatial learning, CA2 and hippocampal network activity), Cellular composition and properties (CA2 interneurons), and Conclusion.

### **VI.2.b - Paper**

## Résumé

L'hippocampe est une structure cérébrale cruciale pour la mémoire et l'apprentissage. Ces fonctions sont assurées par l'activité coordonnée des neurones hippocampiques au cours d'oscillations au sein du réseau neuronal. Différents profils d'activité rythmique sont rencontrés dans l'hippocampe, notamment les oscillations theta et gamma ainsi que les "sharp wave ripples". Toutefois, les mécanismes sous-jacents ne sont pas intégralement élucidés. En effet, plusieurs structures cérébrales connectées à l'hippocampe participent à la genèse de ces oscillations, cependant leurs contributions respectives demeurent méconnues. En particulier, le noyau supramammillaire hypothalamique (SuM) est une région fortement impliquée dans les oscillations theta qui afférente l'aire CA2, zone hippocampique longtemps négligée. De fait, la physiologie de cette connexion hypothalamo-hippocampique n'a jamais été examinée jusqu'à présent. Pourtant, de récentes études *in vivo* ont révélé un rôle de l'aire CA2 dans la genèse des "sharp wave ripples" et le codage spatial, suggérant de ce fait des contributions spécifiques de cette région aux fonctions hippocampiques. Ainsi, l'élucidation des mécanismes gouvernant l'activité de réseau de l'aire CA2, de son influence par les afférences du SuM et des conséquences sur les efférences hippocampiques sont nécessaires pour améliorer la compréhension des fonction mnésiques de l'hippocampe.

Afin de répondre à ces questions, nous avons combinés des approches histologiques, pharmacologiques, électrophysiologiques *ex vivo*, optogénétiques et chimiogénétiques sur tranches d'hippocampe de souris génétiquement modifiées. Cela nous a tout d'abord permis de caractériser les mécanismes associés aux oscillations gamma-mimétiques induites par l'agoniste cholinergique carbachol dans l'aire CA2, à l'échelle cellulaire et à celle du réseau neuronal. Lors de ce régime d'activité, nous avons mis en évidence que les neurones pyramidaux de CA2 déchargent des bouffées de potentiels d'action couplés à la phase de l'oscillation. Par la suite, nous avons prouvé que les neurones pyramidaux superficiels et profonds de CA2 reçoivent différents degrés d'excitation mono-synaptique et d'inhibition di-synaptique de la part des afférences du SuM. De plus, nous avons démontré que les afférences du SuM recrutent des interneurons en panier parvalbumine-immunopositifs qui contrôlent la précision temporelle des potentiels d'action émis par les neurones pyramidaux de CA2 via un processus d'inhibition anticipée. De surcroît, nous avons prouvé que l'inhibition recrutée par le SuM exerce un contrôle temporel sur la décharge des bouffées de potentiels d'action par les neurones pyramidaux de CA2 en présence de carbachol. Enfin, nous avons observé que l'activation des afférences du SuM au niveau de l'aire CA2 provoque une réduction prolongée d'activité dans l'aire CA1 en conditions de tonus cholinergique élevé. Ainsi, nos résultats mettent en exergue un rôle crucial du SuM dans le contrôle de l'activité de l'aire CA2 et ses conséquences sur les efférences de l'hippocampe. En conclusion, nous postulons que la connexion entre le SuM et l'aire CA2 sous-tend des aspects capitaux de la rythmogenèse hippocampique et des fonctions associées.

Mots-clés : hippocampe, hypothalamus, aire CA2, SuM, carbachol, oscillations, décharge en bouffée, interneurons en panier parvalbumine-immunopositifs, inhibition anticipée

# Abstract

The hippocampus is a brain structure critically involved in learning and memory. These functions depend on the coordinated activity of hippocampal neurons during network oscillations. Different rhythmic patterns of activity exist in the hippocampus such as oscillations in the theta and gamma range as well as sharp wave ripples, however their underlying mechanisms are not fully understood. Indeed, several brain structures connected to the hippocampus participate in the generation of these oscillations, but their respective contributions remain elusive. Notably, the hypothalamic supramammillary nucleus (SuM) is strongly involved in theta oscillations and projects to the long-overlooked hippocampal area CA2. Even so, the physiology of this hypothalamo-hippocampal long-range input has never been investigated. Interestingly, recent *in vivo* studies have revealed a role of area CA2 in the generation of sharp wave ripples and spatial coding, suggesting specific contributions of area CA2 to hippocampal network function. Therefore, information regarding the mechanism governing network activity in area CA2, how it is influenced by SuM inputs and the consequences on hippocampal output is required to better understand hippocampal-dependent learning and memory.

To address these questions, we combined histology, pharmacology, *ex vivo* electrophysiology, optogenetics and chemogenetics on acute hippocampal slices from genetically-engineered mouse lines. This first allowed us to characterize the cellular and circuit mechanisms of gamma-like oscillations induced by the cholinergic agonist carbachol in area CA2. In this regime, we found that CA2 pyramidal neurons fire bursts of action potentials that show phase-coupling to the oscillation. Next, we proved that SuM inputs differentially drive mono-synaptic excitation and di-synaptic inhibition onto deep and superficial CA2 pyramidal neurons. In addition, we demonstrated that parvalbumin-expressing basket cells are strongly recruited by SuM inputs and control the timing and precision of CA2 pyramidal neurons action potential firing via feedforward inhibition. Moreover, we showed that the SuM inhibitory drive onto CA2 pyramidal neurons exerts a temporal control on their bursting of action potential in the presence of carbachol. Finally, we observed that activation of SuM inputs to area CA2 result in a prolonged reduction of activity in area CA1 under conditions of elevated cholinergic tone. Altogether, our results highlight a critical role of the SuM in controlling area CA2 activity and thereby influences the hippocampal output. To conclude, we postulate that the SuM to area CA2 connection underlies key aspects of hippocampal rhythmogenesis and associated functions.

**Keywords** : hippocampus, hypothalamus, area CA2, SuM, carbachol, oscillations, burst firing, parvalbumin-expressing basket cell, feedforward inhibition.